Tidal Response Of Planetary Fluids (*TROPF)*
User's Manual with Examples
v1.0, August 11, 2019

Robert H. Tyler[1,2]
1) Geodesy and Geophysics Laboratory, NASA Goddard Space Flight Center
2) Joint Center for Earth Systems Technology, University of Maryland Baltimore County
rtyler@umbc.edu; (01) 301 614 6472

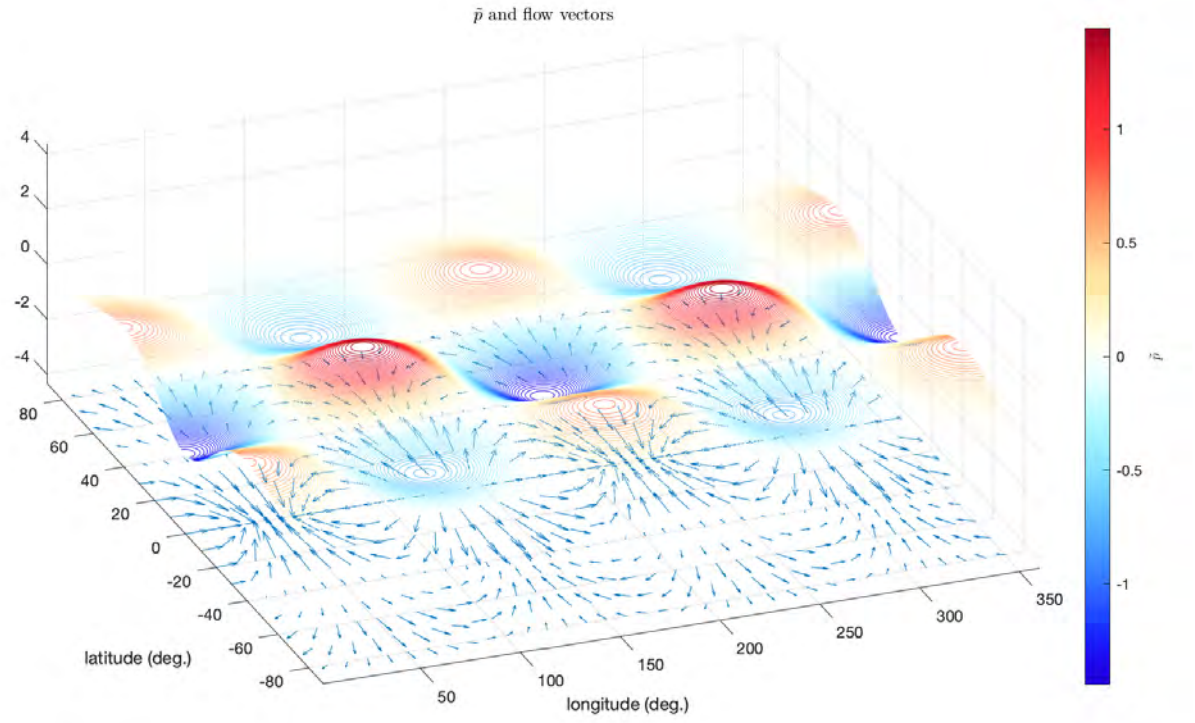

Summary

This document provides a users's manual as well as application examples for the *Tidal Response Of Planetary Fluids* (*TROPF*) software package. In planetary science, the tidal response of fluid media (e.g. ocean, atmosphere, magma, core fluids) depends on input parameters that are not well constrained and must often be considered over a very wide range. This creates a computational challenge as millions of tidal scenarios may be required to adequately sample the solution domain describing the range of tidal response behavior. *TROPF* is designed and optimized to meet this challenge. The *TROPF* package includes several different solvers using either spherical-harmonic or finite-volume base functions. Using factorized sparse matrix operations, the primary solver (`tropf.m`) can provide high-resolution tidal response solutions at a rate of about 1 million solutions per minute on a standard desktop computer (each solution is, more specifically, for an individual vertical mode or layer.) Validations provided show that the different solvers provide solutions that agree with each other to within either machine precision or the theoretical limits of the resolution chosen. *TROPF* is developed in the *MATLAB* language but can also be run in *Octave*. Portability to *Python* and other languages is also fairly easy as the instructions for building the operator matrices are described here in detail and the coding of core *TROPF* routines adheres to generic sparse matrix operations and avoids functions specific to *MATLAB*.

The equations solved by *TROPF* are generalized forms that cover the different governing equations used in a wide range of fluid tidal applications. In the simplest example of a thin, hydrostatic, uniform-density ocean, the equations solved reduce to the Laplace Tidal Equations and continuity equation. Extensions to this can include a wide variety of dissipation processes (e.g. Rayleigh drag, eddy viscosity including harmonic, biharmonic, and hyperharmonic forms) as well as other parameterized effects such as self gravity and coupling with an overlying ice shell. In applications to atmospheric tides (potentially thick, compressible, stratified, nonhydrostatic fluids) the equations solved are those from Classical Tidal Theory, which are understood here as representing a fairly general set of equations for conservation of momentum and energy but under the limitation that the horizontal and vertical dependencies remain separable (such that the separation of variables technique applies).

Configuration scripts are included for running the demos and validation studies described in this manual. In addition, the Applications Chapter, includes a comprehensive suite of generic tidal studies covering the tides in two-body (synchronous as well as nonsychronous) systems. Specific applications can then be treated by using one of these examples as a starting template (or simply rescaling the results these examples already provide). It is expected that more examples will be added to these applications and it is therefore recommended that the user first ensure they have the latest software and documentation.

Contents

List of Figures

List of Tables

CHAPTER 1

Introduction

1.1. Quick Start

This document provides extensive details on the formulation and methodology used in *TROPF* as well as the input parameters and results for several demos, validations, and applications. The user wishing to gain an initial hands-on quick start in exploring the software is recommended to start by opening and running the scripts in the directory TROPF /Demos. This might be followed by opening and running scripts in TROPF /Validations, and finally the various application subdirectories under TROPF /Studies provide a suite of configured examples.

Specific details related to code and function calls are best described within the documentation provided in the *TROPF* files. This manual focuses more on the theory and methodology behind *TROPF*. But it also provides a simple description of the higher-level (macro) function calls, including configured examples that can be easily modified for specific applications. Further examples will be added and so the user should first ensure that they have the latest version of the *TROPF* package.

1.2. An Efficient Approach in Estimating Tides of Planetary Fluids

The key feature distinguishing *TROPF* from other approaches more common in terrestrial fluid tidal studies is the recognition that in planetary applications the required input parameters for calculating the tides are typically not well constrained and must be considered over a very large range. When considering exoplanetary tidal fluids, the vast range of input parameters may in fact represent treatment of a vast range of potential scenarios. Because the tidal response can depend very sensitively on these parameters, millions of tidal solutions may need to be calculated to sample the full range of tidal response behaviors. This creates a practical demand for computational speed but also a potential storage challenge as each tidal scenario involves a data set describing a number of solution variables and their temporal and spatial distribution.

These challenges can be regarded as resolved with *TROPF*. The *TROPF* package includes several different formulations and solution approaches to the governing equations from Classical Tidal Theory. In the fastest, millions of solutions can be calculated to high resolution (e.g. spherical-harmonic degree 500) essentially in real time (several minutes) on a standard computer, solving the speed challenge and also the storage problem as solutions can simply be regenerated when needed.[1]

Let us describe this unique challenge in planetary applications more precisely for what follows. In planetary applications, the tidal response must often be considered over a rotating fully spherical domain. The governing equations to be solved therefore cannot use f-plane, beta-plane or other such simplifying approximations appropriate only for regional domains. On the hand, the assumption of spherically-symmetric environmental parameters is often a good one (such would not be the case for Earth's ocean, for example) and this can be exploited in the formulation. Once a set of governing equations and a general solution method have been established, we may regard this as a function that takes input parameters and returns the solution variables. The solution 'domain' or 'solution space' of this function covers the set of all possible tidal solutions that can be obtained from all possible combinations of the input parameters. It is helpful to think of the N_p input parameters as forming an N_p -dimensional space, with each parameter forming an axes, or independent degree of freedom. Associated with each point in the space is the set of solution variables describing the tidal response. If there are N_s parameters describing the solution, then one could envision the exhaustive description of all tidal scenarios fully described by an N_s–component tensor field in an N_p-dimensional space.

[1] In a benchmark study using a Mac Pro 3.5 GHz 6-Core Intel Xeon E5 with 65 GB RAM, solutions to truncation degree 500 were calculated at a rate of 562122 per minute. Using a MacBook Pro 2.8 GHz Intel Core i7 with 16 GB RAM, the rate was 70673 solutions per minute.

From a practical point, the solution tensor has many parameters describing the spatiotemporal distribution of each solution variable and so one must first decide how to compactify the description of each solution set. A useful approach for planetary tidal applications is as follows. Of all the potential tidal scenarios, the ones most interesting are often the ones with the most power. In this case, the tidal scenario can be compactly characterized by the time-averaged total power of the tidal fluid. For better inter-comparison between fluids with different volumes and densities, one may consider the averaged power density per unit fluid mass (or unit fluid volume). In either case, the domain of tidal solutions is now conveniently characterized by a scalar field in an N_p-dimensional space. As will be shown in applications, this characterization is a good starting point for exploring tidal behaviors. Note that it also presents an additional requirement that integration over solution products be computationally fast in order to calculate the averages.

It could seem to be a problem that the domain of the solutions may not be bounded. But the parameter axes of the solution space may be truncated when an asymptotic behavior of the solution is recognized. The domain of interest must then simply capture the subdomain of tidal behaviors.

Another important point in understanding the *TROPF* approach is that the dimensionality of the domain may be reduced simply through nondimensionalization of the parameters and operators in the governing equations. Physical parameters may be combined into a smaller set of degenerate combinations. The result is that nondimensional "generic" solutions are obtained which may be rescaled and interpreted for specific applications. The full set of generic solutions then comprise the domain of tidal response behaviors.

A large, comprehensive set of these generic solutions for cases of two-body synchronous and nonsynchronous systems is provided in the Applications chapter and it is expected that these generic solutions can be simply rescaled initially for most specific applications. Extensions to the simple assumptions here can then reached by modifying the associated configuration scripts. Hence, the *TROPF* package includes templates that can be used for most fluid tidal applications.

1.3. The Solution Domain in *TROPF*

Within the codification of the *TROPF* software, the dimensionality of the domain of tidal response solutions is set by the number of input free parameters. In the current version of the main solver (`tropf.m`), the function call appears as

$$\text{[Dns,Rns,pns, calWns,calDns,calEKns,calEPns,knFsF]} \;=$$
$$\text{tropf(N,tilOm, tilom,s,Gns,Kns,dns,ens, tilalpd,tilalpr,tilnusqns).}$$

The input parameters are clumped into three groups. The first includes two methodological parameters, where N is the number of terms in the spherical-harmonic expansion and $\tilde{\Omega}$ ('`tilOm`') is the nondimensionalized rotation rate of the fluid (see Table 1 for definitions of parameters). These methodological parameters are not regarded as free parameters since accurate solutions should be independent of reasonable choices for these parameters. The choice of methodological parameters concerns only the convenience and efficiency in the method. In all applications to be described in this document, we take $N = 500$ (which is typically much higher than needed but easy and affordable) and $\tilde{\Omega} = 1$. The latter selection simply sets the nondimensionalization factor Ω_s for temporal frequencies to be equal to the rotation rate Ω. While this is a suitable choice for most applications, this input parameter is included to allow a necessarily different choice for the non-rotating case.

The next six input parameters characterize the nondimensional forcing. The first, $\tilde{\omega}$ ('`tilom`') is the nondimensional forcing frequency. It is a real scalar but may be either positive or negative depending on the direction of propagation of the forcing (as formulated in Chapter 2). The parameter s (a non-negative scalar) is the longitudinal wave number of the forcing, and $\mathbf{G}^{\mathbf{s}}_{\mathbf{n}}$ ('`Gns`') is a column vector with the spherical-harmonic coefficients for the various degrees $n = s, s+1, ...$ of the prescribed tidal potential. The vectors $\mathbf{K}^{\mathbf{s}}_{\mathbf{n}}$, $\mathbf{d}^{\mathbf{s}}_{\mathbf{n}}$, $\mathbf{e}^{\mathbf{s}}_{\mathbf{n}}$ ('`Kns`, `dns`, `ens`') allow for the specification of non-tidal forces which, however, are not considered in the examples to be discussed in this document.

The final clump of input parameters describe the response properties of the fluid media. The parameters $\tilde{\alpha}_d$ and $\tilde{\alpha}_r$ ('`tilalpd`, `tilalpr`'), when entered as scalars are the 'Rayleigh' drag coefficients for the horizontally divergent and rotational components of the flow, respectively. (Distinguishing between the two flow components is important because only the divergent flow leads to vertical motion, which may be damped by ice cover for example). More generally, the parameters $\tilde{\alpha}_d$ and $\tilde{\alpha}_r$ may be entered as row vectors ($\tilde{\alpha}_{d,b}$, $\tilde{\alpha}_{r,b}$), where $b = 0, 1, 2....$ In this case $\tilde{\alpha}_{d,0}, \tilde{\alpha}_{r,0}$ are the Rayleigh drag coefficients, $\tilde{\alpha}_{d,1}$, $\tilde{\alpha}_{r,1}$ are coefficients

for harmonic eddy viscosity, $\tilde{\alpha}_{d,2}$, $\tilde{\alpha}_{r,2}$ are coefficients for biharmonic eddy viscosity, and continuing through hyperharmonic forms with $b > 2$. Finally, one of the most important parameters controlling the response is the squared slowness parameter $\left(\tilde{\nu}^{\mathbf{2}}\right)^{\mathbf{s}}_{\mathbf{n}}$ ('`tilnusqns`'). The squared slowness is a column vector of complex spherical-harmonic coefficients. When this is entered as a real scalar, the squared slowness is just the squared inverse of a nondimensional fluid wave speed (the scalar squared slowness also becomes equivalent to the Lamb number.) When $\left(\tilde{\nu}^{\mathbf{2}}\right)^{\mathbf{s}}_{\mathbf{n}}$ is entered as a real column vector, then this generalizes to the case where the wave speed becomes dispersive (dependent on degree) and can include, for example, the effects of self gravity. When $\left(\tilde{\nu}^{\mathbf{2}}\right)^{\mathbf{s}}_{\mathbf{n}}$ is entered with complex components, the imaginary part represents dissipation associated with the vertical momentum balance. It can be prescribed to include such effects as Newtonian cooling in atmospheres and viscoelastic ice-coupling in oceans.

The output variables of `tropf.m` include the primary solution variables, which are the coefficient vectors for the divergent and rotational flow potentials, $\mathbf{D}^{\mathbf{s}}_{\mathbf{n}}$, $\mathbf{R}^{\mathbf{s}}_{\mathbf{n}}$ ('`Dns,Rns`'), and the dynamic pressure variable $\mathbf{p}^{\mathbf{s}}_{\mathbf{n}}$ ('`pns`')). Also included are several variables that involve averages (performed analytically using the spherical-harmonic coefficients) over the globe and tidal cycle. The variable $\mathbf{W}^{\mathbf{s}}_{\mathbf{n}}$ ('`calWns`') is a column vector of spherical-harmonic coefficients for the average work performed by tidal forces on the fluid. The average total work is simply the sum of the elements in this vector, but the vector is output to provide the additional information on the spectral dependence. Similarly, $\mathbf{D}^{\mathbf{s}}_{\mathbf{n}}$ ('`calDns`') is the vector for the coefficients for average dissipation, and $\mathbf{E}^{\mathbf{s}}_{\mathbf{K},\mathbf{n}}$ ('`calEKns`') and $\mathbf{E}^{\mathbf{s}}_{\mathbf{P},\mathbf{n}}$ ('`calEPns`') are the vectors for the coefficients for average kinetic and potential energy densities, respectively. The final output parameter $k^{s_F}_{n_F}$ ('knFsF') is the complex Love number describing the ratio of the the nondimensional pressure response and nondimensional applied tidal potential. Note that while the Love number concerns only the degree (n_F) and order (s_F) of the applied tidal potential, the response will generally include a spectrum over all degrees. Hence, except for limiting cases where spherical-harmonics become eigenfunctions for the equations controlling the ocean's response, a Love number cannot by itself characterize the tidal response.

1.4. The *TROPF* Software Package

The *TROPF* package is installed by unzipping TROPF.zip in the directory desired and modifying the path in TROPF /`scr_startup_tropf.m` accordingly.

The directory structure of the *TROPF* package includes TROPF /Libraries which contains all the *TROPF* calculation software. Functions for the primary method (based in spherical harmonics) are found in TROPF /Libraries /Lib_tropfSH /Functions. A smaller set of functions for the alternative method (based in finite-volume discretization and used here primarily for cross validation) are included in TROPF /Libraries /Lib_tropfFV.

Most users will probably use the macro function Lib_tropfSH /Functions /`tropf.m` to obtain the spherical-harmonic coefficients of the tidal response as well as the product averages. Then, if mapping (synthesizing) the solution to plot solutions on a global grid, the macro Lib_tropfSH /Functions /`buildMovie.m` can be used to both map the fields as well as calculate and map the flow velocity vectors. Note that to preserve high accuracy the post-processing to obtain the auxiliary solution variables (e.g. product integrals, and the derivatives needed to calculate velocity) is done analytically with the spherical-harmonic coefficients rather than numerically with the gridded solutions. Hence, the mapping of solutions to a grid should be thought of as part of the plotting software rather than part of the core calculation routines. The documentation within these two macro functions describes other subfunctions within the library that are called. Notable are a large number of functions named `build_L*.m` that build the individual suboperator matrices listed in Table 3.

A macro `tropf_sas.m` is also included. This alternative to `tropf.m` uses a formulation of the governing equations previously developed and used first in [Tyler, 2011]. Whereas `tropf_sas.m` solves a symmetric/antisymmetric system of equations in two variables (the flow potentials $\mathbf{D}^{\mathbf{s}}_{\mathbf{n}}$, $\mathbf{R}^{\mathbf{s}}_{\mathbf{n}}$), `tropf.m` solves a higher-order equation for one variable ($\mathbf{p}^{\mathbf{s}}_{\mathbf{n}}$ or alternatively $\mathbf{D}^{\mathbf{s}}_{\mathbf{n}}$). In the Validations it is shown that both `tropf.m` and `tropf_sas.m` produce the same solutions to within machine precision. The use of `tropf.m` is preferred here for reasons of efficiency.

The directory TROPF /Demos includes demonstration scripts, TROPF /Validations provides the scripts used in Chapter 5, and TROPF /Studies provides scripts used in the example applications described in Chapter 7.

1.5. *TROPF* Development

The development of the *TROPF* formulations and solution methods have the following history. [Tyler, 2008, 2009] first treated dynamic tides in ice-covered oceans on Europa and Enceladus using an analytical approach based on perturbations of the inviscid Laplace Tidal Equations. The tangential stress at the ocean/ice interface and seafloor was considered as a perturbation on the inviscid solution, while the normal stresses associated with vertical motion were justifiably ignored because the (obliquity) tidal force component initially considered excited only Class II (Rossby) waves which involve no vertical flow velocities.

If a near-inviscid, horizontally nondivergent flow response could be generally expected for the tidal response due to other tidal forces, then a simple approach for obtaining tidal response solutions would be to construct them from the known eigenmodes of the Laplace Tidal Equations and tidal forcing. But such is not the case as the response due to other tidal forces will involve rotational gravity waves and therefore vertical motion which attempts to lift the ice (requiring normal stress with the ice and not just tangential stress). Because this normal coupling with the ice can be expected to lead to strong damping (especially for thick ice shells), a more general solution approach was needed to extend this work and include the response to other (e.g. eccentricity) tidal forces and under conditions where dissipation may be very strong.

To address this, the precursor to *TROPF* was a method introduced in [Tyler, 2011]. In the Longuet-Higgins [1968] study of the eigenfunctions of the unforced, inviscid Laplace Tidal Equations, the governing equations were translated into operator matrices acting on the coefficients of a spherical-harmonic expansion of the Helmholtz flow potentials. In [Tyler, 2011], the Longuet-Higgins approach was extended and restructured into essentially a response (rather than eigen) function problem for the forced, dissipative equations, with the interpretation of parameters generalized to include both barotropic as well as equivalent barotropic (stratified) tidal dynamics. This approach has been used by Tyler in treating a variety of tidal fluids (oceans, magma, core fluid, atmosphere), including stratified layers [Tyler, 2011, 2014, Tyler and Kuang, 2014, Tyler et al., 2015, Tyler, 2019]. It has also been adopted and extended by others investigating the satellite oceans [Chen et al., 2014, Matsuyama, 2014, Beuthe, 2016, Matsuyama et al., 2018]. (This method is included in the *TROPF* package as the function `tropf_sas.m`, as described in Section 1.4.)

In *TROPF*, there has been a complete reformulation of the equations solved and the optimal method for obtaining solutions. This has been aimed at providing both computational efficiency as well as versatility in the tidal fluids that can be considered. The equations solved in *TROPF* are general forms which essentially preserve the mathematical separability of horizontal and vertical dependencies in Classical Tidal Theory but otherwise remove any unnecessary assumptions that would restrict applicability or the implementation of further extensions. Notable is the generalization from simply a squared wave speed (inverse of the Lamb parameter) to a slowness operator which allows dispersion, self-gravity and the parameterized dissipation of a viscoelastic 'membrane' ice shell (see Appendix D). The slowness operator is also the basis for the vertical modes of a potentially complex atmosphere (Appendix A) and it is expected that this element will receive further discussion and examples in future versions of this manual. Indeed, a goal is to add further examples to the Applications Chapter that can be used as templates and starting points for future studies. Contributions are welcome from the community of *TROPF* users.

TROPF has been developed and optimized in the *Matlab* language. It will also run in the nonproprietary *Octave* language but this may need refining based on feedback from *Octave* users. One sees immediately that *Octave* tends to be slower, and some of the plotting software of *Octave* does not include all the elements in *Matlab*. The core *TROPF* functions can also be readily translated to other languages such as *Python* and *Mathematica*. These core routines are essentially just the algorithmic instructions for building the suboperator matrices as described in Table 2, the coded form of which exists as the library of `build_L*.m` files. A forum on *TROPF*, regarded in this larger context of a set of algorithms independent of the language, would help organize the continued development.

Development of the *TROPF* software package and documentation was supported by the NASA Cassini Data Analyses Program, and the Planetary Geodesy GSFC Internal Scientist Funding Model (ISMF, Planetary Geodesy). The precursor software was developed with support from the NASA Outer Planets Program.

CHAPTER 2

Gravitational Potential and Tidal Forces

Pierre-Simon Laplace developed spherical-harmonic functions in the context of creating a series expansion for the gravitational potential of an external point-mass source projected onto a sphere. The small parameter he used to find an efficiently quick decay in the amplitude of the terms in the series was the ratio of the radius of the sphere to the distance to the external body. In planetary applications this ratio is typically small and justifies a truncation of the series. In tidal applications, one is interested only in the differential pull of the gravitational forces. In this case, only the gravitational potential terms with spatial curvature are of interest, which precludes the zeroth and first order terms in the expansion. What is considered the "tidal potential" then starts with the second-order 'degree-two' terms, and one finds that the higher-order terms can often be neglected.

In the next section, we derive the degree-two gravitational potential for the case of a two-body system with arbitrary rotation, eccentricity, and obliquity. This is then transformed to the coordinates of the rotating spherical body experiencing the tides. Finally, approximate forms assuming small eccentricity and obliquity are provided.

2.1. Tidal Gravitational Potential

Consider the tidal forces of a body of mass M_p on another of mass M_s. Let $\mathbf{r}_p$ and $\mathbf{r}_s$ describe the respective position vectors of their centers of mass. The distance between their centers is $d = ||\mathbf{d}||$, where $\mathbf{d} = \mathbf{r}_p - \mathbf{r_s}$. For convenience, we choose the center of mass M_s to be located at the origin of the reference frame (i.e. $\mathbf{r}_s \equiv \mathbf{0}$).

At a position $\mathbf{r}$, the gravitational potential of M_p is

$$\Phi = -\frac{GM_p}{\left(r^2 + d^2 - 2dr\cos\psi\right)^{1/2}} = -\frac{GM_p}{d_0}\left(\frac{d_0}{d}\right)\left(\left(\frac{r}{d}\right)^2 + 1 - 2\left(\frac{r}{d}\right)\cos\psi\right)^{-1/2} \tag{2.1.1}$$

where $\cos\psi = \mathbf{r}\cdot\mathbf{d}/(rd)$, with $r = ||\mathbf{r}||$, and G is the gravitational constant. Recognizing the Taylor series expansion of the Legendre generating functions, we may write (2.1.1) as

$$\Phi = -\frac{GM_p}{d}\Sigma_{n=0}^{\infty}\left(\frac{r}{d}\right)^n P_n\left(\cos\psi\right), \tag{2.1.2}$$

where P_n is the Legendre function of degree n. We write this equivalently as

$$\Phi = -\frac{GM_p}{d_0}\Sigma_{n=0}^{\infty}\left(\frac{r_0}{d_0}\right)^n\left(\frac{r}{r_0}\right)^n\left(\frac{d}{d_0}\right)^{-(n+1)} P_n\left(\cos\psi\right), \tag{2.1.3}$$

where r_0 and d_0 are arbitrary reference constants which may be conveniently prescribed to be the mean radius (of M_s) and orbital separation, respectively. We then assume that GM_p/d_0 and $(r_0/d_0)^n$ are independent of time (i. e. constants). When one considers the potential on surfaces of uniform r, the factor $(r/r_0)^n$ is also a constant. The spatiotemporal dependence of Φ is then fully contained within $(d/d_0)^{-(n+1)} P_n\left(\cos\psi\right)$ through the dependencies of d and $\cos\psi$ which we next express in a convenient coordinate system.

Consider a non-rotating spherical coordinate system with origin at $\mathbf{r}_s = \mathbf{0}$. Let the right-hand coordinates r, θ, φ include colatitude θ measured from the spin axis of M_s, and longitude φ increasing in the prograde sense of rotation. While r and θ are the same coordinates in a frame rotating with M_s, the use of longitude φ will ultimately be replaced by co-rotating longitude ϕ.

The position vector of the center of mass of M_p can be described in this frame with coordinates $d(t)$, $\theta_p(t)$, $\varphi_p(t)$. From the definition $\cos(\psi) = \mathbf{r} \cdot \mathbf{d}/(rd)$, one may easily assemble the Cartesian components of the dot product to find

$$\cos\psi = \sin(\theta)\cos(\varphi)\sin(\theta_p)\cos(\varphi_p) + \sin(\theta)\sin(\varphi)\sin(\theta_p)\sin(\varphi_p) + \cos(\theta)\cos(\theta_p) \tag{2.1.4}$$

or, using the product-to-sum trigonometric identity,

$$\cos(\psi) = \sin(\theta)\sin(\theta_p)\cos(\varphi - \varphi_p) + \cos(\theta)\cos(\theta_p). \tag{2.1.5}$$

Combining (2.1.3) and (2.1.5), we may then write the gravitational potential in the r, θ, φ coordinate system as

$$\Phi = -\frac{GM_p}{d_0}\Sigma_{n=0}^{\infty}\left(\frac{r_0}{d_0}\right)^n\left(\frac{r}{r_0}\right)^n\left(\frac{d}{d_0}\right)^{-(n+1)} P_n\left(\sin(\theta)\sin(\theta_p)\cos(\varphi-\varphi_p) + \cos(\theta)\cos(\theta_p)\right). \tag{2.1.6}$$

The coordinates d, φ_p, θ_p describing the location of M_p may vary with time. Expressions for these dependencies vary with the application.

Finally, to be considered a "tidal" component of the gravitational potential there must be curvature in the field. Another way of saying this is that tidal forces (proportional to the gradient of the potential) must involve differential pull. Let Φ_n refer to the individual terms in the sum (2.1.6). Because $P_0(x) = 1$,

$$\Phi_0 = -\frac{GM_p}{d_0}\left(\frac{d}{d_0}\right)^{-1} = -\frac{GM_p}{d}, \tag{2.1.7}$$

which is simply the instantaneous potential at $\mathbf{r}_s \equiv \mathbf{0}$ due to M_p. This component has no spatial gradient nor associated force. Because $P_1(x) = x$,

$$\Phi_1 = -\frac{GM_p}{d_0}\left(\frac{r_0}{d_0}\right)\left(\frac{r}{r_0}\right)\left(\frac{d}{d_0}\right)^{-2}\left(\sin(\theta)\sin(\theta_p)\cos(\varphi-\varphi_p) + \cos(\theta)\cos(\theta_p)\right). \tag{2.1.8}$$

Recalling (2.1.5), we see that Φ_1 varies through space as $r\cos\psi$ which shows only a constant gradient and no curvature. Indeed, $\Phi_0 + \Phi_1$ provides the forces associated with maintaining the orbit of the bodies but includes no differential components giving "tidal" forces.

The "tidal" gravitational potential evidently starts with Φ_2. Given that $\Phi_n \propto (r_0/d_0)^n$ by (2.1.6), and that in nearly all applications r_0/d_0 is much less than unity, we can conclude that the tidal potential is dominantly described by Φ_2, which we may write, using (2.1.5) and Legendre/trigonometric identities, as

$$\begin{aligned}\Phi_2 &= -\frac{GM_p}{d_0}\left(\frac{r_0}{d_0}\right)^2\left(\frac{r}{r_0}\right)^2\left(\frac{d}{d_0}\right)^{-3} P_2(\cos\psi) \\ &= -\frac{GM_p}{d_0}\left(\frac{r_0}{d_0}\right)^2\left(\frac{r}{r_0}\right)^2\left(\frac{d}{d_0}\right)^{-3} P_2\left(\sin(\theta)\sin(\theta_p)\cos(\varphi-\varphi_p) + \cos(\theta)\cos(\theta_p)\right) \\ &= -\frac{GM_p}{d_0}\left(\frac{r_0}{d_0}\right)^2\left(\frac{r}{r_0}\right)^2\left(\frac{d}{d_0}\right)^{-3}\left(\frac{1}{2}\left(3\left(\sin(\theta)\sin(\theta_p)\cos(\varphi-\varphi_p) + \cos(\theta)\cos(\theta_p)\right)^2 - 1\right)\right).\end{aligned} \tag{2.1.9}$$

2.1.1. Tidal Potential Represented with Spherical Harmonics. Here we rewrite Φ_2 in a form amenable for representation with a spherical-harmonic expansion.

Using the identities between trigonometric and associated Legendre functions P_n^s, we may rewrite the last equality in (2.1.9) as

$$\begin{aligned}\Phi_2 = &-\frac{GM_p}{d_0}\left(\frac{r_0}{d_0}\right)^2\left(\frac{r}{r_0}\right)^2\{\\ &\left(\frac{d}{d_0}\right)^{-3}\left(\frac{1}{2}\left(\cos^2(\theta_p)-1\right)\right)P_0^0(\cos\theta)\\ &+\left(\frac{d}{d_0}\right)^{-3}\left(\cos^2(\theta_p)\right)P_2^0(\cos(\theta))\\ &+\left(\frac{d}{d_0}\right)^{-3}\left(-\cos(\theta_p)\sin(\theta_p)\cos(\varphi-\varphi_p)\right)P_2^1(\cos(\theta))\\ &+\left(\frac{d}{d_0}\right)^{-3}\left(\frac{1}{2}\sin^2(\theta_p)\cos^2(\varphi-\varphi_p)\right)P_2^2(\cos(\theta))\\ &\},\end{aligned} \tag{2.1.10}$$

which, using $P_2^0(x) = P_0^0(x) - \frac{1}{2}P_2^2(x)$ to remove the P_0^0 term, can be written

$$\begin{aligned}\Phi_2 = &-\frac{GM_p}{d_0}\left(\frac{r_0}{d_0}\right)^2\left(\frac{r}{r_0}\right)^2\{\\ &\left(\frac{d}{d_0}\right)^{-3}\frac{1}{2}\left(3\cos^2(\theta_p)-1\right)P_2^0(\cos(\theta))\\ &+\left(\frac{d}{d_0}\right)^{-3}\left(-\cos(\theta_p)\sin(\theta_p)\cos(\varphi-\varphi_p)\right)P_2^1(\cos(\theta))\\ &+\left(\frac{d}{d_0}\right)^{-3}\left\{\left(\frac{1}{4}\sin^2(\theta_p)\cos(2(\varphi-\varphi_p))\right)\right\}P_2^2(\cos(\theta))\\ &\},\end{aligned} \tag{2.1.11}$$

or, using trigonometric power-reduction identities,

$$\begin{aligned}\Phi_2 = &-\frac{GM_p}{d_0}\left(\frac{r_0}{d_0}\right)^2\left(\frac{r}{r_0}\right)^2\{\\ &\left(\frac{d}{d_0}\right)^{-3}\frac{1}{4}\left(3\cos(2\theta_p)+1\right)P_2^0(\cos(\theta))\\ &+\left(\frac{d}{d_0}\right)^{-3}\left(-\frac{1}{2}\sin(2\theta_p)\cos(\varphi-\varphi_p)\right)P_2^1(\cos(\theta))\\ &+\left(\frac{d}{d_0}\right)^{-3}\left\{\left(\frac{1}{2}\left(1-\cos(2\theta_p)\right)\cos(2(\varphi-\varphi_p))\right)\right\}P_2^2(\cos(\theta))\\ &\}.\end{aligned} \tag{2.1.12}$$

In this section we have described Φ_2 as a sum of terms in $P_n^s(\cos(\theta))$ with factors involving parameters with dependencies that have not yet been prescribed. Such prescription is done in the next section and approximations are used to expand these factors in their time/longitude Fourier modes, as required for spherical-harmonic representation. Alternatively, one may retain the more general forms here by performing the Fourier expansion of these factors numerically using ephemerides data.

2.1.2. Tidal Potential Represented with Spherical Harmonics and Harmonic Time Dependence. Let us now adopt a reference frame rotating with M_s at frequency Ω. The longitude coordinate ϕ in the rotating frame is related to the non-rotating longitude φ by

$$\varphi = \phi + \Omega t. \tag{2.1.13}$$

Let us assume sinusoidal time dependencies describing the orbit of M_p:

$$\frac{d}{d_0} \equiv 1 - e\cos(\Omega_o t + \lambda_d), \tag{2.1.14}$$

$$\cos(\theta_p) \equiv -\delta\cos(\Omega_o t + \lambda_o), \tag{2.1.15}$$

$$\varphi_p \equiv \Omega_o t + \lambda_p + 2e\sin(\Omega_o t), \tag{2.1.16}$$

where e is the eccentricity parameter, δ is the sine of the declination amplitude (i.e. $\delta = \sin(\theta_\delta)$ with θ_δ the maximum angle of M_p away from the spin equator on M_s), Ω_o is the orbital frequency of the M_p, M_s system, t is time, and λ_d, λ_o, λ_p allow phase offsets to be prescribed. For consistency in the limiting case of synchronous rotation, one should take $\lambda_d = \lambda_p$. It is also convenient to choose $t = 0$ to occur at the pericenter of the orbit, in which case $\lambda_d = \lambda_p = 0$.

First, substituting using (2.1.14, 2.1.15) in (2.1.11) or (2.1.12), we may write

$$\begin{aligned}
\Phi_2 = -\frac{GM_p}{d_0}\left(\frac{r_0}{d_0}\right)^2\left(\frac{r}{r_0}\right)^2 \{ & \\
(1 - e\cos(\Omega_o t + \lambda_d))^{-3}\frac{1}{2}\left(3\delta^2\cos^2(\Omega_o t + \lambda_o) - 1\right)P_2^0(\cos(\theta)) & \\
+ (1 - e\cos(\Omega_o t + \lambda_d))^{-3}\left(\delta\cos(\Omega_o t + \lambda_o)\left(1 - \delta^2\cos^2(\Omega_o t + \lambda_o)\right)^{1/2}\cos(\varphi - \varphi_p)\right)P_2^1(\cos(\theta)) & \\
+ (1 - e\cos(\Omega_o t + \lambda_d))^{-3}\left\{\left(\frac{1}{4}\left(1 - \delta^2\cos^2(\Omega_o t + \lambda_o)\right)\cos(2(\varphi - \varphi_p))\right)\right\}P_2^2(\cos(\theta)) & \\
\}. &
\end{aligned} \tag{2.1.17}$$

A simple substitution for φ, φ_p using (2.1.13, 2.1.16) then provides a description of Φ_2 as a function of time and the local (rotating) coordinates. Each of the factors multiplying a P_2^s term in the curly brackets is then a function describing the longitude/time dependence. We need to decompose these factors into their Fourier modes in order to represent the field with a spherical-harmonic expansion. A general approach is to empirically fit ephemerides data to these longitude/time functions to recover the coefficients. Here we continue by finding an approximate analytical fit.

If we assume δ and e are small parameters and perform a Taylor/Maclaurin expansion, keeping only the lowest-order terms, we have

$$\begin{aligned}
\Phi_2 = -\frac{GM_p}{d_0}\left(\frac{r_0}{d_0}\right)^2\left(\frac{r}{r_0}\right)^2 \{ & \\
(1 + 3e\cos(\Omega_o t + \lambda_d))\left(-\frac{1}{2}\right)P_2^0(\cos(\theta)) & \\
(1 + 3e\cos(\Omega_o t + \lambda_d))(\delta\cos(\Omega_o t + \lambda_o)\cos(\varphi - \varphi_p))P_2^1(\cos(\theta)) & \\
(1 + 3e\cos(\Omega_o t + \lambda_d))\left(\frac{1}{4}\cos(2(\varphi - \varphi_p))\right)P_2^2(\cos(\theta)) & \\
\}, &
\end{aligned} \tag{2.1.18}$$

which, further neglecting terms involving products of δ and e and applying power-reduction identities becomes

(2.1.19)

$$\begin{aligned}\Phi_2 = &-\frac{GM_p}{d_0}\left(\frac{r_0}{d_0}\right)^2\left(\frac{r}{r_0}\right)^2\{\\ &-\frac{1}{2}\left(1+3e\cos(\Omega_o t+\lambda_d)\right)P_2^0\left(\cos\left(\theta\right)\right)\\ &+\frac{1}{2}\delta\left(\cos\left(\Omega_o t+\lambda_o-\varphi+\varphi_p\right)+\cos\left(\Omega_o t+\lambda_o+\varphi-\varphi_p\right)\right)P_2^1\left(\cos\left(\theta\right)\right)\\ &+\left(\frac{1}{4}\cos\left(2\left(\varphi-\varphi_p\right)\right)+\frac{3}{8}e\left(\cos\left(\Omega_o t+\lambda_d-2\left(\varphi-\varphi_p\right)\right)+\cos\left(\Omega_o t+\lambda_d+2\left(\varphi-\varphi_p\right)\right)\right)\right)P_2^2\left(\cos\left(\theta\right)\right).\end{aligned}$$

Finally, we substitute using (2.1.13) and (2.1.16) in (2.1.19) and again retain only the lowest-order terms in e, δ. To simplify the expression, let us also choose $\lambda_d = \lambda_p = 0$ (equivalent to choosing $t = 0$ at pericenter, as described above). The degree-two component of the gravitational potential valid to lowest order in δ, e can then be written as

(2.1.20)

$$\begin{aligned}\Phi_2 = &-\frac{GM_p}{d_0}\left(\frac{r_0}{d_0}\right)^2\left(\frac{r}{r_0}\right)^2\{\\ &-\frac{1}{2}\left(1+3e\cos(\Omega_o t)\right)P_2^0\left(\cos\left(\theta\right)\right)\\ &+\frac{1}{2}\delta\left(\cos\left(\phi+\left(\Omega-2\Omega_o\right)t-\lambda_o\right)+\cos\left(\phi+\Omega t+\lambda_o\right)\right)P_2^1\left(\cos\left(\theta\right)\right)\\ &+\left(\frac{1}{4}\cos\left(2\phi+\left(2\Omega-2\Omega_o\right)t\right)+e\left(\frac{7}{8}\cos\left(2\phi+\left(2\Omega-3\Omega_o\right)t\right)-\frac{1}{8}\cos\left(2\phi+\left(2\Omega-\Omega_o\right)t\right)\right)\right)P_2^2\left(\cos\left(\theta\right)\right)\\ &\},\end{aligned}$$

or, in the general form most convenient for solutions with *TROPF*:

(2.1.21)

$$\begin{aligned}\Phi_2 = &-\frac{GM_p}{d_0}\left(\frac{r_0}{d_0}\right)^2\left(\frac{r}{r_0}\right)^2\{\\ &-\frac{1}{2}P_2^0\left(\cos\left(\theta\right)\right)\\ &+\frac{1}{4}\left(\frac{1}{2}\mathrm{e}^{i(2\phi-\{2\Omega_o-2\Omega\}t)}+\frac{1}{2}\mathrm{e}^{-i(2\phi-\{2\Omega_o-2\Omega\}t)}\right)P_2^2\left(\cos\left(\theta\right)\right)\\ &+\frac{1}{2}\delta\left(\frac{1}{2}\mathrm{e}^{i(\phi-\{-\Omega\}t+\lambda_o)}+\frac{1}{2}\mathrm{e}^{-i(\phi-\{-\Omega\}t+\lambda_o)}\right)P_2^1\left(\cos\left(\theta\right)\right)\\ &+\frac{1}{2}\delta\left(\frac{1}{2}\mathrm{e}^{i(\phi-\{2\Omega_o-\Omega\}t-\lambda_o)}+\frac{1}{2}\mathrm{e}^{-i(\phi-\{2\Omega_o-\Omega\}t-\lambda_o)}\right)P_2^1\left(\cos\left(\theta\right)\right)\\ &-\frac{3}{2}e\left(\frac{1}{2}\mathrm{e}^{-i\{\Omega_o\}t}+\frac{1}{2}\mathrm{e}^{i\{\Omega_o\}t}\right)P_2^0\left(\cos\left(\theta\right)\right)\\ &-\frac{1}{8}e\left(\frac{1}{2}\mathrm{e}^{i(2\phi-\{\Omega_o-2\Omega\}t)}+\frac{1}{2}\mathrm{e}^{-i(2\phi-\{\Omega_o-2\Omega\}t)}\right)P_2^2\left(\cos\left(\theta\right)\right)\\ &+\frac{7}{8}e\left(\frac{1}{2}\mathrm{e}^{i(2\phi-\{3\Omega_o-2\Omega\}t)}+\frac{1}{2}\mathrm{e}^{-i(2\phi-\{3\Omega_o-2\Omega\}t)}\right)P_2^2\left(\cos\left(\theta\right)\right)\\ &\}.\end{aligned}$$

We see by (2.1.21) that the terms in the degree-two tidal potential depend on radius only through the common factor preceding the curly brackets. Within the curly brackets, the first two terms describe some combination of a static tidal pull and a time-dependent pull due to nonsynchronous rotation. These are the leading (zeroth-order) terms in the Taylor-McLaurin expansion for small e, δ and should (see below for

exceptions) be larger in amplitude than the other (first-order) terms involving the small parameters e, δ as factors. Two limiting cases for these leading terms follow.

First (the limit $|\Omega_o| << |\Omega|$), consider the case in which M_s rotates much faster than the orbital rate of the M_s, M_p system. In this case, we see that the static tidal potential in (2.1.21) is given by the P_2^0 term and the time-dependent part is given by the first P_2^2 term and describes simply retrograde propagation countering the rotation. Explicitly, for small e, δ, the degree-two potential is approximately

$$
\begin{aligned}
(2.1.22) \qquad \Phi_2 = & -\frac{GM_p}{d_0}\left(\frac{r_0}{d_0}\right)^2\left(\frac{r}{r_0}\right)^2\{ \\
& -\frac{1}{2}P_2^0\left(\cos\left(\theta\right)\right) \\
& +\frac{1}{4}\left(\frac{1}{2}\mathrm{e}^{i(2\phi-\{2\Omega_o-2\Omega\}t)}+\frac{1}{2}\mathrm{e}^{-i(2\phi-\{2\Omega_o-2\Omega\}t)}\right)P_2^2\left(\cos\left(\theta\right)\right) \\
& \}.
\end{aligned}
$$

Second (the limit $\Omega_o = \Omega$), consider the case of synchronous rotation. In this case, the general form (2.1.21) reduces to

$$
\begin{aligned}
(2.1.23) \qquad \Phi_2 = & -\frac{GM_p}{d_0}\left(\frac{r_0}{d_0}\right)^2\left(\frac{r}{r_0}\right)^2\{ \\
& -\frac{1}{2}P_2^0\left(\cos\left(\theta\right)\right) \\
& +\frac{1}{4}\left(\frac{1}{2}\mathrm{e}^{i(2\phi)}+\frac{1}{2}\mathrm{e}^{-i(2\phi)}\right)P_2^2\left(\cos\left(\theta\right)\right) \\
& +\frac{1}{2}\delta\left(\frac{1}{2}\mathrm{e}^{i(\phi+\Omega t+\lambda_o)}+\frac{1}{2}\mathrm{e}^{-i(\phi+\Omega t+\lambda_o)}\right)P_2^1\left(\cos\left(\theta\right)\right) \\
& +\frac{1}{2}\delta\left(\frac{1}{2}\mathrm{e}^{i(\phi-\Omega t-\lambda_o)}+\frac{1}{2}\mathrm{e}^{-i(\phi-\Omega t-\lambda_o)}\right)P_2^1\left(\cos\left(\theta\right)\right) \\
& -\frac{3}{2}e\left(\frac{1}{2}\mathrm{e}^{-i\Omega t}+\frac{1}{2}\mathrm{e}^{i\Omega t}\right)P_2^0\left(\cos\left(\theta\right)\right) \\
& -\frac{1}{8}e\left(\frac{1}{2}\mathrm{e}^{i(2\phi+\Omega t)}+\frac{1}{2}\mathrm{e}^{-i(2\phi+\Omega t)}\right)P_2^2\left(\cos\left(\theta\right)\right) \\
& +\frac{7}{8}e\left(\frac{1}{2}\mathrm{e}^{i(2\phi-\Omega t)}+\frac{1}{2}\mathrm{e}^{-i(2\phi-\Omega t)}\right)P_2^2\left(\cos\left(\theta\right)\right) \\
& \},
\end{aligned}
$$

and we see that the leading terms become time-independent and provide only a static tidal potential (which does no work). We also see that the amplitude (though not sign) of the forcing frequency becomes Ω for all the time-dependent terms. For easy reference, we will refer to the three eccentricity components (i.e. the last three lines with the factor e) as follows: The first (degree 2, order 0) we shall denote "G20"; the second (degree 2, order 2, retrograde propagation) is "G22W"; the third (degree 2, order 2, prograde propagation) is "G22E". The "W" and "E" reflect a nominal westward and eastward propagation, respectively. Of course this choice in nomenclature makes sense only if prograde rotation is eastward. Similarly, the two obliquity terms (degree two, order 0 terms involving factor δ) shall be referred to as G21W and G21E respectively.

2.1.3. Summary. In summary, a general expression for the degree-two tidal potential represented in the rotating-frame coordinates is (2.1.17), and the the time/longitude dependence can be Fourier expanded to deliver spherical-harmonic terms. When the parameters e, δ are small, we have more immediately the spherical-harmonic terms described in (2.1.21). The latter becomes, in the fast-rotation limit, (2.1.22), and in the synchronous-rotation limit (2.1.23). It can be justifiable to ignore higher-order terms but there are several important considerations. First, the leading terms may collapse into static components that can perform no work on the fluid. Second, the temporal frequencies of the various terms are not the same (e. g. one may need to retain the P_2^1 terms, even though they appear with the small factor δ, because they are

the leading terms at that frequency). Third, the largest forces do not necessarily lead to the largest tidal responses. When considering an inertial fluid capable of being resonantly forced, the response amplitudes are not simply commensurate with the force amplitudes.

CHAPTER 3

Equations Governing the Fluid Response

As will be described in this chapter, the tidal response is obtained by combining an equation for the balance of horizontal momentum (3.1.2), a description of the forces and how they depend on the fluid pressure (3.1.5), and a second relationship between pressure and flow (3.2.2) which is needed to close the system. Five different formulations of the governing equation(s) are obtained by combining these.

The second relationship (3.2.2) is written in a generic form with initially unspecified operators L_h and L_V. The best formulation and method to use can depend on how these operators are specified and this is highly dependent on the application. In all the cases considered here, $L_h = I$ (the identity operator). But L_V depends strongly on what medium is being considered. In the simplest case (e.g. a uniform-density, hydrostatic fluid), L_V reduces simply to a scalar factor (the squared slowness). In the most complex case (a stratified, compressible, non-hydrostatic fluid), L_V represents a differential operator describing the vertical balance of momentum and energy (see Appendix A for details on how L_V can be selected to represent the vertical balance in different media).

The presentation of formulae below is not the most conventional for two reasons that essentially anticipate the solution method to be applied. First, all parameters, variables, and operators are nondimensionalized to reduce any redundancy in the solution domain axes (parameters in the equations are combined into a reduced set of degenerate combinations). Second, operators are factored into suboperators. This has an advantage in applying the solution methods because the suboperators can be readily translated into numerical matrix operators and it is also clear which of these suboperators have inverses that can be calculated analytically rather than numerically. The operator-matrix factorization provides speed and simplicity in the *TROPF* solution routines and the presentation below is aimed at including a description of the operator factorizations such that the matrix factorizations used in *TROPF* easily follow.

3.1. Horizontal Momentum Equations

3.1.1. Vector Momentum Equation. The momentum equation describing the horizontal components of the flow velocity vector $\mathbf{u}_H$ is

$$[\partial_t + L_\alpha + f\hat{\mathbf{r}}\times]\,\mathbf{u}_H = \mathbf{F}_H/\rho_0, \tag{3.1.1}$$

where L_α is an operator such that $L_\alpha \mathbf{u}_H$ describes the dissipation rate, f is the Coriolis parameter, $\hat{\mathbf{r}}$ is the radial/upward unit vector, $\mathbf{F}_H$ is the force vector, and $\rho_0 = \rho_0(r)$ represents an assumed equilibrium mass density dependent on only the vertical coordinate r. In the spherical coordinates adopted below, r shall represent radius and $\mathbf{u}_H$ may be regarded as the flow vector components tangent to spherical surfaces centered at $\mathbf{r} = 0$.

Using definitions in Tables 1 and 2, we may write (3.1.1) in nondimensional form as

$$L_{\tilde{u}}\tilde{\mathbf{u}}_H = \tilde{\mathbf{F}}_H. \tag{3.1.2}$$

A solution for the flow vector in terms of the force is

$$\tilde{\mathbf{u}}_H = L_{\tilde{u}}^{-1}\tilde{\mathbf{F}}_H, \tag{3.1.3}$$

where, for a wide range of assumptions, the inverse operator

$$L_{\tilde{u}}^{-1} = \left[\left[\tilde{\partial}_t + L_{\tilde{\alpha}}\right]^2 + \tilde{f}^2\right]^{-1}\left[\tilde{\partial}_t + L_{\tilde{\alpha}} - \tilde{f}\hat{\mathbf{r}}\times\right] \tag{3.1.4}$$

can be derived analytically (or, more generally, numerically). A simple example of an analytically derived inverse $L_{\tilde{u}}^{-1}$ is one with harmonic time dependence and a simple drag dissipation formulation such that the operators $\tilde{\partial}_t$ and $L_{\tilde{\alpha}}$ can be regarded as complex coefficients and manipulated algebraically. In this case, $L_{\tilde{u}}^{-1} = \left(\left(\tilde{\partial}_t + L_{\tilde{\alpha}}\right)^2 + \tilde{f}^2\right)^{-1}\left(\tilde{\partial}_t + L_{\tilde{\alpha}} - \tilde{f}\hat{\mathbf{r}}\times\right)$ and involves only arithmetic. (Note that square brackets will often be used when the expression enclosed should be regarded as an operator and not simply a factor.)

Solutions for the velocity may be obtained provided $\tilde{\mathbf{F}}_H$ is known. But because $\tilde{\mathbf{F}}_H$ generally depends on $\tilde{\mathbf{u}}_H$, an additional equation relating the two is needed to close the system (as shall be discussed in Section 3.2).

We shall assume the force can be written in the form

$$\tilde{\mathbf{F}}_H = -\tilde{\nabla}_H\left(\tilde{p} - \tilde{\mathfrak{G}}\right) + \tilde{\mathbf{F}}_H^{(p)}, \tag{3.1.5}$$

where $\tilde{p}$ is the dynamic (flow-dependent) "pressure" variable, $\tilde{\mathfrak{G}}$ is a prescribed scalar field, and $\tilde{\mathbf{F}}_H^{(p)}$ represents any additional prescribed horizontal force vector. This does not yet close the system but instead simply replaces the need for an additional relationship relating $\tilde{\mathbf{F}}_H$ and $\tilde{\mathbf{u}}_H$ with the need for a relationship relating $\tilde{p}$ and $\tilde{\mathbf{u}}_H$. The choices for the latter relationship are, however, more restricted because of the appearance of $\tilde{p}$ in the gradient operator (3.1.5).

3.1.2. Scalar Momentum Equations. We consider now an alternate formulation for the horizontal momentum balance that provides more versatility by distinguishing between horizontally divergent and horizontally rotational components of the flow field. The distinction is potentially important because only the horizontally divergent component is coupled to vertical motion through the continuity equation, and vertical motion may be subject to distinct processes (e.g. Newtonian cooling, normal stress with an ice shell) which are not active on the divergence-free components of the flow. This formulation also leads to convenience when adopting spherical-harmonic bases later.

Consider a Helmholtz decomposition

$$\tilde{\mathbf{u}}_H = \tilde{\nabla}_H\tilde{\mathfrak{D}} + \tilde{\nabla}_H\times(\tilde{\mathfrak{R}}\hat{\mathbf{r}}), \tag{3.1.6}$$

where $\tilde{\mathfrak{D}}$, $\tilde{\mathfrak{R}}$ are scalar fields representing, respectively, potentials for the divergent and rotational components of $\tilde{\mathbf{u}}_H$, and the 'H' subscript on the gradient operator emphasizes that only horizontal components are considered.

Using (3.1.6), let us now restrict the prescription of $L_{\tilde{\alpha}}$ such that it can be written in the form

$$L_{\tilde{\alpha}}\tilde{\mathbf{u}}_H = \tilde{\nabla}_H L_{\tilde{\alpha}_d}\tilde{\mathfrak{D}} + \tilde{\nabla}_H\times(\hat{\mathbf{r}}L_{\tilde{\alpha}_r}\tilde{\mathfrak{R}}), \tag{3.1.7}$$

where dissipation has been parameterized such that it may be represented by (potentially different) operators $L_{\tilde{\alpha}_d}$, $L_{\tilde{\alpha}_r}$ on the respective Helmholtz potentials $\tilde{\mathfrak{D}}$, $\tilde{\mathfrak{R}}$.

Using (3.1.6, 3.1.7) and $i = (-1)^{1/2}$, while performing the alternate operations $\left[i\tilde{\nabla}_H\cdot\right]$ and $\left[-\tilde{\nabla}_H\cdot\hat{\mathbf{r}}\times\right]$ on (3.1.2), we may rewrite the equations governing the horizontal momentum balance as

$$\left[i\tilde{\nabla}_H^2\left[\tilde{\partial}_t + L_{\tilde{\alpha}_d}\right] + i\tilde{\nabla}_H\cdot\tilde{f}\hat{\mathbf{r}}\times\tilde{\nabla}_H\right]\tilde{\mathfrak{D}} + \left[\tilde{\nabla}_H\cdot\tilde{f}\tilde{\nabla}_H\right]i\tilde{\mathfrak{R}} = i\tilde{\nabla}_H\cdot\left(\tilde{\mathbf{F}}_H\right), \tag{3.1.8}$$

$$\left[i\tilde{\nabla}_H^2\left[\tilde{\partial}_t + L_{\tilde{\alpha}_r}\right] + i\tilde{\nabla}_H\cdot\tilde{f}\hat{\mathbf{r}}\times\tilde{\nabla}_H\right]i\tilde{\mathfrak{R}} + \left[\tilde{\nabla}_H\cdot\tilde{f}\tilde{\nabla}_H\right]\tilde{\mathfrak{D}} = -\tilde{\nabla}_H\cdot\left(\hat{\mathbf{r}}\times\tilde{\mathbf{F}}_H\right). \tag{3.1.9}$$

These two scalar equations (3.1.8, 3.1.9) may be used instead of the two-component vector equation (3.1.2).

3.1.3. Scalar Momentum Equations in Spherical Coordinates. Here we adopt a spherical coordinate system rotating about its polar axis, assume harmonic dependencies in time and longitude, and further restrict the form of the dissipation operators.

In spherical coordinates (where θ is colatitude, ϕ is longitude, and r is radius), $f = 2\Omega\cos(\theta)$, with Ω the angular rotation rate of the coordinate system,

$$[\nabla_H\cdot f\hat{\mathbf{r}}\times\nabla_H] = \left[i\frac{2\Omega}{r^2}\partial_\phi\right], \tag{3.1.10}$$

$$[\nabla_H \cdot f\nabla_H] = \left[\frac{2\Omega}{r^2}\left[\cos\theta\nabla_H^2 + \sin^2\theta\frac{\partial}{\partial\cos\theta}\right]\right], \tag{3.1.11}$$

or, in non-dimensional form,

$$\left[\tilde{\nabla}_H \cdot \tilde{f}\hat{\mathbf{r}}\times\tilde{\nabla}_H\right] = \left[i\tilde{\Omega}\partial_\phi\right], \tag{3.1.12}$$

$$\left[\tilde{\nabla}_H \cdot \tilde{f}\tilde{\nabla}_H\right] = \left[\tilde{\Omega}\cos\theta\tilde{\nabla}_H^2 + \tilde{\Omega}\sin^2\theta\frac{\partial}{\partial\cos\theta}\right]. \tag{3.1.13}$$

Let us assume that both $\tilde{\mathbf{F}}_H$ and the solutions have a longitude/time dependence that can be written in the form $\mathrm{e}^{i(s\phi-\tilde{\omega}\tilde{t})}$, where s is a non-negative integer, and $\tilde{\omega}$ is the non-dimensional frequency (note that $\tilde{\omega}\tilde{t} = \omega t$). Positive $\tilde{\omega}$ corresponds with prograde (i.e. same sense as rotation) propagation while negative $\tilde{\omega}$ corresponds with retrograde propagation. Using these assumptions and (3.1.5, 3.1.10-3.1.13) in (3.1.8, 3.1.9), the horizontal momentum equations become

$$\left[\left[\tilde{\nabla_H}^2\right][\tilde{\omega} + iL_{\tilde{\alpha}_d}] - s\tilde{\Omega}\right]\tilde{\mathfrak{D}} + \left[\tilde{\Omega}\cos\theta\tilde{\nabla_H}^2 + \tilde{\Omega}\sin^2\theta\frac{\partial}{\partial\cos\theta}\right]i\tilde{\mathfrak{R}} = -\tilde{\nabla}_H^2\left(i\tilde{p} - i\tilde{\mathfrak{G}}\right) + \tilde{\nabla_H}\cdot\left(i\tilde{\mathbf{F}}_H^{(p)}\right), \tag{3.1.14}$$

$$\left[\left[\tilde{\nabla_H}^2\right][\tilde{\omega} + iL_{\tilde{\alpha}_r}] - s\tilde{\Omega}\right]i\tilde{\mathfrak{R}} + \left[\tilde{\Omega}\cos\theta\tilde{\nabla_H}^2 + \tilde{\Omega}\sin^2\theta\frac{\partial}{\partial\cos\theta}\right]\tilde{\mathfrak{D}} = -\tilde{\nabla}_H\cdot\left(\hat{\mathbf{r}}\times\tilde{\mathbf{F}}_H^{(p)}\right). \tag{3.1.15}$$

Using operators defined in Table 2, let us write (3.1.14, 3.1.15) more compactly as

$$L_A\tilde{\mathfrak{D}} + L_C i\tilde{\mathfrak{R}} = -L_L\left(i\tilde{p} - i\tilde{\mathfrak{G}}\right) + \tilde{\nabla_H}\cdot\left(i\tilde{\mathbf{F}}_H^{(p)}\right), \tag{3.1.16}$$

$$L_B i\tilde{\mathfrak{R}} + L_C\tilde{\mathfrak{D}} = -\tilde{\nabla}_H\cdot\left(\hat{\mathbf{r}}\times\tilde{\mathbf{F}}_H^{(p)}\right). \tag{3.1.17}$$

In anticipation of the spherical-harmonic expansion used below to obtain solutions, we further restrict the dissipation operators $L_{\tilde{\alpha}_d}$, $L_{\tilde{\alpha}_r}$ to the forms

$$L_{\tilde{\alpha}_d} = \Sigma_b\tilde{\alpha}_{d,b}\tilde{\nabla}_H^{2b} = \tilde{\alpha}_{d,0} + \tilde{\alpha}_{d,1}\tilde{\nabla}_H^2 + \tilde{\alpha}_{d,2}\tilde{\nabla}_H^4 + ..., \tag{3.1.18}$$

$$L_{\tilde{\alpha}_r} = \Sigma_b\tilde{\alpha}_{r,b}\tilde{\nabla}_H^{2b} = \tilde{\alpha}_{r,0} + \tilde{\alpha}_{r,1}\tilde{\nabla}_H^2 + \tilde{\alpha}_{r,2}\tilde{\nabla}_H^4 + ..., \tag{3.1.19}$$

where b is a positive integer ($b = 0, 1, 2...$), and $\tilde{\alpha}_{d,b}$ and $\tilde{\alpha}_{r,b}$ are vectors of coefficients that are either constant or vary only with r. With this restriction, it can be shown using vector calculus identities and (3.1.7) that

$$\begin{aligned} L_{\tilde{\alpha}}\tilde{\mathbf{u}}_H &= \tilde{\nabla}_H L_{\tilde{\alpha}_d}\tilde{\mathfrak{D}} + \tilde{\nabla}_H\times(\hat{\mathbf{r}}L_{\tilde{\alpha}_r}\tilde{\mathfrak{R}}) \\ &= L_{\tilde{\alpha}_d}\tilde{\nabla}_H\tilde{\mathfrak{D}} + L_{\tilde{\alpha}_r}\tilde{\nabla}_H\times(\hat{\mathbf{r}}\tilde{\mathfrak{R}}), \end{aligned} \tag{3.1.20}$$

and therefore there is an equivalence in applying the dissipation operators to the flow potentials rather than the flow velocity. This dissipation form is still quite general and allows representation of Rayleigh drag ($b = 0$), as well as harmonic ($b = 1$) and biharmonic ($b = 2$) eddy viscosity parameterizations as specific cases. The form here need not assume $\tilde{\alpha}_{d,b} = \tilde{\alpha}_{r,b}$, but it does assume that these parameters are independent of the horizontal coordinates..

	dimensional	non-dimensional form
partial time derivative operator (1/s)	∂_t	$\tilde{\partial}_t = (2\Omega_s)^{-1}\partial_t$
horizontal gradient operator (1/m)	∇_H	$\tilde{\nabla}_H = (1/r)^{-1}\nabla_H$
horizontal divergence operator (1/m)	$\nabla_H\cdot$	$(1/r)^{-1}\tilde{\nabla}_H\cdot$
horizontal Laplacian operator (1/m^2)	∇_H^2	$\tilde{\nabla}_H^2 = \left(1/r^2\right)^{-1}\nabla_H^2$
Coriolis parameter (1/s)	f	$\tilde{f} = (2\Omega_s)^{-1} f$
rotation rate (1/s)	Ω	$\tilde{\Omega} = (\Omega_s)^{-1}\Omega$
horizontal flow velocity (m/s)	$\mathbf{u}_H$	$\tilde{\mathbf{u}}_H = (G_s/(2\Omega_s r))^{-1}\mathbf{u}_H$
vertical flow velocity (m/s)	w	$\tilde{w} = (G_s/(2\Omega_s r))^{-1} w$
total force vector (N/m^3)	$\mathbf{F}_H$	$\tilde{\mathbf{F}}_H = (\rho_0 G_s/r)^{-1}\mathbf{F}_H$
time (s)	t	$\tilde{t} = (2\Omega_s)\,t$
frequency (1/s)	ω	$\tilde{\omega} = (2\Omega_s)^{-1}\omega$
dissip. coef. for divergent flow (1/s)	$\alpha_{d,b}$	$\tilde{\alpha}_{d,b} = (2\Omega_s)^{-1}\alpha_{d,b}$
dissip. coef. for rotational flow (1/s)	$\alpha_{r,b}$	$\tilde{\alpha}_{r,b} = (2\Omega_s)^{-1}\alpha_{r,b}$
dissip. coef. for vertical balance (1/s)	$\alpha_{p,}$	$\tilde{\alpha}_p = (2\Omega_s)^{-1}\alpha_p$
longitudinal wave number	s	s
dissipation time scale (s)	$T_{(j)}$	$\tilde{T}_{(j)} = (\tilde{\alpha}_{(j)})^{-1}\lvert\tilde{\omega}\rvert$
wave speed (m/s)	c_e	$\tilde{c}_e = (2\Omega_s r)^{-1} c_e$
slowness (s/m)	ν	$\tilde{\nu} = (2\Omega_s r)\,\nu$
divergent flow potential (m^2/s)	$\mathfrak{D}$	$\tilde{\mathfrak{D}} = \left(\frac{G_s}{2\Omega_s}\right)^{-1}\mathfrak{D}$
rotational flow potential (m^2/s)	$\mathfrak{R}$	$\tilde{\mathfrak{R}} = \left(\frac{G_s}{2\Omega_s}\right)^{-1}\mathfrak{R}$
dynamic pressure (N/m^2)	p	$\tilde{p} = (\rho_0 G_s)^{-1} p$
gravitational potential (m^2/s^2)	$\mathfrak{G}$	$\tilde{\mathfrak{G}} = (G_s)^{-1}\mathfrak{G}$
prescribed force vector (N/m^3)	$\mathbf{F}_H^{(p)}$	$\tilde{\mathbf{F}}_H^{(p)} = (\rho_0 G_s/r)^{-1}\mathbf{F}_H^{(p)}$
work density (W/m^3)	W	$\tilde{W} = \left(\rho_0 G_s^2/(2\Omega_s r^2)\right)^{-1} W$
dissipation density (W/m^3)	D	$\tilde{D} = \left(\rho_0 G_s^2/(2\Omega_s r^2)\right)^{-1} D$
power density (W/m^3)	P	$\tilde{P} = \left(\rho_0 G_s^2/(2\Omega_s r^2)\right)^{-1} P$
kinetic energy density (J/m^3)	E_k	$\tilde{E}_k = \left(\rho_0\left(G_s/(2\Omega_s r)\right)^2\right)^{-1} E_k$
potential energy density (J/m^3)	E_p	$\tilde{E}_p = \left(\rho_0\left(G_s/(2\Omega_s r)\right)^2\right)^{-1} E_p$
divergence source term (1/s)	$\mathfrak{s}$	$\tilde{\mathfrak{s}} = \left(\frac{G_s}{2\Omega_s r^2}\right)^{-1}\mathfrak{s}$

TABLE 1. Definitions of the basic operators and parameters. Here, r is the radius, and $\rho_0 = \rho_0(r)$ is the background density distribution. Nondimensionalization introduces the arbitrary scaling factors Ω_s (with units of s^{-1}), and $G_s = G_s(r)$ (with units of m^2/s^2). In studies involving non-zero rotation and gravitational forcing, we typically assign $\Omega_s = \Omega$, and $G_s = |\mathfrak{G}(r)|$.

3.2. Closing the System of Equations

3.2.1. A Second Relationship. To close the system provided by the horizontal momentum balance, we need a second relationship between the pressure and horizontal flow fields. An appropriate relationship is highly dependent on the fluid medium considered (see Appendix A) and so we want to chose a general form that can cover all of these cases. But we also wish to limit the form to one where the vertical and horizontal dependencies in the governing system remain separable. In all the cases that we shall consider, this relationship can be written generically as

$$\nabla_H \cdot L_h \mathbf{u}_H + \frac{1}{\rho_0}\frac{1}{(2\Omega_s r)^2} L_V \partial_t p = \mathfrak{s}, \tag{3.2.1}$$

Fixed sub operators:
$L_L = \left[\tilde{\nabla}_H^2\right]$
$L_C = \left[\tilde{\Omega}\cos\theta\tilde{\nabla}_H^2 + \tilde{\Omega}\sin^2\theta\frac{\partial}{\partial\cos\theta}\right]$
Prescribed sub operators:
$L_{\tilde{\alpha}_d} = \left[\Sigma_b \tilde{\alpha}_{d,b}\tilde{\nabla}_H^{2b}\right]$
$L_{\tilde{\alpha}_r} = \left[\Sigma_b \tilde{\alpha}_{r,b}\nabla_H^{2b}\right]$
L_h (see Section 3.2.1)
L_V (see Section 3.2.1)
Composite operators:
$L_{\tilde{u}} = \left[\tilde{\partial}_t + L_{\tilde{\alpha}} + \tilde{f}\hat{\mathbf{r}}\times\right]$
$L_M = i\tilde{\omega}^{-1}\mathcal{L}_V^{-1}\left[\tilde{\nabla}_H \cdot L_h L_{\tilde{u}}^{-1}\tilde{\nabla}_H - L_V\tilde{\partial}_t\right]$
$L_A = \left[\left[\tilde{\omega} + iL_{\tilde{\alpha}_d}\right]L_L - s\tilde{\Omega}\right]$
$L_B = \left[\left[\tilde{\omega} + iL_{\tilde{\alpha}_r}\right]L_L - s\tilde{\Omega}\right]$
$L_D = \left[L_A + \tilde{\omega}^{-1}L_L L_V^{-1}L_L\right]$
$L_E = \left[\tilde{\omega}L_A L_L^{-1}L_V + L_L\right]$
$L_F = \left[\tilde{\omega}L_C L_L^{-1}L_V\right]$
$L_{\tilde{p}} = \left[\left[L_L^{-1}\right]\left[L_A - L_C L_B^{-1}L_C\right]\left[\tilde{\omega}L_L^{-1}L_V\right] + I\right]$
$L_{\tilde{\mathfrak{D}}} = \left[\left[L_L^{-1}\right]\left[L_D - L_C L_B^{-1}L_C\right]\right]$
$L_{\tilde{\mathfrak{R}}} = \left[\left[L_L^{-1}\right]\left[L_C - L_D L_C^{-1}L_B\right]\right]$

TABLE 2. Additional non-dimensional operators. Operators in the governing equations are composed of the fixed and prescribed sub operators (as well as the identity operator I).

or, in non-dimensional form

$$\tilde{\nabla}_H \cdot L_h\tilde{\mathbf{u}}_H + L_V\tilde{\partial}_t\tilde{p} = \tilde{\mathfrak{s}}, \tag{3.2.2}$$

where the prescription of the non-dimensional operators L_h and L_V, and the source term $\tilde{\mathfrak{s}}$ vary with the application.

The approach for combining (3.2.2) with the horizontal-momentum formulations and the selection of a basis for obtaining solutions depends much on which, if any, of the operators $\tilde{\partial}_t$, L_h, L_V have a simple analytical inverse. In the simplest case, all three of these operators are algebraic factors. In many applications, we take $\tilde{\partial}_t = -i\tilde{\omega}$, $L_h = I$, and $L_V = \tilde{\nu}^2$, where $\tilde{\nu}$ is the (potentially complex) slowness parameter. In this case, let us define the squared wave speed

$$\tilde{c}_e^2 = 1/\text{real}(\tilde{\nu}^2) \tag{3.2.3}$$

and attenuation constant

$$\tilde{\alpha}_p = \left(i\tilde{\partial}_t\right)\tilde{c}_e^2\text{imag}\left(\tilde{\nu}^2\right) = \tilde{\omega}\text{imag}\left(\tilde{\nu}^2\right)/\text{real}(\tilde{\nu}^2), \tag{3.2.4}$$

such that

$$L_V = \tilde{\nu}^2 = \frac{1}{\tilde{c}_e^2}\left[1 + \frac{\tilde{\alpha}_p}{\tilde{\partial}_t}\right] = \frac{1}{\tilde{c}_e^2}\left[1 + i\frac{\tilde{\alpha}_p}{\tilde{\omega}}\right], \tag{3.2.5}$$

and (3.2.2) becomes

$$\tilde{\nabla}_H \cdot \tilde{\mathbf{u}}_H + \frac{1}{\tilde{c}_e^2}\left[\tilde{\partial}_t + \tilde{\alpha}_p\right]\tilde{p} = \tilde{\mathfrak{s}}. \tag{3.2.6}$$

We may regard $\tilde{\alpha}_p$ as an attenuation constant associated with a tendency for $\tilde{p}$ to relax to the state $\tilde{p} = \tilde{c}_e^2\tilde{\mathfrak{s}}/\tilde{\alpha}_p$. When, for example, we choose $\tilde{\mathfrak{s}} = 0$, the relaxed state is $\tilde{p} = 0$. Independent of the flow, there is then an added tendency for the perturbations $\tilde{p}$ to dissipate with time over a time scale $\tilde{\alpha}_p^{-1}$. This

Fixed sub operators:
$L_L = \mathrm{diag}(-\mathbf{n}(\mathbf{n}+1))$
$L_C = \mathrm{diag}_{(-1)}\left\{-\tilde{\Omega}\mathbf{n}\left(\mathbf{n}+2\right)\left(\mathbf{n}-s+1\right)/\left(2\mathbf{n}+1\right)\right\}$ $+\mathrm{diag}_{(+1)}\left\{-\tilde{\Omega}\left(\mathbf{n}-1\right)\left(\mathbf{n}+1\right)\left(\mathbf{n}+s\right)/\left(2\mathbf{n}+1\right)\right\}$
Prescribed sub operators:
$L_{\tilde{\alpha}_d} = \Sigma_b \tilde{\alpha}_{d,b} \mathrm{diag}\left\{(-\mathbf{n}(\mathbf{n}+1))^b\right\} = \Sigma_b \tilde{\alpha}_{d,b} L_L^b$
$L_{\tilde{\alpha}_r} = \Sigma_b \tilde{\alpha}_{r,b} \mathrm{diag}\left\{(-\mathbf{n}(\mathbf{n}+1))^b\right\} = \Sigma_b \tilde{\alpha}_{r,b} L_L^b$
$L_h = I$
$L_V = \mathrm{diag}\left\{\left(\tilde{\nu}^{\mathbf{2}}\right)_{\mathbf{n}}^{s}\right\}$
Composite operators:
$L_A = \left[\left[\tilde{\omega} + iL_{\tilde{\alpha}_d}\right] L_L - s\tilde{\Omega} I\right]$
$L_B = \left[\left[\tilde{\omega} + iL_{\tilde{\alpha}_r}\right] L_L - s\tilde{\Omega} I\right]$
$L_D = \left[L_A + \tilde{\omega}^{-1} L_L L_V^{-1} L_L\right]$
$L_E = \left[\tilde{\omega} L_A L_L^{-1} L_V + L_L\right]$
$L_F = \left[\tilde{\omega} L_C L_L^{-1} L_V\right]$
$L_{\tilde{p}} = \left[\left[L_L^{-1}\right]\left[L_A - L_C L_B^{-1} L_C\right]\left[\tilde{\omega} L_L^{-1} L_V\right] + I\right]$
$L_{\tilde{\mathfrak{D}}} = \left[\left[L_L^{-1}\right]\left[L_D - L_C L_B^{-1} L_C\right]\right]$
$L_{\tilde{\mathfrak{R}}} = \left[\left[L_L^{-1}\right]\left[L_C - L_D L_C^{-1} L_B\right]\right]$

TABLE 3. Matrices (L) representing the operators (L) in Table 2 as used in the spherical-harmonic method. Here $\mathbf{n}$ is a column vector of degrees $n = s, s+1, ..N_{trunc}$, "diag" indicates the vector argument is placed on the main diagonal of a square matrix, while "$\mathrm{diag}_{(-1)}, \mathrm{diag}_{(+1)}$" indicate placement on the first lower and first upper subdiagonals, respectively (the last vector element is clipped in the case of the lower diagonal, and the first element is clipped in the case of the upper diagonal). Analytical inverses of all the sub matrices can be obtained by taking the reciprocal of the diagonal entries, with the exception of the non-diagonal matrix L_C for which the inverse L_C^{-1} is calculated numerically.

parameterization can be used to represent pressure transfer due to subscale wave processes, Newtonian cooling, and other dynamics that are not explicitly resolved in the equations. We shall refer to these various parameterizations generically as "Newtonian radiation". We shall, in our applications, require that $\tilde{\alpha}_p$ is real and positive, such that Newtonian radiation is a dissipative process associated with the leakage of energy and momentum through unresolved dynamics. More generally, there are selections for $\tilde{\alpha}_p, \tilde{\mathfrak{s}}$ which would in fact perform work on the fluid.

Importantly, the spherical-harmonic method to be described in Section 4.2 permits an easy generalization $\tilde{\nu}^2 \to \tilde{\nu}^2_{(n)}$ in which the slowness becomes a function of the spherical-harmonic degree n. One can still apply (3.2.3–3.2.6) provided an explicit or implicit indexing is included to recall that constants vary with degree. For example, $\tilde{c}_e^2 \to \tilde{c}^2_{e;(n)} = 1/\mathrm{Real}(\tilde{\nu}^2_{(n)})$, where $\tilde{c}^2_{e;(n)}$ is the wave speed at degree n. The wave speed is then dispersive because propagation depends on the spatial scale of the wave. This can allow added realism in the wave dynamics, but also represent other effects such as self gravity.

3.2.2. Combining with Vector Momentum Equation. Substituting using (3.1.3) and (3.1.5), we can write (3.2.2) as

$$\left[\tilde{\nabla}_H \cdot L_h L_{\tilde{u}}^{-1} \tilde{\nabla}_H - L_V \tilde{\partial}_t\right] \tilde{p} = \left[\tilde{\nabla}_H \cdot L_h L_{\tilde{u}}^{-1}\right] \left\{\tilde{\nabla}_H \tilde{\mathfrak{G}} + \tilde{\mathbf{F}}_H^{(p)}\right\} - \tilde{\mathfrak{s}}, \tag{3.2.7}$$

which is now a closed equation in the single variable $\tilde{p}$. Alternatively, we may regard the solution variable as $\left\{\tilde{p} - \tilde{\mathfrak{G}}\right\}$ and rewrite (3.2.7) as

$$\left[\tilde{\nabla}_H \cdot L_h L_{\tilde{u}}^{-1} \tilde{\nabla}_H - L_V \tilde{\partial}_t\right] \left\{\tilde{p} - \tilde{\mathfrak{G}}\right\} = L_V \tilde{\partial}_t \tilde{\mathfrak{G}} + \left[\tilde{\nabla}_H \cdot L_h L_{\tilde{u}}^{-1}\right] \tilde{\mathbf{F}}_H^{(p)} - \tilde{\mathfrak{s}}, \tag{3.2.8}$$

or, assuming a temporal dependence $\mathrm{e}^{-i\tilde{\omega}\tilde{t}}$ such that $\tilde{\partial}_t \to -i\tilde{\omega}$, more compactly as

$$L_M \left\{ \tilde{p} - \tilde{\mathfrak{G}} \right\} = \tilde{\mathfrak{G}} + \tilde{Q}_M, \tag{3.2.9}$$

where L_M is described in Table 2 and

$$\tilde{Q}_M = i\tilde{\omega}^{-1} \mathcal{L}_V^{-1} \left\{ \left[\tilde{\nabla}_H \cdot L_h L_{\tilde{u}}^{-1} \right] \tilde{\mathbf{F}}_H^{(p)} - \tilde{\mathfrak{s}} \right\}. \tag{3.2.10}$$

The solution can then be written symbolically as

$$\left\{ \tilde{p} - \tilde{\mathfrak{G}} \right\} = L_M^{-1} \left\{ \tilde{\mathfrak{G}} + \tilde{Q}_M \right\}, \tag{3.2.11}$$

where we see that the operator L_M^{-1} fully describes how forcing generates the dynamic anomaly $\left\{ \tilde{p} - \tilde{\mathfrak{G}} \right\}$. Inspection of L_M, L_M^{-1} and their suboperators can then suggest appropriate solution methods.

3.2.3. Combining with Scalar Momentum Equations. In this section we combine (3.2.1), assuming $L_h = I$, with (3.1.16, 3.1.17).

Assuming $\tilde{\partial}_t \to -i\tilde{\omega}$ and using (3.1.6), we may write (3.2.2) as

$$i\tilde{p} = \tilde{\omega}^{-1} L_V^{-1} \left\{ L_L \tilde{\mathfrak{D}} - \tilde{\mathfrak{s}} \right\}, \tag{3.2.12}$$

or

$$\tilde{\mathfrak{D}} = \tilde{\omega} L_L^{-1} L_V i\tilde{p} + L_L^{-1} \tilde{\mathfrak{s}}. \tag{3.2.13}$$

Combining (3.2.12) with (3.1.16,3.1.17) we obtain the closed system of two equations governing $\tilde{\mathfrak{D}}, \tilde{\mathfrak{K}}$

$$L_D \left\{ \tilde{\mathfrak{D}} \right\} + L_C \left\{ i\tilde{\mathfrak{K}} \right\} = L_L \left\{ i\tilde{\mathfrak{G}} \right\} + \tilde{Q}_{s1}, \tag{3.2.14}$$

$$L_B \left\{ i\tilde{\mathfrak{K}} \right\} + L_C \left\{ \tilde{\mathfrak{D}} \right\} = \tilde{Q}_{s2}, \tag{3.2.15}$$

where

$$\tilde{Q}_{s1} = +\tilde{\omega}^{-1} L_L L_V^{-1} \tilde{\mathfrak{s}} + \tilde{\nabla}_H \cdot \left(i\tilde{\mathbf{F}}_H^{(p)} \right), \tag{3.2.16}$$

$$\tilde{Q}_{s2} = -\tilde{\nabla} \cdot \left(\hat{\mathbf{r}} \times \tilde{\mathbf{F}}_H^{(p)} \right). \tag{3.2.17}$$

Once $\tilde{\mathfrak{D}}, \tilde{\mathfrak{K}}$ are obtained, we may calculate $\tilde{p}$ using (3.2.12), and $\tilde{\mathbf{u}}_H$ using (3.1.6).

An alternative system involving the solution variables $\tilde{\mathfrak{D}}, \tilde{p}$ instead of $\tilde{\mathfrak{D}}, \tilde{\mathfrak{K}}$ is obtained by using (3.2.13) to replace $\tilde{\mathfrak{D}}$ in (3.2.14, 3.2.15):

$$L_E \left\{ i\tilde{p} \right\} + L_C \left\{ i\tilde{\mathfrak{K}} \right\} = L_L \left\{ i\tilde{\mathfrak{G}} \right\} + \tilde{Q}_{s3}, \tag{3.2.18}$$

$$L_B \left\{ i\tilde{\mathfrak{K}} \right\} + L_F \left\{ i\tilde{p} \right\} = \tilde{Q}_{s4}, \tag{3.2.19}$$

where

$$\tilde{Q}_{s3} = \left[\tilde{\nabla}_H \cdot \left(i\tilde{\mathbf{F}}_H^{(p)} \right) - L_A L_L^{-1} \left\{ \tilde{\mathfrak{s}} \right\} \right], \tag{3.2.20}$$

$$\tilde{Q}_{s4} = -\tilde{\nabla} \cdot \left(\hat{\mathbf{r}} \times \tilde{\mathbf{F}}_H^{(p)} \right) - L_C L_L^{-1} \left\{ \tilde{\mathfrak{s}} \right\}. \tag{3.2.21}$$

Finally, (3.2.14, 3.2.15) can be combined to write higher-order governing equations in a single variable

$$L_{\tilde{p}} \left\{ i\tilde{p} \right\} = i\tilde{\mathfrak{G}} + \tilde{Q}_{\tilde{p}}, \tag{3.2.22}$$

$$L_{\tilde{\mathfrak{D}}}\left\{\tilde{\mathfrak{D}}\right\} = i\tilde{\mathfrak{G}} + \tilde{Q}_{\tilde{\mathfrak{D}}}, \tag{3.2.23}$$

$$L_{\tilde{\mathfrak{R}}}\left\{i\tilde{\mathfrak{R}}\right\} = i\tilde{\mathfrak{G}} + \tilde{Q}_{\tilde{\mathfrak{R}}}, \tag{3.2.24}$$

where

$$\tilde{Q}_{\tilde{p}} = -\left[L_L^{-1}\left[L_A - L_C L_B^{-1} L_C\right] L_L^{-1}\right]\tilde{\mathfrak{s}} + L_L^{-1}\left\{\tilde{\nabla_H}\cdot\left(i\tilde{\mathbf{F}}_H^{(p)}\right)\right\} + \left[L_L^{-1} L_C L_B^{-1}\right]\left\{\tilde{\nabla}\cdot\left(\hat{\mathbf{r}}\times\tilde{\mathbf{F}}_H^{(p)}\right)\right\}, \tag{3.2.25}$$

$$\tilde{Q}_{\tilde{\mathfrak{D}}} = \tilde{\omega}^{-1} L_V^{-1}\tilde{\mathfrak{s}} + L_L^{-1}\left\{\tilde{\nabla_H}\cdot\left(i\tilde{\mathbf{F}}_H^{(p)}\right)\right\} + \left[L_L^{-1} L_C L_B^{-1}\right]\left\{\tilde{\nabla}\cdot\left(\hat{\mathbf{r}}\times\tilde{\mathbf{F}}_H^{(p)}\right)\right\}, \tag{3.2.26}$$

$$\tilde{Q}_{\tilde{\mathfrak{R}}} = \tilde{\omega}^{-1} L_V^{-1}\tilde{\mathfrak{s}} + L_L^{-1}\left\{\tilde{\nabla_H}\cdot\left(i\tilde{\mathbf{F}}_H^{(p)}\right)\right\} + \left[L_L^{-1} L_C L_B^{-1} - L_{\tilde{\mathfrak{R}}} L_B^{-1}\right]\left\{\tilde{\nabla}\cdot\left(\hat{\mathbf{r}}\times\tilde{\mathbf{F}}_H^{(p)}\right)\right\}. \tag{3.2.27}$$

The uncoupled forms of the governing equations (3.2.22–3.2.24) are regarded here as the most insightful because the tidal response for each of the variables $\tilde{p}$, $\tilde{\mathfrak{D}}$, $\tilde{\mathfrak{R}}$ is individually described by the operators $L_{\tilde{p}}$, $L_{\tilde{\mathfrak{D}}}$, $L_{\tilde{\mathfrak{R}}}$. Indeed, we may write the solutions as

$$i\tilde{p} = L_{\tilde{p}}^{-1}\left\{i\tilde{\mathfrak{G}} + \tilde{Q}_{\tilde{p}}\right\}, \tag{3.2.28}$$

$$\tilde{\mathfrak{D}} = L_{\tilde{\mathfrak{D}}}^{-1}\left\{i\tilde{\mathfrak{G}} + \tilde{Q}_{\tilde{\mathfrak{D}}}\right\}, \tag{3.2.29}$$

$$i\tilde{\mathfrak{R}} = L_{\tilde{\mathfrak{R}}}^{-1}\left\{i\tilde{\mathfrak{G}} + \tilde{Q}_{\tilde{\mathfrak{R}}}\right\}, \tag{3.2.30}$$

where $L_{\tilde{p}}^{-1}$, $L_{\tilde{\mathfrak{D}}}^{-1}$, $L_{\tilde{\mathfrak{R}}}^{-1}$ are response operators which fully describe how forcing is translated into each of the variables $\tilde{p}$, $\tilde{\mathfrak{D}}$, $\tilde{\mathfrak{R}}$.

3.3. Auxiliary Equations

3.3.1. Recursive Solutions. The formulations described above each involve some subset of $\tilde{p}$, $\tilde{\mathbf{u}}_H$, $\tilde{\mathfrak{D}}$, $\tilde{\mathfrak{R}}$ as primary solution variables in the governing equations(s). Here we describe auxiliary formulae that can be used to obtain missing components of this set from the solutions obtained.

Solution of the governing equation in the form (3.2.22) provides only $\tilde{p}$. The horizontal velocity $\tilde{\mathbf{u}}_H$ can be subsequently obtained from (3.1.3). If one needs to also determine the velocity potential functions $\tilde{\mathfrak{D}}$, $\tilde{\mathfrak{R}}$, these can be obtained from $\tilde{\mathbf{u}}_H$ as follows. Applying $\nabla_H\cdot\{\cdot\}$ or alternatively$\nabla_H\cdot(\hat{\mathbf{r}}\times\{\cdot\})$ to (3.1.6) we obtain the elliptic equations

$$\tilde{\nabla}_H^2\tilde{\mathfrak{D}} = \tilde{\nabla}_H\cdot\tilde{\mathbf{u}}_H, \tag{3.3.1}$$

$$\tilde{\nabla}_H^2\tilde{\mathfrak{R}} = \tilde{\nabla}_H\cdot\{\hat{\mathbf{r}}\times\tilde{\mathbf{u}}_H\}, \tag{3.3.2}$$

which may be solved for $\tilde{\mathfrak{D}}$, $\tilde{\mathfrak{R}}$.

In the alternative governing system (3.2.14, 3.2.15), it is $\tilde{\mathfrak{D}}, \tilde{\mathfrak{R}}$ that are the primary solution variables. The horizontal velocity $\tilde{\mathbf{u}}_H$ can be obtained using (3.1.6). One may obtain $\tilde{p}$ from $\tilde{\mathfrak{D}}$ using (3.2.12). If instead the version (3.2.18, 3.2.15) were used, one may use (3.2.13) to obtain the missing $\tilde{\mathfrak{D}}$.

Finally, uncoupled governing equations are given for each of $\tilde{p}, \tilde{\mathfrak{D}}, \tilde{\mathfrak{R}}$ by (3.2.22, 3.2.23, 3.2.24), respectively. One may solve these independently and then use (3.1.3) or (3.1.6) to obtain $\tilde{\mathbf{u}}_H$. Alternatively, we may solve for just one of these and then use recursive formulae to determine the others. For example, if either $\tilde{\mathfrak{D}}$ or $\tilde{\mathfrak{R}}$ has been obtained, we can obtain the other from (3.2.18, 3.2.19) which can be rewritten here as

$$\tilde{\mathfrak{D}} = L_a^{-1}\left\{-L_C\left\{i\tilde{\mathfrak{R}}\right\} + L_L\left\{i\tilde{\mathfrak{G}}\right\} + \tilde{Q}_{s1}\right\}, \tag{3.3.3}$$

$$i\tilde{\mathfrak{R}} = L_B^{-1}\left\{-L_C\left\{\tilde{\mathfrak{D}}\right\} + \tilde{Q}_{s2}\right\}. \tag{3.3.4}$$

Then, one may use (3.2.12) to obtain $\tilde{p}$.

3.3.2. Energy, Power, Work, Dissipation. To obtain the work ($\tilde{W}$) and dissipation ($\tilde{D}$) density rates associated with solutions, we make use of an energy equation. We derive this equation by taking the dot product of $\tilde{\mathbf{u}}_H$ with (3.1.2), assuming (3.1.5) and (3.2.2) with $L_h = 1$, and we then may write the energy equation

$$\tilde{\partial}_t(\tilde{E}_k + \tilde{E}_p) + \tilde{\nabla}\cdot\left\{\left(\tilde{p} - \tilde{\mathfrak{G}}\right)\tilde{\mathbf{u}}_H\right\} = \tilde{W} - \tilde{D}, \tag{3.3.5}$$

where

$$\tilde{E}_k = \frac{1}{2}\left(\tilde{\mathbf{u}}_H\cdot\tilde{\mathbf{u}}_H\right), \tag{3.3.6}$$

is the kinetic energy density,

$$\tilde{E}_p = \frac{1}{2}\left(\left[L_V^{(R)}\right]^{1/2}\tilde{p}\right)^2 = \frac{1}{2}\tilde{p}L_V^{(R)}\tilde{p}, \tag{3.3.7}$$

can be associated with the potential or internal energy density,

$$\tilde{W} = \tilde{\mathfrak{G}}L_V\tilde{\partial}_t\tilde{p} + \left(\tilde{p} - \tilde{\mathfrak{G}}\right)\tilde{\mathfrak{s}} + \tilde{\mathbf{u}}_H\cdot\tilde{\mathbf{F}}^{(p)}, \tag{3.3.8}$$

is the work rate density, and

$$\tilde{D} = \tilde{\mathbf{u}}_H\cdot L_{\tilde{\alpha}}\tilde{\mathbf{u}}_H + \tilde{\omega}\tilde{p}L_V^{(I)}\tilde{p}, \tag{3.3.9}$$

is the dissipation rate density. Above, $L_V^{(R)} = \text{real}\{L_V\}$, and $L_V^{(I)} = \text{imaginary}\{L_V\}$.

Of particular interest in characterizing the tidal response are the integrals (or averages) of the above densities over the global fluid and tidal cycle. We now provide the relationships above in alternate forms which help perform these integrals when the solutions are represented in a spherical-harmonic expansion. These integrals are converted to spatiotemporal averages to make tidal fluids of different size and tidal period more directly comparable.

A utility in the Helmholtz expansion of flow field (aside from allowing different dissipation functions for the divergent and rotational components) is that the global average of dissipation and kinetic energy densities can be calculated directly from the spherical-harmonic coefficients of the primary solution variables. Using (3.1.6, 3.1.7, 3.1.20) and vector-calculus identities,

$$\begin{aligned}\tilde{E}_k &= \frac{1}{2}\left(\tilde{\nabla}_H\tilde{\mathfrak{D}} + \tilde{\nabla}_H\times(\hat{\mathbf{r}}\tilde{\mathfrak{R}})\right)\cdot\left(\tilde{\nabla}_H\tilde{\mathfrak{D}} + \tilde{\nabla}_H\times(\hat{\mathbf{r}}\tilde{\mathfrak{R}})\right)\\ &= -\frac{1}{2}\tilde{\mathfrak{D}}\tilde{\nabla}_H^2\tilde{\mathfrak{D}} - \frac{1}{2}\tilde{\mathfrak{R}}\tilde{\nabla}_H^2\tilde{\mathfrak{R}}\\ &\quad + \tilde{\nabla}_H\cdot\tilde{\nabla}_H\left(\frac{1}{4}\left(\tilde{\mathfrak{D}}^2 + \tilde{\mathfrak{R}}^2\right)\right)\\ &\quad + \tilde{\nabla}_H\cdot\left(\tilde{\mathfrak{R}}\hat{\mathbf{r}}\times\tilde{\nabla}_H\tilde{\mathfrak{D}}\right),\end{aligned} \tag{3.3.10}$$

while

$$
\begin{aligned}
\tilde{D} = &\left(\tilde{\nabla}_H\tilde{\mathfrak{D}} + \tilde{\nabla}_H \times (\tilde{\mathfrak{R}}\hat{\mathbf{r}})\right) \cdot \left(\tilde{\nabla}_H L_{\tilde{\alpha}_d}\tilde{\mathfrak{D}} + \tilde{\nabla}_H \times (\hat{\mathbf{r}} L_{\tilde{\alpha}_r}\tilde{\mathfrak{R}})\right) \\
= &- L_{\tilde{\alpha}_d}\left\{\tilde{\mathfrak{D}}\right\}\tilde{\nabla}_H^2\tilde{\mathfrak{D}} \\
&- L_{\tilde{\alpha}_r}\left\{\tilde{\mathfrak{R}}\right\}\tilde{\nabla}_H^2\tilde{\mathfrak{R}} \\
&+ \tilde{\omega}\tilde{p}L_V^{(I)}\tilde{p} \\
&+ \tilde{\nabla}_H \cdot \left(L_{\tilde{\alpha}_r}\left\{\tilde{\mathfrak{R}}\right\}\hat{\mathbf{r}} \times \tilde{\nabla}_H\tilde{\mathfrak{D}} + \tilde{\mathfrak{R}}\hat{\mathbf{r}} \times \tilde{\nabla}_H L_{\tilde{\alpha}_d}\left\{\tilde{\mathfrak{D}}\right\}\right) \\
&+ \tilde{\nabla}_H \cdot \left(L_{\tilde{\alpha}_r}\left\{\tilde{\mathfrak{R}}\right\}\hat{\mathbf{r}} \times \tilde{\nabla}_H\tilde{\mathfrak{D}} + \tilde{\mathfrak{R}}\hat{\mathbf{r}} \times \tilde{\nabla}_H L_{\tilde{\alpha}_d}\left\{\tilde{\mathfrak{D}}\right\}\right).
\end{aligned}
\tag{3.3.11}
$$

These forms show components involving the divergence that vanish when integrated over the surface of a sphere. The remaining terms involve simply products of terms with operators that do not change the order of the spherical harmonics. This is in contrast to the previous forms involving $\tilde{\mathbf{u}}_H$, which is not fully represented in the spherical-harmonic expansions involving only order s. To obtain the integrals/averages of $\tilde{W}$, $\tilde{D}$, $\tilde{E}_k$, $\tilde{E}_p$ directly from the spherical-harmonic coefficients we shall use the forms (3.3.8–3.3.11) together with properties of integrals of propagating spherical harmonics as discussed in Appendix B. Under an assumed balance, the average power density $\tilde{P}$ can be defined as the average of either the work or dissipation rates, i.e.

$$\tilde{P} = \bar{\tilde{W}} = \bar{\tilde{D}}. \tag{3.3.12}$$

Note that when $L_{\tilde{\alpha}_d} = L_{\tilde{\alpha}_r} = \tilde{\alpha}$, where $\tilde{\alpha}$ is a constant drag coefficient common for both the divergent and rotational flow components, and when L_V is given by (3.2.5), where $\tilde{\alpha}_p$ is a constant, it can be shown using (3.3.11) that the average dissipation (and therefore power) is simply proportional to a weighted combination of kinetic and potential energy densities:

$$\tilde{P} = 2\tilde{\alpha}\bar{\tilde{E}}_k + 2\tilde{\alpha}_p\bar{\tilde{E}}_p. \tag{3.3.13}$$

CHAPTER 4

Solution Methods

In this section we describe several methods for solving the equations governing the fluid tidal response. The primary methods to be discussed are based in spherical-harmonics. A finite-volume method is first briefly described.

4.1. Finite-Volume Method

Here we describe a method for solving (3.2.9) using the finite-volume method.

We shall assume $\tilde{\partial}_t \rightarrow -i\tilde{\omega}$ and that the operators $L_{\tilde{\alpha}}$, L_h and L_V similarly reduce to coefficients (prescribed constants or spatially varying parameters). This model can then represent, for example, tides in a uniform-density ocean with variable bathymetry (in which case, $L_h = \tilde{h} = h/H$, where h is the variable fluid thickness and H is a reference constant depth, $L_V = (2\Omega_s r)^2 (gH)^{-1}$ is a uniform constant, $\tilde{Q}_M = 0$, and $-\tilde{\mathfrak{G}}$ is the prescribed tidal gravitational potential).

We assume that the solution variable $\left\{\tilde{p} - \tilde{\mathfrak{G}}\right\}$ is discretized on a uniform spherical grid axially aligned with the rotation axis. The challenge then reduces to finding an appropriate discretization of the operator L_M (see Table 2).

Note that using standard vector identities we can rewrite (3.2.9) as

$$\tilde{\nabla}_H \cdot \left(-\tilde{C}_f \tilde{\nabla}_H \left(\tilde{p} - \tilde{\mathfrak{G}}\right) + \left(\tilde{p} - \tilde{\mathfrak{G}}\right) \tilde{\mathbf{v}}_f\right) - i\tilde{\omega} L_V \left(\tilde{p} - \tilde{\mathfrak{G}}\right) = i\tilde{\omega} L_V \left\{\tilde{\mathfrak{G}} + \tilde{Q}_M\right\}, \tag{4.1.1}$$

where $\tilde{C}_f = L_h \left[\frac{-i\tilde{\omega}+L_{\tilde{\alpha}}}{[-i\tilde{\omega}+L_{\tilde{\alpha}}]^2+\tilde{f}^2}\right]$, $\tilde{\mathbf{v}}_f = \tilde{\nabla}_H(\psi_s) \times \hat{\mathbf{r}}$, and $\psi_s = L_h \frac{\tilde{f}}{[-i\tilde{\omega}+L_{\tilde{\alpha}}]^2+\tilde{f}^2}$ can be regarded as a stream function for the propagation velocity associated with the combined effects of beta drift, drag, and topography (ψ_s is a version of the 'string function' described in [Tyler and Käse, 2000, 2001]). We see that (4.1.1) has the form of a conservative advection-diffusion elliptic equation, where $\tilde{C}_f$ is a spatially varying diffusion coefficient and $\tilde{\mathbf{v}}_f$ is a prescribed advection velocity. This can be readily solved using the finite-volume method on a uniform spherical grid. One integrates 3.2.9 over a control volume and applies Gauss' law to replace the divergence operation with a sum of diffusive and advective fluxes across the boundaries which must balance the prescribed forcing term.

Once the solution for $\tilde{p}$ is obtained, one may (using (3.1.2, 3.1.5)) calculate $\tilde{\mathbf{u}}_H$ as

$$\tilde{\mathbf{u}}_H = \left(\left(\tilde{\partial}_t + L_{\tilde{\alpha}}\right)^2 + \tilde{f}^2\right)^{-1} \left(\tilde{\partial}_t + L_{\tilde{\alpha}} - \tilde{f}\hat{\mathbf{r}}\times\right) \left\{-\tilde{\nabla}_H \left(\tilde{p} - \tilde{\mathfrak{G}}\right) + \tilde{\mathbf{F}}_H^{(p)}\right\}. \tag{4.1.2}$$

4.2. Spherical-Harmonic Method

4.2.1. Expanding Variables in Spherical-Harmonic Bases. In the spherical-harmonic method, the solution variables are first expanded in spherical-harmonic bases. Then the continuous governing (and auxiliary) equations are replaced with algebraic equations describing the relationships between the expansion coefficients. Solutions for the coefficients are then obtained through solution of the resulting system.

Let us expand the primary solution variables and forcing components in terms of propagating spherical harmonics (see Appendix B for more details)

$$\tilde{\mathfrak{D}} = \Sigma_{n=s}^{\infty} P_n^s(\cos\theta) \left(D_n^s e^{i(s\phi - \tilde{\omega}\tilde{t})} + \left\{D_n^s e^{i(s\phi-\tilde{\omega}\tilde{t})}\right\}^*\right) \tag{4.2.1}$$

$$i\tilde{\mathfrak{R}} = \Sigma_{n=s}^{\infty} P_n^s(\cos\theta) \left(R_n^s e^{i(s\phi - \tilde{\omega}\tilde{t})} - \left\{R_n^s e^{i(s\phi-\tilde{\omega}\tilde{t})}\right\}^*\right) \tag{4.2.2}$$

$$i\tilde{p} = \Sigma_{n=s}^{\infty} P_n^s(\cos\theta)\left(p_n^s \mathrm{e}^{i(s\phi-\tilde{\omega}\tilde{t})} - \left\{p_n^s \mathrm{e}^{i(s\phi-\tilde{\omega}\tilde{t})}\right\}^*\right) \tag{4.2.3}$$

$$i\tilde{\mathfrak{G}} = \Sigma_{n=s}^{\infty} P_n^s(\cos\theta)\left(G_n^s \mathrm{e}^{i(s\phi-\tilde{\omega}\tilde{t})} - \left\{G_n^s \mathrm{e}^{i(s\phi-\tilde{\omega}\tilde{t})}\right\}^*\right) \tag{4.2.4}$$

$$\tilde{\mathfrak{s}} = \Sigma_{n=s}^{\infty} P_n^s(\cos\theta)\left(K_n^s \mathrm{e}^{i(s\phi-\tilde{\omega}\tilde{t})} + \left\{K_n^s \mathrm{e}^{i(s\phi-\tilde{\omega}\tilde{t})}\right\}^*\right) \tag{4.2.5}$$

$$\tilde{\nabla_H} \cdot \left(i\tilde{\mathbf{F}}_H^{(p)}\right) = \Sigma_{n=s}^{\infty} P_n^s(\cos\theta)\left(d_n^s \mathrm{e}^{i(s\phi-\tilde{\omega}\tilde{t})} - \left\{d_n^s \mathrm{e}^{i(s\phi-\tilde{\omega}\tilde{t})}\right\}^*\right) \tag{4.2.6}$$

$$\tilde{\nabla}_H \cdot \left(\hat{\mathbf{r}} \times \tilde{\mathbf{F}}_H^{(p)}\right) = \Sigma_{n=s}^{\infty} P_n^s(\cos\theta)\left(e_n^s \mathrm{e}^{i(s\phi-\tilde{\omega}\tilde{t})} + \left\{e_n^s \mathrm{e}^{i(s\phi-\tilde{\omega}\tilde{t})}\right\}^*\right) \tag{4.2.7}$$

where P_n^s are the Associated Legendre functions of degree n and order (also called "rank") s, and $\{\cdot\}^*$ is the complex-conjugate operator.

Now truncate the expansions above to degree $N_{trunc} = s + N - 1$ (where N is then the number of terms included in the expansion) and consider the vector of complex propagating spherical harmonic functions

$$\mathbf{Y}_{\mathbf{n}}^{\mathbf{s};\tilde{\omega}}(\cos\theta, s\phi - \tilde{\omega}\tilde{t}) = \mathbf{P}_{\mathbf{n}}^{\mathbf{s}} \mathrm{e}^{i(s\phi-\tilde{\omega}\tilde{t})}, \tag{4.2.8}$$

where $\mathbf{P}_{\mathbf{n}}^{\mathbf{s}}(\cos\theta)$ is a column vector of Associated Legendre functions $P_n^s(\cos\theta)$ evaluated at θ and spanning $n = s, s+1, ...N_{trunc}$. In most cases, a range of θ values are needed and $\mathbf{P}_{\mathbf{n}}^{\mathbf{s}}(\cos\theta)$ becomes a matrix with each column corresponding to each value θ. Using a similar bold-face notation to represent coefficient vectors (e.g. $\mathbf{D}_{\mathbf{n}}^{\mathbf{s}}$ for the column vector of D_n^s coefficients), the sums (4.2.1–4.2.7) can be written

$$\tilde{\mathfrak{D}} = \left(\mathbf{Y}_{\mathbf{n}}^{\mathbf{s};\tilde{\omega}}\right)^T \mathbf{D}_{\mathbf{n}}^{\mathbf{s}} + \left\{\left(\mathbf{Y}_{\mathbf{n}}^{\mathbf{s};\tilde{\omega}}\right)^T \mathbf{D}_{\mathbf{n}}^{\mathbf{s}}\right\}^* \tag{4.2.9}$$

$$i\tilde{\mathfrak{R}} = \left(\mathbf{Y}_{\mathbf{n}}^{\mathbf{s};\tilde{\omega}}\right)^T \mathbf{R}_{\mathbf{n}}^{\mathbf{s}} + \left\{\left(\mathbf{Y}_{\mathbf{n}}^{\mathbf{s};\tilde{\omega}}\right)^T \mathbf{R}_{\mathbf{n}}^{\mathbf{s}}\right\}^* \tag{4.2.10}$$

$$i\tilde{p} = \left(\mathbf{Y}_{\mathbf{n}}^{\mathbf{s};\tilde{\omega}}\right)^T \mathbf{p}_{\mathbf{n}}^{\mathbf{s}} + \left\{\left(\mathbf{Y}_{\mathbf{n}}^{\mathbf{s};\tilde{\omega}}\right)^T \mathbf{p}_{\mathbf{n}}^{\mathbf{s}}\right\}^* \tag{4.2.11}$$

$$i\tilde{\mathfrak{G}} = \left(\mathbf{Y}_{\mathbf{n}}^{\mathbf{s};\tilde{\omega}}\right)^T \mathbf{G}_{\mathbf{n}}^{\mathbf{s}} + \left\{\left(\mathbf{Y}_{\mathbf{n}}^{\mathbf{s};\tilde{\omega}}\right)^T \mathbf{G}_{\mathbf{n}}^{\mathbf{s}}\right\}^* \tag{4.2.12}$$

$$\tilde{\mathfrak{s}} = \left(\mathbf{Y}_{\mathbf{n}}^{\mathbf{s};\tilde{\omega}}\right)^T \mathbf{K}_{\mathbf{n}}^{\mathbf{s}} + \left\{\left(\mathbf{Y}_{\mathbf{n}}^{\mathbf{s};\tilde{\omega}}\right)^T \mathbf{K}_{\mathbf{n}}^{\mathbf{s}}\right\}^* \tag{4.2.13}$$

$$\tilde{\nabla_H} \cdot \left(i\tilde{\mathbf{F}}_H^{(p)}\right) = \left(\mathbf{Y}_{\mathbf{n}}^{\mathbf{s};\tilde{\omega}}\right)^T \mathbf{d}_{\mathbf{n}}^{\mathbf{s}} + \left\{\left(\mathbf{Y}_{\mathbf{n}}^{\mathbf{s};\tilde{\omega}}\right)^T \mathbf{d}_{\mathbf{n}}^{\mathbf{s}}\right\}^* \tag{4.2.14}$$

$$\tilde{\nabla} \cdot \left(\hat{\mathbf{r}} \times \tilde{\mathbf{F}}_H^{(p)}\right) = \left(\mathbf{Y}_{\mathbf{n}}^{\mathbf{s};\tilde{\omega}}\right)^T \mathbf{e}_{\mathbf{n}}^{\mathbf{s}} + \left\{\left(\mathbf{Y}_{\mathbf{n}}^{\mathbf{s};\tilde{\omega}}\right)^T \mathbf{e}_{\mathbf{n}}^{\mathbf{s}}\right\}^*. \tag{4.2.15}$$

In *TROPF*, s and $\tilde{\omega}$ are constant within an expansion and sub/super scripts on solution variables can be withheld. But we can more clearly label the field (e.g. $\tilde{\mathfrak{D}}^{s,\tilde{\omega}}$ instead of $\tilde{\mathfrak{D}}$) where confusion could arise (when combining solutions from different forcing, for example).

For convenience in the final expressions of these expansions in the governing equations, some variables have been multiplied by i. The factor i can be instead easily moved to the coefficients on the right side. For example (4.2.12) can be written as

$$\tilde{\mathfrak{G}} = \left(\mathbf{Y}_{\mathbf{n}}^{\mathbf{s};\tilde{\omega}}\right)^T (-i\mathbf{G}_{\mathbf{n}}^{\mathbf{s}}) + \left\{\left(\mathbf{Y}_{\mathbf{n}}^{\mathbf{s};\tilde{\omega}}\right)^T (-i\mathbf{G}_{\mathbf{n}}^{\mathbf{s}})\right\}^*. \tag{4.2.16}$$

4.2.2. Matrix Equations Governing Primary Solution Variables. Finally, we consider the results of operators L (in Table 2) acting on an element $Y_n^{s;\tilde{\omega}}$ of $\mathbf{Y}_{\mathbf{n}}^{\mathbf{s};\tilde{\omega}}$. These results are used to replace the operators L with coefficient matrices L (in Table 3) that multiply the column vector of spherical-harmonic coefficients. We require that the result of an operation, for example $L\tilde{\mathfrak{D}}$, can be adequately represented within the same truncated expansion (i. e. the operators L can lead to terms of degree reaching outside of the truncation, and we ignore these). Because the result $L\tilde{\mathfrak{D}}$ remains within the same expansion basis, we expect that there is a matrix L for which

$$L\left\{\left(\mathbf{Y}_{\mathbf{n}}^{\mathbf{s};\tilde{\omega}}\right)^T \mathbf{D}_{\mathbf{n}}^{\mathbf{s}}\right\} = \left(\mathbf{Y}_{\mathbf{n}}^{\mathbf{s};\tilde{\omega}}\right)^T L\mathbf{D}_{\mathbf{n}}^{\mathbf{s}}. \tag{4.2.17}$$

To find the matrices L, we apply the operator L and then collect terms $Y_n^{s;\tilde{\omega}}$ of common degree into rows of a system of equations. Operators which do not alter the degree of $Y_n^{s;\tilde{\omega}}$ lead simply to diagonal matrices.

Following this approach, the governing equations for the system in $\tilde{\mathfrak{D}}, \tilde{\mathfrak{R}}$ (3.2.14, 3.2.15, using 3.2.16, 3.2.17) are replaced with

$$L_D\left\{\mathbf{D}_{\mathbf{n}}^{\mathbf{s}}\right\} + L_C\left\{\mathbf{R}_{\mathbf{n}}^{\mathbf{s}}\right\} = L_L\left\{\mathbf{G}_{\mathbf{n}}^{\mathbf{s}}\right\} + \mathbf{Q}_{\mathbf{s1},\mathbf{n}}^{\mathbf{s}}, \tag{4.2.18}$$

$$L_B\left\{\mathbf{R}_{\mathbf{n}}^{\mathbf{s}}\right\} + L_C\left\{\mathbf{D}_{\mathbf{n}}^{\mathbf{s}}\right\} = \mathbf{Q}_{\mathbf{s2},\mathbf{n}}^{\mathbf{s}}, \tag{4.2.19}$$

where

$$\mathbf{Q}_{\mathbf{s1},\mathbf{n}}^{\mathbf{s}} = \tilde{\omega}^{-1} L_L L_V^{-1}\left\{\mathbf{K}_{\mathbf{n}}^{\mathbf{s}}\right\} + \mathbf{d}_{\mathbf{n}}^{\mathbf{s}}, \tag{4.2.20}$$

$$\mathbf{Q}_{\mathbf{s2},\mathbf{n}}^{\mathbf{s}} = -\mathbf{e}_{\mathbf{n}}^{\mathbf{s}}. \tag{4.2.21}$$

Similarly, the governing equations for the system in $\tilde{\mathfrak{D}}, \tilde{p}$ (3.2.18, 3.2.19, using 3.2.20, 3.2.21) are replaced with

$$L_E\left\{\mathbf{p}_{\mathbf{n}}^{\mathbf{s}}\right\} + L_C\left\{\mathbf{R}_{\mathbf{n}}^{\mathbf{s}}\right\} = L_L\left\{\mathbf{G}_{\mathbf{n}}^{\mathbf{s}}\right\} + \mathbf{Q}_{\mathbf{s3},\mathbf{n}}^{\mathbf{s}}, \tag{4.2.22}$$

$$L_B\left\{\mathbf{R}_{\mathbf{n}}^{\mathbf{s}}\right\} + L_F\left\{\mathbf{p}_{\mathbf{n}}^{\mathbf{s}}\right\} = \mathbf{Q}_{\mathbf{s4},\mathbf{n}}^{\mathbf{s}}, \tag{4.2.23}$$

where

$$\mathbf{Q}_{\mathbf{s3},\mathbf{n}}^{\mathbf{s}} = -L_A L_L^{-1}\left\{\mathbf{K}_{\mathbf{n}}^{\mathbf{s}}\right\} + \mathbf{d}_{\mathbf{n}}^{\mathbf{s}}, \tag{4.2.24}$$

$$\mathbf{Q}_{\mathbf{s4},\mathbf{n}}^{\mathbf{s}} = -L_C L_L^{-1}\left\{\tilde{\mathfrak{s}}\right\} - \mathbf{e}_{\mathbf{n}}^{\mathbf{s}}. \tag{4.2.25}$$

In the alternative, higher-order formulation of governing equations, (3.2.22–3.2.24) become

$$L_{\tilde{p}}\left\{\mathbf{p}_{\mathbf{n}}^{\mathbf{s}}\right\} = \mathbf{G}_{\mathbf{n}}^{\mathbf{s}} + \mathbf{Q}_{\tilde{\mathbf{p}},\mathbf{n}}^{\mathbf{s}}, \tag{4.2.26}$$

$$L_{\tilde{\mathfrak{D}}}\left\{\mathbf{D}_{\mathbf{n}}^{\mathbf{s}}\right\} = \mathbf{G}_{\mathbf{n}}^{\mathbf{s}} + \mathbf{Q}_{\tilde{\mathfrak{D}},\mathbf{n}}^{\mathbf{s}}, \tag{4.2.27}$$

$$L_{\tilde{\mathfrak{R}}}\left\{\mathbf{R}_{\mathbf{n}}^{\mathbf{s}}\right\} = \mathbf{G}_{\mathbf{n}}^{\mathbf{s}} + \mathbf{Q}_{\tilde{\mathfrak{R}},\mathbf{n}}^{\mathbf{s}}, \tag{4.2.28}$$

where

$$\mathbf{Q}_{\tilde{\mathbf{p}},\mathbf{n}}^{\mathbf{s}} = -\left[L_L^{-1}\left[L_A - L_C L_B^{-1} L_C\right] L_L^{-1}\right]\left\{\mathbf{K}_{\mathbf{n}}^{\mathbf{s}}\right\} + L_L^{-1}\left\{\mathbf{d}_{\mathbf{n}}^{\mathbf{s}}\right\} + \left[L_L^{-1} L_C L_B^{-1}\right]\left\{\mathbf{e}_{\mathbf{n}}^{\mathbf{s}}\right\}, \tag{4.2.29}$$

$$\mathbf{Q}_{\tilde{\mathfrak{D}},\mathbf{n}}^{\mathbf{s}} = \tilde{\omega}^{-1} L_V^{-1}\left\{\mathbf{K}_{\mathbf{n}}^{\mathbf{s}}\right\} + L_L^{-1}\left\{\mathbf{d}_{\mathbf{n}}^{\mathbf{s}}\right\} + \left[L_L^{-1} L_C L_B^{-1}\right]\left\{\mathbf{e}_{\mathbf{n}}^{\mathbf{s}}\right\}, \tag{4.2.30}$$

$$\mathbf{Q}_{\tilde{\mathfrak{R}},\mathbf{n}}^{\mathbf{s}} = \tilde{\omega}^{-1} L_V^{-1}\left\{\mathbf{K}_{\mathbf{n}}^{\mathbf{s}}\right\} + L_L^{-1}\left\{\mathbf{d}_{\mathbf{n}}^{\mathbf{s}}\right\} + \left[L_L^{-1} L_C L_B^{-1} - L_{\tilde{\mathfrak{R}}} L_B^{-1}\right]\left\{\mathbf{e}_{\mathbf{n}}^{\mathbf{s}}\right\}. \tag{4.2.31}$$

Solutions are then represented as

$$\mathbf{p}_{\mathbf{n}}^{\mathbf{s}} = L_{\tilde{p}}^{-1}\left\{\mathbf{G}_{\mathbf{n}}^{\mathbf{s}} + \mathbf{Q}_{\tilde{\mathbf{p}},\mathbf{n}}^{\mathbf{s}}\right\}, \tag{4.2.32}$$

$$\mathbf{D}_{\mathbf{n}}^{\mathbf{s}} = L_{\tilde{\mathfrak{D}}}^{-1}\left\{\mathbf{G}_{\mathbf{n}}^{\mathbf{s}} + \mathbf{Q}_{\tilde{\mathfrak{D}},\mathbf{n}}^{\mathbf{s}}\right\}, \tag{4.2.33}$$

$$\mathbf{R}_{\mathbf{n}}^{\mathbf{s}} = L_{\tilde{\mathfrak{R}}}^{-1}\left\{\mathbf{G}_{\mathbf{n}}^{\mathbf{s}} + \mathbf{Q}_{\tilde{\mathfrak{R}},\mathbf{n}}^{\mathbf{s}}\right\}. \tag{4.2.34}$$

These are three uncoupled equations that can be used to obtain the solutions $\mathbf{p}_{\mathbf{n}}^{\mathbf{s}}$, $\mathbf{D}_{\mathbf{n}}^{\mathbf{s}}$, $\mathbf{R}_{\mathbf{n}}^{\mathbf{s}}$ or any subset. Any one of the three equations can be regarded as a governing equation for the tidal response because once any one of the solutions $\mathbf{p}_{\mathbf{n}}^{\mathbf{s}}$, $\mathbf{D}_{\mathbf{n}}^{\mathbf{s}}$, $\mathbf{R}_{\mathbf{n}}^{\mathbf{s}}$ are obtained, the others can be obtained using the relationships below (which are the matrix-equation versions of 3.2.12, 3.2.13, 3.2.14, 3.2.15):

$$\mathbf{p}_{\mathbf{n}}^{\mathbf{s}} = \tilde{\omega}^{-1} L_V^{-1}\left\{L_L \mathbf{D}_{\mathbf{n}}^{\mathbf{s}} - \mathbf{K}_{\mathbf{n}}^{\mathbf{s}}\right\}, \tag{4.2.35}$$

$$\mathbf{D}_{\mathbf{n}}^{\mathbf{s}} = L_L^{-1}\left\{\tilde{\omega} L_V\left\{\mathbf{p}_{\mathbf{n}}^{\mathbf{s}}\right\} + \mathbf{K}_{\mathbf{n}}^{\mathbf{s}}\right\}, \tag{4.2.36}$$

$$\mathbf{D}_{\mathbf{n}}^{\mathbf{s}} = L_D^{-1}\left\{-L_C\left\{\mathbf{R}_{\mathbf{n}}^{\mathbf{s}}\right\} + L_L\left\{\mathbf{G}_{\mathbf{n}}^{\mathbf{s}}\right\} + \mathbf{Q}_{\mathbf{s1},\mathbf{n}}^{\mathbf{s}}\right\}, \tag{4.2.37}$$

$$\mathbf{R}_{\mathbf{n}}^{\mathbf{s}} = L_B^{-1}\left\{-L_C\left\{\mathbf{D}_{\mathbf{n}}^{\mathbf{s}}\right\} + \mathbf{Q}_{\mathbf{s2},\mathbf{n}}^{\mathbf{s}}\right\}. \tag{4.2.38}$$

4.2.3. Matrix Equations for Auxiliary Variables. The last section provided matrix equations for calculating the primary solution variables (regarded here as the coefficient vectors $\mathbf{D}_{\mathbf{n}}^{\mathbf{s}}$, $\mathbf{R}_{\mathbf{n}}^{\mathbf{s}}$, $\mathbf{p}_{\mathbf{n}}^{\mathbf{s}}$). These variables may then be mapped to a 3D (lon, lat, time) grid.

Auxiliary variables that are post-processed from the primary variables can be calculated numerically with the gridded data. But most can also be calculated analytically directly from the spherical-harmonic coefficients. The latter approach will be more accurate and computational faster.

Which auxiliary variables can be calculated analytically with the spherical-harmonic coefficients? This depends on the kinds of operations that need to be performed to produce these variables. As detailed in Appendix B, time and space derivatives can be performed directly with the $TROPF$ coefficients. Integrals of products (as needed for work and dissipation) can also be calculated analytically with the $TROPF$ coefficients so long as they remain in the same $TROPF$ expansion bases which expand in degree n but not both degree and order n, s. A case where this can be a limitation is in calculating products involving velocity terms. As will be shown next, calculating some of the velocity components involve $\partial_\theta P_n^s(\cos\theta)$, the result of which can include terms at different order s. Hence, one can indeed calculate the velocities analytically from the spherical-harmonic coefficients but this may not be true for calculating products of the velocity with other variables.

4.2.3.1. *Calculating the Flow Velocity.* Formulae for the spatial derivatives and gradient of the propagating spherical-harmonic components are described in Section B.1.2. Using (3.1.6) with (4.2.9, 4.2.10), we may derive an analytical expression for the divergent $\tilde{\mathbf{u}}_d$ and rotational $\tilde{\mathbf{u}}_r$ velocity vectors:

$$\begin{aligned}\tilde{\mathbf{u}}_d = \tilde{\nabla}_H \tilde{\mathfrak{D}} = &\left(\mathrm{e}^{i(s\phi-\omega t)}(\partial_\theta \mathbf{P}_{\mathbf{n}}^{\mathbf{s}})^T\left\{\mathbf{D}_{\mathbf{n}}^{\mathbf{s}}\right\} + \left\{\mathrm{e}^{i(s\phi-\omega t)}(\partial_\theta \mathbf{P}_{\mathbf{n}}^{\mathbf{s}})^T\left\{\mathbf{D}_{\mathbf{n}}^{\mathbf{s}}\right\}\right\}^*\right)\hat{\theta} \\ &+ \left(\mathrm{e}^{i(s\phi-\omega t)}(\frac{1}{\sin\theta}\mathbf{P}_{\mathbf{n}}^{\mathbf{s}})^T\left\{is\mathbf{D}_{\mathbf{n}}^{\mathbf{s}}\right\} + \left\{\mathrm{e}^{\mathbf{i}(\mathbf{s}\phi-\omega\mathbf{t})}\left(\frac{\mathbf{1}}{\sin\theta}\mathbf{P}_{\mathbf{n}}^{\mathbf{s}}\right)^T\left\{is\mathbf{D}_{\mathbf{n}}^{\mathbf{s}}\right\}\right\}^*\right)\hat{\phi},\end{aligned} \tag{4.2.39}$$

$$\begin{aligned}\tilde{\mathbf{u}}_r = \tilde{\nabla}_H \tilde{\mathfrak{R}} \times \hat{\mathbf{r}} = &\left(\mathrm{e}^{i(s\phi-\omega t)}(\frac{1}{\sin\theta}\mathbf{P}_{\mathbf{n}}^{\mathbf{s}})^T\left\{s\mathbf{R}_{\mathbf{n}}^{\mathbf{s}}\right\} + \left\{\mathrm{e}^{\mathbf{i}(\mathbf{s}\phi-\omega\mathbf{t})}\left(\frac{\mathbf{1}}{\sin\theta}\mathbf{P}_{\mathbf{n}}^{\mathbf{s}}\right)^T\left\{s\mathbf{R}_{\mathbf{n}}^{\mathbf{s}}\right\}\right\}^*\right)\hat{\theta} \\ &- \left(\mathrm{e}^{i(s\phi-\omega t)}(\partial_\theta \mathbf{P}_{\mathbf{n}}^{\mathbf{s}})^T\left\{-i\mathbf{R}_{\mathbf{n}}^{\mathbf{s}}\right\} + \left\{\mathrm{e}^{i(s\phi-\omega t)}(\partial_\theta \mathbf{P}_{\mathbf{n}}^{\mathbf{s}})^T\left\{-i\mathbf{R}_{\mathbf{n}}^{\mathbf{s}}\right\}\right\}^*\right)\hat{\phi},\end{aligned} \tag{4.2.40}$$

where $\partial_\theta \mathbf{P}_{\mathbf{n}}^{\mathbf{s}}$ can be evaluated using (B.1.21). The total velocity is $\tilde{\mathbf{u}} = \tilde{\mathbf{u}}_d + \tilde{\mathbf{u}}_r$.

In the summation form, the velocities are

(4.2.41)
$$\tilde{\mathbf{u}}_d = \Sigma_{n=s}^{\infty} \partial_\theta P_n^s(\cos\theta) \left\{ D_n^s \mathrm{e}^{i(s\phi-\omega t)} + \left(D_n^s \mathrm{e}^{i(s\phi-\omega t)} \right)^* \right\} \hat{\theta} + \frac{P_n^s(\cos\theta)}{\sin\theta} \left\{ isD_n^s \mathrm{e}^{i(s\phi-\omega t)} + \left(isD_n^s \mathrm{e}^{i(s\phi-\omega t)} \right)^* \right\} \hat{\phi},$$

(4.2.42)
$$\tilde{\mathbf{u}}_r = \Sigma_{n=s}^{\infty} \frac{P_n^s(\cos\theta)}{\sin\theta} \left\{ sR_n^s \mathrm{e}^{i(s\phi-\omega t)} + \left(sR_n^s \mathrm{e}^{i(s\phi-\omega t)} \right)^* \right\} \hat{\theta} + \partial_\theta P_n^s(\cos\theta) \left\{ iR_n^s \mathrm{e}^{i(s\phi-\omega t)} + \left(iR_n^{s*} \mathrm{e}^{i(s\phi-\omega t)} \right)^* \right\} \hat{\phi}.$$

4.2.3.2. *Average of Products (average Power, Work, Dissipation).* Formulae for analytical calculation of products of variables with respect to time, longitude, latitude or some combination of these is given in Appendix B.1.3. Particularly useful is the formula for the simultaneous average over the forcing period and sphere (Appendix B.1.3.5). This can be used to provide the average work and dissipation. The averages of these, by an assumed balance, are equal and can be referred to as the average power. To calculate this from the spherical-harmonic coefficients consider the product $\left\{ \tilde{\mathfrak{G}} \right\} \left\{ L_V \tilde{\partial}_t \tilde{p} \right\}$ representing the tidal work term in (3.3.8). We first expand using (4.2.11, 4.2.12), replacing the operator L_V with the operator matrix L_V, then use formulae in (B.1.3.5) to evaluate the average product from the coefficients.

CHAPTER 5

Validation of *TROPF*

5.1. Checking Eigenvalues of Governing Equations

A script used for calculating the results presented in this section can be found as TROPF /Validations /`scr_val_eigs.m`.

Here we check the *TROPF* implementation of the homogeneous (force-free) versions of the governing equations (4.2.26, 4.2.27, 4.2.28). These equations are based in the same underlying equations and they each have a different form only because they are posed in terms of a different solution variable. Once any one of these three is solved, the others can be obtained through auxiliary relationships and so any one of the three equations can be regarded as a governing equation for the system.

Because these equations reflect the same system, we expect that the matrices $L_{\tilde{p}}$, $L_{\tilde{\mathfrak{D}}}$, $L_{\tilde{\mathfrak{R}}}$ should include the same eigenvalues. Below, we will verify this using parameters taken for the study of tides in Jupiter. The reason for choosing these parameters is that in [Ioannou and Lindzen, 1993a] the eigenvalues were listed and offer then opportunity for an independent validation. That is, this section shows (1) that the eigenvalues of $L_{\tilde{p}}$, $L_{\tilde{\mathfrak{D}}}$, $L_{\tilde{\mathfrak{R}}}$ match each other, and (2) that they match values independently derived using a formulation different than these (the eigenvalues in [Ioannou and Lindzen, 1993a] can be regarded as the eigenvalues of the operator L_M in the dissipation-free limit). The configuration of the forcing, as assumed in [Ioannou and Lindzen, 1993a], describes the tidal pull of Io (in an equatorial, circular orbit) on Jupiter. This is then the lowest-order degree-two, sectoral tidal force described in (2.1.21). The frequency is not $\tilde{\omega} = -1$, as is the case in the limit of a more distant moon, but rather $\tilde{\omega} = -0.766$ because Io progresses non-negligibly in its orbit during a rotation period of Jupiter.

Under these assumptions, there are no dissipation terms (nor forcing) in the equations and the wave speed is nondispersive. Therefore, $L_{\tilde{\alpha}_d}, L_{\tilde{\alpha}_r}$ become null matrices and L_V becomes a real constant (or a real constant repeated along a diagonal), which by (3.2.2) can be written as $L_V = \tilde{c}_e^{-2}$ (or $\tilde{c}_e^{-2} I$). We see (consulting Table 2) that $L_{\tilde{p}}$ will become the null operator if $L_V = -1/\lambda_j$, where λ_j is one of the eigenvalues of the matrix $\left[\left[L_L^{-1}\right]\left[L_A - L_C L_B^{-1} L_C\right]\left[\tilde{\omega} L_L^{-1}\right]\right]$. We see that for choices of squared wave speed $\tilde{c}_e^2 = \tilde{c}_{e,j}^2 = -\lambda_j$, the matrix $L_{\tilde{p}}$ becomes null, at least in this dissipation-free and non-dispersive case. Even in the more realistic cases, the establishment here of $\tilde{c}_{e,j}^2$ provides useful insight in explaining where the resonant peaks occur in the solution domain.

The script used for calculating the eigenvalues and generating the plots in this section can be found in TROPF /Validations /`scr_val_eigs.m`. In Figure 5.1.1, the first 30 eigenvalues for the matrices $L_{\tilde{p}}$, $L_{\tilde{\mathfrak{D}}}$, $L_{\tilde{\mathfrak{R}}}$ (labeled 'A, B, C', respectively) are shown to agree. 'Symmetric' refer to modes that are symmetric about the equator while 'asymmetric' refers to modes that are in this case antisymmetric about the equator. The first 60 eigenvalues are listed in Table 1 assuming $N = 120$ and can be seen to be very close to those in [Ioannou and Lindzen, 1993a] for the larger eigenvalues. Tables 2, 3 show the eigenvalues when more terms are included in the expansion. Comparison between the Tables 1, 2, 3 is useful in showing the dependence of the eigenvalues on N, particularly for the smaller eigenvalues. From this we see that accurate estimates of even the large eigenvalues (and low-degree solutions) depend on a suitably large expansion. Because *TROPF* is fast, this is not likely a problem as even the case with $N = 1500$ is calculated by *TROPF* essentially instantaneously. Hence, in configuring *TROPF* configurations the user can simply err on the side of large N and accuracy of solutions can be examined by comparing with results from other N choices.

We can be more rigorous in checking the agreement of the eigenvalues of $L_{\tilde{p}}$, $L_{\tilde{\mathfrak{D}}}$, $L_{\tilde{\mathfrak{R}}}$ by assigning non-zero dissipation terms. In this case, the eigenvalues are complex. We choose a configuration identical to that above for Jupiter but add three random numbers (between 0 and 1) for $\tilde{\alpha}_{d,0}$, $\tilde{\alpha}_{r,0}$, $\tilde{\alpha}_p$ to assign non-zero dissipation. Figure 5.1.2 shows that the real and imaginary components agree.

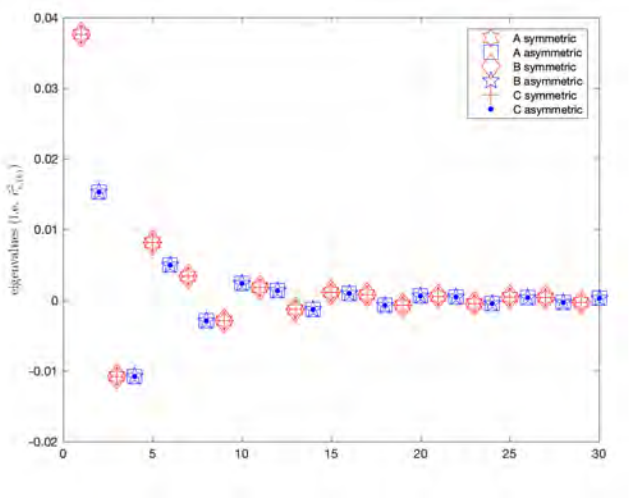

FIGURE 5.1.1. Validation showing that three different *TROPF* formulations (A, B, C) have the same symmetric and asymmetric eigenvalues (only the first 30 of 1500 eigenvalues calculated are shown).

symmetric			asymmetric		
3.7584906e-02	1.5927870e-04	4.2170353e-05	1.5263228e-02	-1.4838821e-04	-4.1634774e-05
-1.0791703e-02	-1.4838821e-04	-4.1634774e-05	-1.0791978e-02	1.4749385e-04	4.0992826e-05
8.0986251e-03	1.3696982e-04	3.8430877e-05	4.9829481e-03	1.2753302e-04	3.8021889e-05
3.3650696e-03	-1.2022874e-04	-3.7138735e-05	-2.9216440e-03	-1.2022874e-04	-3.7138735e-05
-2.9216440e-03	1.1903872e-04	3.4381851e-05	2.4216344e-03	1.1136547e-04	3.4260046e-05
1.8247906e-03	1.0441080e-04	-3.3326678e-05	1.4237640e-03	-9.9383578e-05	-3.3326670e-05
-1.3197428e-03	-9.9383578e-05	2.9982110e-05	-1.3197428e-03	9.8087709e-05	-2.9973145e-05
1.1415373e-03	9.2321999e-05	-2.9973223e-05	9.3549512e-04	8.7050038e-05	2.9934868e-05
7.8052622e-04	-8.3523230e-05	-2.6638625e-05	-7.4667652e-04	-8.3523230e-05	-2.6638346e-05
-7.4667652e-04	8.2217026e-05	2.5304898e-05	6.6106321e-04	7.7775558e-05	2.5282764e-05
5.6704260e-04	7.3684460e-05	-2.2943560e-05	4.9172650e-04	-7.1176624e-05	-2.2943043e-05
-4.7916955e-04	-7.1176624e-05	2.0426915e-05	-4.7916955e-04	6.9907831e-05	2.0415664e-05
4.3046682e-04	6.6414250e-05	-1.8845103e-05	3.7997360e-04	6.3176127e-05	-1.8844402e-05
3.3786548e-04	-6.1377774e-05	1.5414113e-05	-3.3324884e-04	-6.1377774e-05	1.5408359e-05
-3.3324884e-04	6.0169152e-05	-1.4419173e-05	3.0238451e-04	5.7371839e-05	-1.4418382e-05
2.7221022e-04	5.4765136e-05	1.0324821e-05	2.4633522e-04	-5.3471143e-05	1.0322090e-05
-2.4505471e-04	-5.3471143e-05	-9.7402640e-06	-2.4505471e-04	5.2332185e-05	-9.7395157e-06
2.2398021e-04	5.0057332e-05	5.2129709e-06	2.0453473e-04	4.7930949e-05	5.2119679e-06
-1.8772900e-04	-4.6999203e-05	-4.8716450e-06	-1.8772900e-04	-4.6999203e-05	-4.8711341e-06
1.8751509e-04	4.5921369e-05	1.3035022e-07	1.7253407e-04	4.4110164e-05	1.3033172e-07

TABLE 1. The first 60 symmetric and asymmetric eigenvalues for Jupiter parameters and $N = 120$.

5.2. Checking Solutions From Different *TROPF* Spherical-Harmonic Formulations

A script used for calculating the results presented in this section can be found as TROPF /Validations /`scr_val_compareSHMethods.m`.

In the last section, we saw that the different formulations (4.2.26, 4.2.27, 4.2.28) provided the same eigenvalues—a reasonable validation that the three consistently represent the homogenous equations, at least within the spherical-harmonic bases assumed in all three. We extend the check here by considering

symmetric			asymmetric		
3.7584906e-02	1.5927870e-04	4.2296217e-05	1.5263228e-02	-1.4838821e-04	-4.1634775e-05
-1.0791703e-02	-1.4838821e-04	-4.1634775e-05	-1.0791978e-02	1.4749385e-04	4.0638067e-05
8.0986251e-03	1.3696982e-04	3.9075541e-05	4.9829481e-03	1.2753302e-04	3.7601425e-05
3.3650696e-03	-1.2022874e-04	-3.7138882e-05	-2.9216440e-03	-1.2022874e-04	-3.7138882e-05
-2.9216440e-03	1.1903872e-04	3.6209173e-05	2.4216344e-03	1.1136547e-04	3.4892834e-05
1.8247906e-03	1.0441080e-04	3.3646989e-05	1.4237640e-03	-9.9383578e-05	-3.3333689e-05
-1.3197428e-03	-9.9383578e-05	-3.3333689e-05	-1.3197428e-03	9.8087709e-05	3.2466692e-05
1.1415373e-03	9.2321999e-05	3.1347424e-05	9.3549512e-04	8.7050038e-05	3.0285051e-05
7.8052622e-04	-8.3523230e-05	-3.0084645e-05	-7.4667652e-04	-8.3523230e-05	-3.0084645e-05
-7.4667652e-04	8.2217026e-05	2.9275780e-05	6.6106321e-04	7.7775558e-05	2.8316130e-05
5.6704260e-04	7.3684460e-05	2.7402902e-05	4.9172650e-04	-7.1176624e-05	-2.7288432e-05
-4.7916955e-04	-7.1176624e-05	-2.7288432e-05	-4.7916955e-04	6.9907831e-05	2.6533148e-05
4.3046682e-04	6.6414250e-05	2.5704154e-05	3.7997360e-04	6.3176127e-05	2.4913411e-05
3.3786548e-04	-6.1377774e-05	-2.4864657e-05	-3.3324884e-04	-6.1377774e-05	-2.4864657e-05
-3.3324884e-04	6.0169152e-05	2.4158601e-05	3.0238451e-04	5.7371839e-05	2.3437581e-05
2.7221022e-04	5.4765142e-05	-2.2750004e-05	2.4633522e-04	-5.3471143e-05	-2.2750004e-05
-2.4505471e-04	-5.3471143e-05	2.2748362e-05	-2.4505471e-04	5.2332129e-05	2.2089103e-05
2.2398021e-04	5.0057708e-05	2.1458092e-05	2.0453473e-04	4.7928389e-05	-2.0894059e-05
-1.8772900e-04	-4.6999203e-05	-2.0894059e-05	-1.8772900e-04	-4.6999203e-05	2.0853737e-05
1.8751509e-04	4.5932088e-05	2.0274558e-05	1.7253407e-04	4.4057954e-05	1.9719176e-05

TABLE 2. The first 60 symmetric and asymmetric eigenvalues for Jupiter parameters and $N = 1000$.

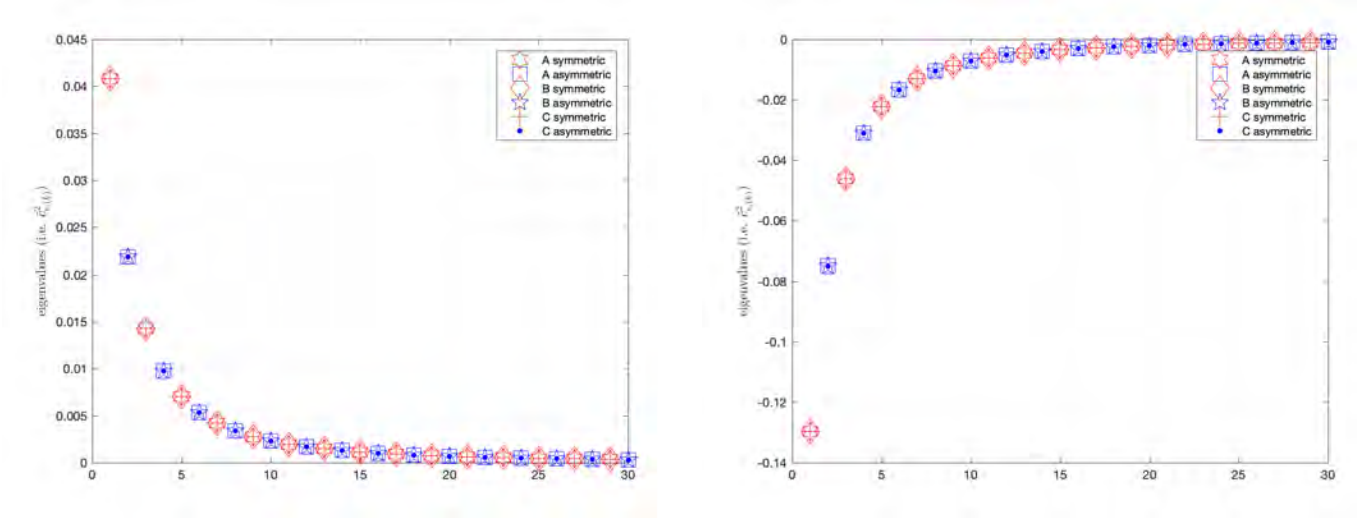

(A) (B)

FIGURE 5.1.2. Similar to Figure 5.1.1 but for more general case with dissipation, in which case the eigenvalues have real (a) and imaginary (b) components.

the solutions to the non-homogeneous problem as recovered by the functions `tropf.m` and `tropf_sas.m`. While the governing equation in `tropf.m` is (4.2.27, or alternatively 4.2.26), the governing equation in `tropf_sas.m` is the system (4.2.18, 4.2.19). The script we used for this comparison is TROPF /Validations /`scr_val_compareSHMethods.m`.

symmetric			asymmetric		
3.7584906e-02	1.5927870e-04	4.2296217e-05	1.5263228e-02	-1.4838821e-04	-4.1634775e-05
-1.0791703e-02	-1.4838821e-04	-4.1634775e-05	-1.0791978e-02	1.4749385e-04	4.0638067e-05
8.0986251e-03	1.3696982e-04	3.9075541e-05	4.9829481e-03	1.2753302e-04	3.7601425e-05
3.3650696e-03	-1.2022874e-04	-3.7138882e-05	-2.9216440e-03	-1.2022874e-04	-3.7138882e-05
-2.9216440e-03	1.1903872e-04	3.6209173e-05	2.4216344e-03	1.1136547e-04	3.4892834e-05
1.8247906e-03	1.0441080e-04	3.3646989e-05	1.4237640e-03	-9.9383578e-05	-3.3333689e-05
-1.3197428e-03	-9.9383578e-05	-3.3333689e-05	-1.3197428e-03	9.8087709e-05	3.2466692e-05
1.1415373e-03	9.2321999e-05	3.1347424e-05	9.3549512e-04	8.7050038e-05	3.0285051e-05
7.8052622e-04	-8.3523230e-05	-3.0084645e-05	-7.4667652e-04	-8.3523230e-05	-3.0084645e-05
-7.4667652e-04	8.2217026e-05	2.9275780e-05	6.6106321e-04	7.7775558e-05	2.8316130e-05
5.6704260e-04	7.3684460e-05	2.7402902e-05	4.9172650e-04	-7.1176624e-05	-2.7288432e-05
-4.7916955e-04	-7.1176624e-05	-2.7288432e-05	-4.7916955e-04	6.9907831e-05	2.6533148e-05
4.3046682e-04	6.6414250e-05	2.5704154e-05	3.7997360e-04	6.3176127e-05	2.4913411e-05
3.3786548e-04	-6.1377774e-05	-2.4864657e-05	-3.3324884e-04	-6.1377774e-05	-2.4864657e-05
-3.3324884e-04	6.0169152e-05	2.4158601e-05	3.0238451e-04	5.7371839e-05	2.3437581e-05
2.7221022e-04	5.4765142e-05	-2.2750004e-05	2.4633522e-04	-5.3471143e-05	-2.2750004e-05
-2.4505471e-04	-5.3471143e-05	2.2748362e-05	-2.4505471e-04	5.2332129e-05	2.2089103e-05
2.2398021e-04	5.0057708e-05	2.1458092e-05	2.0453473e-04	4.7928389e-05	-2.0894059e-05
-1.8772900e-04	-4.6999203e-05	-2.0894059e-05	-1.8772900e-04	-4.6999203e-05	2.0853737e-05
1.8751509e-04	4.5932088e-05	2.0274558e-05	1.7253407e-04	4.4057954e-05	1.9719176e-05

TABLE 3. The first 60 symmetric and asymmetric eigenvalues for Jupiter parameters and $N = 1500$.

The dissipation parameters were assigned randomly, and results were also examined with varying assumptions on the force configuration. The solution components were inspected to determine the maximum value of the absolute differences. The solution components examined include the spatiotemporal integrals for work and dissipation. Because the spatial and harmonic-degree distributions differ between the unaveraged power, work, and dissipation, it is very unlikely that their integrals would agree spuriously. In any case, the solutions compared also included the solution variables $\tilde{p}$, $\tilde{\mathfrak{D}}$, $\tilde{\mathfrak{R}}$. In all cases, the maximum differences were seen to be at machine precision (e.g. 10^{-17}). The high level of agreement indicate that both `tropf.m` and `tropf_sas.m` produce the same solutions to high accuracy.

5.3. Checking *TROPF* Solutions With a Finite-Volume Model

A script used for calculating the results presented in this section can be found as TROPF /Validations /`scr_compareSHvsFV.m`.

While the *TROPF* package is primarily based in methods using spherical-harmonic bases, a fully-independent finite-volume package is also included in the library directory TROPF /Libraries /Lib_tropfFV. The finite-volume model is based on flux-conserving finite-differences on a regular, global (including the poles) spherical grid. The formulation solved is that described in Section 4.1, which is different than any of the formulations used in the spherical-harmonic *TROPF* routines. Because both the formulation and the bases are completely different in these solution approaches, agreement provides very strong validation.

In Figure 5.3.1, we compare $\tilde{p}$ from the two methods using the Jupiter parameters above and selecting $\tilde{c}_e^2 = 10^{-2}$ and the non-zero dissipation parameter $\tilde{\alpha}_{d,0} = \tilde{\alpha}_{r,0} = 10^{-1}$. The finite-volume grid is discretized at 1×1 degree resolution and $N = 500$ terms are used in the spherical-harmonic expansion. As we can see in Figure 5.3.1, the differences between the solutions are small, despite the completely different methods. Some experimentation in varying $\tilde{\alpha}_{d,0}$ show that the differences are due to inaccuracies in the finite-volume method, as there are singularities in this approach at the critical latitudes when $\tilde{\alpha}_{d,0} \to 0$. This is further supported by results in Section 5.4 where *TROPF* solutions are compared against analytical solutions and found to show residuals much smaller than the differences here with the finite-volume solutions.

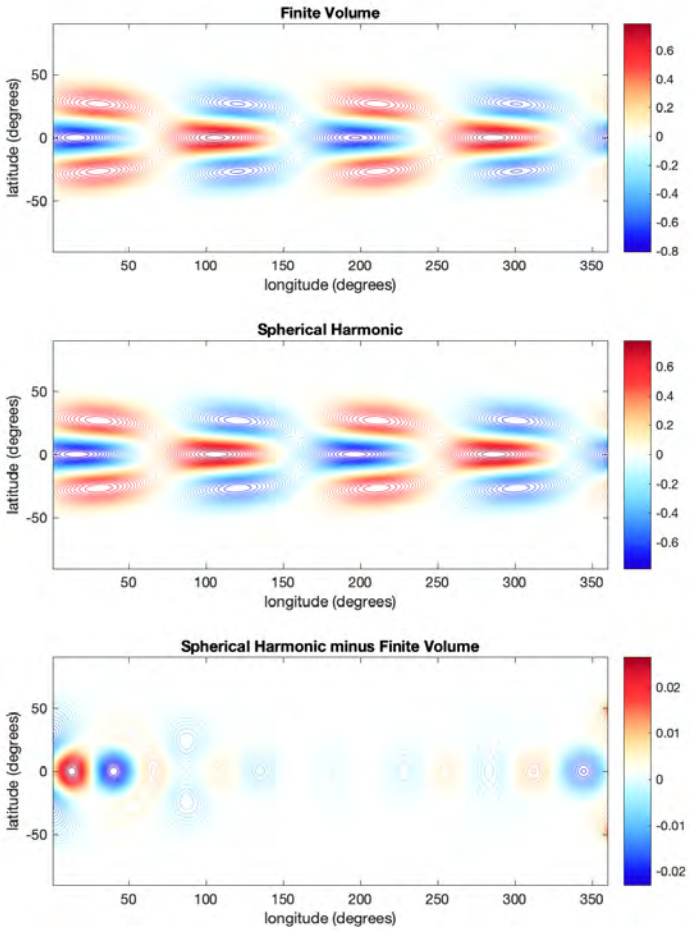

FIGURE 5.3.1. Comparison of solution $\tilde{p}$ obtained using *TROPF* finite-volume and spherical-harmonic methods. The differences (bottom panel) are small and reduce further with increased resolution. (See Section 5.3 for parameter assumptions).

5.4. Checking *TROPF* Against Analytical Solutions

A script used for calculating the results presented in this section can be found as TROPF /Validations /`scr_compareSHvsAnaly.m`.

The previous sections provide general validation of the *TROPF* solutions. To gain a more quantitative description of the accuracy, we compare *TROPF* solutions against analytical forms obtained in several limits. It is convenient to obtain the analytical solutions from the governing equation in the form (4.1.1).

Consider the case of a non-rotating ($\tilde{f} = 0$) fluid with $L_h = 1$, $L_{\tilde{\alpha}}$ described by a real constant, the forcing $\tilde{\mathfrak{G}}$ prescribed as a spherical harmonic of degree n and order s, and $\tilde{\mathbf{F}}_H^{(p)} = 0$. In this case,

$$\tilde{C}_f = \left(\frac{1}{(-i\tilde{\omega} + L_{\tilde{\alpha}})} \right) \tag{5.4.1}$$

is uniform, $\tilde{\mathbf{v}}_f = 0$, and the solution of (4.1.1) is

$$\left(\tilde{p} - \tilde{\mathfrak{G}} \right) = \left(\tilde{C}_f \frac{n(n+1)}{i\tilde{\omega} L_V} - 1 \right)^{-1} \tilde{\mathfrak{G}}, \tag{5.4.2}$$

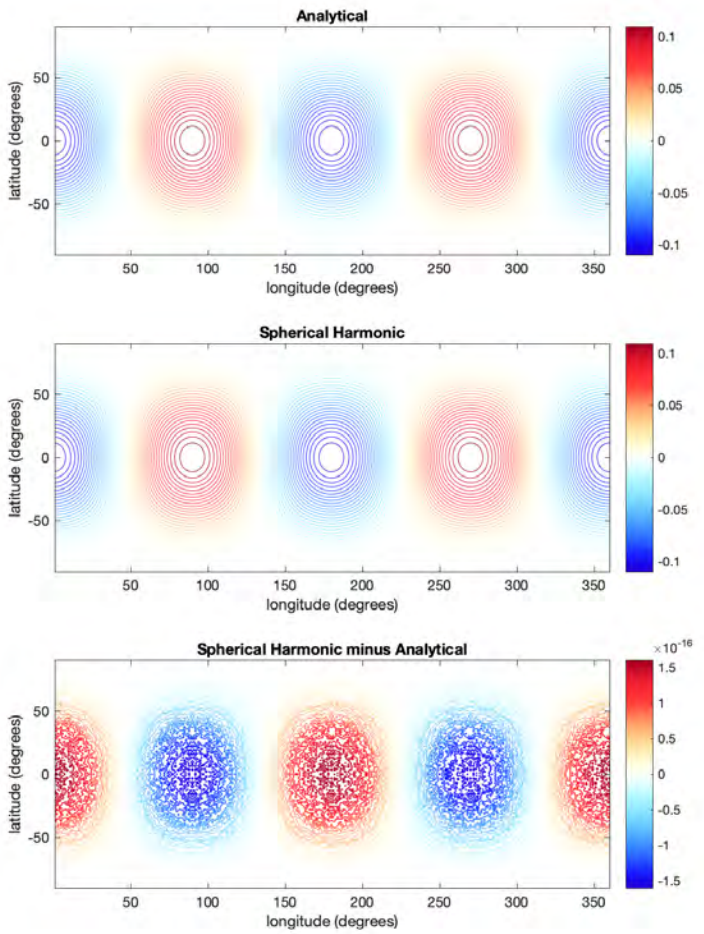

FIGURE 5.4.1. Comparison of solution $\tilde{p}$ obtained using `tropf.m` and analytical solution (assuming zero rotation and zero dissipation — see Section 5.4 for parameter assumptions). Differences (bottom frame) are extremely small.

or

$$\tilde{p} = \left(\left(\tilde{C}_f \frac{n(n+1)}{i\tilde{\omega} L_V} - 1 \right)^{-1} + 1 \right) \tilde{\mathfrak{G}}. \tag{5.4.3}$$

Note that from the analytical solution (5.4.3), when $\tilde{\omega}^2 \to \pm\infty$, $\tilde{p} \to 0$, while for $\tilde{\omega}^2 = L_{\tilde{\alpha}} = 0$, the solution is $\tilde{p} = \tilde{\mathfrak{G}}$. We first verify that *TROPF* solutions properly approach these limits. Further, let us check *TROPF* solutions quantitatively against the analytical form. We consider parameters just as in Section 5.3 except that $\tilde{\Omega} = 0$ for non-rotation, and we consider alternate limits of either $L_{\tilde{\alpha}} = 0$ (results shown in Figure 5.4.1) or $\tilde{\omega} = 0$ (results shown in Figure 5.4.2). The differences are seen to be extremely small, and decrease further with increased N; for example, the maximum residual in Figure 5.4.1 decreases from 3.75×10^{-16} to 1.66×10^{-16} when N increases from 500 to 1000.

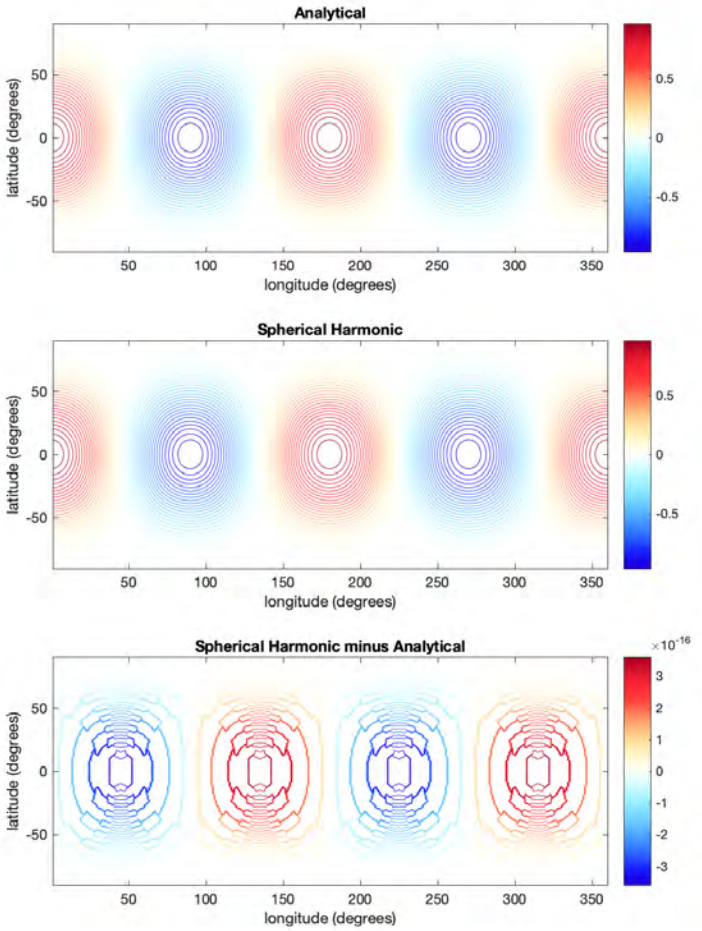

FIGURE 5.4.2. Comparison of solution $\tilde{p}$ obtained using `tropf.m` and analytical solution (assuming zero rotation and zero frequency — see Section 5.4 for parameter assumptions). Differences (bottom frame) are extremely small.

CHAPTER 6

Initial Insight Into the Tidal Response

The response of a global rotating fluid to forces can show a wide range of behavior, with sharp transitions following even subtle changes in parameters. Three important aspects in understanding this variety are the following:

(1) Different forces produce different responses. This is a rather obvious aspect.
(2) Different compositions of the fundamental restoring forces acting on the fluid produce different responses. When the fluid is perturbed by external forcing, there are three important restoring forces that attempt to return it to equilibrium: gravity, Coriolis, and the beta effect (due to the variation of the Coriolis parameter with latitude). While gravity may be uniform, Coriolis and beta vary with latitude and so the local mixture of restoring forces vary. In addition to these forces, there are also the forces associated with dissipative processes to consider.
(3) For some combinations of parameters, wave oscillations can be resonantly forced. Fluids (by definition) respond readily to forces and can retain momentum in normal modes of oscillation, the specifics of which depend on the fluid's internal parameters. If the forces are such as to constructively interfere with these oscillations, the amplitudes can be resonantly amplified.

These elements are of course treated in detail in standard texts of Geophysical Fluid Dynamics, and the reader is also referred to specialized papers treating fluid tidal dynamics such as [Longuet-Higgins, 1968]. Here, we provide only some lateral insight through examination of the behavior of *TROPF* operators already presented.

When the fluid is perturbed by forces, waves in the fluid attempt to restore the equilibrium. If wave speeds can keep up with propagation speeds of the forces (both applied forces as well as the fictitious inertial forces due to the rotating frame), there can be a quasistatic equilibrium. If not, a more interesting fluid response can result. This is why the parameter $\tilde{c}_e^2$ is prominent in the formulations. It is a measure of the relative amplitude of the fluid wave speed c_e to the speed of equatorial rotation. A large $\tilde{c}_e^2$ would suggest that the fluid can respond instantaneously to forces and the so-called "equilibrium tide" would be the response to tidal forces.

But this is incomplete. We see in the fundamental equations that $\tilde{c}_e^2$ enters not in the momentum equation (3.1.2) but only the second relationship (e.g. 3.2.6). We see from (3.2.6) that $\tilde{c}_e^2$ is related only to the horizontally divergent component of the flow and can be quite irrelevant in describing the wave speeds of non-divergent flow components. The horizontally divergent flow leads to vertical motion and therefore necessarily involves gravity as a restoring force. However, disturbances due to forcing can also be propagated through horizontally non-divergent Rossby waves, the speed of which is not predicted by $\tilde{c}_e^2$. The tidal response then involves some combination of gravity waves and Rossby waves (together with inertial oscillations) and these waves have been described as Class I and Class II oscillations, respectively (see, for example, [Longuet-Higgins, 1968]). The Rossby waves are also called Rossby-Haurwitz waves, or planetary waves. This latter term can surely be confusing in extraterrestrial applications (as is "gravity wave", for that matter). o

To gain some intuition into the gravity and Rossby wave oscillations that will be involved in the fluid tidal response, recall that each of the primary solution variables ($\tilde{p}$, $\tilde{\mathfrak{D}}$, $\tilde{\mathfrak{K}}$) is individually governed by the uncoupled equations (3.2.22–3.2.24), and solutions can therefore be immediately described as in (3.2.28–3.2.30). The operators $L_{\tilde{p}}$, $L_{\tilde{\mathfrak{D}}}$, $L_{\tilde{\mathfrak{K}}}$ and their inverses then fully control how forces translate into fluid response ($\tilde{p}$, $\tilde{\mathfrak{D}}$, $\tilde{\mathfrak{K}}$). To proceed further, we refer to the matrix forms of these equations (4.2.26–4.2.28 and 4.2.32–4.2.34) involving the operators $L_{\tilde{p}}$, $L_{\tilde{\mathfrak{D}}}$, $L_{\tilde{\mathfrak{K}}}$ and their inverses. The gravity and Rossby response limits will next be described by the conditions for which suboperators within $L_{\tilde{p}}$, $L_{\tilde{\mathfrak{D}}}$, $L_{\tilde{\mathfrak{K}}}$ become null.

6.1. Gravity Wave Response

First, in the case of no rotation ($\tilde{\Omega} = 0$) the operator L_C becomes null (see Table 3). In this case,

$$L_{\tilde{p}} = \left[\tilde{\omega} L_L^{-1} L_A L_L^{-1} L_V + I\right] \tag{6.1.1}$$

and

$$L_{\tilde{\mathfrak{D}}} = \left[L_L^{-1} L_D\right] = \left[L_L^{-1} L_A + \tilde{\omega}^{-1} L_V^{-1} L_L\right]. \tag{6.1.2}$$

The suboperator matrices in (6.1.1, 6.1.2) are all diagonal, in which case the inverses $L_{\tilde{p}}^{-1}$, $L_{\tilde{\mathfrak{D}}}^{-1}$ can be calculated analytically and solutions immediately obtained using (4.2.32, 4.2.33). Another result of this diagonality is that the response of $\tilde{p}$ and $\tilde{\mathfrak{D}}$ will occur at the same degree as the prescribed forcing. This implies that it is rotation (absent here) that scatters energy between degrees.

Because of the L_C^{-1} in $L_{\tilde{\mathfrak{R}}}$, when L_C becomes null then the solution for $\mathbf{R}_{\mathbf{n}}^{\mathbf{s}}$ (and therefore $\tilde{\mathfrak{R}}$) must vanish and the flow is irrotational. More carefully, provided the application of $L_C L_D^{-1} L_L$ to the forcing terms on the right of (4.2.28) causes them to vanish, then the resulting equation can be written as

$$L_B \left\{\mathbf{R}_{\mathbf{n}}^{\mathbf{s}}\right\} = \left[\tilde{\omega} + i L_{\tilde{\alpha}_r}\right] \left[L_L\right] \left\{\mathbf{R}_{\mathbf{n}}^{\mathbf{s}}\right\} = 0. \tag{6.1.3}$$

The suboperator matrix $[L_L]$ is never null (except in the case $n = 0$), and the suboperator $[\tilde{\omega} + i L_{\tilde{\alpha}_r}]$ is never null (except when both $\tilde{\omega} I$ and $L_{\tilde{\alpha}_r}$ are null). As a result, in wave applications we expect that (6.1.3) can only be satisfied by the vanishing of $\mathbf{R}_{\mathbf{n}}^{\mathbf{s}}$ (and therefore $\tilde{\mathfrak{R}}$); the fluid response is irrotational.

For some parameter choices, the operators $L_{\tilde{p}}$ and $L_{\tilde{\mathfrak{D}}}$ may also become null (or approximately so), describing the condition for free oscillations as well as resonant forcing. The requirement is that L_D become null (in addition to the assumption $\tilde{\Omega} = 0$). For example, let $L_V = 1/\tilde{c}_e^2$, assume no dissipation ($L_{\tilde{\alpha}_d}$ and $L_{\tilde{\alpha}_r}$ are null), and define the horizontal wavenumber $\tilde{\kappa} = (n(n+1))^{1/2}$. In this case, the operators $L_{\tilde{p}}$, $L_{\tilde{\mathfrak{D}}}$ applied to a spherical harmonic of degree n are null if the phase speed

$$\frac{\tilde{\omega}}{\tilde{\kappa}} = \tilde{c}_e, \tag{6.1.4}$$

which describes the condition for free gravity-wave oscillations in the nonrotating, dissipation-free fluid.

If instead of $\tilde{\Omega} = 0$, we assume only $\tilde{\Omega} << \tilde{\omega}$, the condition (6.1.4) is replaced with

$$\frac{\left(\tilde{\omega}\left(\tilde{\omega} - s\tilde{\Omega}\right)\right)^{1/2}}{\kappa} = \tilde{c}_e, \tag{6.1.5}$$

which describes the condition for gravity waves weakly modified by rotation.

When trying to determine the conditions for resonant forcing, the diagonality of the governing operator matrices requires that in the solution all of the parameters $\tilde{\omega}$, s, and κ follow that of the forcing. The question of resonant forcing then reduces to determining what value $\tilde{c}_e$ satisfies (6.1.4, or 6.1.5). In the example where $\tilde{c}_e = (gh)^{1/2}$ this can be further reduced to determining what fluid thicknesses h will result in a resonantly amplified response. One can also see from (6.1.5) that the first effects of weak rotation are to decrease the resonant $\tilde{c}_e$ values.

Examples on Earth of a near gravity-wave response to forcing (or initial conditions) include ocean swell and tsunamis. Both of these have frequencies much higher than the rotation rate as well as wavelengths longer than the ocean depth. As we add rotation, energy is scattered between spatial scales and the resonant $\tilde{c}_e$ is decreased.

6.2. Rossby Wave Response

Consider again the case of no dissipation ($L_{\tilde{\alpha}_d}$ and $L_{\tilde{\alpha}_r}$ are null). The suboperators L_A and L_B become null if

$$\tilde{\omega} = -\frac{s\tilde{\Omega}}{n(n+1)}, \tag{6.2.1}$$

which is the condition for the so-called Class II oscillations. In Table 1, we show the frequency $\tilde{\omega}$ required (given s and n) for (6.2.1) to be satisfied, where it is also assumed that the scaling frequency Ω_s has been chosen to be equal to the rotation rate Ω such that $\tilde{\Omega} = 1$.

	$s=1$	$s=2$	$s=3$	$s=4$	$s=5$	$s=6$	$s=7$	$s=8$	$s=9$	$s=10$
$n=1$	0.5000									
$n=2$	0.1667	0.3333								
$n=3$	0.08333	0.1667	0.2500							
$n=4$	0.05000	0.1000	0.1500	0.2000						
$n=5$	0.03333	0.06667	0.1000	0.1333	0.1667					
$n=6$	0.02381	0.04762	0.07143	0.09524	0.1190	0.1428				
$n=7$	0.01786	0.03571	0.05357	0.07143	0.08928	0.1071	0.1250			
$n=8$	0.01389	0.02778	0.04167	0.05555	0.06944	0.08333	0.09722	0.1111		
$n=9$	0.01111	0.02222	0.03333	0.04444	0.05556	0.06667	0.07778	0.08889	0.1000	
$n=10$	0.009091	0.01818	0.02727	0.03636	0.04545	0.05454	0.06363	0.07272	0.08181	0.09090

TABLE 1. The retrograde frequency (i.e. $-\tilde{\omega}$) required for the Class II oscillations of degree n and order s (assuming $\tilde{\Omega}=1$).

If L_B is null then it can be shown that because of the L_B^{-1} suboperators in $L_{\tilde{p}}$ and $L_{\tilde{\mathfrak{D}}}$, $\tilde{p}$ and $\tilde{\mathfrak{D}}$ must vanish, while

$$L_{\tilde{\mathfrak{R}}} = \left[L_L^{-1} L_C\right] \tag{6.2.2}$$

and therefore only rotational (horizontally nondivergent) flow can be forced.

In CITELH, where a more restricted form of the governing equations is used, this limit is obtained alternatively in the limit of vanishing Lamb number. In the more general treatment here, this can be understood as the limit where L_V^{-1} becomes null.

6.3. Creeping Flow Response

In some applications (e.g. a magma ocean, as in [Tyler et al., 2015]), dissipation may be very strong, and rather than assuming $L_{\tilde{\alpha}_d}$ and $L_{\tilde{\alpha}_r}$ are null, it may make more sense to assume $L_{\tilde{\alpha}_d}^{-1}$ and $L_{\tilde{\alpha}_r}^{-1}$ are null (or approximately so). In this latter case,

$$L_{\tilde{p}} = \left[i\tilde{\omega} L_L^{-1} L_{\tilde{\alpha}_d} L_V\right], \tag{6.3.1}$$

$$L_{\tilde{\mathfrak{D}}} = \left[i L_{\tilde{\alpha}_d}\right], \tag{6.3.2}$$

and one can also show (similar to preceding examples) that the flow is irrotational (i. e. $\tilde{\mathfrak{R}}$ vanishes).

6.4. Quasi-Static (Equilibrium Tide) Response

Consider the case now where L_V becomes null. We have

$$L_{\tilde{p}} = I, \tag{6.4.1}$$

which, by (4.2.26), and assuming here $Q^s_{\tilde{p},n}=0$, indicates the equilibrium solution $\mathbf{p^s_n} = \mathbf{G^s_n}$ and consequently $\tilde{p} = \tilde{\mathfrak{G}}$.

One can also show that because both $L_{\tilde{\mathfrak{D}}}$ and $L_{\tilde{\mathfrak{R}}}$ retain suboperators L_V^{-1}, $\tilde{\mathfrak{D}}$ and $\tilde{\mathfrak{R}}$ must vanish. That is, in the equilibrium tide approximation, the flow velocity is vanishingly weak.

CHAPTER 7

Applications

7.1. Nonsynchronous–Rapid Rotation

Perhaps the simplest tidal case to first consider is that of a two-body system where the body experiencing the tides rotates rapidly relative to the mean motion of the tide-raising, second body. Assuming the eccentricity e is small, the tidal forces associated with the eccentricity can be neglected in this case because the zeroth-order term (in the expansion parameter e) of the tidal potential does not vanish—as it does in the synchronous rotation case, for example. We are then considering here a circular orbit with small obliquity and rotation rate much faster than the orbital rate ($|\tilde{\Omega}| >> |\tilde{\Omega}_o|$). Without this approximation, the forcing frequency $\tilde{\omega}$ becomes a free parameter which adds a new dimension to the solution domain which we will explore in Section 7.2. As it turns out, the approximation is a pretty good one for many applications.

In this case, the tidal potential (2.1.21) is approximately

$$
\begin{aligned}
(7.1.1) \qquad \Phi_2 = & -\frac{GM_p}{d_0}\left(\frac{r_0}{d_0}\right)^2\left(\frac{r}{r_0}\right)^2\{ \\
& -\frac{1}{2}P_2^0\left(\cos\left(\theta\right)\right) \\
& +\frac{1}{4}\left(\frac{1}{2}\mathrm{e}^{i(2\phi-\{2\Omega\}t)}+\frac{1}{2}\mathrm{e}^{-i(2\phi-\{2\Omega\}t)}\right)P_2^2\left(\cos\left(\theta\right)\right) \\
& +\delta\left(\frac{1}{2}\mathrm{e}^{i(\phi-\{-\Omega\}t+\lambda_o)}+\frac{1}{2}\mathrm{e}^{-i(\phi-\{-\Omega\}t+\lambda_o)}\right)P_2^1\left(\cos\left(\theta\right)\right) \\
& \},
\end{aligned}
$$

where we see there are no longer any terms dependent on the eccentricity parameter e. There is a term dependent on the obliquity parameter δ that remains as it is the leading term at that frequency (i. e. $\{-\Omega\}$). The P_2^0 term is independent of time and therefore does no work.

This limiting case $|\Omega_o| << |\Omega|$ is useful in that the forcing frequencies depend then only on the rotation rate. Note also that the factors preceding the large curly brackets are constant on a spherical surface and therefore act only as scaling factors when solving the horizontal balance equations. Nondimensionalized forms of the forces can then be considered generically and the solutions obtained can be re-scaled appropriately for any specific application. The goal in this section is not a specific application but rather to describe generically the full range of tidal response behaviors permitted under this assumed tidal forcing. Hence, the force parameters are set but the fluid response parameters are treated as free parameters that must be explored over the full range of response behaviors.

Specifically, we choose the forcing potential to be $\mathfrak{G} = -\Phi_2$ and treat the P_2^2 and P_2^1 terms in (7.1.1) separately. When considering the P_2^2 term, we nondimensionalize $\mathfrak{G}$ using the scaling factor

$$
(7.1.2) \qquad G_s = \frac{GM_p}{d_0}\left(\frac{r_0}{d_0}\right)^2\left(\frac{r}{r_0}\right)^2\left(\frac{1}{4}\right)\left(\left|P_2^2\left(\cos\theta\right)\right|\right),
$$

while when considering the P_2^1 term we choose

$$
(7.1.3) \qquad G_s = \frac{GM_p}{d_0}\left(\frac{r_0}{d_0}\right)^2\left(\frac{r}{r_0}\right)^2(\delta)\left(\left|P_2^1\left(\cos\theta\right)\right|\right),
$$

where the factors in vertical bars indicate the maximum absolute value of the Associated Legendre function taken over the range of colatitudes. With these choices, $\tilde{\mathfrak{G}}$ has unit amplitude, as does $\tilde{p}$ in the case of an equilibrium-tide solution.

symmetric			asymmetric		
8.9855736e-02	2.2953422e-04	6.0256838e-05	4.2009958e-02	2.1899082e-04	5.8813980e-05
2.4193812e-02	2.0915740e-04	5.7422329e-05	1.5687197e-02	1.9997162e-04	5.6079491e-05
1.0981751e-02	1.9137785e-04	5.4783209e-05	8.1113419e-03	1.8332630e-04	5.3531356e-05
6.2334673e-03	1.7577229e-04	5.2321925e-05	4.9386410e-03	1.6867567e-04	5.1153020e-05
4.0085215e-03	1.6200024e-04	5.0022851e-05	3.3180975e-03	1.5571333e-04	4.8929724e-05
2.7916320e-03	1.4978537e-04	4.7872040e-05	2.3810805e-03	1.4418955e-04	4.6848282e-05
2.0547785e-03	1.3890150e-04	4.5857015e-05	1.7911729e-03	1.3389908e-04	4.4896877e-05
1.5751832e-03	1.2916208e-04	4.3966580e-05	1.3960024e-03	1.2467204e-04	4.3064900e-05
1.2457226e-03	1.2041210e-04	4.2190674e-05	1.1184500e-03	1.1636680e-04	4.1342800e-05
1.0097194e-03	1.1252197e-04	4.0520229e-05	9.1609816e-04	1.0886456e-04	3.9721964e-05
8.3491228e-04	1.0538260e-04	3.8947057e-05	7.6405405e-04	1.0206505e-04	3.8194605e-05
7.0184395e-04	9.8901705e-05	3.7463749e-05	6.4693034e-04	9.5883166e-05	3.6753671e-05
5.9821564e-04	9.3000727e-05	3.6063591e-05	5.5480106e-04	9.0246326e-05	3.5392764e-05
5.1594497e-04	8.7612492e-05	3.4740481e-05	4.8103101e-04	8.5092290e-05	3.4106064e-05
4.4954356e-04	8.2679277e-05	3.3488868e-05	4.2104861e-04	8.0367460e-05	3.2888274e-05
3.9517872e-04	7.8151258e-05	3.2303693e-05	3.7162116e-04	7.6025472e-05	3.1734560e-05
3.5010842e-04	7.3985249e-05	3.1180335e-05	3.3041055e-04	7.2026059e-05	3.0640503e-05
3.1232907e-04	7.0143666e-05	3.0114570e-05	2.9569186e-04	6.8334109e-05	2.9602062e-05
2.8034915e-04	6.6593679e-05	2.9102526e-05	2.6617007e-04	6.4918899e-05	2.8615528e-05
2.5303987e-04	6.3306508e-05	2.8140653e-05	2.4085761e-04	6.1753446e-05	2.7677500e-05

TABLE 1. The first 60 symmetric and asymmetric eigenvalues for (rapid rotation) parameters and $N = 120$.

In terms of the coefficient vector $\mathbf{G}^{\mathbf{s}}_{\mathbf{n}}$ needed to force the governing equation (e.g. 4.2.26), this unit-amplitude normalization is given by assigning the non-zero value $\mathbf{G}^{\mathbf{s}}_{\mathbf{n}}(n_F - s_F + 1) = -i/\left(2|P^{s_F}_{n_F}(\cos\theta)\,|\right)$, where $(n_F - s_F + 1)$ is the index of the vector element, with n_F, s_F the degree and order of the forcing term considered. The vector elements of $\mathbf{Q}^{\mathbf{s}}_{\tilde{\mathbf{p}},\mathbf{n}}$ (as well as $\mathbf{K}^{\mathbf{s}}_{\mathbf{n}}$, $\mathbf{d}^{\mathbf{s}}_{\mathbf{n}}$, $\mathbf{e}^{\mathbf{s}}_{\mathbf{n}}$ on which it depends through (4.2.29)) are all zero as we are only considering the tidal force.

The frequency $\tilde{\omega}$ is now set by the forcing term in (7.1.1) considered ($\tilde{\omega} = -1$ in the sectoral (P^2_2) case, and $\tilde{\omega} = -1/2$ in the tesseral (P^1_2) case) but there remain other parameters controlling the fluid response to be chosen. These parameters are ultimately coded in the operators $L_{\tilde{\alpha}_d}$, $L_{\tilde{\alpha}_r}$, L_V, or more specifically their matrix representations $L_{\tilde{\alpha}_d}$, $L_{\tilde{\alpha}_r}$, L_V, which from Table 2 we see require specification of the parameters $\tilde{\alpha}_{d,b}$, $\tilde{\alpha}_{r,b}$, and the slowness vector $\left(\tilde{\nu}^2\right)^s_n$. There are also two methodological parameters to choose: Ω_s (the scaling factor to nondimensionalize Ω) and N (the number of spherical-harmonic terms in the expansion.) We choose $\Omega_s = \Omega$, and $N = 500$ in this and all following applications to be discussed. Next, we describe several cases involving different assumptions on the parameters $\tilde{\alpha}_{d,b}$, $\tilde{\alpha}_{r,b}$, $\left(\tilde{\nu}^2\right)^s_n$.

7.1.1. Eigenvalues.

7.1.2. Dissipation of Kinetic Energy. We first consider the case where the average dissipation rate (per unit volume) is proportional to the average kinetic energy (per unit volume). This is attained by specifying $\tilde{\alpha}_{d,0} = \tilde{\alpha}_{r,0} = \tilde{\alpha}_0$, and $\tilde{\nu}^2 = 1/\tilde{c}^2_e$. In this case, the tidal response has only two input parameters, which we conveniently present as the squared wave speed $\tilde{c}^2_e$ and the dissipation time scale $\tilde{T} = (\tilde{\alpha}_0)^{-1}|\tilde{\omega}|$. We consider these to be two independent degrees of freedom controlling the tidal response and consider ranges in these parameters to completely cover the space of solution behaviors. Hence, $\tilde{c}^2_e$ and $\tilde{T}$ can be regarded as the coordinates of a parameter space describing the solution domain. Solution components can be plotted as a function of $\tilde{c}^2_e$ and $\tilde{T}$. For each of the two tidal force components in this example, 563124 tidal-response solutions were calculated (using `tropf.m`) to resolve the solution behavior seen in the parameter space. The ranges for $\tilde{c}^2_e$ and $\tilde{T}$ were chosen not through plausibility consideration for any specific application but rather to cover the full range of tidal response behaviors the governing equations permit.

symmetric			asymmetric		
3.7584906e-02	1.5927870e-04	4.2296217e-05	1.5263228e-02	-1.4838821e-04	-4.1634775e-05
-1.0791703e-02	-1.4838821e-04	-4.1634775e-05	-1.0791978e-02	1.4749385e-04	4.0638067e-05
8.0986251e-03	1.3696982e-04	3.9075541e-05	4.9829481e-03	1.2753302e-04	3.7601425e-05
3.3650696e-03	-1.2022874e-04	-3.7138882e-05	-2.9216440e-03	-1.2022874e-04	-3.7138882e-05
-2.9216440e-03	1.1903872e-04	3.6209173e-05	2.4216344e-03	1.1136547e-04	3.4892834e-05
1.8247906e-03	1.0441080e-04	3.3646989e-05	1.4237640e-03	-9.9383578e-05	-3.3333689e-05
-1.3197428e-03	-9.9383578e-05	-3.3333689e-05	-1.3197428e-03	9.8087709e-05	3.2466692e-05
1.1415373e-03	9.2321999e-05	3.1347424e-05	9.3549512e-04	8.7050038e-05	3.0285051e-05
7.8052622e-04	-8.3523230e-05	-3.0084645e-05	-7.4667652e-04	-8.3523230e-05	-3.0084645e-05
-7.4667652e-04	8.2217026e-05	2.9275780e-05	6.6106321e-04	7.7775558e-05	2.8316130e-05
5.6704260e-04	7.3684460e-05	2.7402902e-05	4.9172650e-04	-7.1176624e-05	-2.7288432e-05
-4.7916955e-04	-7.1176624e-05	-2.7288432e-05	-4.7916955e-04	6.9907831e-05	2.6533148e-05
4.3046682e-04	6.6414250e-05	2.5704154e-05	3.7997360e-04	6.3176127e-05	2.4913411e-05
3.3786548e-04	-6.1377774e-05	-2.4864657e-05	-3.3324884e-04	-6.1377774e-05	-2.4864657e-05
-3.3324884e-04	6.0169152e-05	2.4158601e-05	3.0238451e-04	5.7371839e-05	2.3437581e-05
2.7221022e-04	5.4765142e-05	-2.2750004e-05	2.4633522e-04	-5.3471143e-05	-2.2750004e-05
-2.4505471e-04	-5.3471143e-05	2.2748362e-05	-2.4505471e-04	5.2332129e-05	2.2089103e-05
2.2398021e-04	5.0057708e-05	2.1458092e-05	2.0453473e-04	4.7928389e-05	-2.0894059e-05
-1.8772900e-04	-4.6999203e-05	-2.0894059e-05	-1.8772900e-04	-4.6999203e-05	2.0853737e-05
1.8751509e-04	4.5932088e-05	2.0274558e-05	1.7253407e-04	4.4057954e-05	1.9719176e-05

TABLE 2. The first 60 symmetric and asymmetric eigenvalues for Jupiter parameters and $N = 1500$

The solution component we first describe is the tidal power $\tilde{\mathcal{P}}$, which by assumption is equivalent to the average of either the work $\tilde{W}$ or dissipation $\tilde{D}$ densities. This is an insightful place to start analyses as the tidal power provides a description of the rate at which spin/orbit energy is transferred to the fluid (and ultimately dissipative heat). High-power tidal solutions are typically the most interesting. Note that $\tilde{\mathcal{P}}$ (when dimensionalized) is a volumetric density. An even better initial diagnostic describing the total power would be $\tilde{\mathcal{P}}$ integrated through the thickness of the fluid layer to obtain the average power per unit surface area (i.e. the total power divided by the global surface area). In general, this requires additional, application-specific assumptions. But for the class of thin-shell, hydrostatic fluids (oceans are a common example) where the wave speed is non-dispersive and given by the shallow-water wave speed, $c_e^2 = gh$, the fluid thickness h is proportional to c_e^2 and therefore $\tilde{c}_e^2$. Hence the nondimensional average power per surface area is described by the product $\tilde{c}_e^2\bar{\tilde{\mathcal{P}}}$.

The function `tropf.m` returns not only the coefficient vectors for the solution variables but also the spatiotemporal averaged work and dissipation densities $\bar{\tilde{W}}$, $\bar{\tilde{D}}$. We first confirm that $\bar{\tilde{W}}$ and $\bar{\tilde{D}}$ are equivalent. The maximum difference between these in the 563124 solutions is found to be 1.4×10^{-13} and this difference decreases as N is raised further above the $N = 500$ assumed here. This small difference (relative to the standard deviation of 2.8 seen in either) suggests that the solutions are highly accurate. Considering that the spatial distribution (and distribution with degree) of $\tilde{W}$ and $\tilde{D}$ can be quite different, the fact that their averages match so closely, and over such a large range of input parameters, would not be expected if the solutions were not highly accurate.

Note that in this specific application (where $L_{\tilde{\alpha}} \to \tilde{\alpha}_0$, and $L_V \to \tilde{\nu}^2 = 1/\tilde{c}_e^2$ such that by (3.2.4) $\tilde{\alpha}_p = 0$, and (3.3.13) becomes $\tilde{P} = 2\tilde{\alpha}_0\bar{\tilde{E}}_k$. Using the definition of $\tilde{T}$ in Table 1, we can write this further as $\tilde{P} = 2|\tilde{\omega}|\tilde{T}^{-1}\bar{\tilde{E}}_k$. Hence, the tidal power is proportional to the kinetic energy and inversely proportional to the dissipation time scale $\tilde{T}$.

In Figure 7.1.1 the space of solutions for $\tilde{\mathcal{P}}$ are shown for forcing given by the sectoral component (i.e. the term involving P_2^2 in (7.1.1)). The high-power solutions are contained in a broad ridge centered on the critically damped case ($\tilde{T} = 1$) where the dissipation and forcing time scales are equivalent. In (a) we see additionally a "picket fence" of resonance peaks associated with resonantly forced rotational-gravity waves. If

	$s=1$	$s=2$	$s=3$	$s=4$	$s=5$	$s=6$	$s=7$	$s=8$	$s=9$	$s=10$
$n=1$	0.5000									
$n=2$	0.1667	0.3333								
$n=3$	0.08333	0.1667	0.2500							
$n=4$	0.05000	0.1000	0.1500	0.2000						
$n=5$	0.03333	0.06667	0.1000	0.1333	0.1667					
$n=6$	0.02381	0.04762	0.07143	0.09524	0.1190	0.1428				
$n=7$	0.01786	0.03571	0.05357	0.07143	0.08928	0.1071	0.1250			
$n=8$	0.01389	0.02778	0.04167	0.05555	0.06944	0.08333	0.09722	0.1111		
$n=9$	0.01111	0.02222	0.03333	0.04444	0.05556	0.06667	0.07778	0.08889	0.1000	
$n=10$	0.009091	0.01818	0.02727	0.03636	0.04545	0.05454	0.06363	0.07272	0.08181	0.09090

TABLE 3. The retrograde frequency (i.e. $-\tilde{\omega}$) required for the Class II oscillations of degree n and order s.

not for the Coriolis force, there would only be one peak; rotation is responsible for scattering energy through degrees and thereby the excitation of the subharmonic resonances. The power seen in Figure 7.1.1 decreases for large (positive) $\tilde{c}_e^2$ because the wave speeds become fast enough to maintain a quasi-static adjustment and near equilibrium-tide solution. The exact equilibrium tide solution has zero associated power and so this provides the expected asymptotic behavior as $\tilde{c}_e^2 \to \infty$. As $\tilde{T}$ decreases below the critically damped case ($\tilde{T}=1$), the power $\tilde{P} = 2|\tilde{\omega}|\tilde{T}^{-1}\bar{\tilde{E}}_k$ ultimately decreases because kinetic energy $\bar{\tilde{E}}_k$ decreases more quickly than does $\tilde{T}$. As $\tilde{T}$ increases above $\tilde{T}=1$, power decreases (because of the inverse dependence on $\tilde{T}$) and the resonance peaks become more focused. Because there are vertical structures for which the squared wave speeds can be negative (the case of 'negative equivalent depths' in other literature), we include panel (b). In this case, the rotational-gravity resonances are seen to be absent for negative $\tilde{c}_e^2$, but this is not necessarily true for other forcing frequencies (as would result when we relax the assumption that $\Omega_o = 0$). This figure then provides a usefully compact description of the full range of tidal power scenarios for this assumed forcing and dissipation process.

In Figure 7.1.2 we show $\tilde{\mathcal{P}}$ for the case of the tesseral forcing component. Many of the descriptions are similar to the case for sectoral forcing just discussed. A major difference, however, is that the rotational-gravity resonances are weak relative to a broad resonance ridge associated with the excitation of Rossby waves. It is a peculiarity of the parameters in this configuration that Class II (Rossby) waves dominate the response. In this case of tesseral forcing, the parameters ($\tilde{\omega} = -1/2$, $s=1$) allow for excitation of Class II oscillations for degree $n=1$ (see Table 3). (More carefully, the description as a Class II oscillation is only valid in the inviscid limit $\tilde{T} \to \infty$.) This is then an example where the response is predominantly at a different degree than the forcing.

In Figures 7.1.3, 7.1.4, we show the product $\tilde{c}_e^2\tilde{\mathcal{P}}$, which is intended to represent the depth-integrated power as described above. This assumes that the fluid thickness is proportional to $\tilde{c}_e^2$, which is probably not tenable for any applications with negative $\tilde{c}_e^2$ and so a second panel showing the negative $\tilde{c}_e^2$ region of the parameter space is not included.

Aside from the average power density, there are other average variables that are useful for characterizing the solutions. In Figures 7.1.5 and 7.1.6, we show the kinetic- and potential- energy densities of the tidal responses due to the sectoral and tesseral force terms, respectively. These are volumetric densities (when dimensionalized, they have units of $\mathrm{J/m^3}$).

In Figures 7.1.7 and 7.1.8 we show the admittance at the forcing degree. This is equivalent to k_2 which is a complex number describing the ratio of degree-two coefficients p_2^s/G_2^s describing the response and forcing. In the cases of both sectoral and tesseral forcing, we see that for large-amplitude $\tilde{c}_e^2$, there is a section of the parameter space where the tidal response is close to the equilibrium-tide response (in which case the amplitude of k_2 is close to 1, and the phase close to zero). Over most of the parameter space, however, the solution is not close to the equilibrium tide response and can show amplitudes much larger than 1 (note in the figures that the color scale is truncated to amplitudes ≤ 1.5 for visualization) and large phase lags.

7.1.3. Dissipation of Potential Energy. Here we consider a case identical to the last (Section 7.1.2) except that we assume the average dissipation is proportional to the potential (rather than kinetic) energy density. Note that in this case, the response to the tesseral force component is a Class II oscillation for which there is no vertical motion and consequently no potential energy nor dissipation/work /power. (By contrast, the similar case in Section 7.1.2 retained dissipation.) Hence, in this section we plot the power results only for the sectoral component.

In Figure 7.1.10, we show the product $\tilde{c}_e^2\tilde{\mathcal{P}}$, which is intended to represent the depth-integrated power as described above. This assumes that the fluid thickness is proportional to $\tilde{c}_e^2$, which is probably not tenable for any applications with negative $\tilde{c}_e^2$ and so a second panel showing the negative $\tilde{c}_e^2$ region of the parameter space is not included.

Aside from the average power density, there are other average variables that are useful for characterizing the solutions. In Figure 7.1.11, we show the kinetic- and potential- energy densities of the tidal responses due to the sectoral and tesseral force terms, respectively. These are volumetric densities (when dimensionalized, they have units of $\mathrm{J/m^3}$).

In Figure 7.1.12, we show the admittance at the forcing degree. This is equivalent to k_2 which is a complex number describing the ratio of degree-two coefficients p_2^s/G_2^s describing the response and forcing.

7.1.4. Summary of Results. The first important result is that the average power is indeed a useful parameter for characterizing the tidal response of planetary fluids. This is not only because the power is itself the primary parameter of interest for many applications, including estimates of the tidal heat generated, but also because the behavior of many other parameters track that seen in the power.

The cases described show that low-power equilibrium-tide solutions are possible but only over a relatively small section of the domain of solutions. In other cases, the power can be elevated many orders of magnitude when the sectoral or tesseral tidal forces resonantly excite rotational gravity waves, or the retrograde propagating component of the tesseral force resonantly excites a Rossby wave (Class II oscillation). The power (dissipation) also shows an expected tendency to increase near critical damping ($\tilde{T} = 1$) where the forcing and dissipation time scales match.

Although the forcing is of spherical-harmonic degree 2 for all the forcing components, the tidal response includes a spectrum over degrees because of the scattering of energy to other degrees by rotation. We have described here the k_2 admittance and see that the departure of k_2 from that expected for a near-equlibrium tide solution is predicted by the same domain regions where the power is elevated.

For completeness in this initial example, we have included the solution domain extending into the region of negative $\tilde{c}_e^2$ (or negative "equivalent depth"). But the physical interpretation of these solutions is difficult outside of a specific application where the nature of negative $\tilde{c}_e^2$ is described.

7.2. Nonsynchronous–Arbitrary Rotation

In situations of either close orbits or slow rotation, the assumption $|\tilde{\Omega}| >> |\tilde{\Omega}_o|$ used in the last section may not be valid. Relaxing this assumption introduces a new free parameter, the forcing frequency $\tilde{\omega}$, increasing the dimensionality of the solution domain to 3 (over 2 in the last section). But we expect that the elevated power near critical damping is already understood. So to complete this study of tides generated under nonsynchronous rotation, let us consider here only a 2-D slice through the 3-D solution domain at a constant $\tilde{T} = 100$. The reason for assuming a highly underdamped value of $\tilde{T}$ is to retain the sharpness of the resonance peaks. This 2-D slice shall show how the locations of the resonance peaks vary with frequency $\tilde{\omega}$. To reiterate, the solution domain of interest for the general case of arbitrary rotation would have the three axes $\tilde{\omega}$, $\tilde{T}$, $\tilde{c}_e^2$. In Section 7.1 we studied a $\tilde{T}, \tilde{c}_e^2$ slice (with $\tilde{\omega}$ specified by the forcing in the limit of rapid rotation). Here, we specify $\tilde{T}$ and study a $\tilde{\omega}$, $\tilde{c}_e^2$ slice.

7.2.1. Dissipation of Kinetic Energy. We first consider the case where dissipation is proportional to kinetic energy (as in Section 7.1.2). Here, we calculate solutions for 2249124 $\tilde{\omega}$, $\tilde{c}_e^2$ combinations to sample the solution domain for each case discussed.

In Figure 7.2.1 we show $\tilde{P}(\tilde{\omega}, \tilde{c}_e^2)$ for the case of the sectoral forcing. In this case, $\tilde{\omega} = -1$ corresponds to the fast-rotation limit studied in Section 7.1; $\tilde{\omega} < -1$ corresponds to the case of the forcing body in an orbit retrograde with respect to the rotation of the forced body; and $\tilde{\omega} > 0$ corresponds to the forcing body orbiting faster than the rotation of the forced body (and in the same sense). The case $\tilde{\omega} = 0$ corresponds to synchronous rotation with power vanishing (in this case with assumed zero eccentricity.) The results show a

"picket fence" of peaks of elevated power due to resonant excitation of rotational gravity waves (as in Figure 7.1.1) but the peaks are shifted to lower $\tilde{c}_e^2$ as $|\tilde{\omega}| \to 0$. An exception is a peak (near $\tilde{\omega} = -0.17$, for large $\tilde{c}_e^2$) due to resonant excitation of a Rossby wave response.

In Figure 7.2.2 we show $\tilde{P}(\tilde{\omega}, \tilde{c}_e^2)$ for the case of the tesseral forcing. In this case, $\tilde{\omega} = -1/2$ corresponds to the fast-rotation limit studied in Section 7.1; $\tilde{\omega} < -1/2$ corresponds to the case of the forcing body in an orbit retrograde with respect to the rotation of the forced body, and $\tilde{\omega} > 0$ corresponds to the forcing body orbiting faster than the rotation of the forced body (and in the same sense). The case $\tilde{\omega} = 0$ corresponds to synchronous rotation with power vanishing (in this case assumed zero eccentricity.) The results show a "picket fence" of peaks of elevated power due to resonant excitation of rotational gravity resonances (as in Figure 7.1.2) but the peaks are shifted to lower $\tilde{c}_e^2$ as $|\tilde{\omega}| \to 0$. Exceptions are the peaks near $\tilde{\omega} = 0.50$ and 0.083 (for large $\tilde{c}_e^2$) due to resonant excitation Rossby waves.

7.2.2. Dissipation of Potential Energy. Now we consider the case identical to that in Section 7.2.1 but with dissipation proportional to potential energy rather than kinetic energy. We see the same resonance structure as in the kinetic-energy case and the description of corresponding frequency regimes is the same as that discussed in Section 7.2.1. The primary difference between the two cases is the dependence on $\tilde{c}_e^2$ and this follows the description in 7.1.

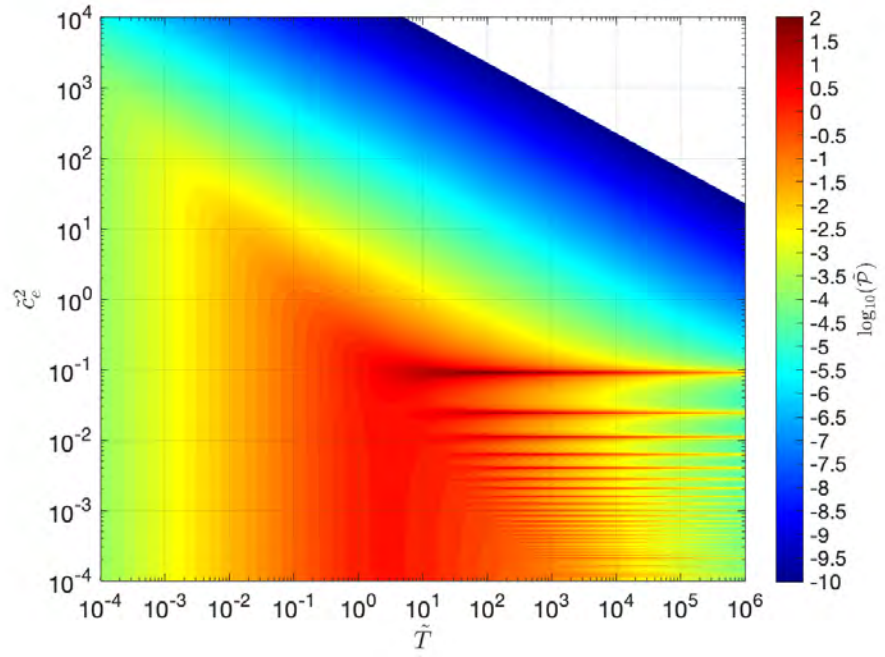

(A)

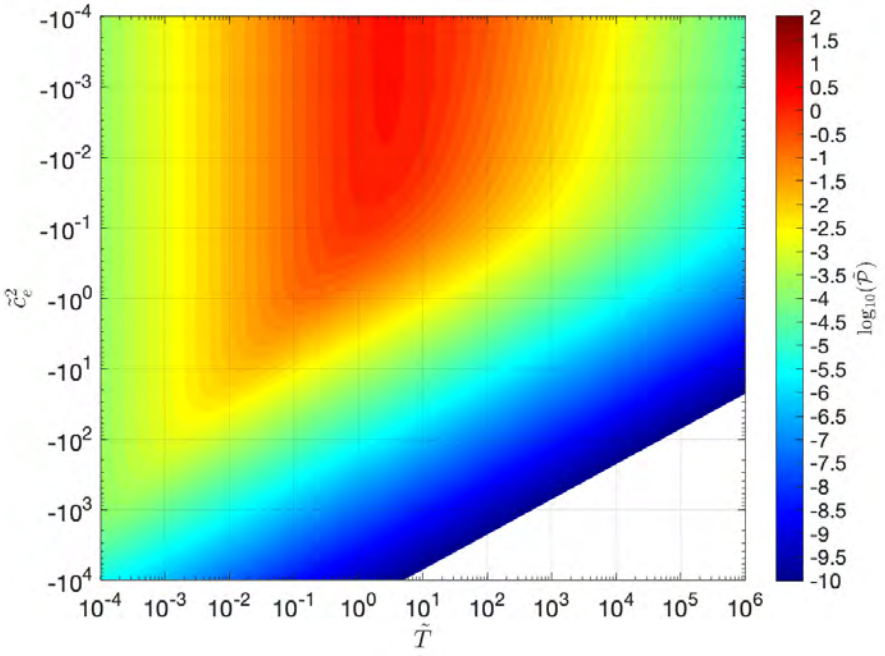

(B)

FIGURE 7.1.1. Tidal power $\tilde{\mathcal{P}}$ as a function of dissipation time scale $\tilde{T}$ and squared wave speed $\tilde{c}_e^2$ (positive (a) and negative (b) values for $\tilde{c}_e^2$ are displayed). Here $\tilde{T}$ refers to a process where dissipation is proportional to kinetic energy, and the forcing considered is the sectoral component in the nonsynchronous rapid rotation limit described in Section 7.1.2.

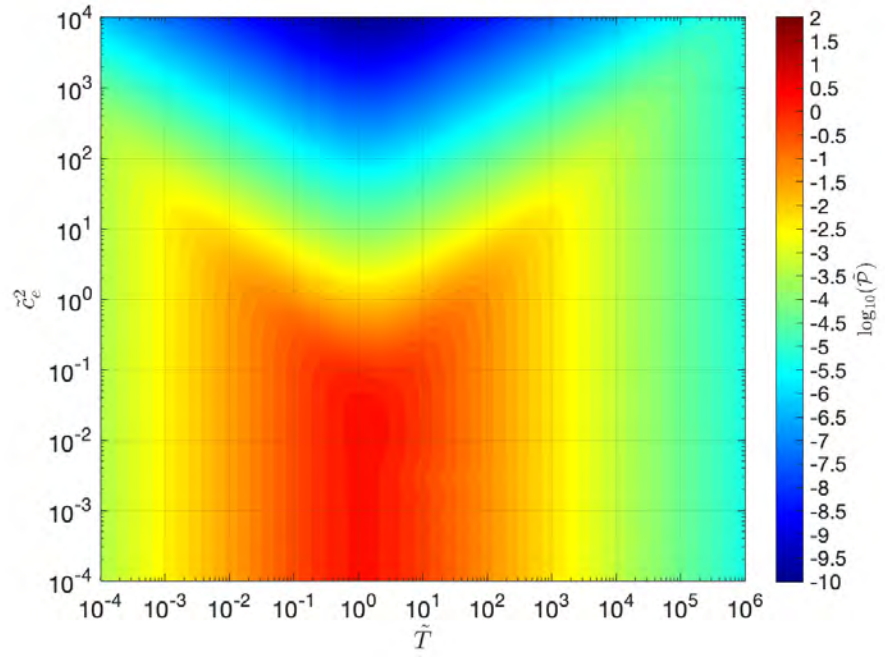

(A)

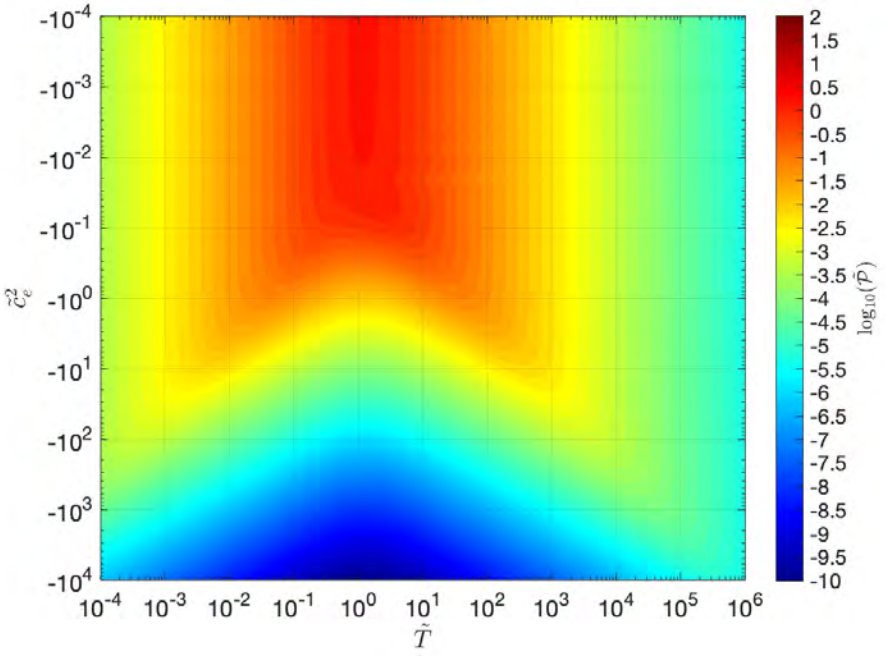

(B)

FIGURE 7.1.2. Tidal power $\tilde{\mathcal{P}}$ as a function of dissipation time scale $\tilde{T}$ and squared wave speed $\tilde{c}_e^2$. (This case is identical to that in Fig. 7.1.1 except that the tesseral tidal force potential is considered.)

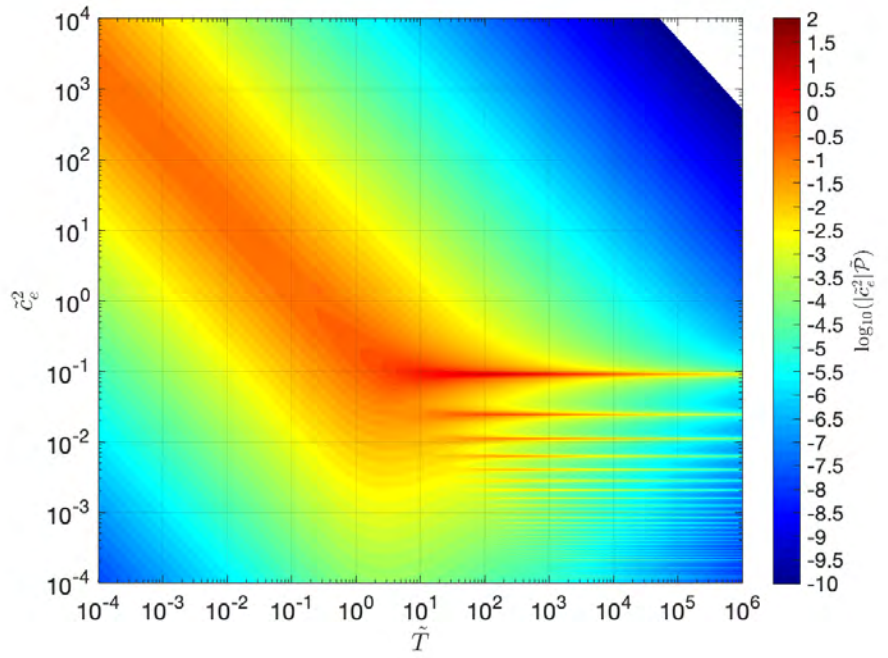

FIGURE 7.1.3. Tidal power integrated over the fluid thickness as represented by the product $\tilde{c}_e^2\tilde{\mathcal{P}}$, where $\tilde{\mathcal{P}}$ is that shown in Figure 7.1.1 (a).

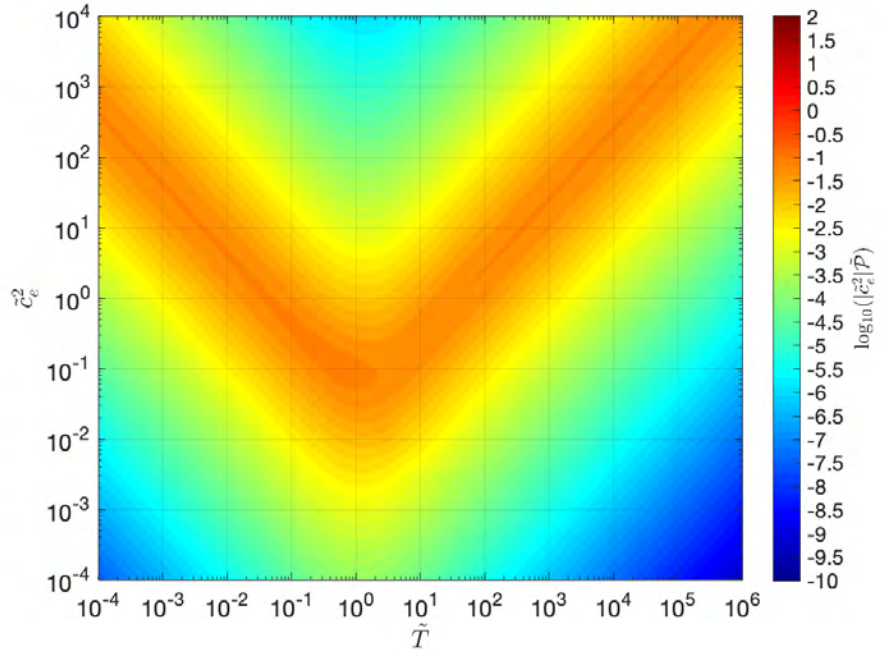

FIGURE 7.1.4. Tidal power integrated over depth as represented by the product $\tilde{c}_e^2\tilde{\mathcal{P}}$, where $\tilde{\mathcal{P}}$ is that shown in Fig. 7.1.2 (a).

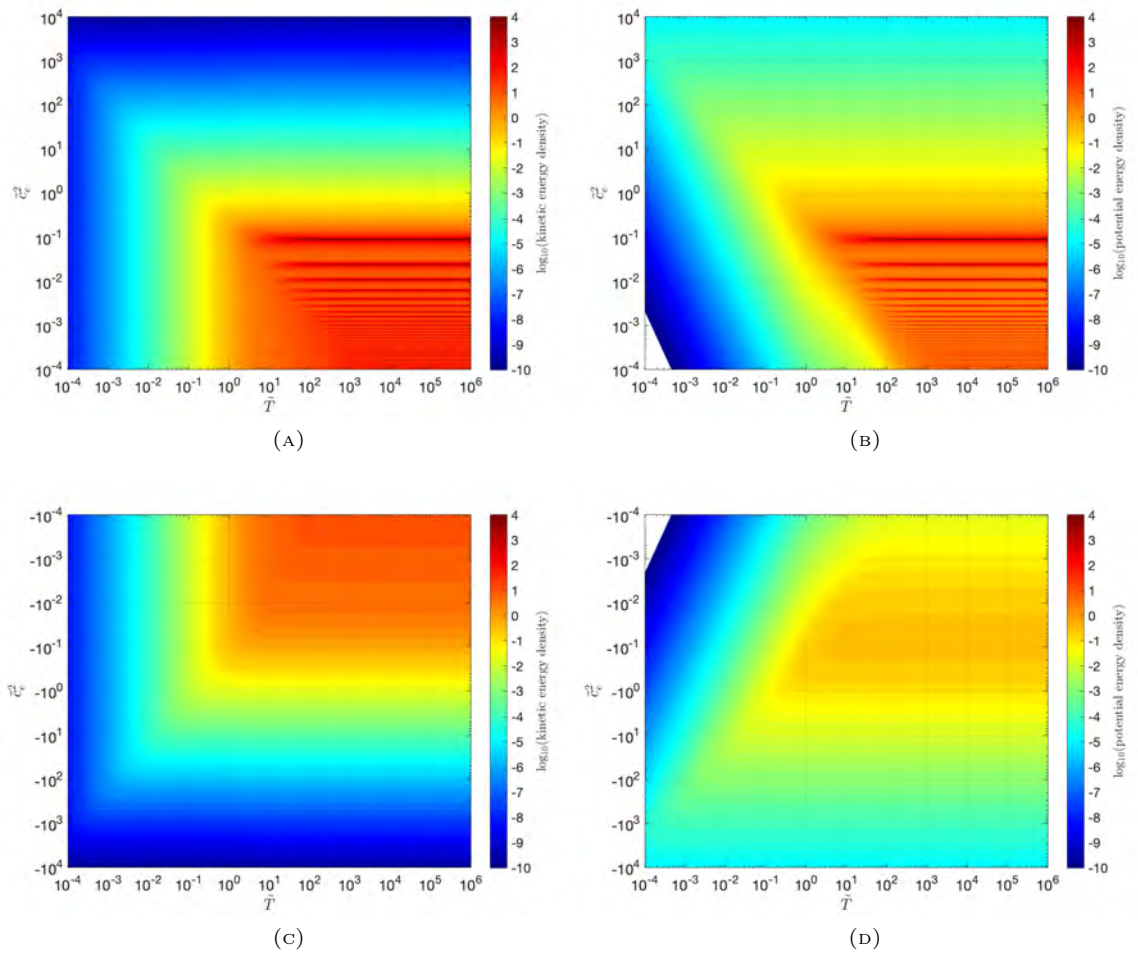

FIGURE 7.1.5. Kinetic energy density (a, c) and potential energy density (b, d) as a function of dissipation time scale $\tilde{T}$ and squared wave speed $\tilde{c}_e^2$ (positive (a) and negative (b) values for $\tilde{c}_e^2$ are displayed). Here $\tilde{T}$ refers to a process where dissipation is proportional to kinetic energy and the forcing is the sectoral component in the nonsynchronous rapid rotation limit described in Section 7.1.2.

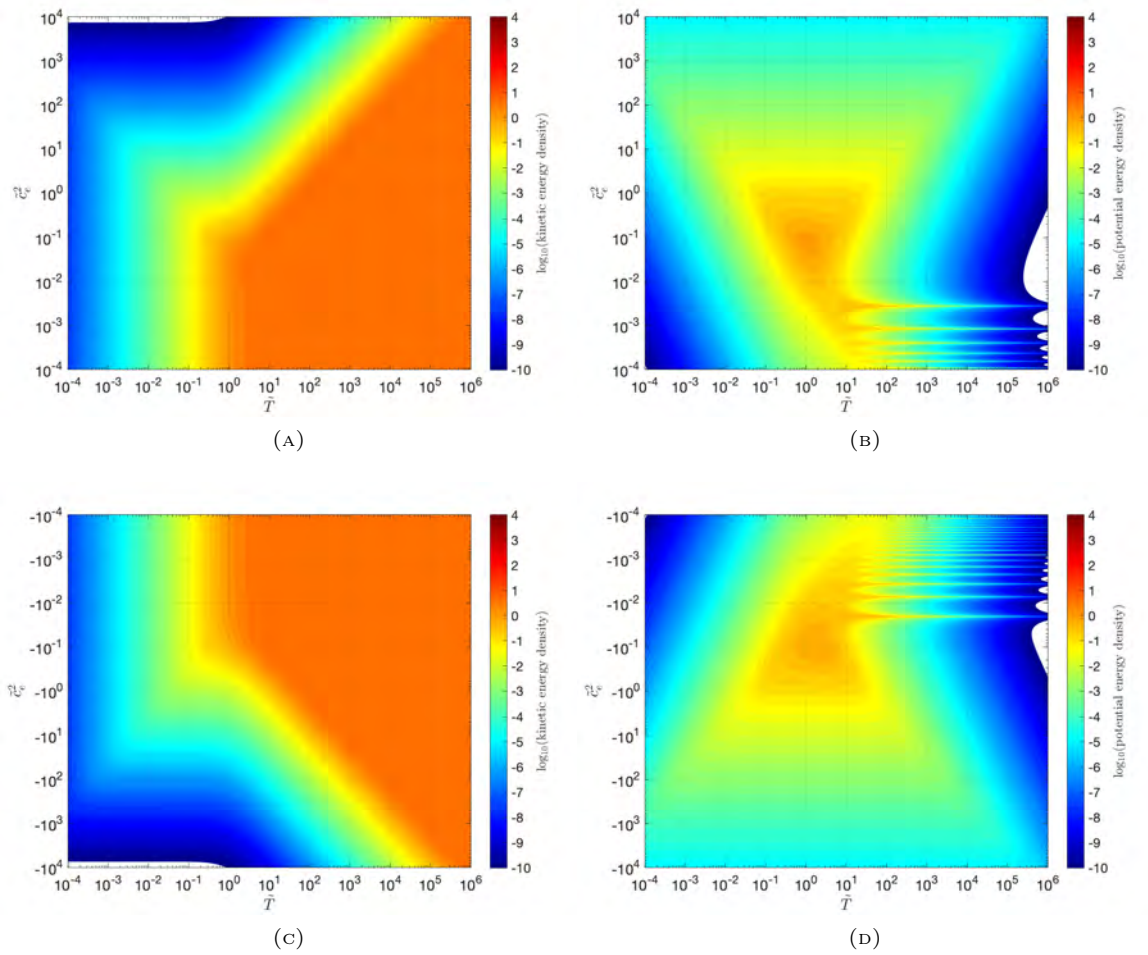

FIGURE 7.1.6. Kinetic energy density (a, c) and potential energy density (b, d) as a function of dissipation time scale $\tilde{T}$ and squared wave speed $\tilde{c}_e^2$ (positive (a, b) and negative (c, d) values for $\tilde{c}_e^2$ are displayed). Here $\tilde{T}$ refers to a process where dissipation is proportional to kinetic energy and the forcing is the tesseral component in the nonsynchronous rapid rotation limit described in Section 7.1.2.

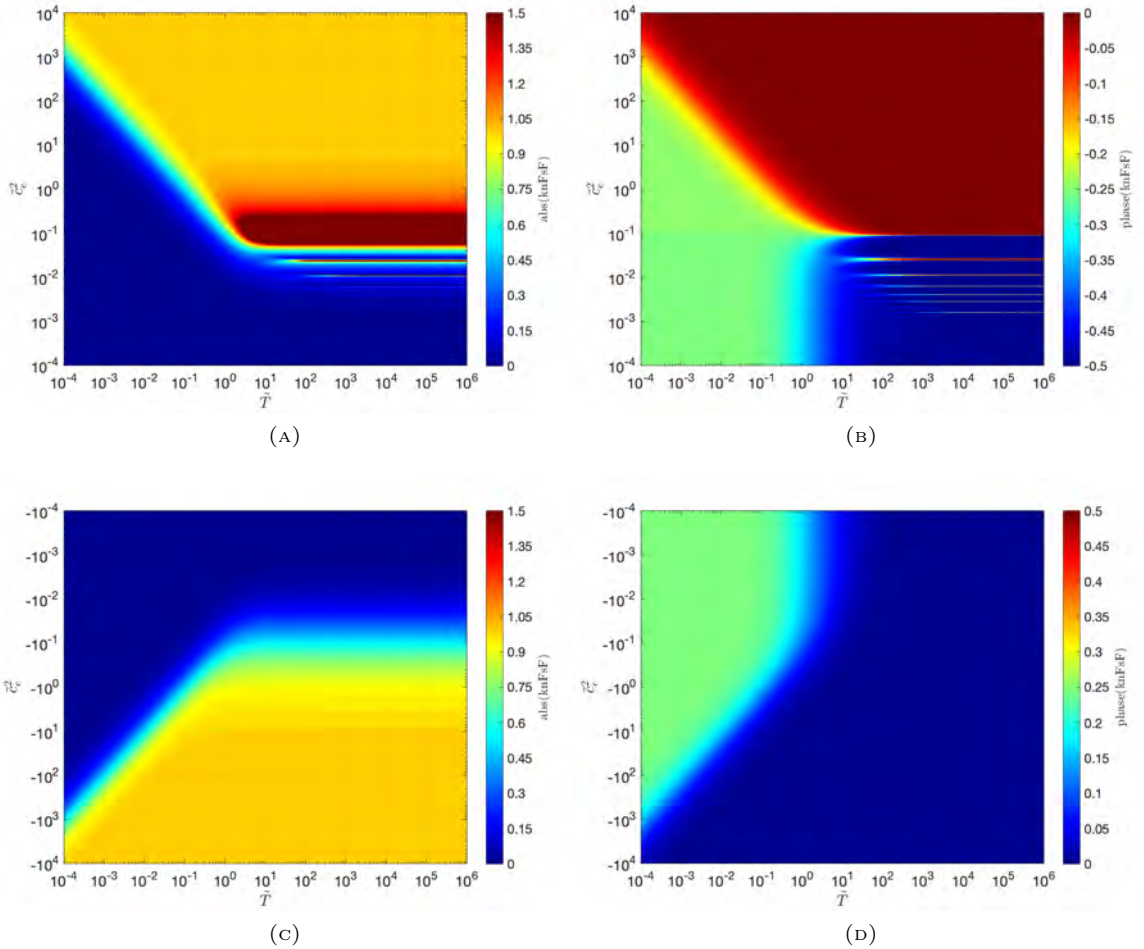

FIGURE 7.1.7. Degree-two admittance (k_2) amplitude (a, c) and phase/(2π) (b, d) as a function of dissipation time scale $\tilde{T}$ and squared wave speed $\tilde{c}_e^2$. Here $\tilde{T}$ refers to a process where dissipation is proportional to kinetic energy and the forcing is the sectoral component in the nonsynchronous rapid rotation limit described in Section 7.1.2.

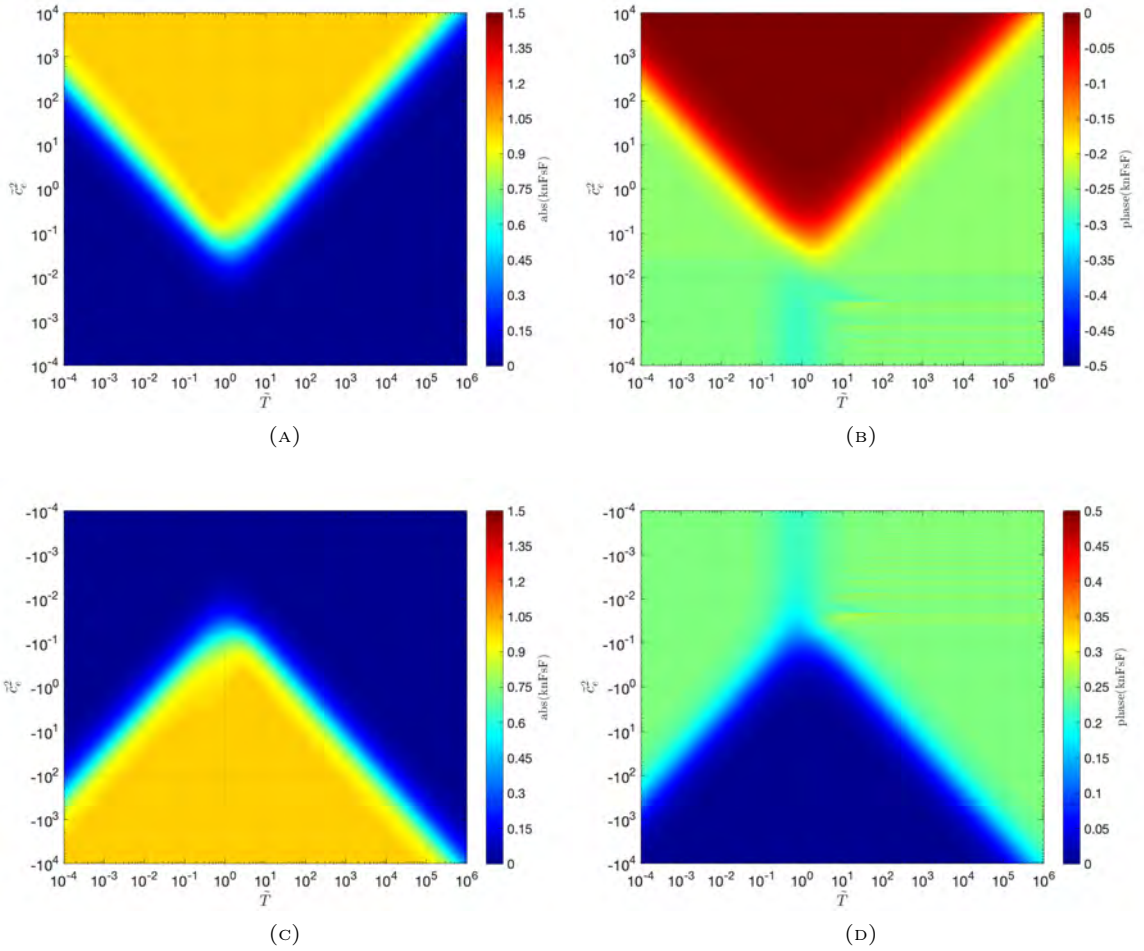

(A) (B)

(C) (D)

FIGURE 7.1.8. Degree-two admittance (k_2) amplitude (a, c) and phase/(2π) (b, d) as a function of dissipation time scale $\tilde{T}$ and squared wave speed $\tilde{c}_e^2$. Here $\tilde{T}$ refers to a process where dissipation is proportional to kinetic energy and the forcing is the tesseral component in the nonsynchronous rapid rotation limit described in Section 7.1.2.

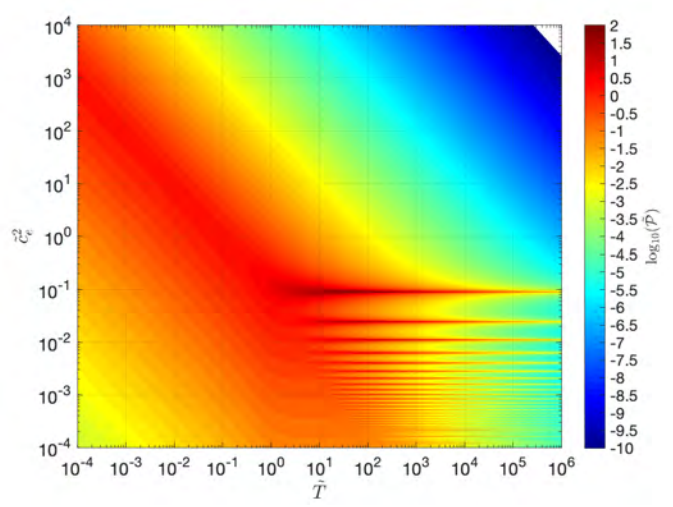

(A)

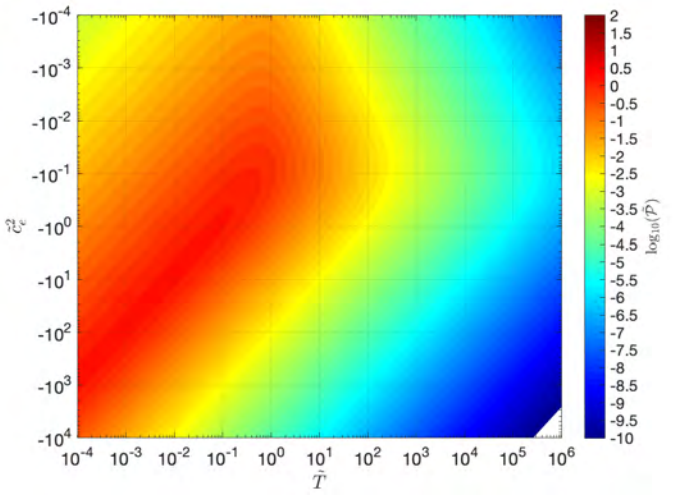

(B)

FIGURE 7.1.9. Tidal power $\tilde{\mathcal{P}}$ as a function of dissipation time scale $\tilde{T}$ and squared wave speed $\tilde{c}_e^2$ (positive (a) and negative (b) values for $\tilde{c}_e^2$ are displayed). Here $\tilde{T}$ refers to a process where dissipation is proportional to potential energy, and the forcing considered is the sectoral component in the nonsynchronous rapid rotation limit described in Section 7.1.3.

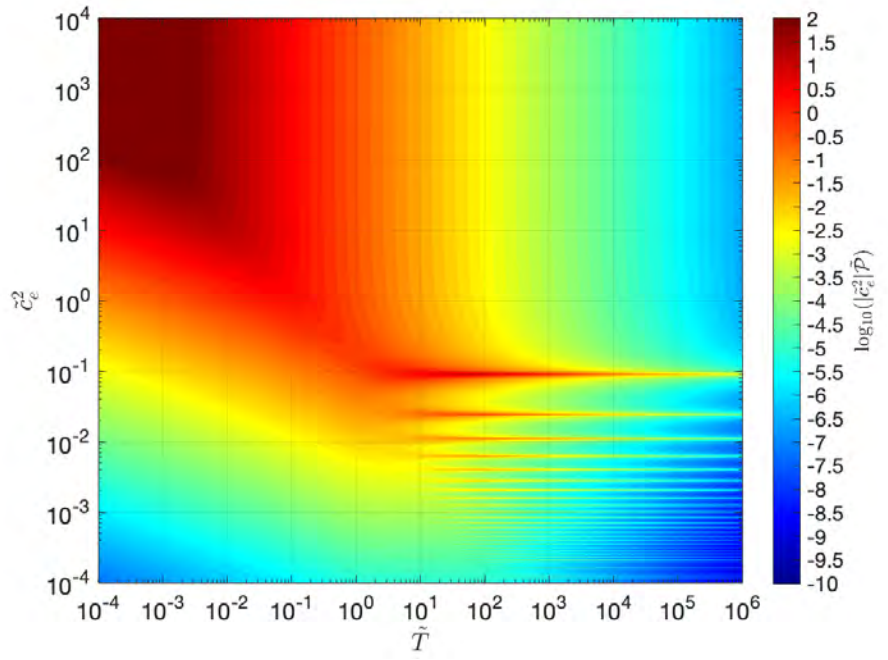

FIGURE 7.1.10. Tidal power integrated over the fluid thickness as represented by the product $\tilde{c}_e^2\tilde{\mathcal{P}}$, where $\tilde{\mathcal{P}}$ is that shown in Figure 7.1.9 (a).

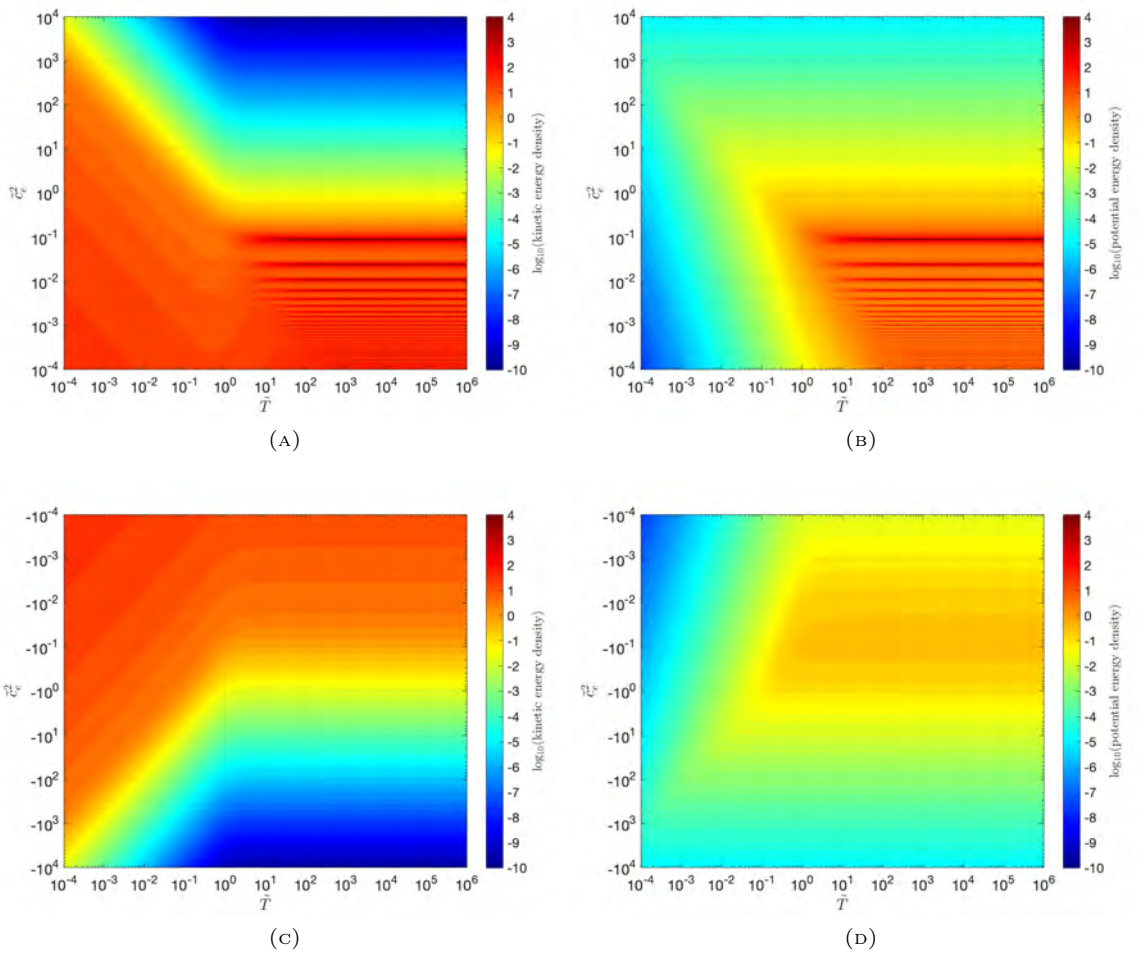

FIGURE 7.1.11. Kinetic energy density (a, c) and potential energy density (b, d) as a function of dissipation time scale $\tilde{T}$ and squared wave speed $\tilde{c}_e^2$ (positive (a, b) and negative (c, d) values for $\tilde{c}_e^2$ are displayed). Here $\tilde{T}$ refers to a process where dissipation is proportional to potential energy and the forcing is the sectoral component in the nonsynchronous rapid rotation limit described in Section 7.1.3.

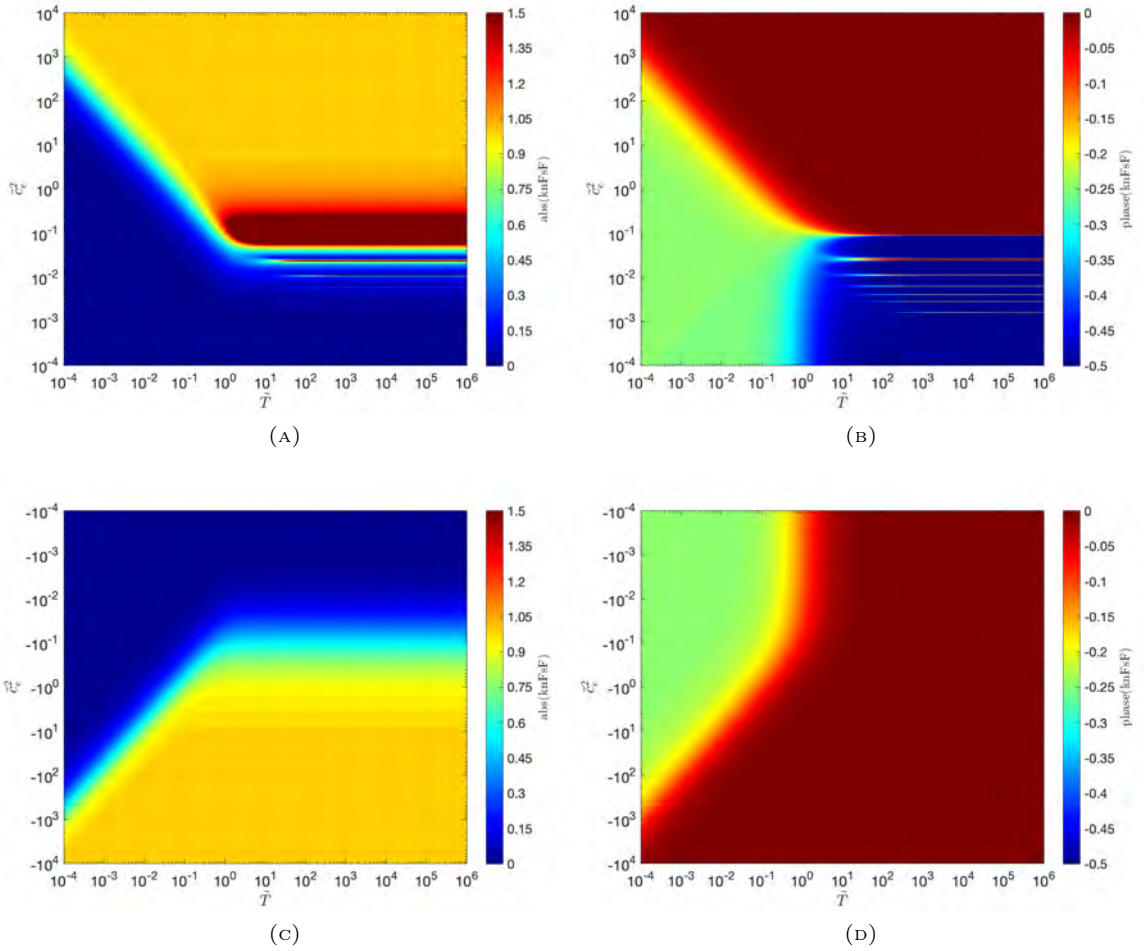

FIGURE 7.1.12. Degree-two admittance (k_2) amplitude (a, c) and phase (b, d) as a function of dissipation time scale $\tilde{T}$ and squared wave speed $\tilde{c}_e^2$. Here $\tilde{T}$ refers to a process where dissipation is proportional to potential energy and the forcing is the sectoral component in the nonsynchronous rapid rotation limit described in Section 7.1.3.

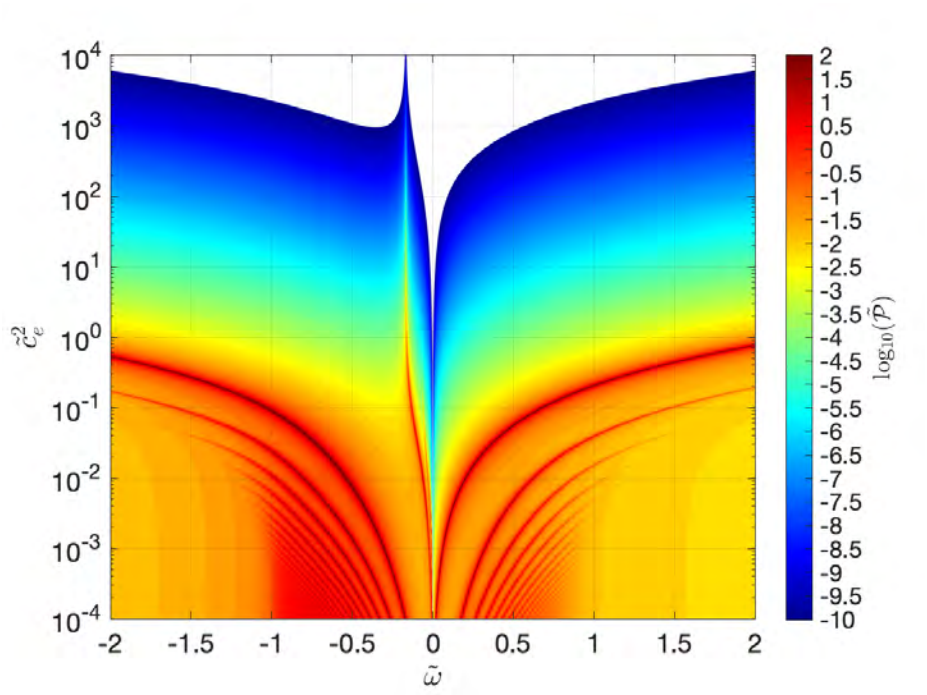

(A)

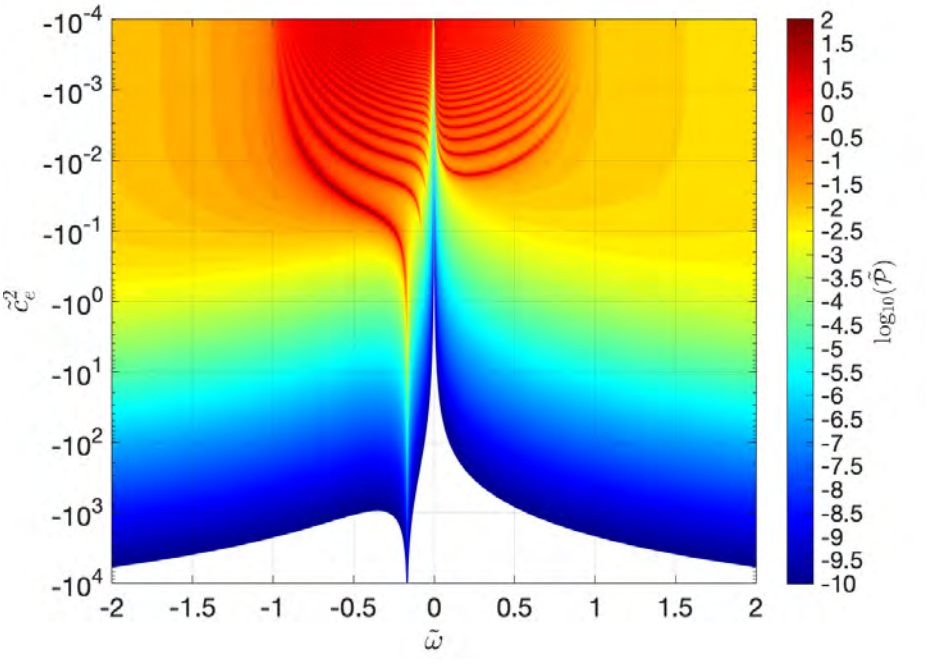

(B)

FIGURE 7.2.1. Tidal power $\tilde{\mathcal{P}}$ as a function of forcing frequency $\tilde{\omega}$ and squared wave speed $\tilde{c}_e^2$ (positive (a) and negative (b) values for $\tilde{c}_e^2$ are displayed). Here $\tilde{T}$ refers to a process where dissipation is proportional to kinetic energy (and is taken here to be $\tilde{T} = 100$), and the forcing considered is the sectoral component in the nonsynchronous arbitrary rotation case described in Section 7.2.1.

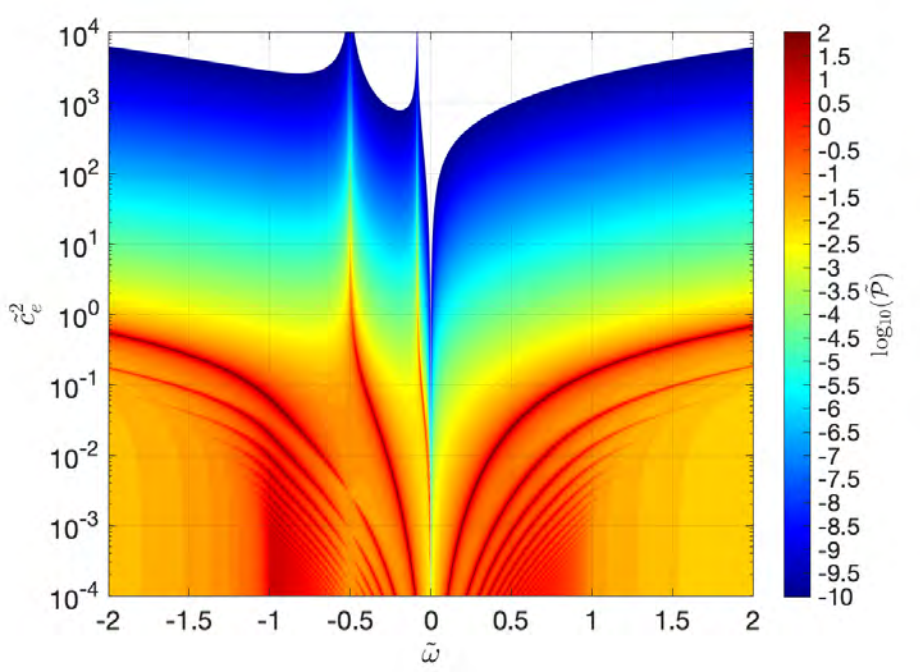

(A)

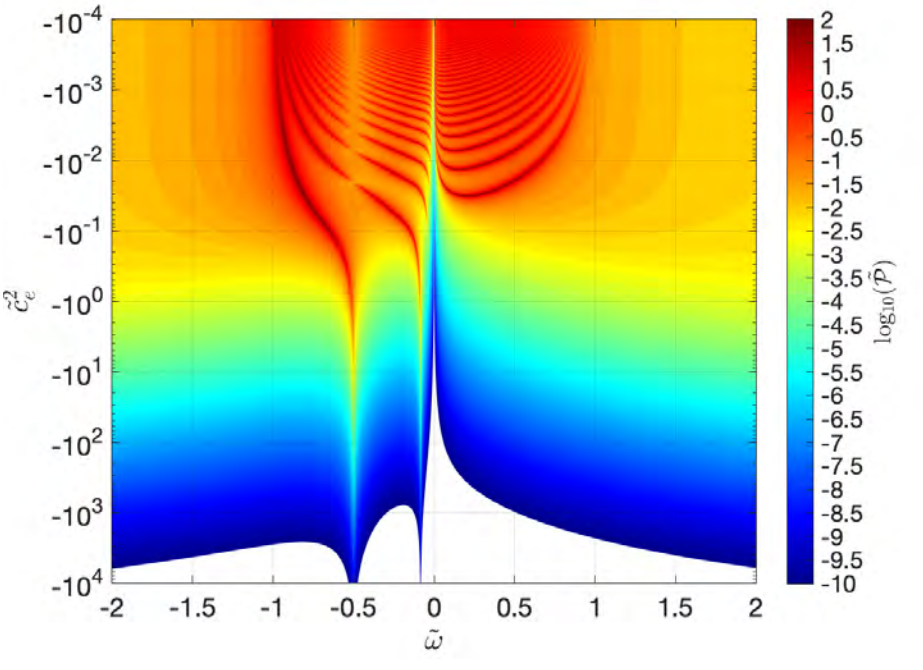

(B)

FIGURE 7.2.2. Tidal power $\tilde{\mathcal{P}}$ as a function of forcing frequency $\tilde{\omega}$ and squared wave speed $\tilde{c}_e^2$ (positive (a) and negative (b) values for $\tilde{c}_e^2$ are displayed). Here $\tilde{T}$ refers to a process where dissipation is proportional to kinetic energy (and is taken here to be $\tilde{T} = 100$), and the forcing considered is the tesseral component in the nonsynchronous arbitrary rotation case described in Section 7.2.1.

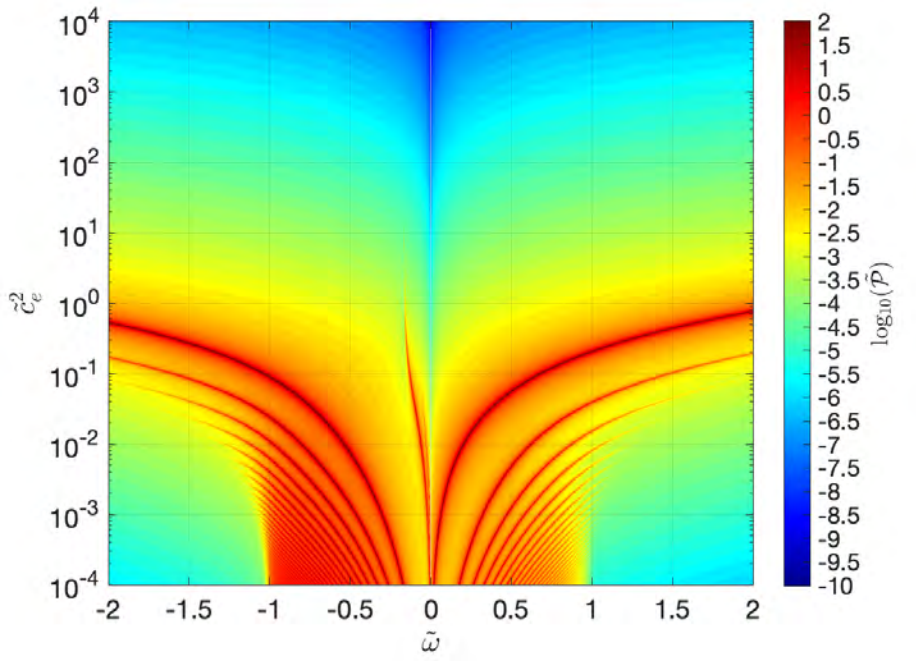

(A)

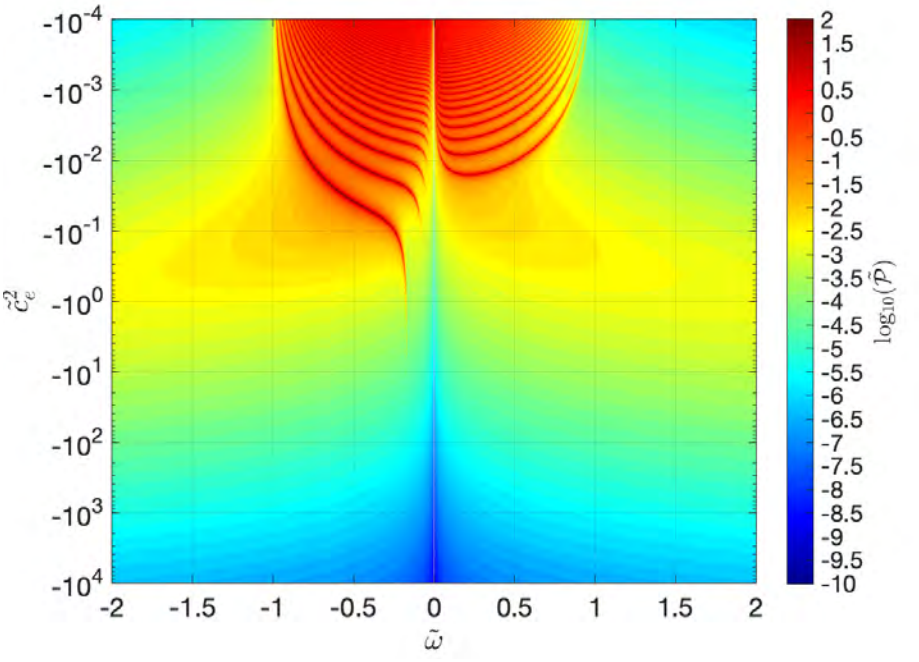

(B)

FIGURE 7.2.3. Tidal power $\tilde{\mathcal{P}}$ as a function of forcing frequency $\tilde{\omega}$ and squared wave speed $\tilde{c}_e^2$ (positive (a) and negative (b) values for $\tilde{c}_e^2$ are displayed). Here $\tilde{T}$ refers to a process where dissipation is proportional to potential energy (and is taken here to be $\tilde{T} = 100$), and the forcing considered is the sectoral component in the nonsynchronous arbitrary rotation case described in Section 7.2.2.

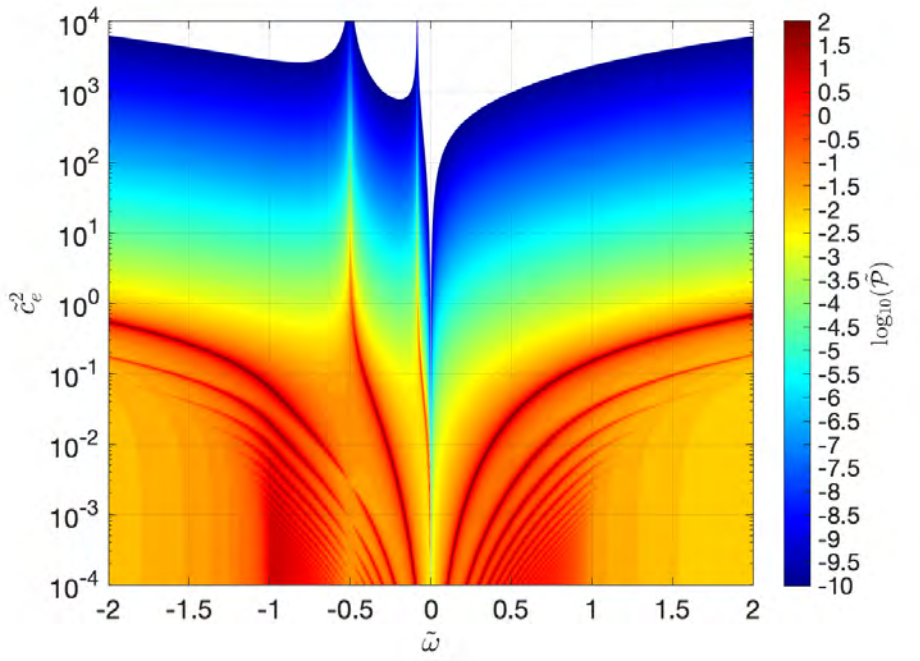

(A)

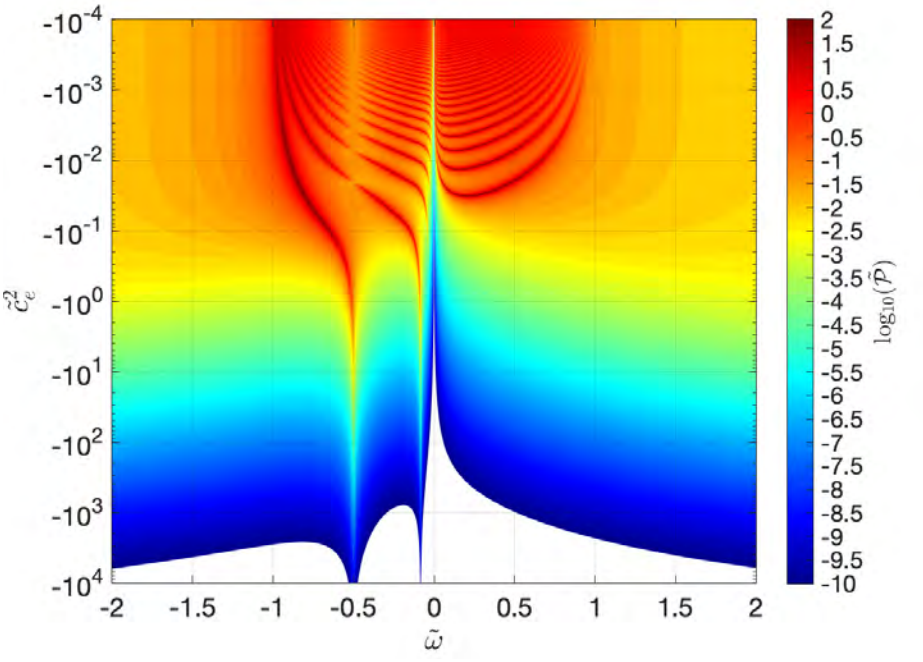

(B)

FIGURE 7.2.4. Tidal power $\tilde{\mathcal{P}}$ as a function of forcing frequency $\tilde{\omega}$ and squared wave speed $\tilde{c}_e^2$ (positive (a) and negative (b) values for $\tilde{c}_e^2$ are displayed). Here $\tilde{T}$ refers to a process where dissipation is proportional to potential energy (and is taken here to be $\tilde{T} = 100$), and the forcing considered is the tesseral component in the nonsynchronous arbitrary rotation case described in Section 7.2.

7.3. Synchronous Rotation

As described in Section 2.1.2, when the body experiencing the tide has spun down to a synchronous orbit, the zeroth-order tidal forces (i.e. zeroth order in the expansion parameter of the eccentricity e or obliquity parameter δ) vanish. Under synchronous rotation, tidal forces then involve the first-order terms—provided, as we shall assume here, that e, δ are small such that these lowest-order terms approximate these forces. These first-order tidal-potential terms are described by (2.1.23) and involve three components (G20, G22W, G22E) associated with eccentricity, and two components (G21W, G21E) associated with obliquity.

Because of the integral properties of the orthogonal spherical-harmonic functions, the average power associated with the eccentricity tidal forces can be obtained by calculating the average power of each of G20, G22W, and G22E, and then summing. Similarly, the average power due to obliquity tidal forces is obtained by summing the average power of G21W, and G21E. For a specific application where e and δ have assigned values, one may also further combine the eccentricity and obliquity average power values to get the total power. For the generic results here, however, e and δ are not assigned but rather removed through nondimensionalization. For this reason, the power domains for eccentricity and obliquity are shown separately.

Before presenting the power domains for the summed eccentricity and summed obliquity parts, we first present the results for each of G20, G22W, G22E, G21W, G21E separately. This will make clear, for example, which resonance peaks are associated with which of the five tidal forces. Furthermore, the admittances must be shown individually as there is not a sensible way of presenting them combined.

The next Section (7.3.1) provides results under the assumption that dissipation is proportional to kinetic energy. Following this, in Section 7.3.2 we provide results for the alternate assumption that dissipation is proportional to potential energy.

7.3.1. Dissipation of Kinetic Energy. Here we assume that the dissipation rate (average power density) is proportional to the kinetic energy density. We provide first the results for the individual G20, G22W, G22E, G21W, G21E components, and then the results for the total combined eccentricity components (G20 + G22W + G22E), and then the total combined obliquity components (G21W + G21E).

7.3.1.1. *Individual Components.* In Figures 7.3.1–7.3.5 we show the average tidal power of the individual components. In Figures 7.3.6–7.3.10 we show the power integrated over the fluid thickness. In Figures 7.3.12–7.3.19 we show the kinetic and potential energy densities. In Figure 7.3.20–7.3.24 we show the admittances.

7.3.1.2. *Combined Components.* In Figure we show the total average power of the eccentricity tidal forces (i.e. G20 + G22W + G22E). In Figure 7.3.26 we show the total average power for the obliquity tidal forces (i.e. G21W + G21E). In Figures 7.3.27 and 7.3.28 we show the power integrated over the fluid thickness for the total eccentricity and obliquity tidal forces, respectively.

7.3.2. Dissipation of Potential Energy. Here we assume that the dissipation rate (average power density) is proportional to the potential energy density. We provide first the results for the individual G20, G22W, G22E, G21W, G21E components, and then the results for the total combined eccentricity components (G20 + G22W + G22E), and then the total combined obliquity components (G21W + G21E).

7.3.2.1. *Individual Components.* In Figures 7.3.29–7.3.32 we show the average tidal power of the individual components. (The dissipation for the G21W result is exactly zero in this case of potential-energy dissipation.) In Figures 7.3.33–7.3.36 we show the power integrated over the fluid thickness. In Figures 7.3.38–7.3.45 we show the kinetic and potential energy densities. In Figure 7.3.46–7.3.50 we show the admittance.

7.3.2.2. *Combined Components.* In Figure we show the total average power of the eccentricity tidal forces (i.e. G20 + G22W + G22E). In Figure 7.3.52 we show the total average power for the obliquity tidal forces (i.e. G21W + G21E). In Figures 7.3.53 and 7.3.54 we show the power integrated over the fluid thickness for the total eccentricity and obliquity tidal forces, respectively.

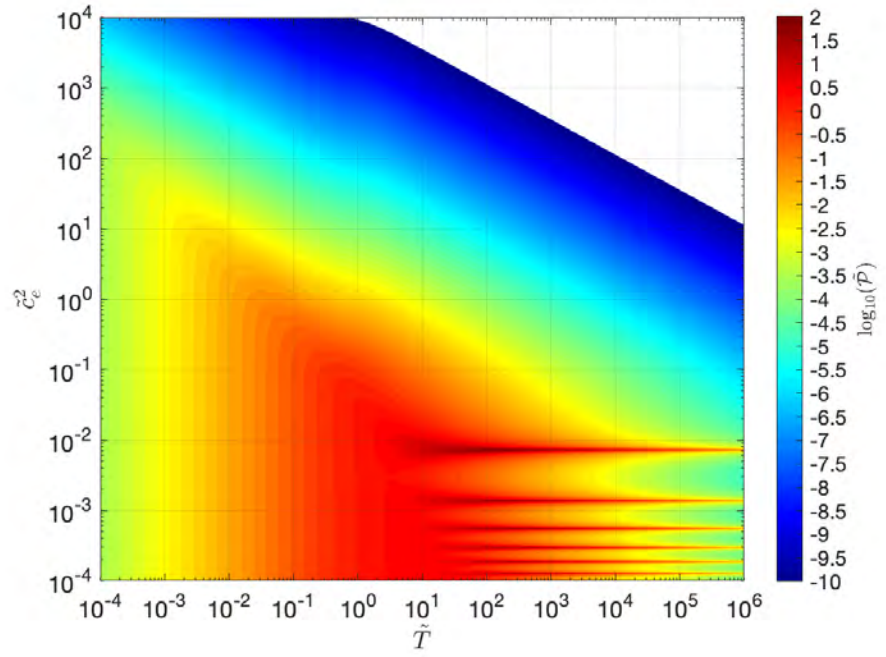

(A)

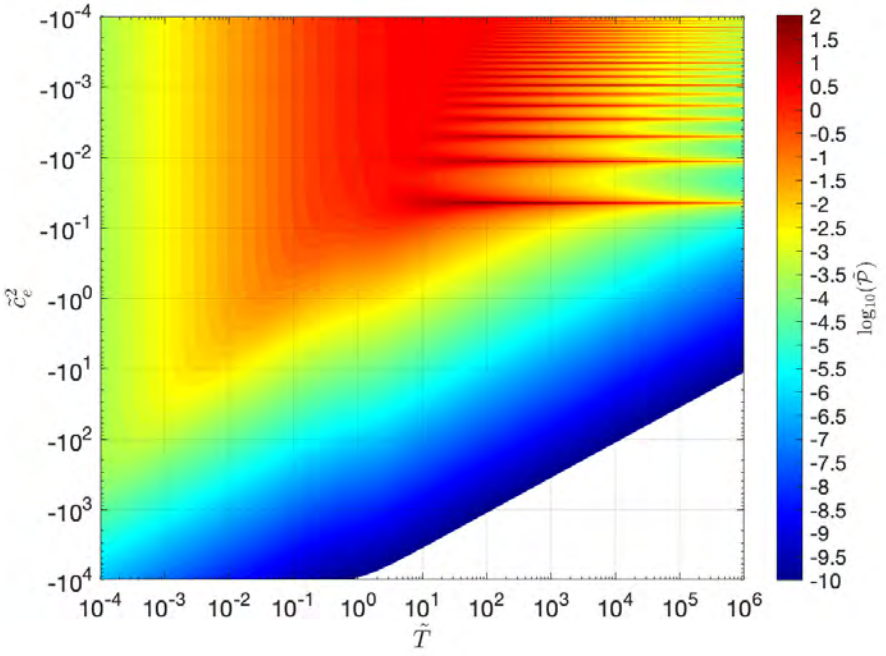

(B)

FIGURE 7.3.1. Tidal power $\tilde{\mathcal{P}}$ as a function of dissipation time scale $\tilde{T}$ and squared wave speed $\tilde{c}_e^2$ (positive (a) and negative (b) values for $\tilde{c}_e^2$ are displayed). Here $\tilde{T}$ refers to a process where dissipation is proportional to kinetic energy, and the forcing considered is the synchronous G20 component (see Section 7.3.1.1).

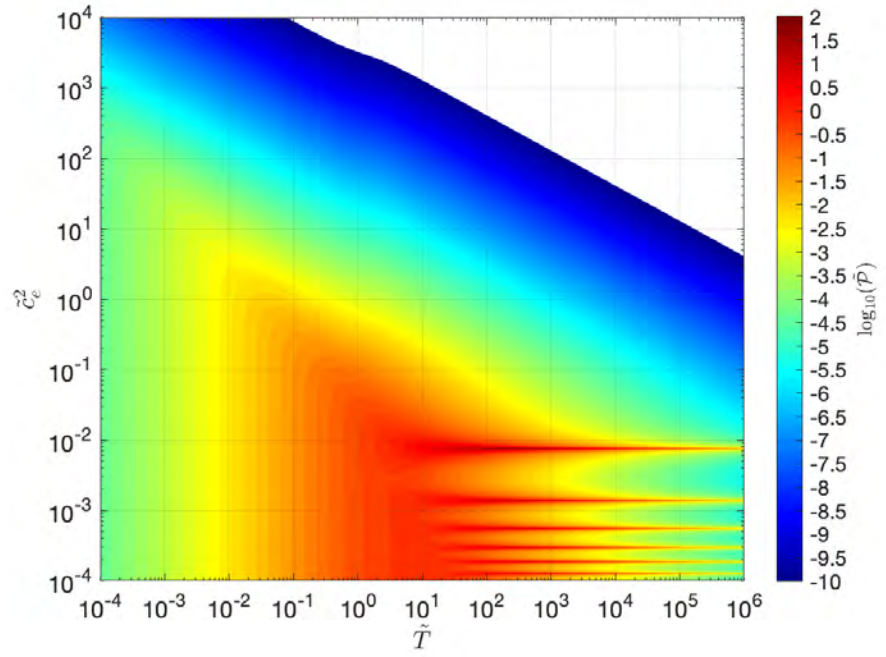

(A)

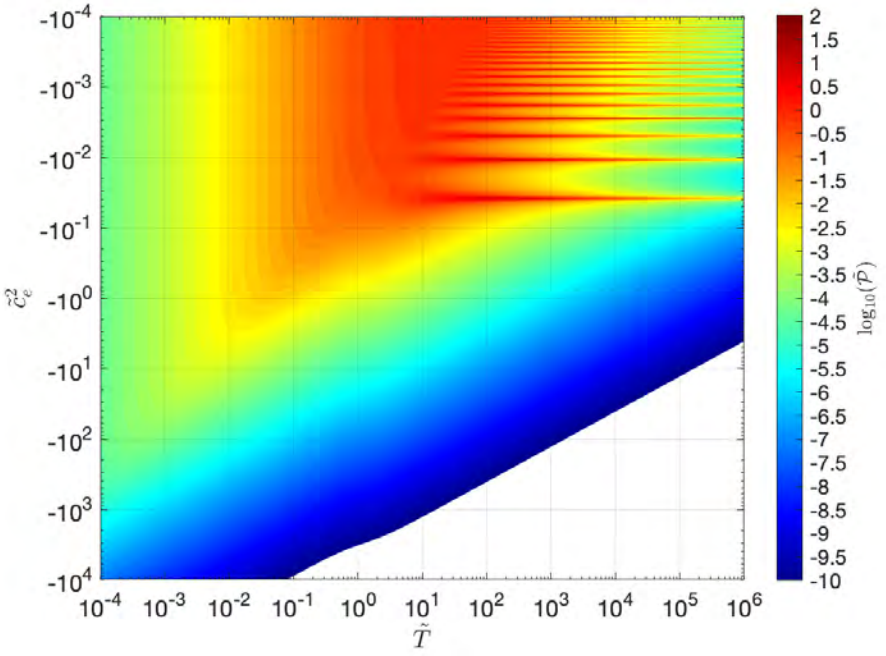

(B)

FIGURE 7.3.2. Tidal power $\tilde{\mathcal{P}}$ as a function of dissipation time scale $\tilde{T}$ and squared wave speed $\tilde{c}_e^2$ (positive (a) and negative (b) values for $\tilde{c}_e^2$ are displayed). Here $\tilde{T}$ refers to a process where dissipation is proportional to kinetic energy, and the forcing considered is the synchronous G22W component (see Section 7.3.1.1).

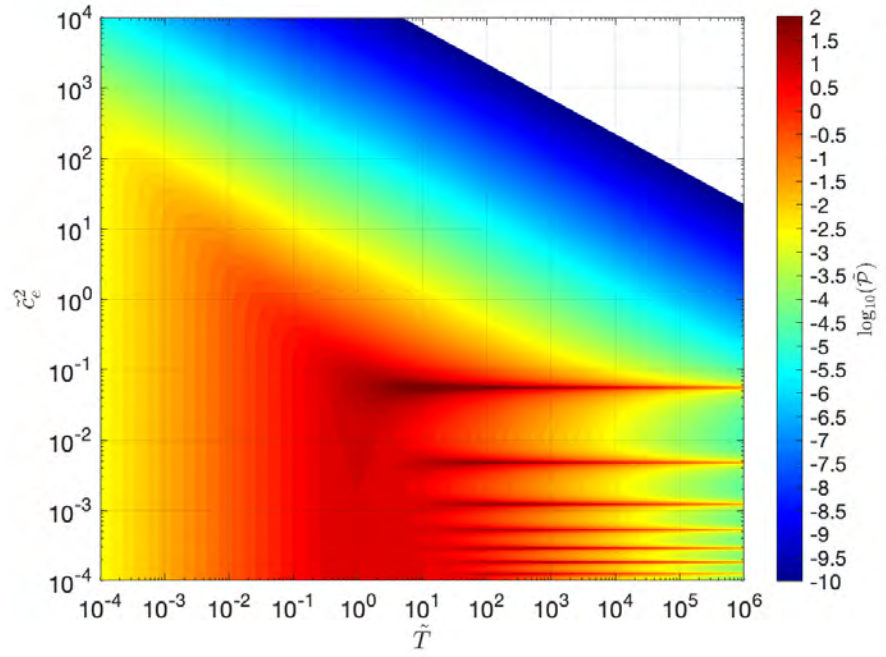

(A)

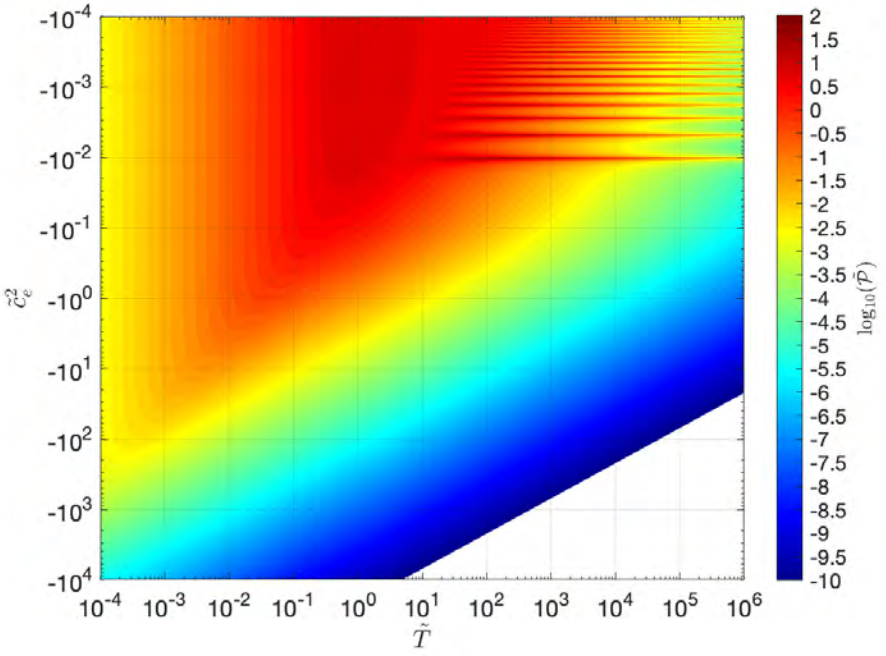

(B)

FIGURE 7.3.3. Tidal power $\tilde{\mathcal{P}}$ as a function of dissipation time scale $\tilde{T}$ and squared wave speed $\tilde{c}_e^2$ (positive (a) and negative (b) values for $\tilde{c}_e^2$ are displayed). Here $\tilde{T}$ refers to a process where dissipation is proportional to kinetic energy, and the forcing considered is the synchronous G22E component (see Section 7.3.1.1).

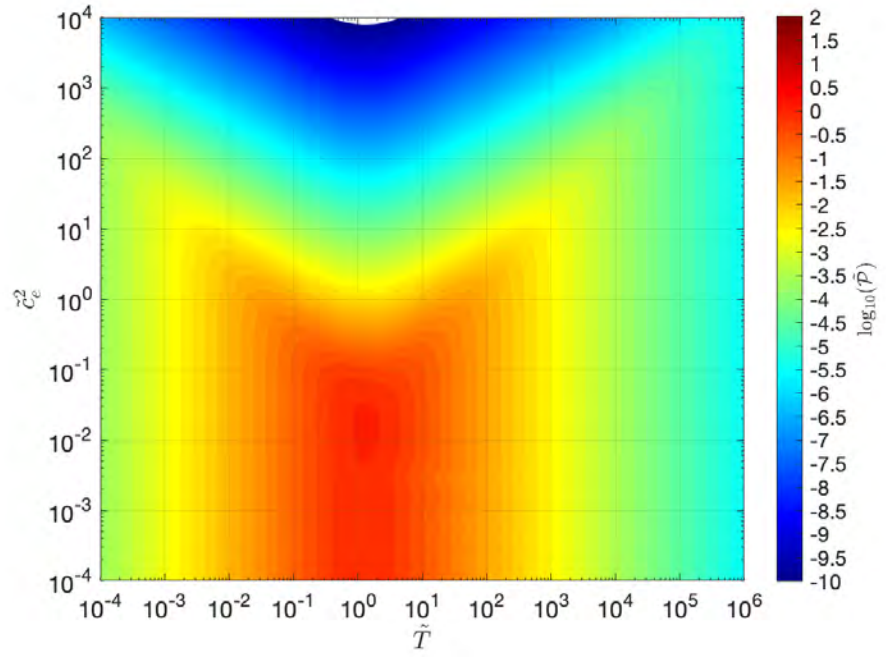

(A)

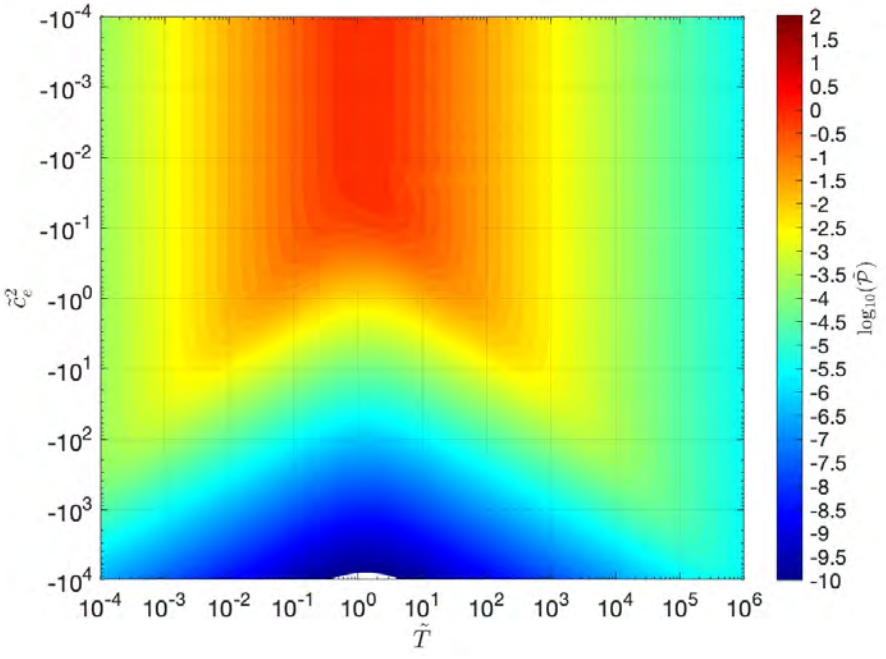

(B)

FIGURE 7.3.4. Tidal power $\tilde{\mathcal{P}}$ as a function of dissipation time scale $\tilde{T}$ and squared wave speed $\tilde{c}_e^2$ (positive (a) and negative (b) values for $\tilde{c}_e^2$ are displayed). Here $\tilde{T}$ refers to a process where dissipation is proportional to kinetic energy, and the forcing considered is the synchronous G21W component (see Section 7.3.1.1).

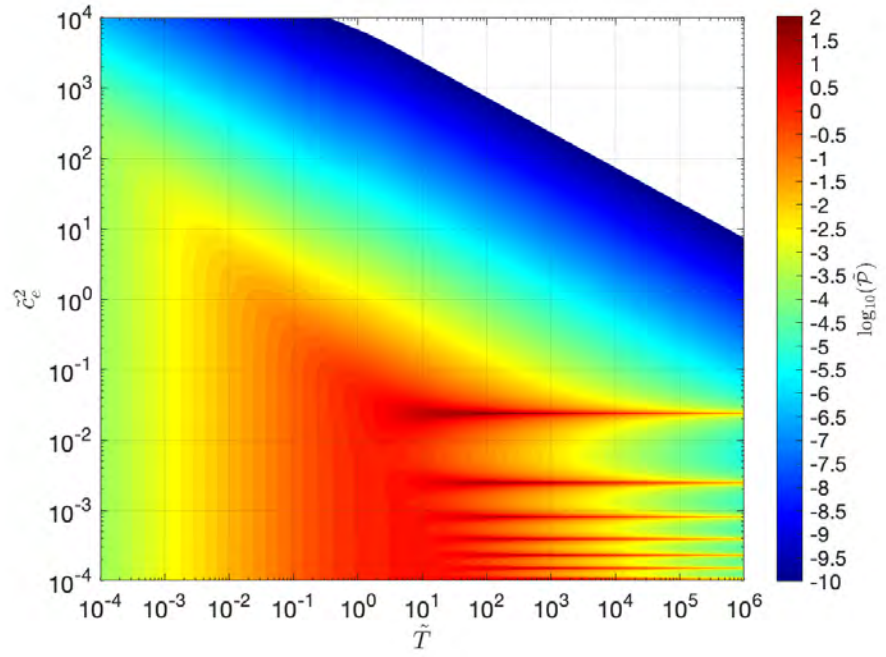

(A)

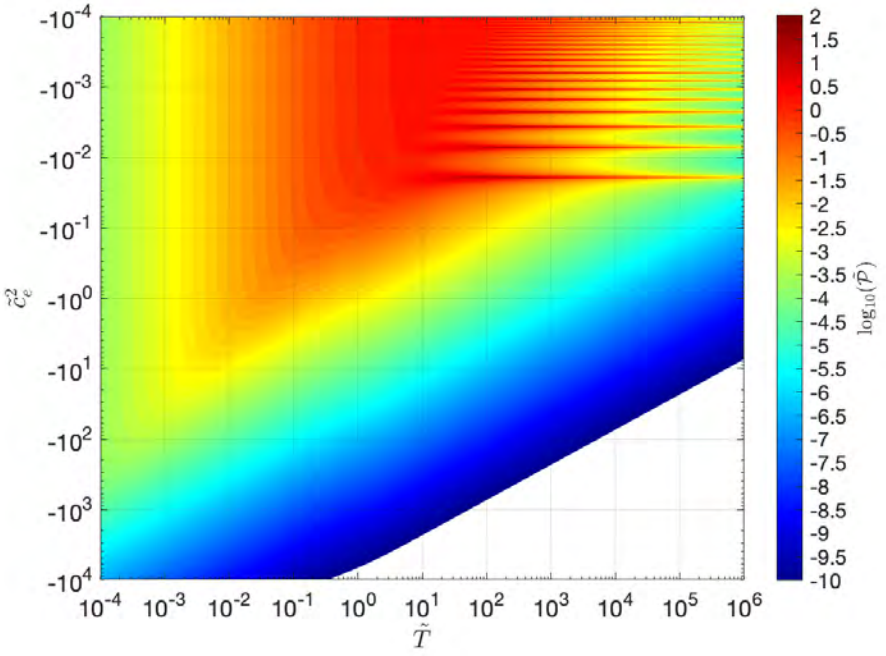

(B)

FIGURE 7.3.5. Tidal power $\tilde{\mathcal{P}}$ as a function of dissipation time scale $\tilde{T}$ and squared wave speed $\tilde{c}_e^2$ (positive (a) and negative (b) values for $\tilde{c}_e^2$ are displayed). Here $\tilde{T}$ refers to a process where dissipation is proportional to kinetic energy, and the forcing considered is the synchronous G21E component (see Section 7.3.1.1).

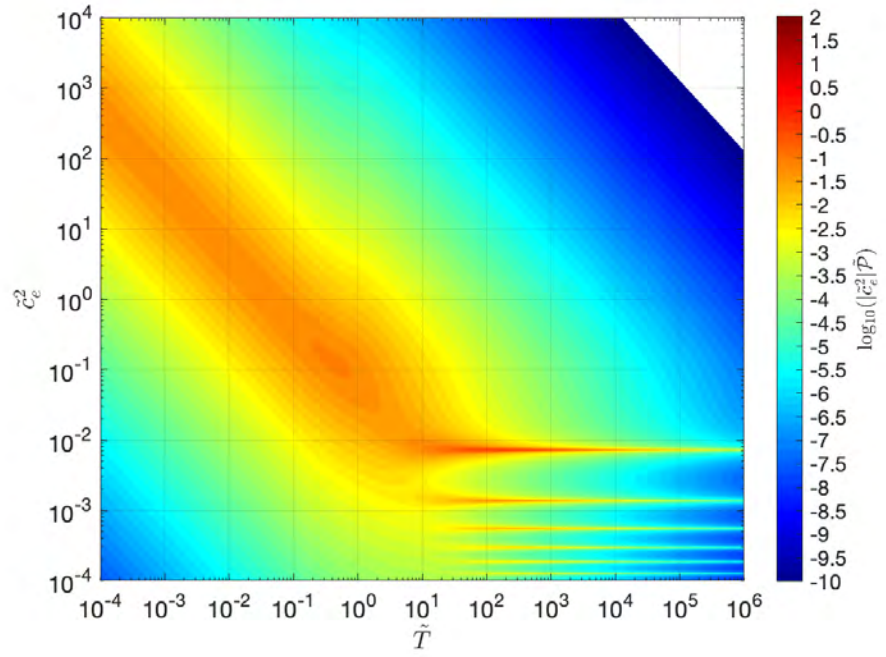

(A)

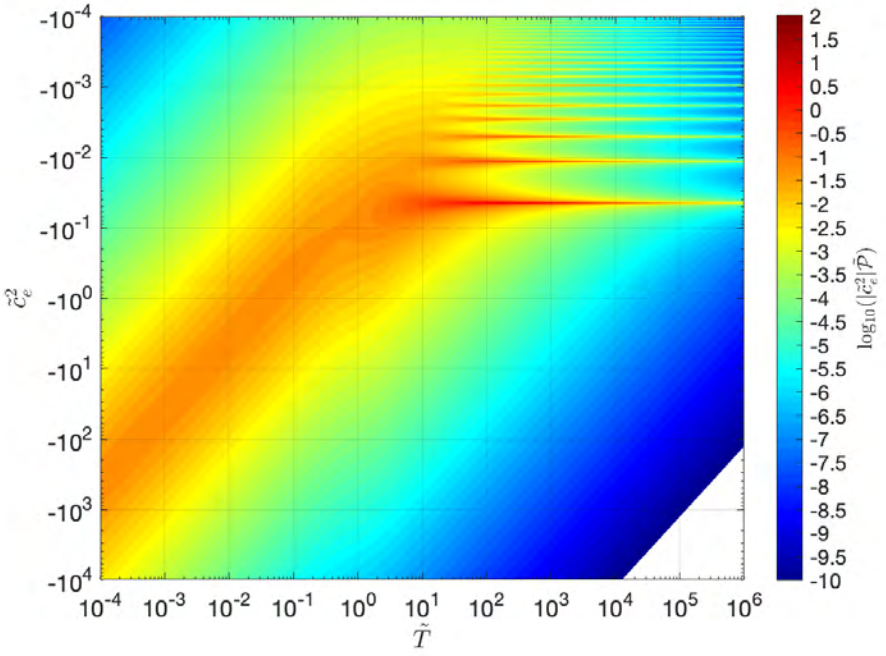

(B)

FIGURE 7.3.6. Tidal power integrated over the fluid thickness as represented by the product $\tilde{c}_e^2\tilde{\mathcal{P}}$, where $\tilde{\mathcal{P}}$ is the G20 component shown in Figure 7.3.1 (a).

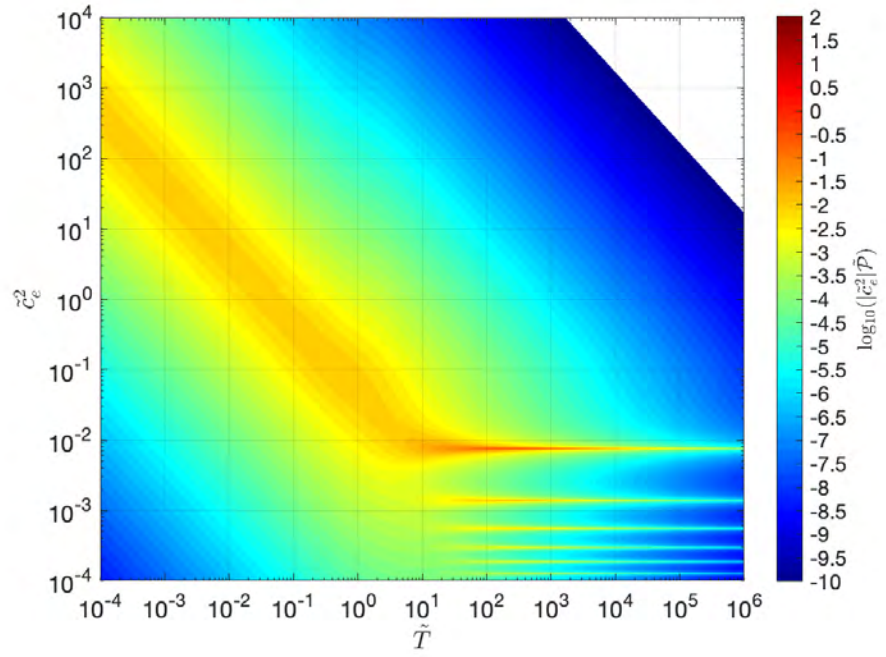

(A)

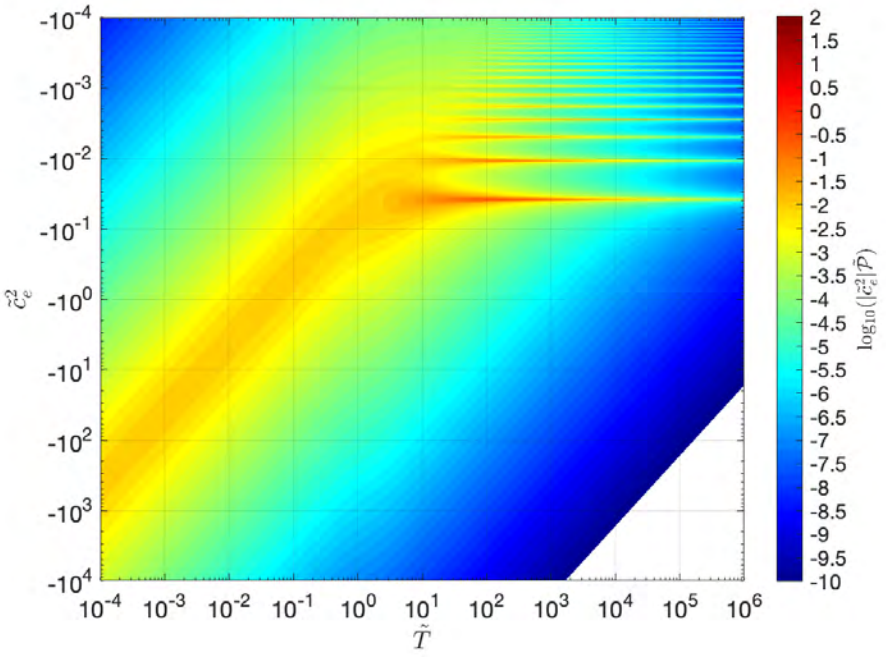

(B)

FIGURE 7.3.7. Tidal power integrated over the fluid thickness as represented by the product $\tilde{c}_e^2\tilde{\mathcal{P}}$, where $\tilde{\mathcal{P}}$ is the G22W component shown in Figure 7.3.2 (a).

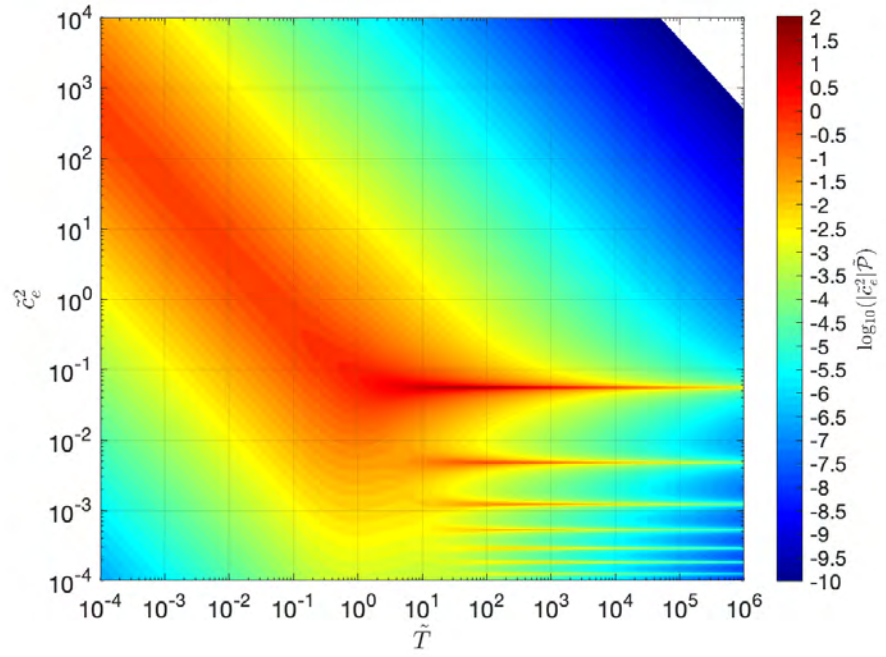

(A)

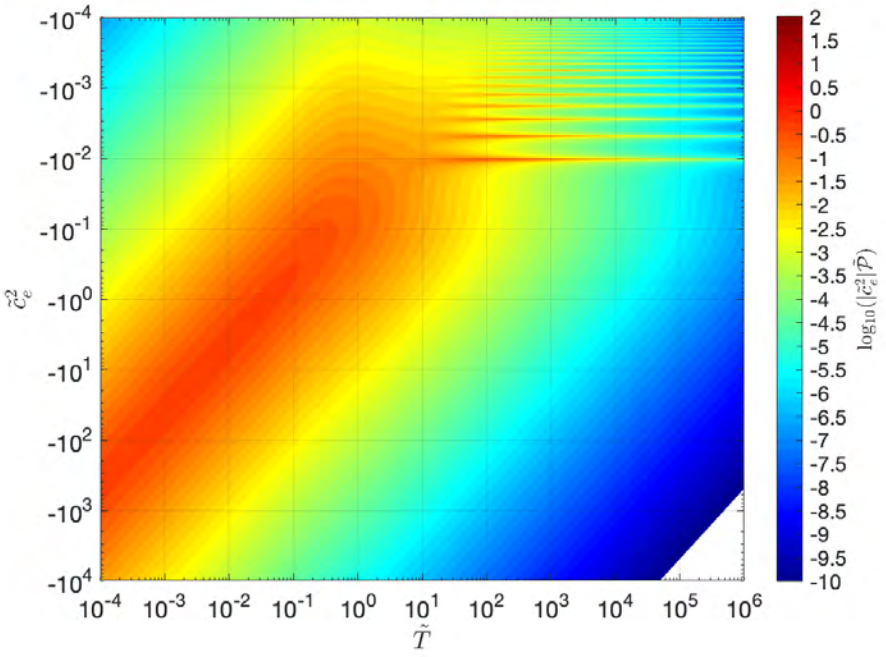

(B)

FIGURE 7.3.8. Tidal power integrated over the fluid thickness as represented by the product $\tilde{c}_e^2\tilde{\mathcal{P}}$, where $\tilde{\mathcal{P}}$ is the G22E component shown in Figure 7.3.3 (a).

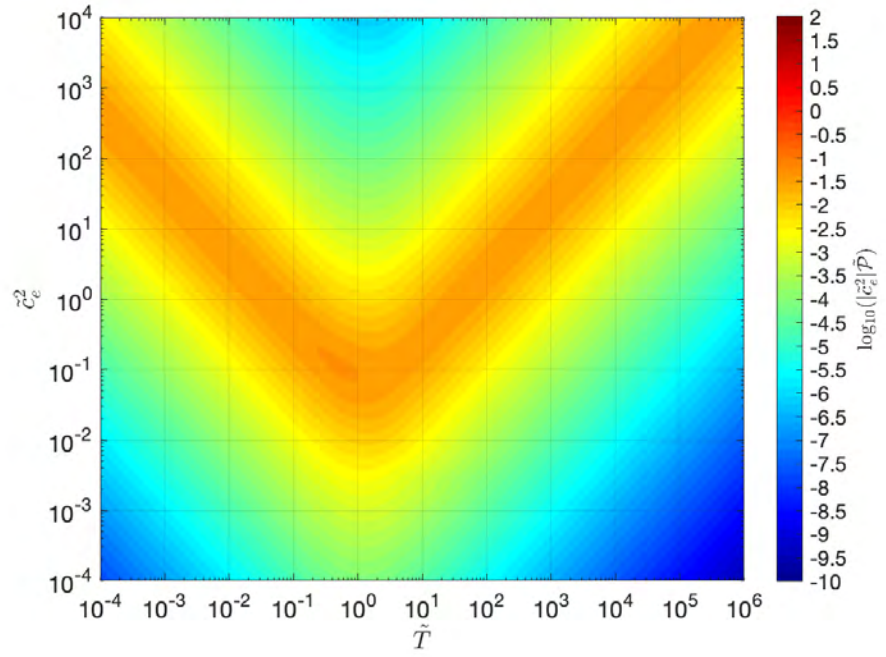

(A)

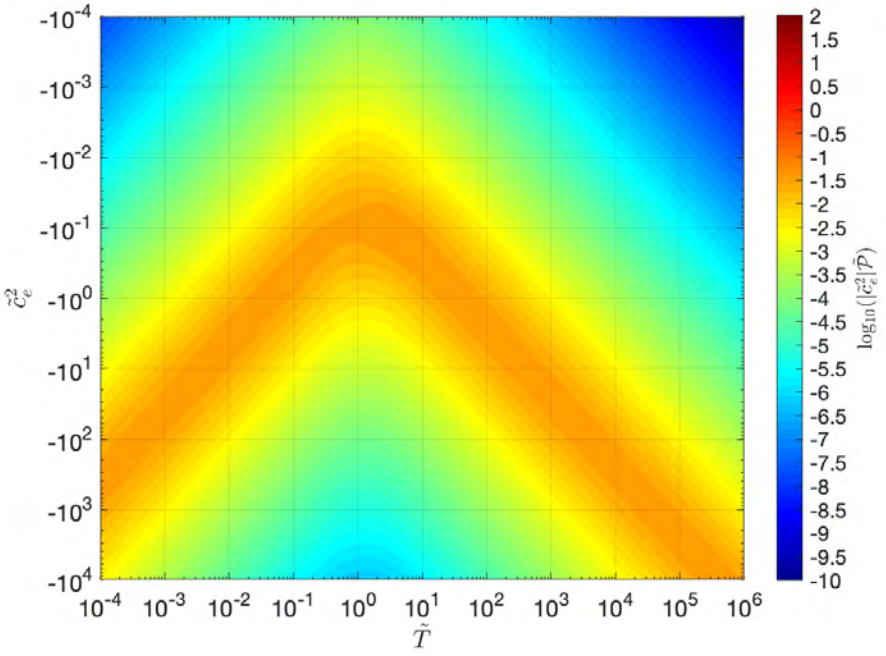

(B)

FIGURE 7.3.9. Tidal power integrated over the fluid thickness as represented by the product $\tilde{c}_e^2\tilde{\mathcal{P}}$, where $\tilde{\mathcal{P}}$ is the G21W component shown in Figure 7.3.4 (a).

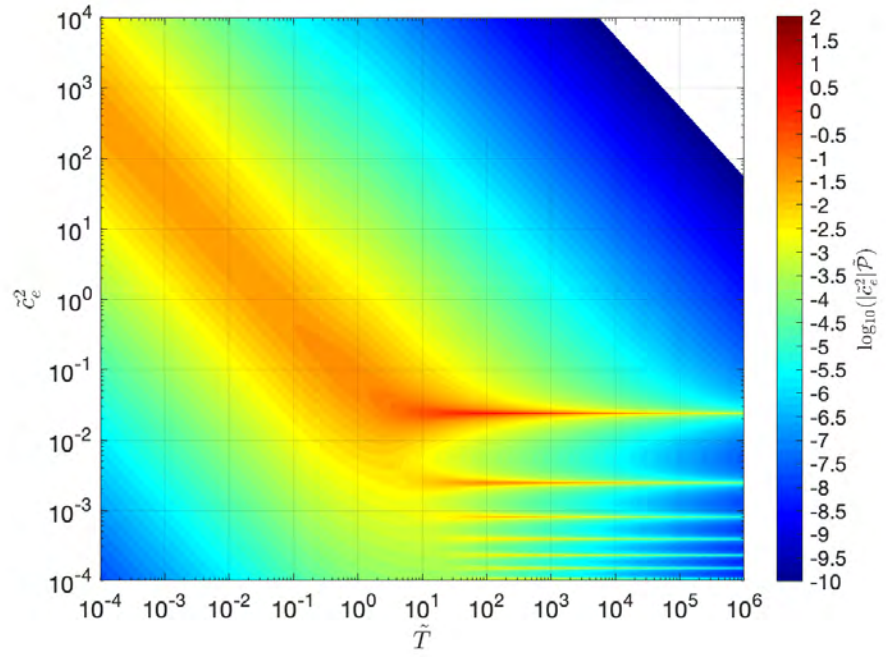

(A)

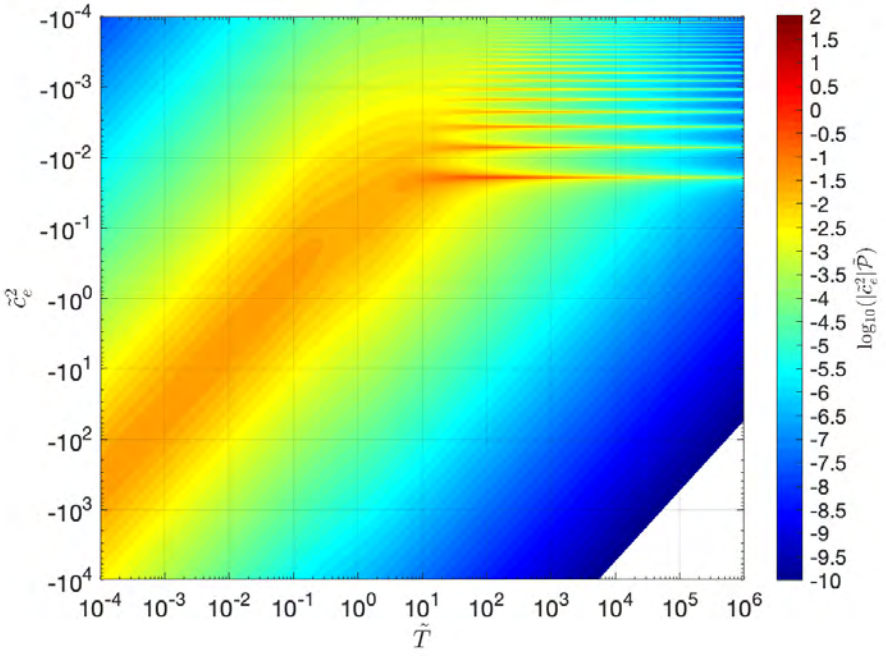

(B)

FIGURE 7.3.10. Tidal power integrated over the fluid thickness as represented by the product $\tilde{c}_e^2\tilde{\mathcal{P}}$, where $\tilde{\mathcal{P}}$ is the G21E component shown in Figure 7.3.5 (a).

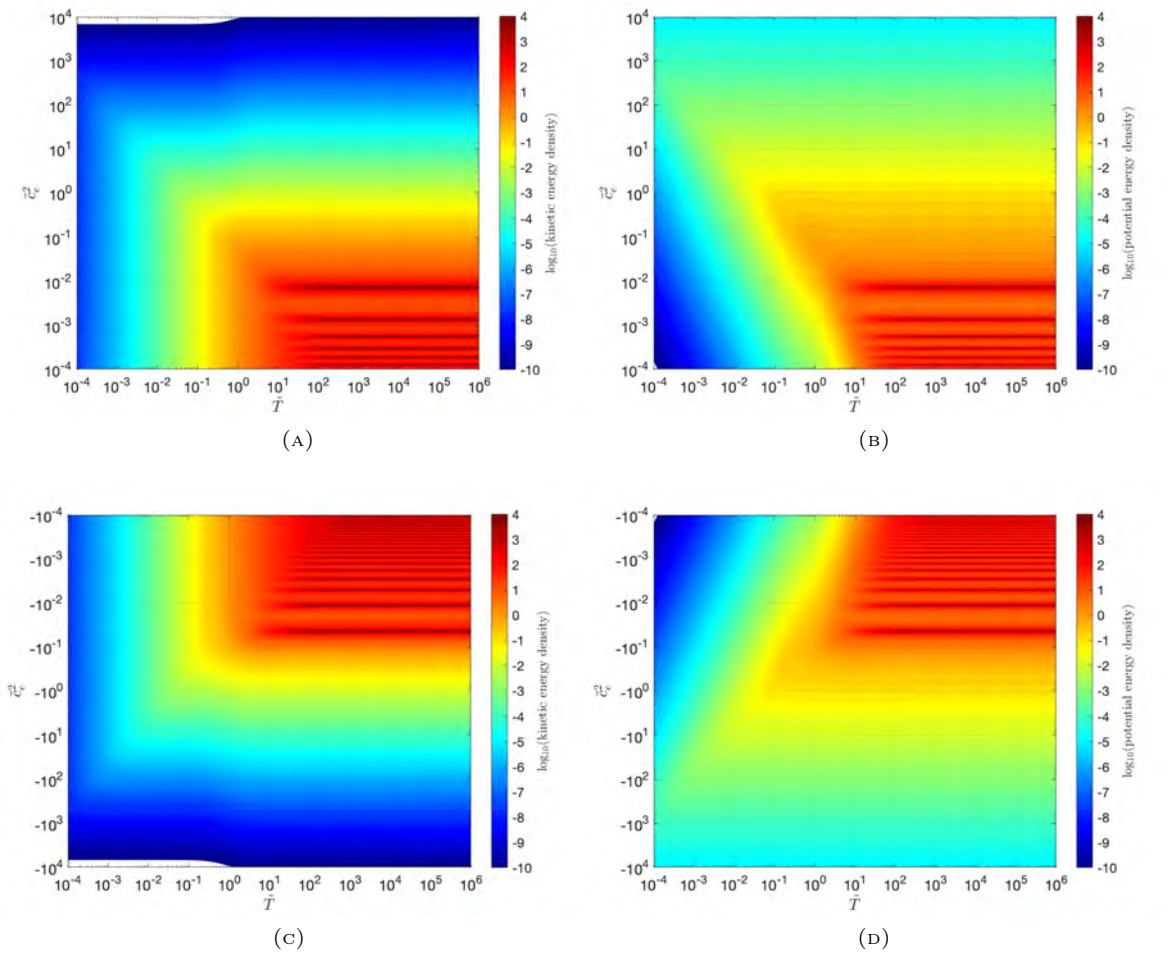

FIGURE 7.3.11

FIGURE 7.3.12. Kinetic energy density (a, c) and potential energy density (b, d) as a function of dissipation time scale $\tilde{T}$ and squared wave speed $\tilde{c}_e^2$ (positive (a, b) and negative (c, d) values for $\tilde{c}_e^2$ are displayed). Here $\tilde{T}$ refers to a process where dissipation is proportional to kinetic energy and the forcing is the G20 component in the nonsynchronous rapid rotation limit described in Section 7.3.1.

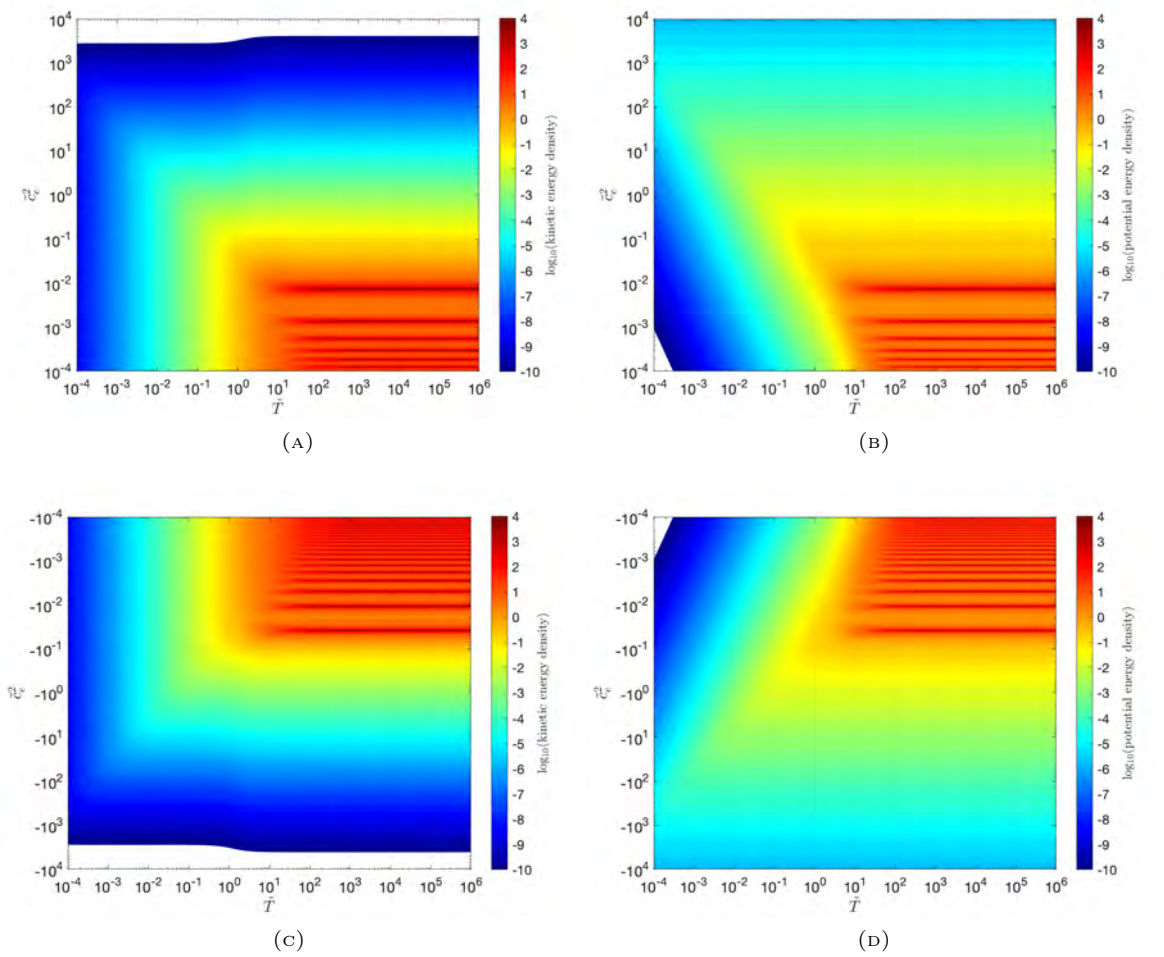

FIGURE 7.3.13

FIGURE 7.3.14. Kinetic energy density (a, c) and potential energy density (b, d) as a function of dissipation time scale $\tilde{T}$ and squared wave speed $\tilde{c}_e^2$ (positive (a, b) and negative (c, d) values for $\tilde{c}_e^2$ are displayed). Here $\tilde{T}$ refers to a process where dissipation is proportional to kinetic energy and the forcing is the G22W component in the nonsynchronous rapid rotation limit described in Section 7.3.1.

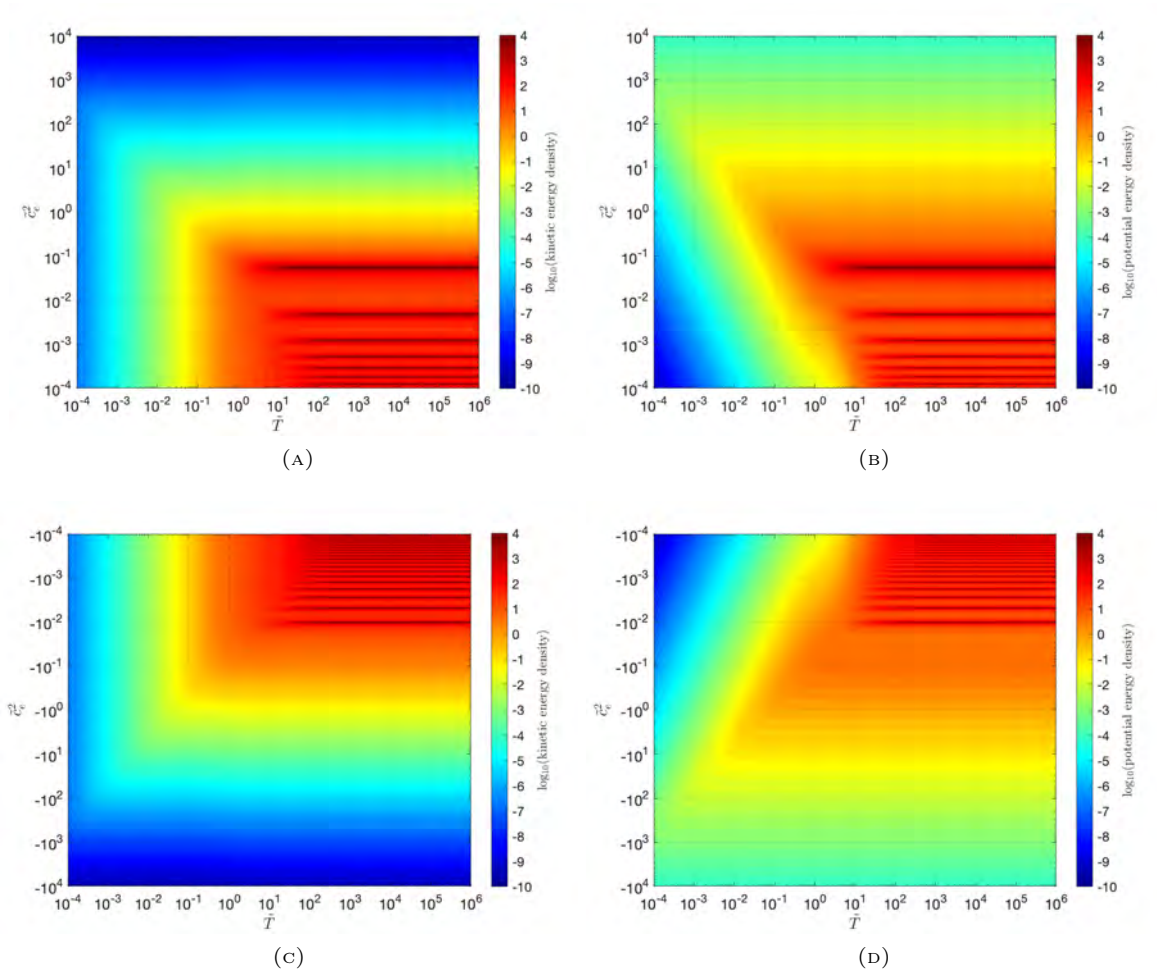

FIGURE 7.3.15

FIGURE 7.3.16. Kinetic energy density (a, c) and potential energy density (b, d) as a function of dissipation time scale $\tilde{T}$ and squared wave speed $\tilde{c}_e^2$ (positive (a, b) and negative (c, d) values for $\tilde{c}_e^2$ are displayed). Here $\tilde{T}$ refers to a process where dissipation is proportional to kinetic energy and the forcing is the G22E component in the nonsynchronous rapid rotation limit described in Section 7.3.1.

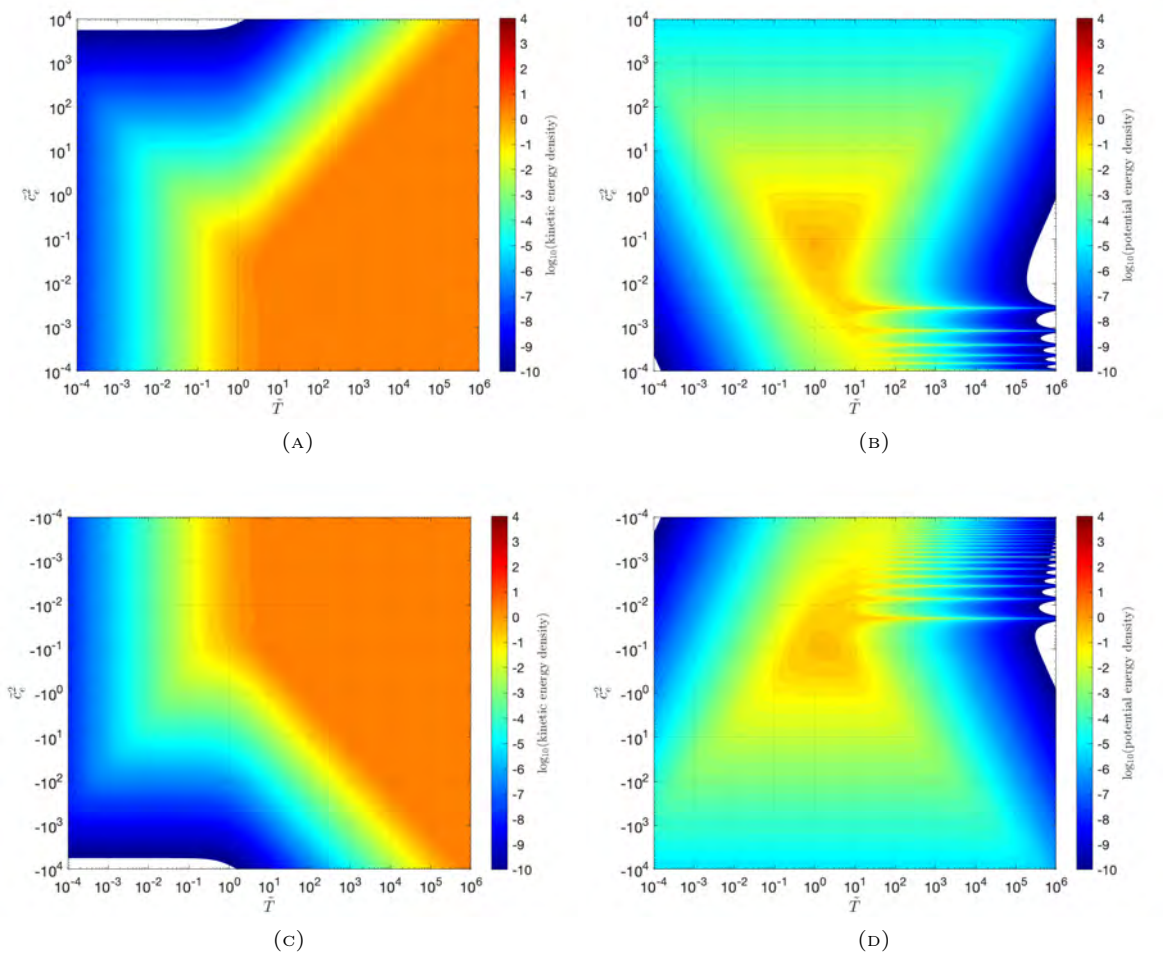

FIGURE 7.3.17

FIGURE 7.3.18. Kinetic energy density (a, c) and potential energy density (b, d) as a function of dissipation time scale $\tilde{T}$ and squared wave speed $\tilde{c}_e^2$ (positive (a) and negative (b) values for $\tilde{c}_e^2$ are displayed). Here $\tilde{T}$ refers to a process where dissipation is proportional to kinetic energy and the forcing is the G21W component in the nonsynchronous rapid rotation limit described in Section 7.3.1.

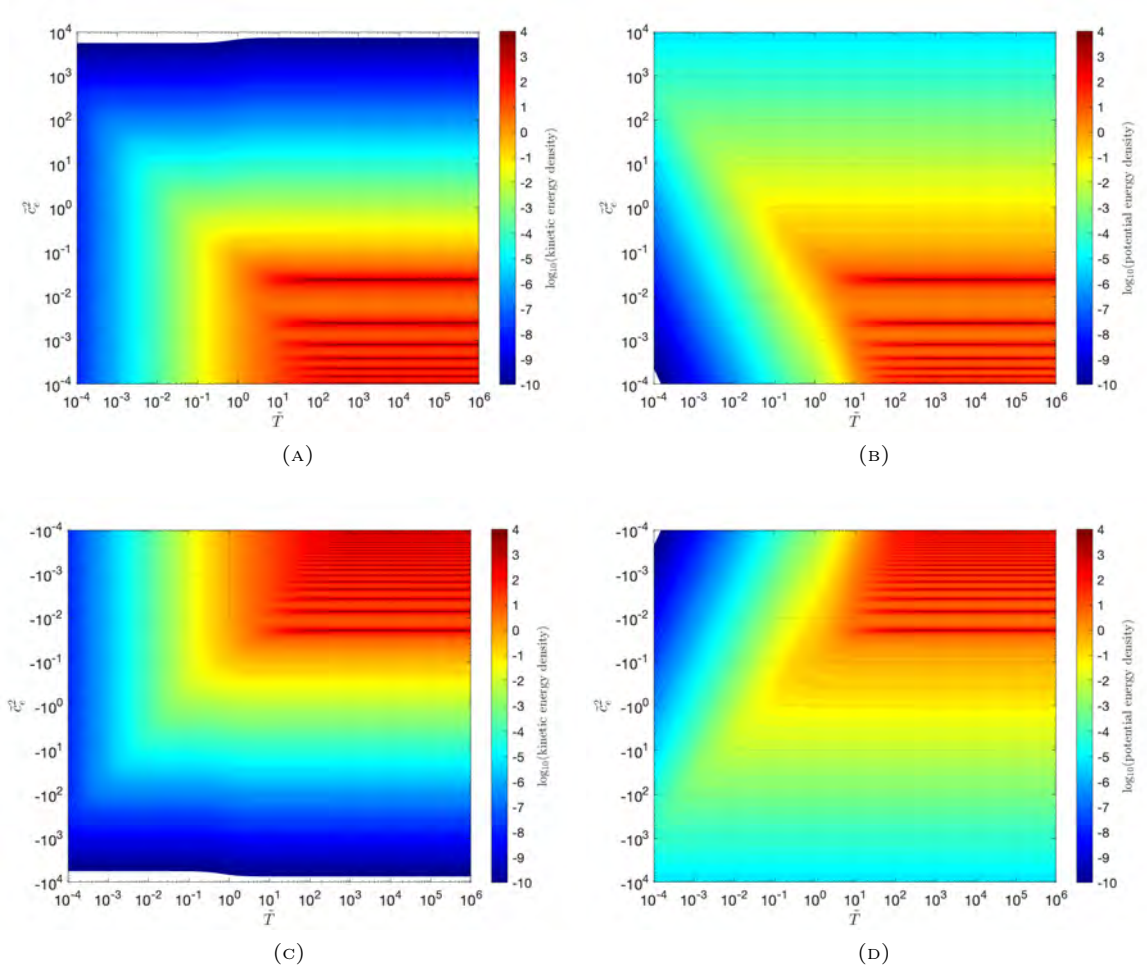

FIGURE 7.3.19. Kinetic energy density (a, c) and potential energy density (b, d) as a function of dissipation time scale $\tilde{T}$ and squared wave speed $\tilde{c}_e^2$ (positive (a) and negative (b) values for $\tilde{c}_e^2$ are displayed). Here $\tilde{T}$ refers to a process where dissipation is proportional to kinetic energy and the forcing is the G21E component in the nonsynchronous rapid rotation limit described in Section 7.3.1.

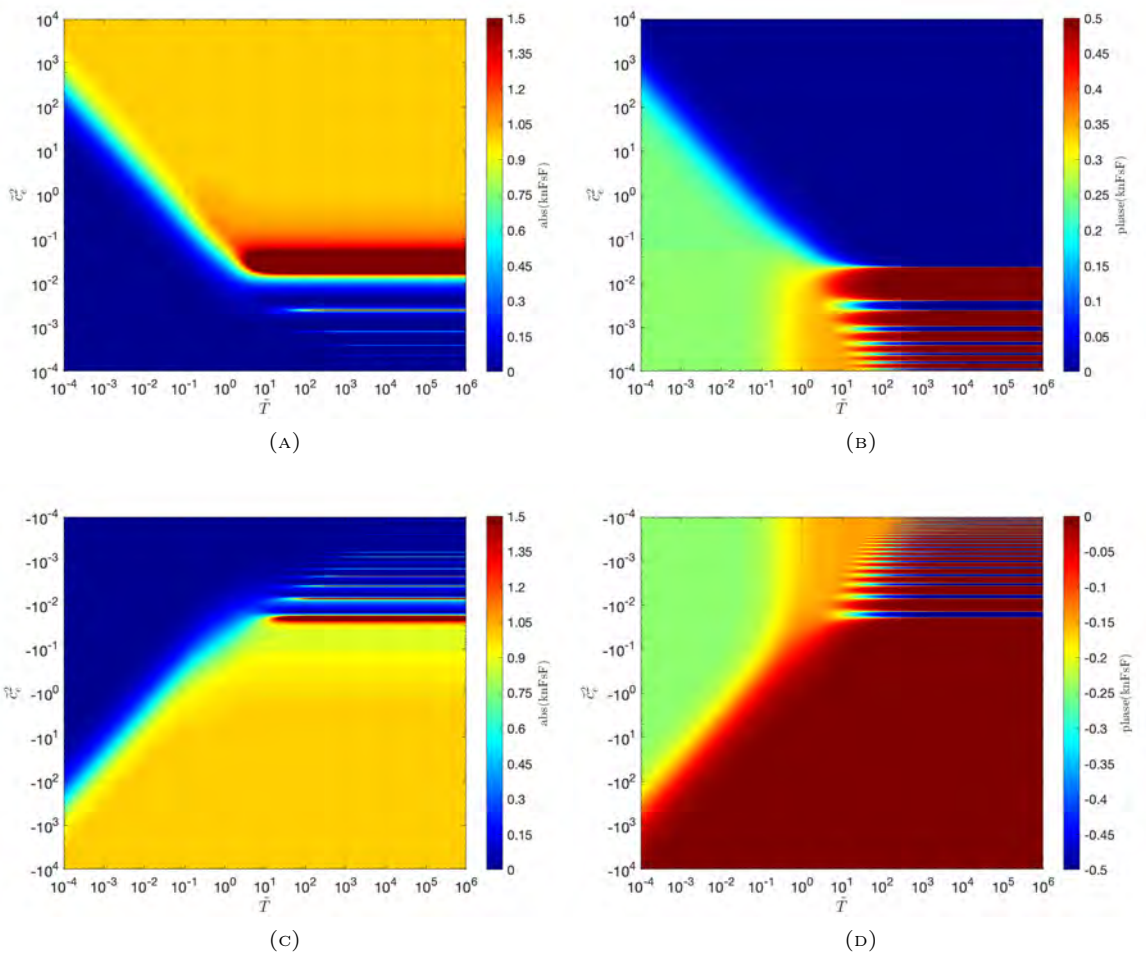

FIGURE 7.3.20. Degree-two admittance (k_2) amplitude (a, c) and phase/(2π) (b, d) as a function of dissipation time scale $\tilde{T}$ and squared wave speed $\tilde{c}_e^2$. Here $\tilde{T}$ refers to a process where dissipation is proportional to kinetic energy and the forcing is the G20 component in the nonsynchronous rapid rotation limit described in Section 7.3.1.

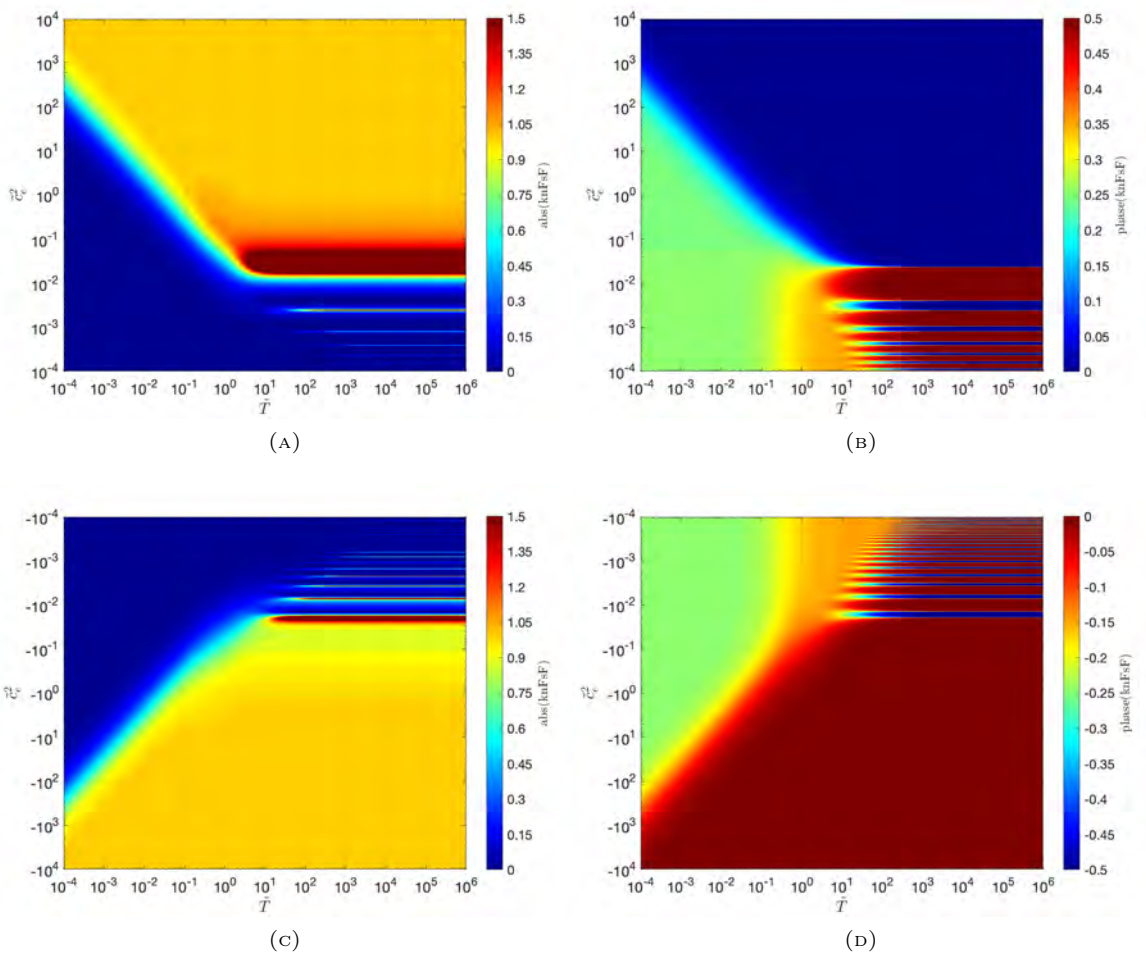

FIGURE 7.3.21. Degree-two admittance (k_2) amplitude (a, c) and phase/(2π) (b, d) as a function of dissipation time scale $\tilde{T}$ and squared wave speed $\tilde{c}_e^2$. Here $\tilde{T}$ refers to a process where dissipation is proportional to kinetic energy and the forcing is the G22W component in the nonsynchronous rapid rotation limit described in Section 7.3.1.

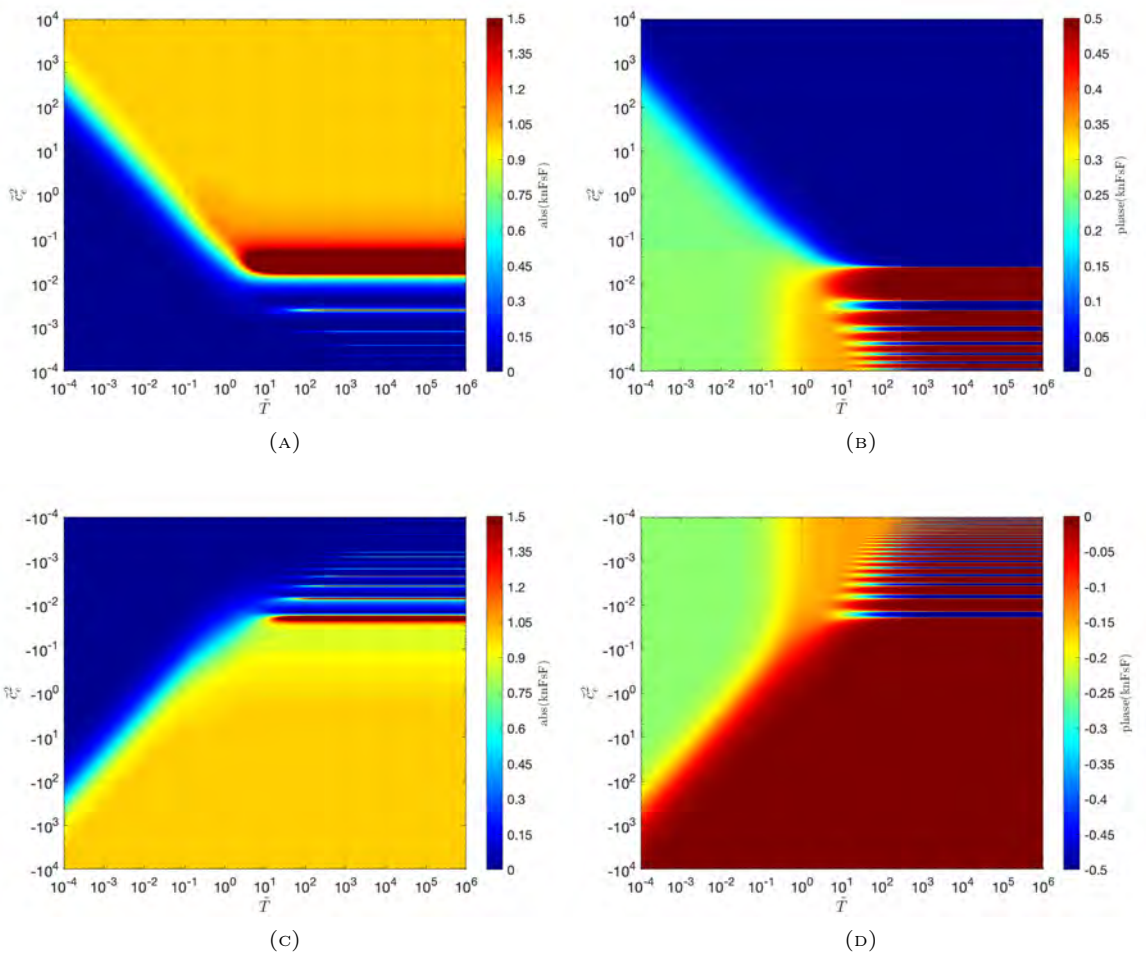

FIGURE 7.3.22. Degree-two admittance (k_2) amplitude (a, c) and phase/(2π) (b, d) as a function of dissipation time scale $\tilde{T}$ and squared wave speed $\tilde{c}_e^2$. Here $\tilde{T}$ refers to a process where dissipation is proportional to kinetic energy and the forcing is the G22E component in the nonsynchronous rapid rotation limit described in Section 7.3.1.

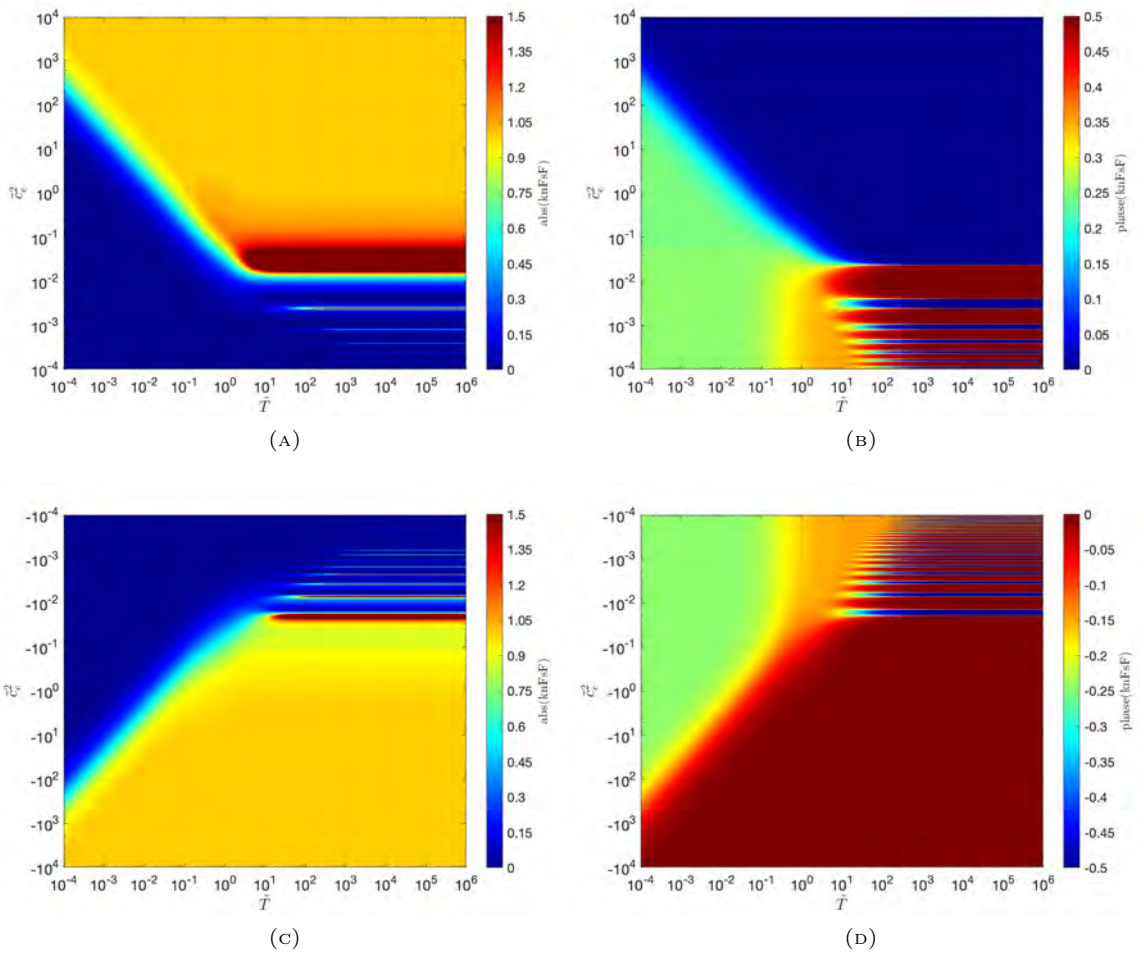

FIGURE 7.3.23. Degree-two admittance (k_2) amplitude (a, c) and phase/(2π) (b, d) as a function of dissipation time scale $\tilde{T}$ and squared wave speed $\tilde{c}_e^2$. Here $\tilde{T}$ refers to a process where dissipation is proportional to kinetic energy and the forcing is the G21W component in the nonsynchronous rapid rotation limit described in Section 7.3.1.

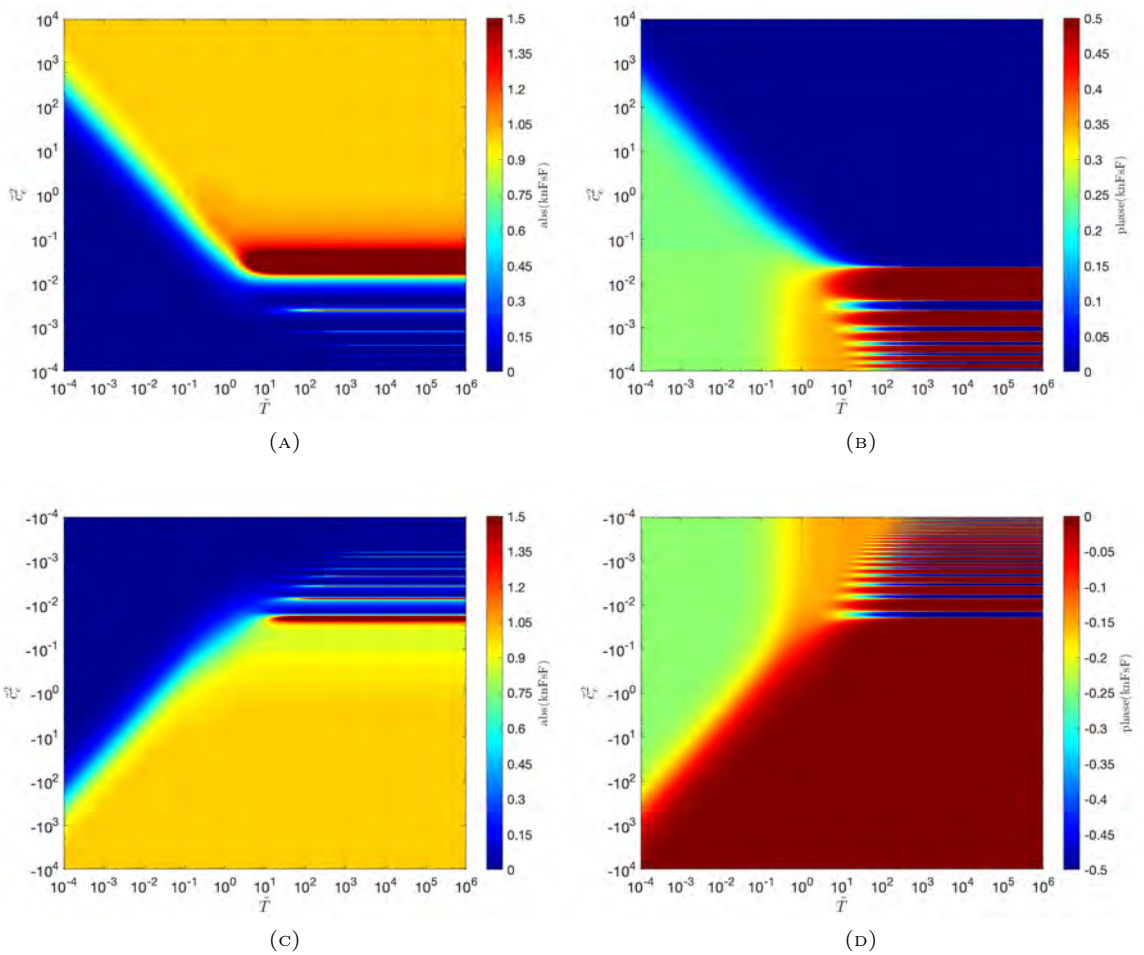

FIGURE 7.3.24. Degree-two admittance (k_2) amplitude (a, c) and phase/(2π) (b, d) as a function of dissipation time scale $\tilde{T}$ and squared wave speed $\tilde{c}_e^2$. Here $\tilde{T}$ refers to a process where dissipation is proportional to kinetic energy and the forcing is the G21E component in the nonsynchronous rapid rotation limit described in Section 7.3.1.

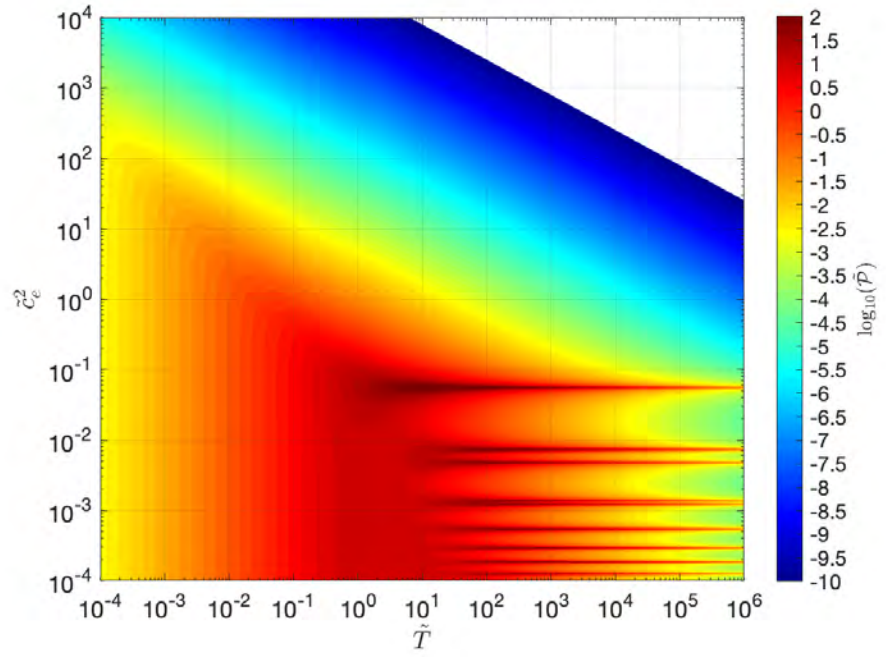

(A)

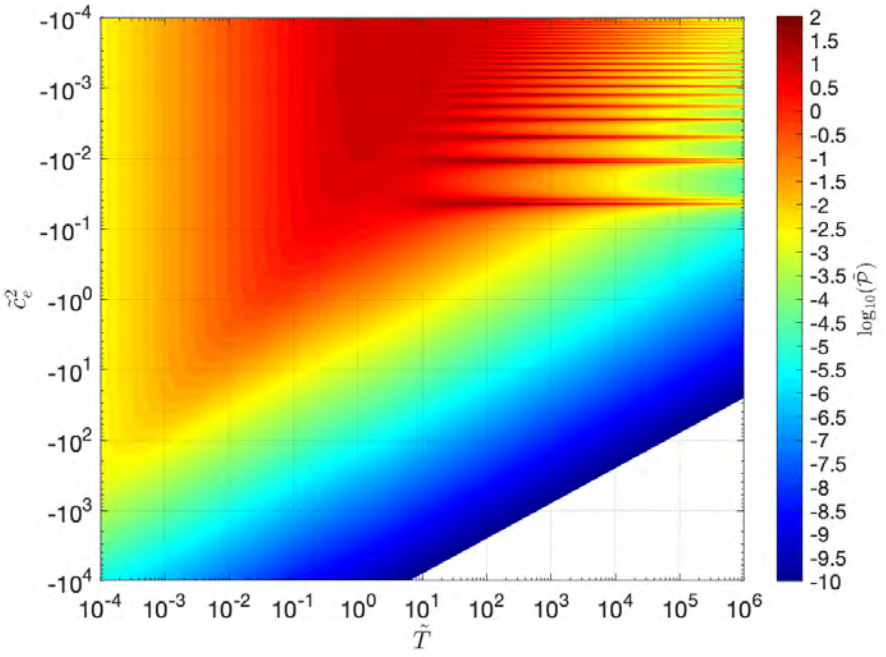

(B)

FIGURE 7.3.25. Tidal power $\tilde{\mathcal{P}}$ as a function of dissipation time scale $\tilde{T}$ and squared wave speed $\tilde{c}_e^2$ (positive (a) and negative (b) values for $\tilde{c}_e^2$ are displayed). Here $\tilde{T}$ refers to a process where dissipation is proportional to kinetic energy, and the forcing considered is due to the eccentricity of a synchronous-rotation orbit (see Section 7.3.1).

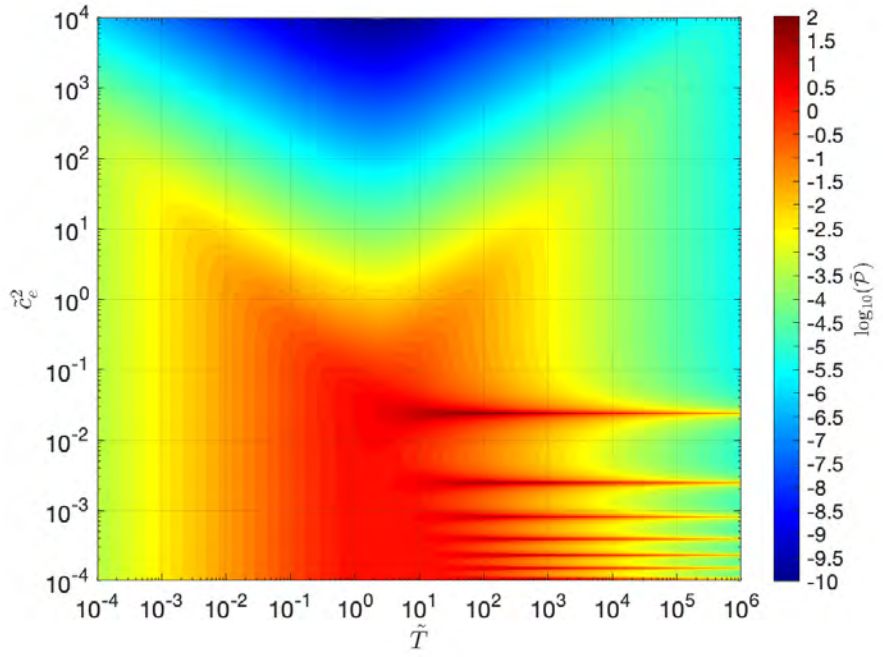

(A)

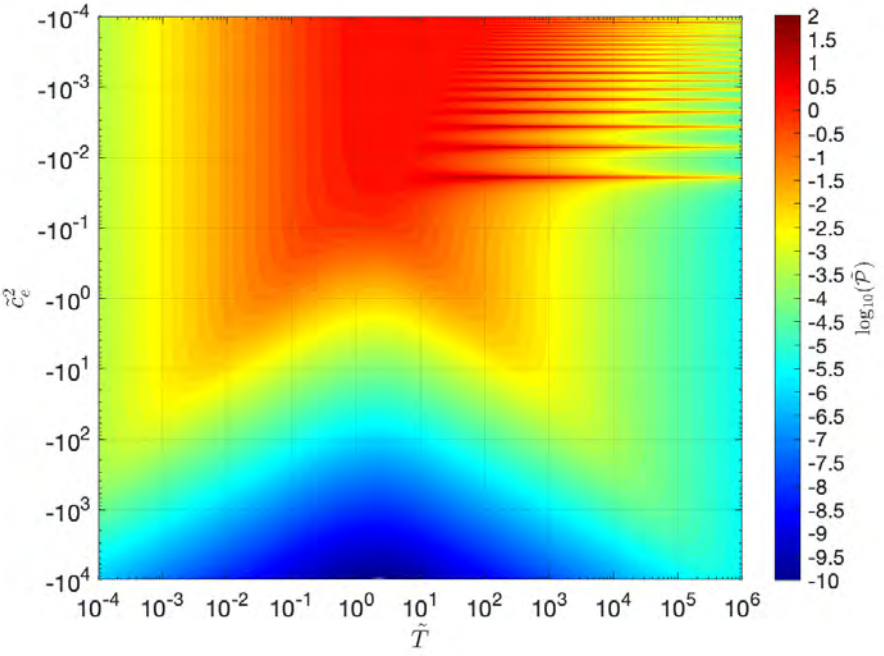

(B)

FIGURE 7.3.26. Tidal power $\tilde{\mathcal{P}}$ as a function of dissipation time scale $\tilde{T}$ and squared wave speed $\tilde{c}_e^2$ (positive (a) and negative (b) values for $\tilde{c}_e^2$ are displayed). Here $\tilde{T}$ refers to a process where dissipation is proportional to kinetic energy, and the forcing considered is due to the obliquity of a synchronous-rotation orbit (see Section 7.3.1).

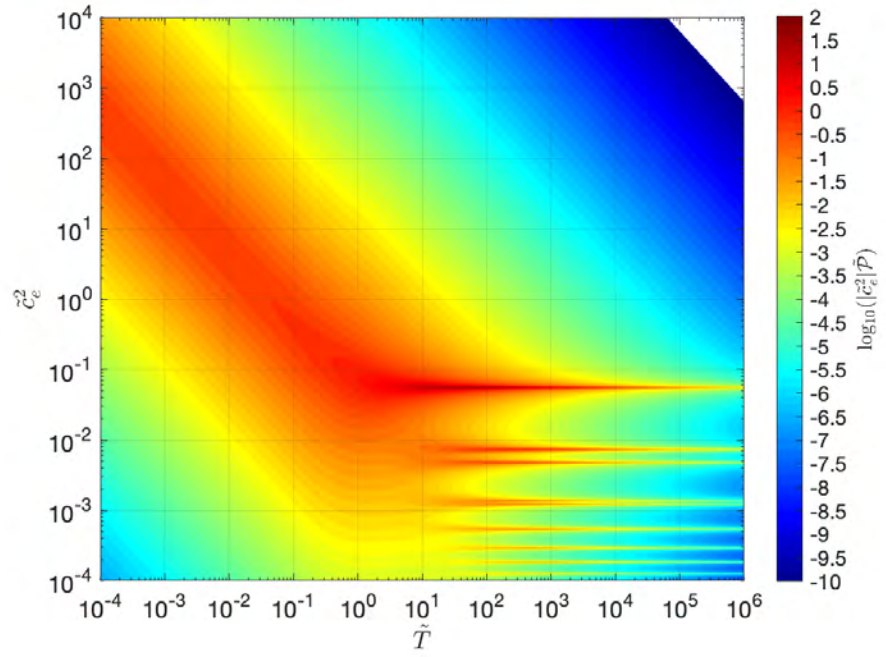

(A)

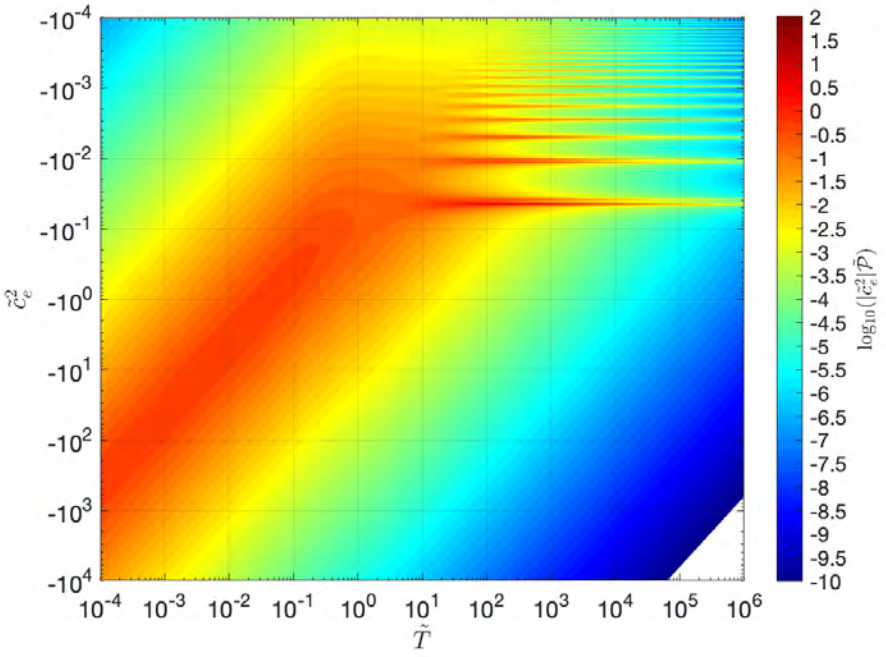

(B)

FIGURE 7.3.27. Tidal power integrated over the fluid thickness as represented by the product $\tilde{c}_e^2\tilde{\mathcal{P}}$, where $\tilde{\mathcal{P}}$ is the combined eccentricity component shown in Figure 7.3.27 (a).

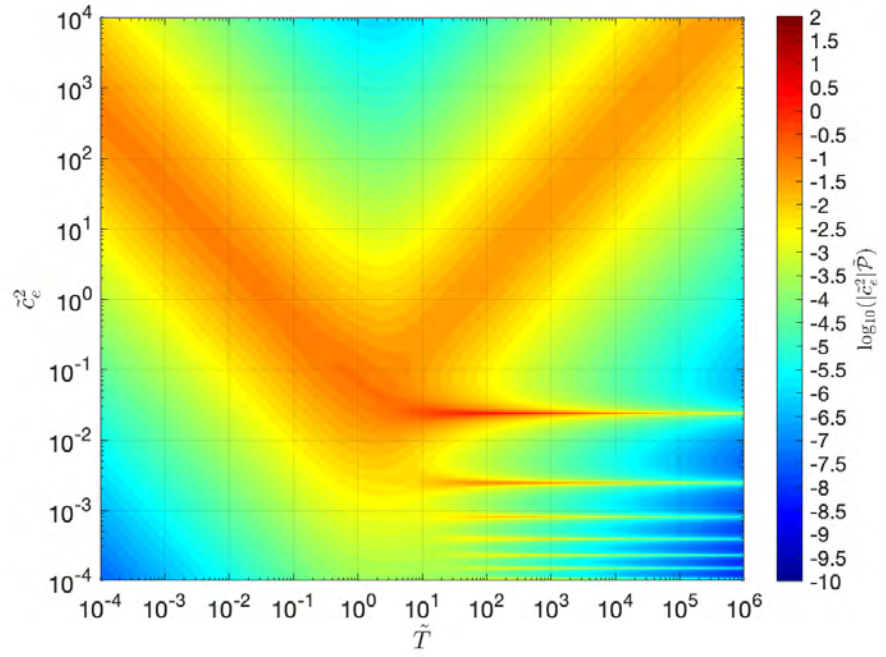

(A)

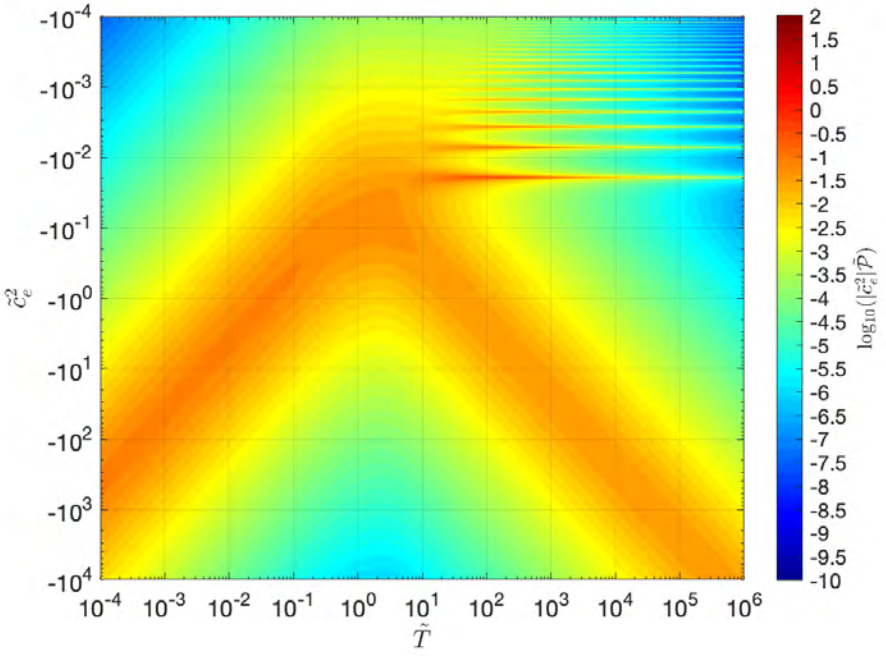

(B)

FIGURE 7.3.28. Tidal power $\tilde{\mathcal{P}}$ as a function of dissipation time scale $\tilde{T}$ and squared wave speed $\tilde{c}_e^2$ (positive (a) and negative (b) values for $\tilde{c}_e^2$ are displayed). Here $\tilde{T}$ refers to a process where dissipation is proportional to kinetic energy, and the forcing considered is due to the obliquity of a synchronous-rotation orbit (see Section 7.3.1).

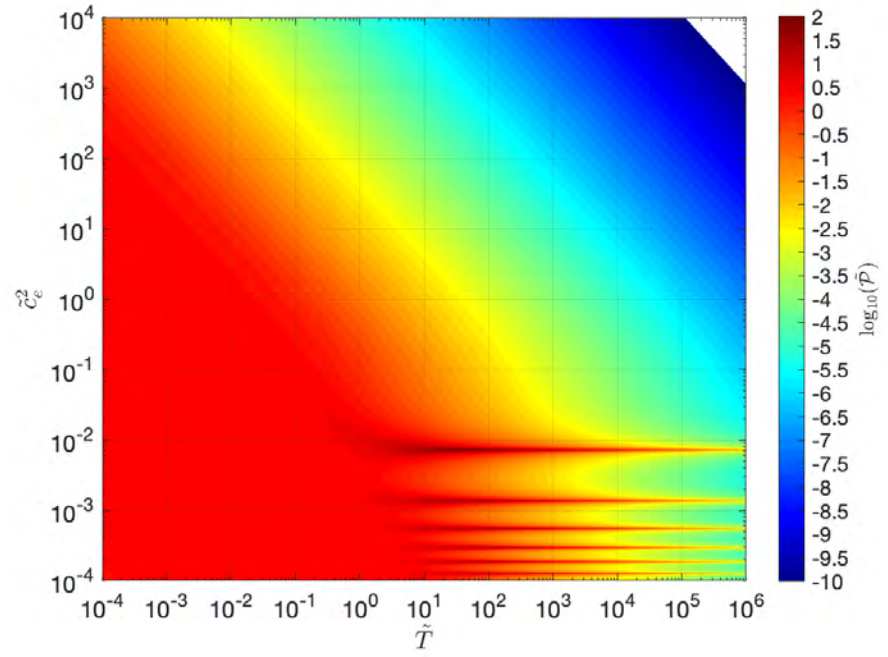

(A)

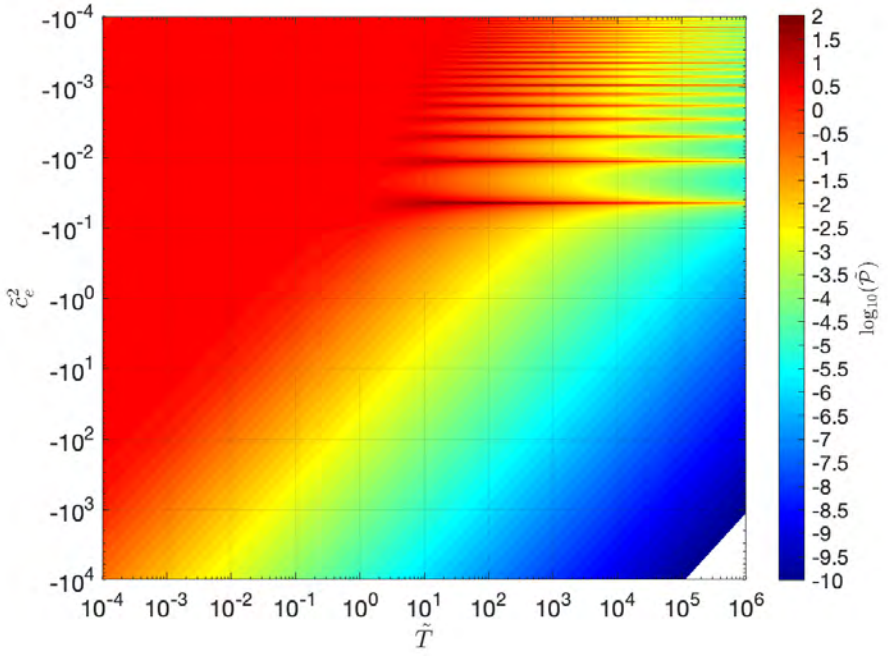

(B)

FIGURE 7.3.29. Tidal power $\tilde{\mathcal{P}}$ as a function of dissipation time scale $\tilde{T}$ and squared wave speed $\tilde{c}_e^2$ (positive (a) and negative (b) values for $\tilde{c}_e^2$ are displayed). Here $\tilde{T}$ refers to a process where dissipation is proportional to potential energy, and the forcing considered is the synchronous G20 component (see Section 7.3.2).

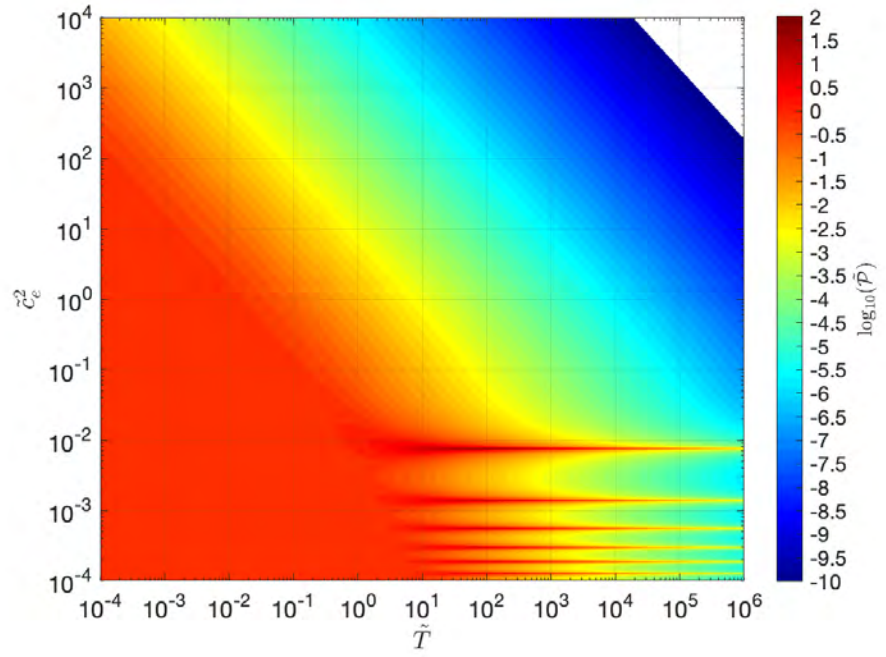

(A)

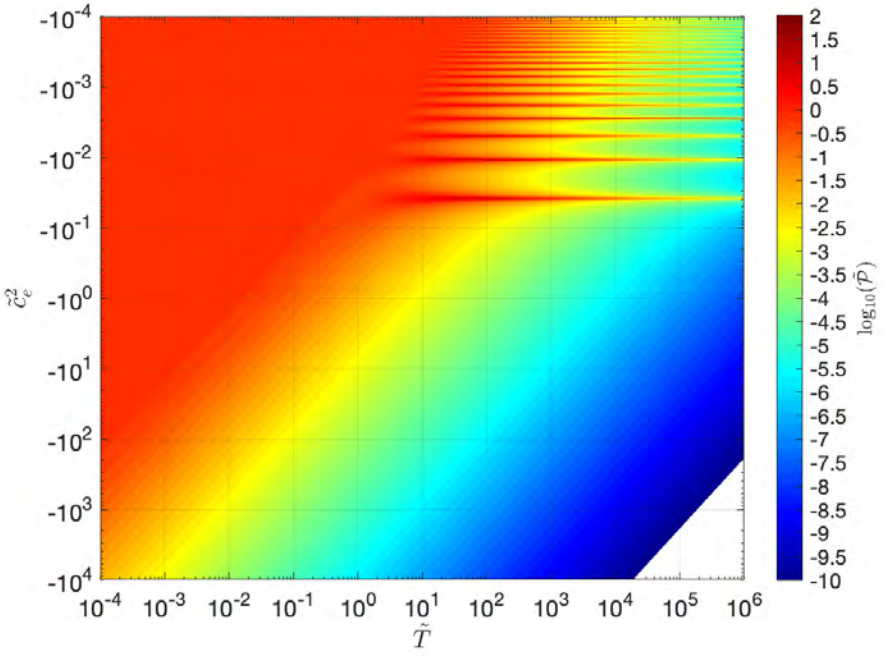

(B)

FIGURE 7.3.30. Tidal power $\tilde{\mathcal{P}}$ as a function of dissipation time scale $\tilde{T}$ and squared wave speed $\tilde{c}_e^2$ (positive (a) and negative (b) values for $\tilde{c}_e^2$ are displayed). Here $\tilde{T}$ refers to a process where dissipation is proportional to potential energy, and the forcing considered is the synchronous G22W component (see Section7.3.2).

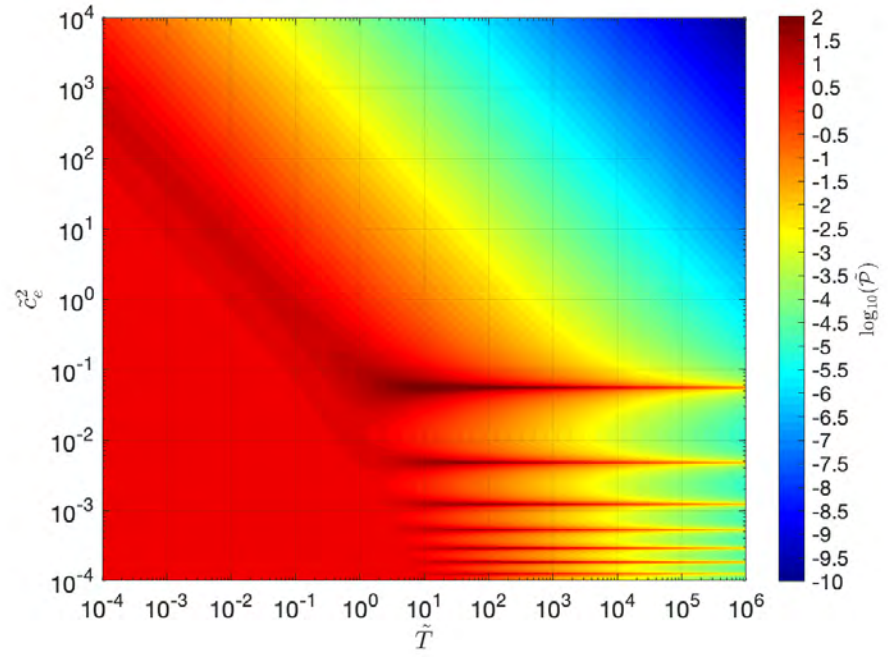

(A)

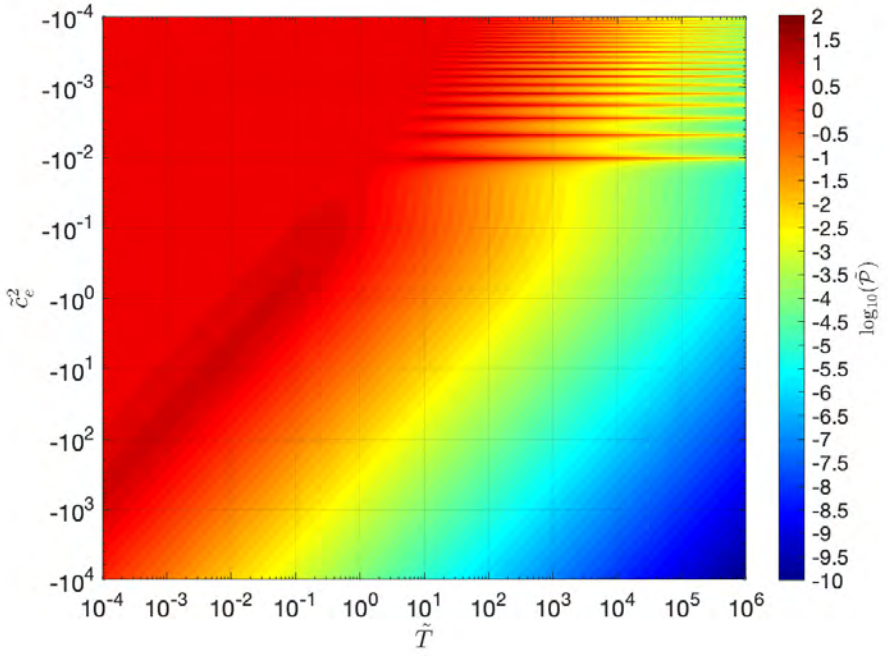

(B)

FIGURE 7.3.31. Tidal power $\tilde{\mathcal{P}}$ as a function of dissipation time scale $\tilde{T}$ and squared wave speed $\tilde{c}_e^2$ (positive (a) and negative (b) values for $\tilde{c}_e^2$ are displayed). Here $\tilde{T}$ refers to a process where dissipation is proportional to potential energy, and the forcing considered is the synchronous G22E component (see Section 7.3.2).

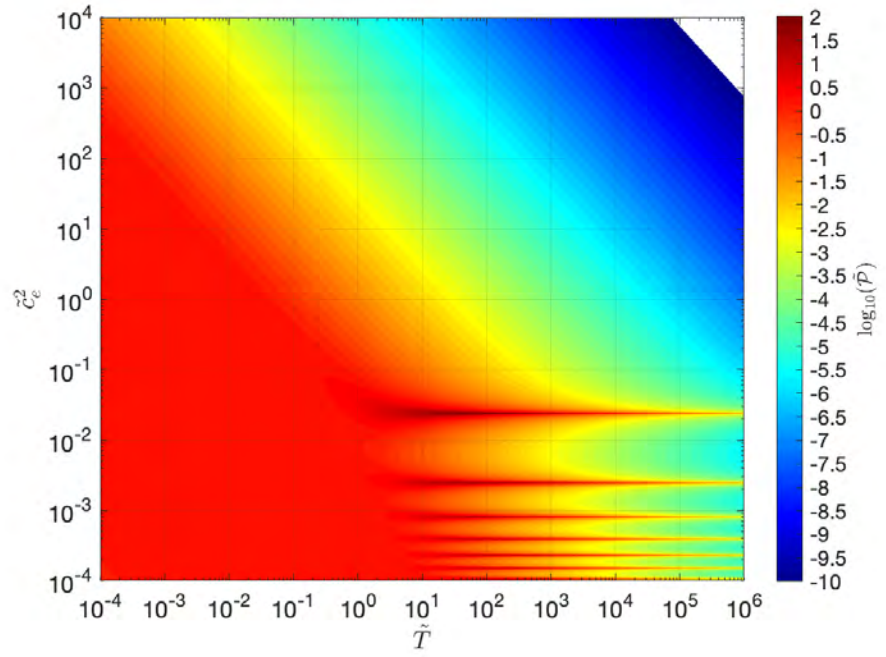

(A)

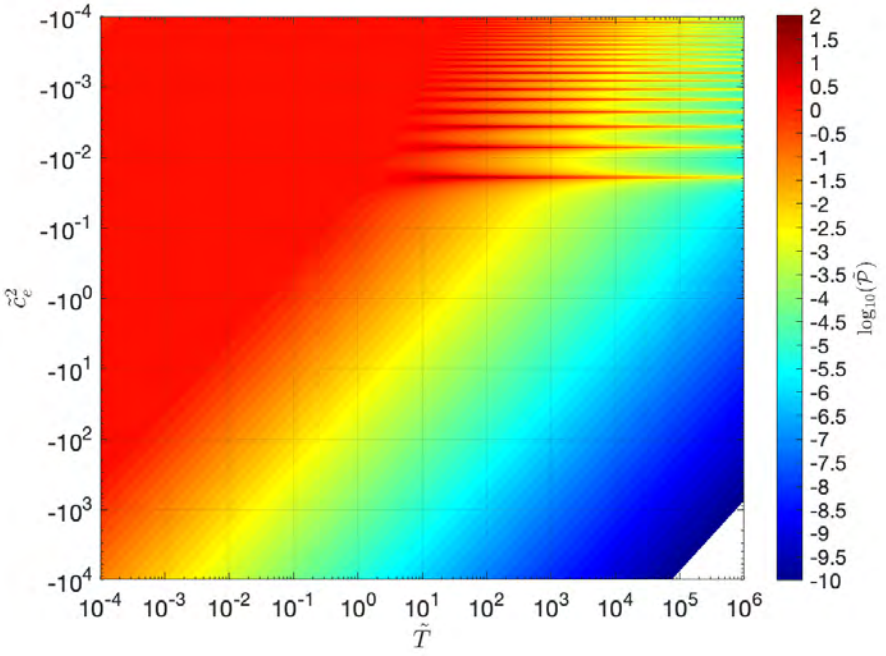

(B)

FIGURE 7.3.32. Tidal power $\tilde{\mathcal{P}}$ as a function of dissipation time scale $\tilde{T}$ and squared wave speed $\tilde{c}_e^2$ (positive (a) and negative (b) values for $\tilde{c}_e^2$ are displayed). Here $\tilde{T}$ refers to a process where dissipation is proportional to potential energy, and the forcing considered is the synchronous G21E component (see Section 7.3.2).

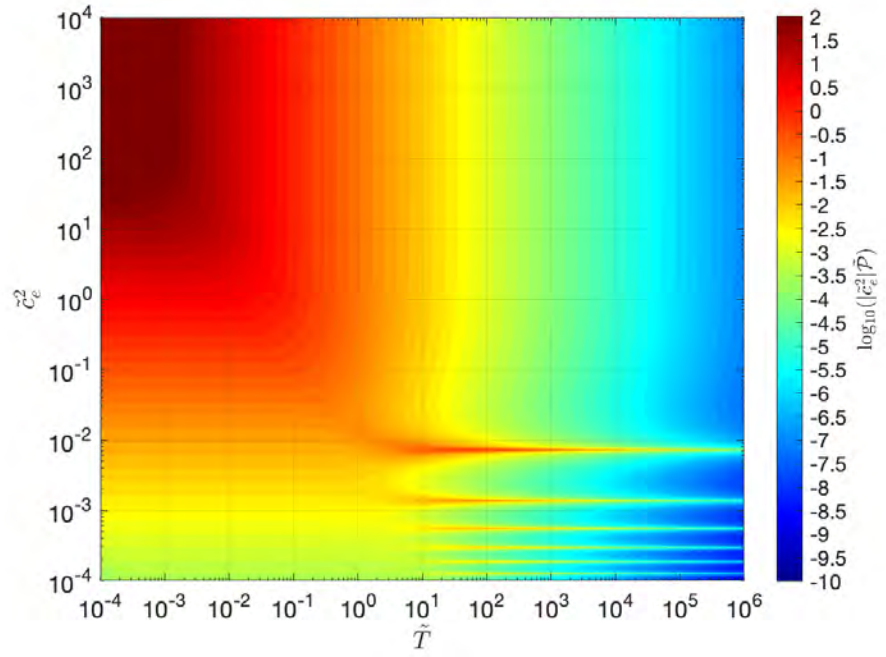

(A)

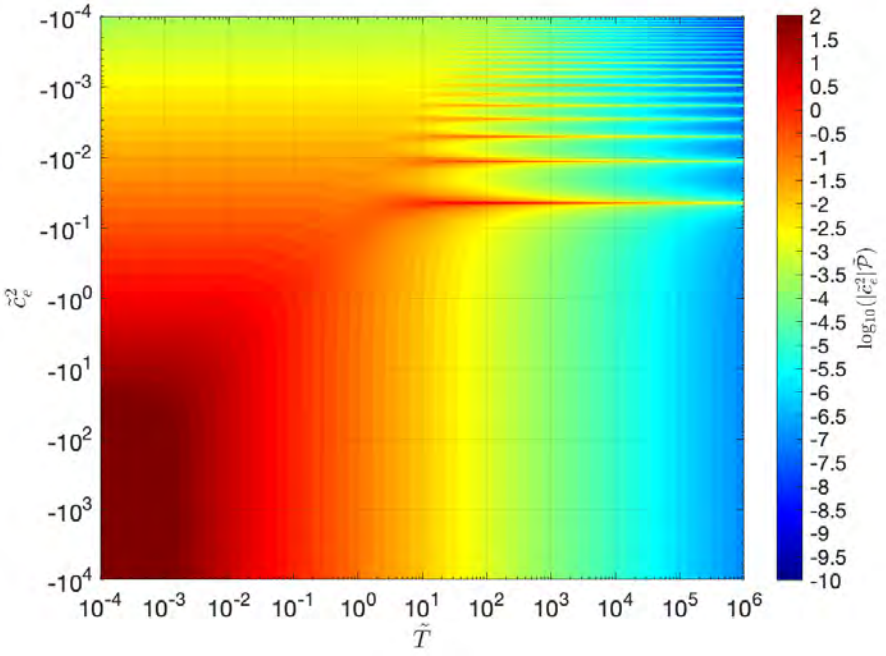

(B)

FIGURE 7.3.33. Tidal power integrated over the fluid thickness as represented by the product $\tilde{c}_e^2\tilde{\mathcal{P}}$, where $\tilde{\mathcal{P}}$ is the G20 component shown in Figure 7.3.29 (a).

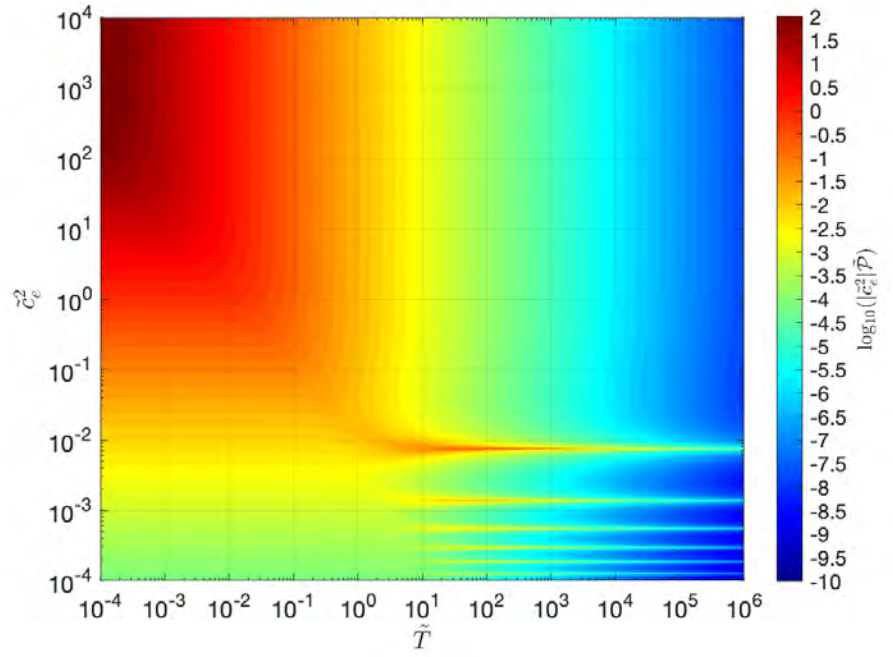

(A)

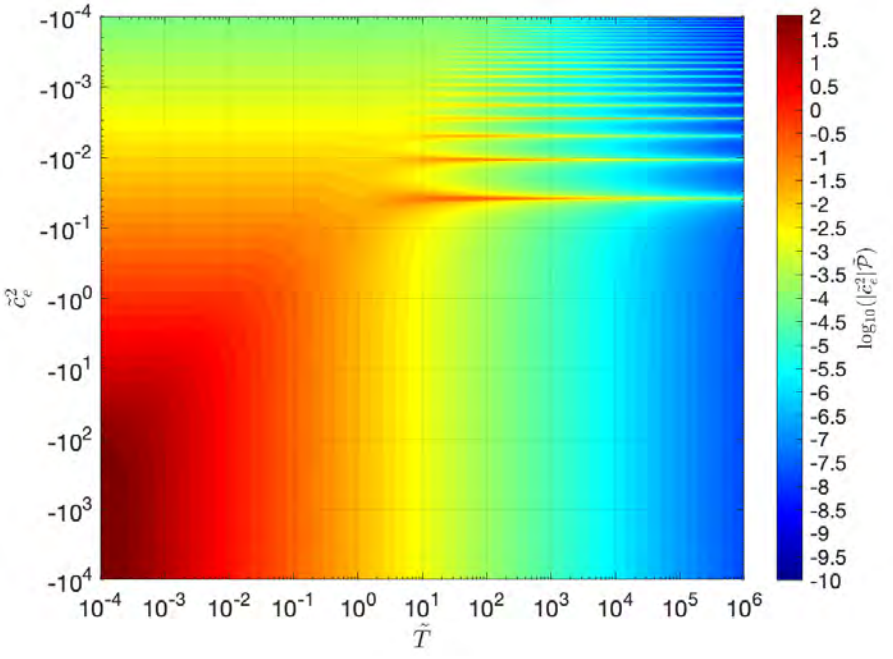

(B)

FIGURE 7.3.34. Tidal power integrated over the fluid thickness as represented by the product $\tilde{c}_e^2\tilde{\mathcal{P}}$, where $\tilde{\mathcal{P}}$ is the G22W component shown in Figure 7.3.30 (a).

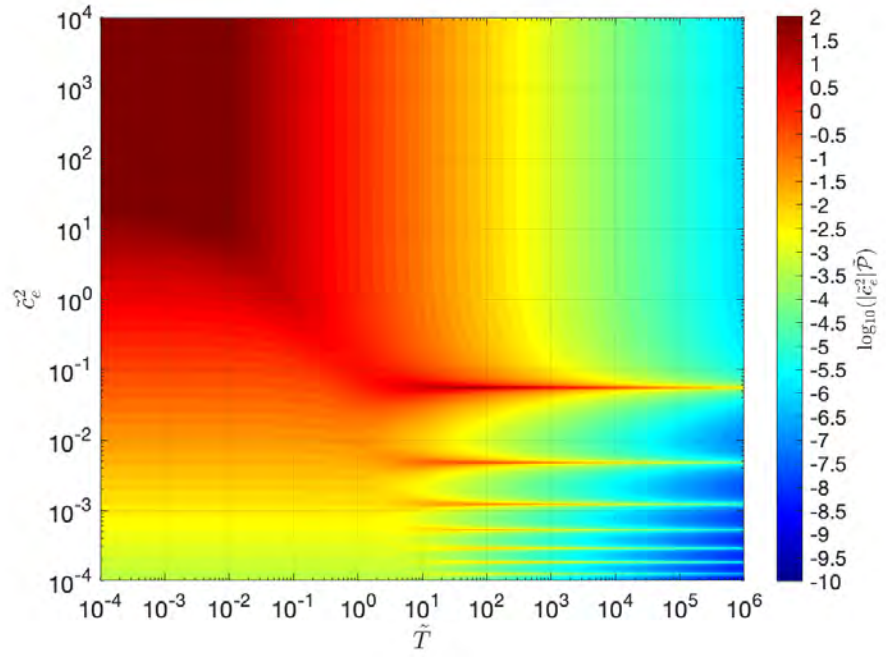

(A)

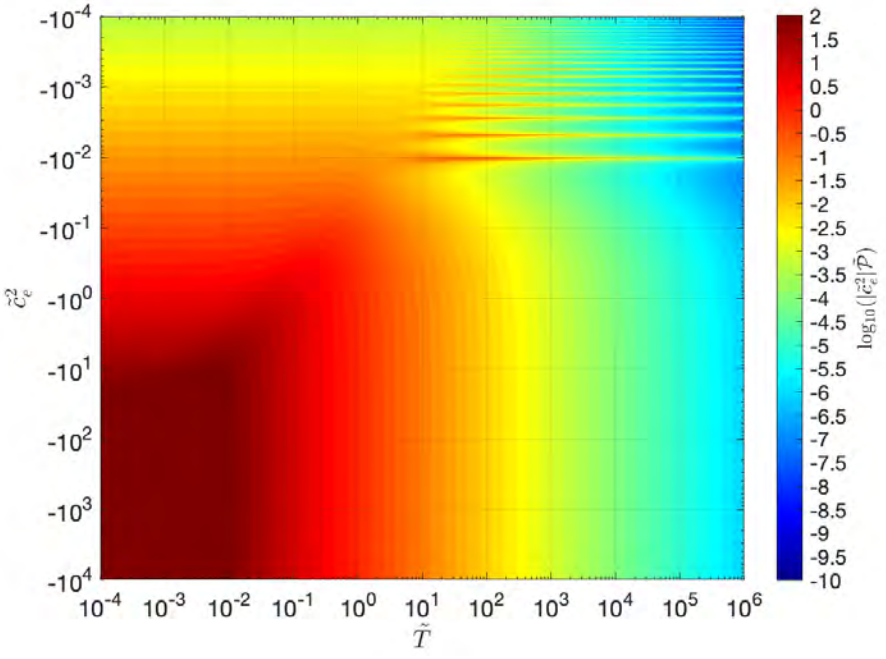

(B)

FIGURE 7.3.35. Tidal power integrated over the fluid thickness as represented by the product $\tilde{c}_e^2\tilde{\mathcal{P}}$, where $\tilde{\mathcal{P}}$ is the G22E component shown in Figure 7.3.31 (a).

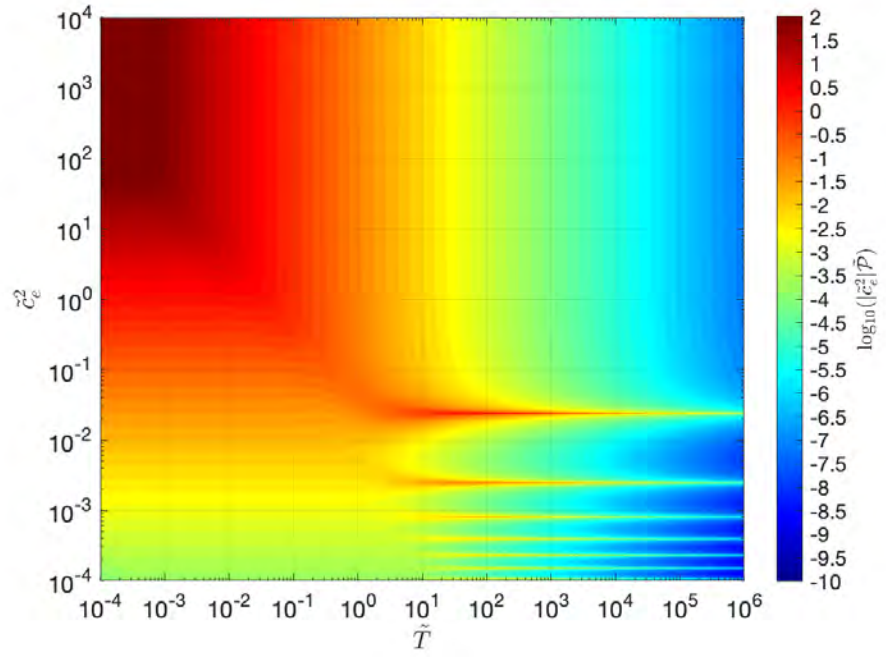

(A)

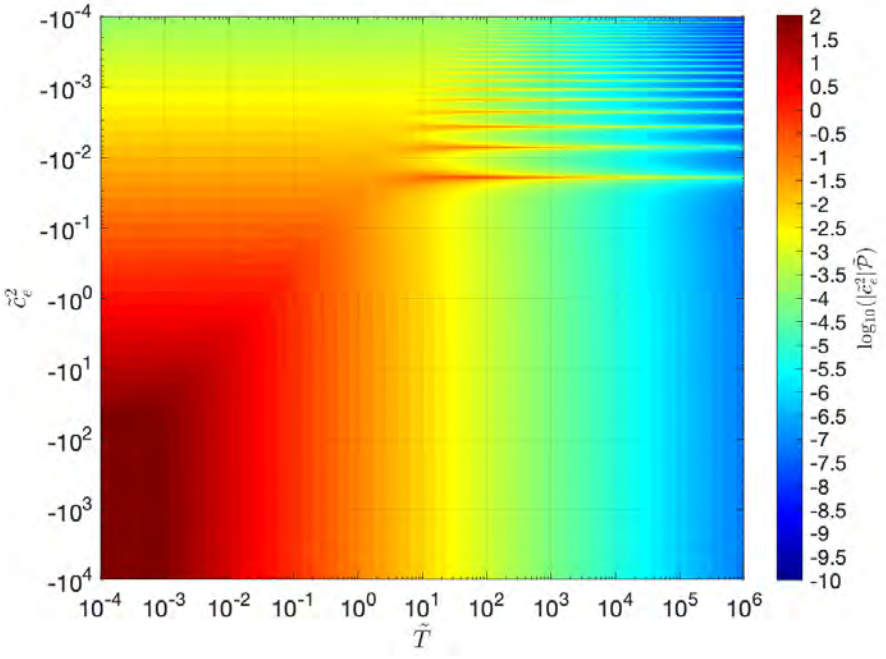

(B)

FIGURE 7.3.36. Tidal power integrated over the fluid thickness as represented by the product $\tilde{c}_e^2\tilde{\mathcal{P}}$, where $\tilde{\mathcal{P}}$ is the G21E component shown in Figure 7.3.32 (a).

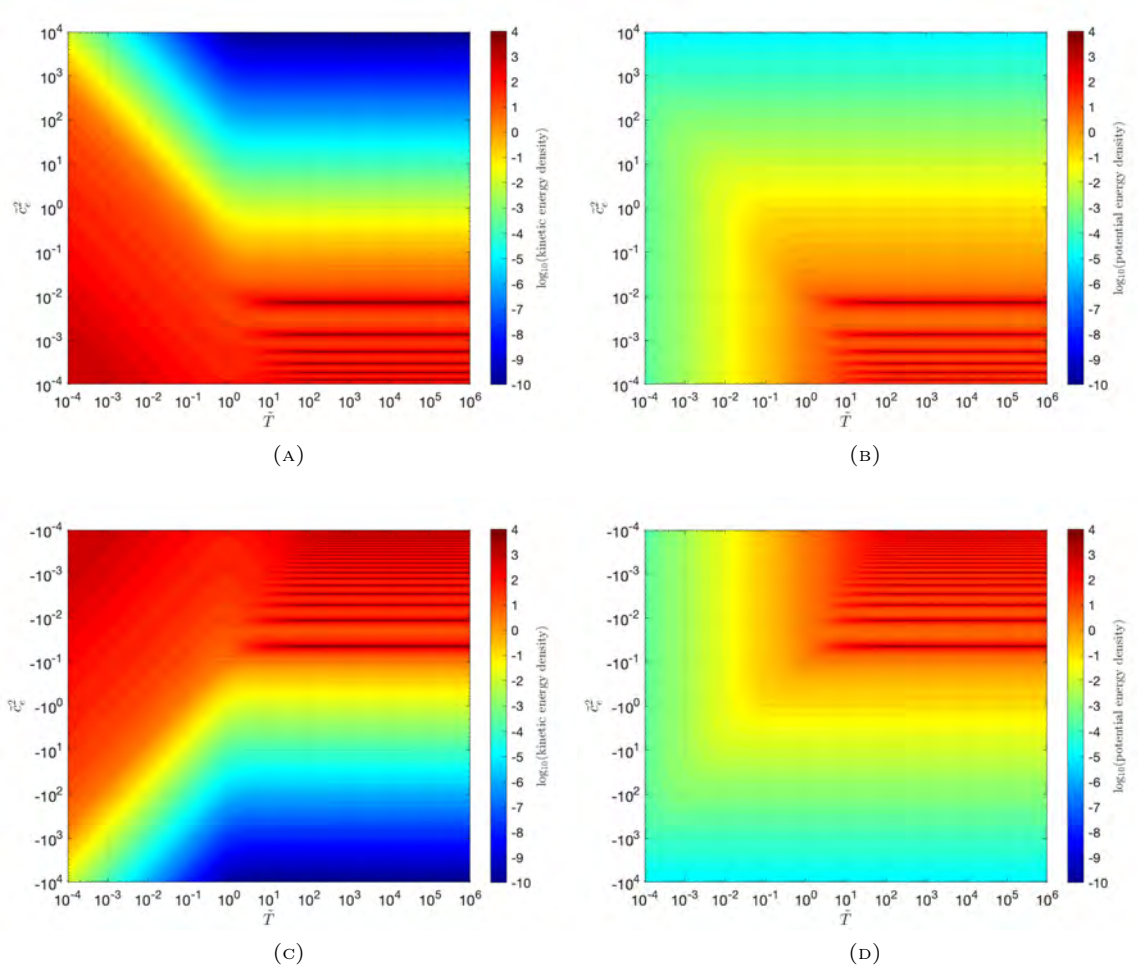

FIGURE 7.3.37

FIGURE 7.3.38. Kinetic energy density (a, c) and potential energy density (b, d) as a function of dissipation time scale $\tilde{T}$ and squared wave speed $\tilde{c}_e^2$ (positive (a) and negative (b) values for $\tilde{c}_e^2$ are displayed). Here $\tilde{T}$ refers to a process where dissipation is proportional to potential energy and the forcing is the G20 component in the nonsynchronous rapid rotation limit described in Section 7.3.2.

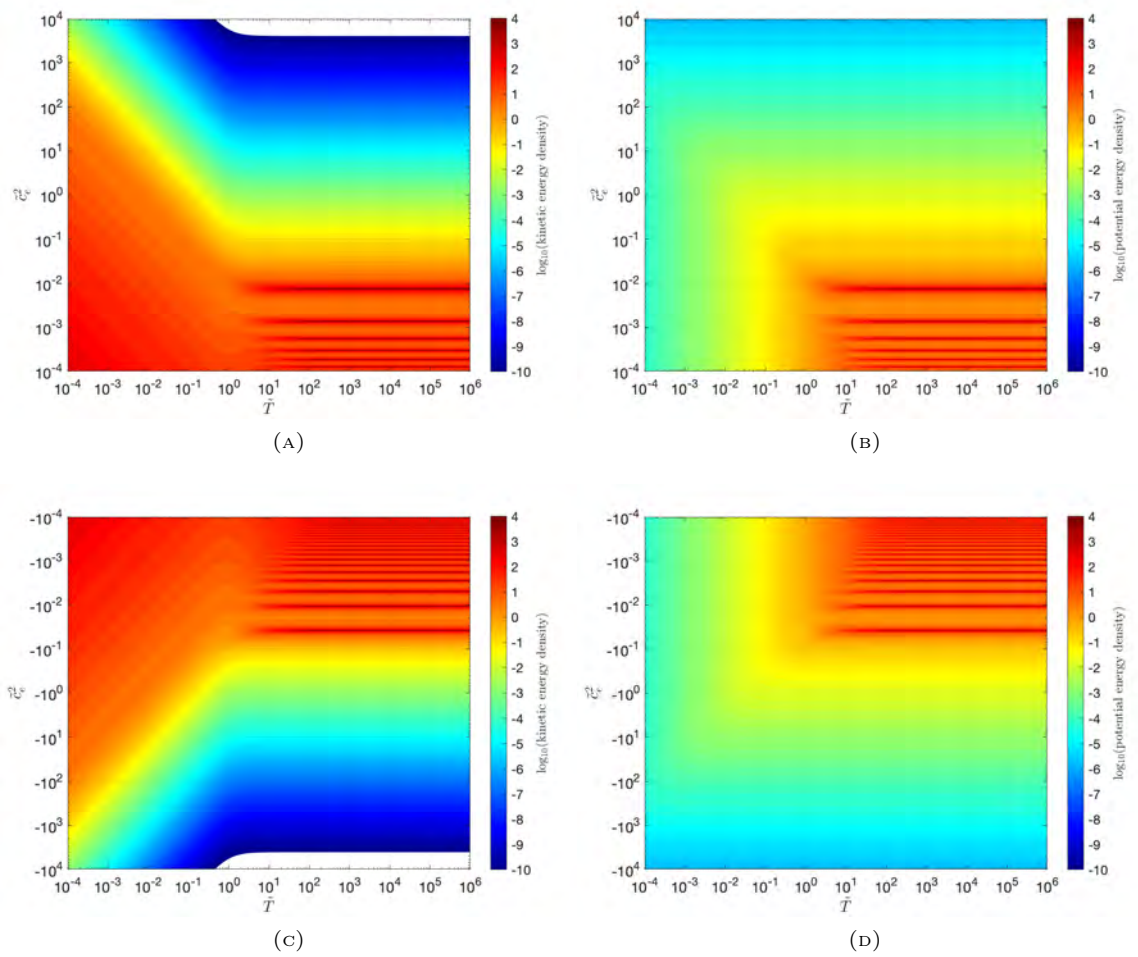

FIGURE 7.3.39

FIGURE 7.3.40. Kinetic energy density (a, c) and potential energy density (b, d) as a function of dissipation time scale $\tilde{T}$ and squared wave speed $\tilde{c}_e^2$ (positive (a) and negative (b) values for $\tilde{c}_e^2$ are displayed). Here $\tilde{T}$ refers to a process where dissipation is proportional to potential energy and the forcing is the G22W component in the nonsynchronous rapid rotation limit described in Section 7.3.2.

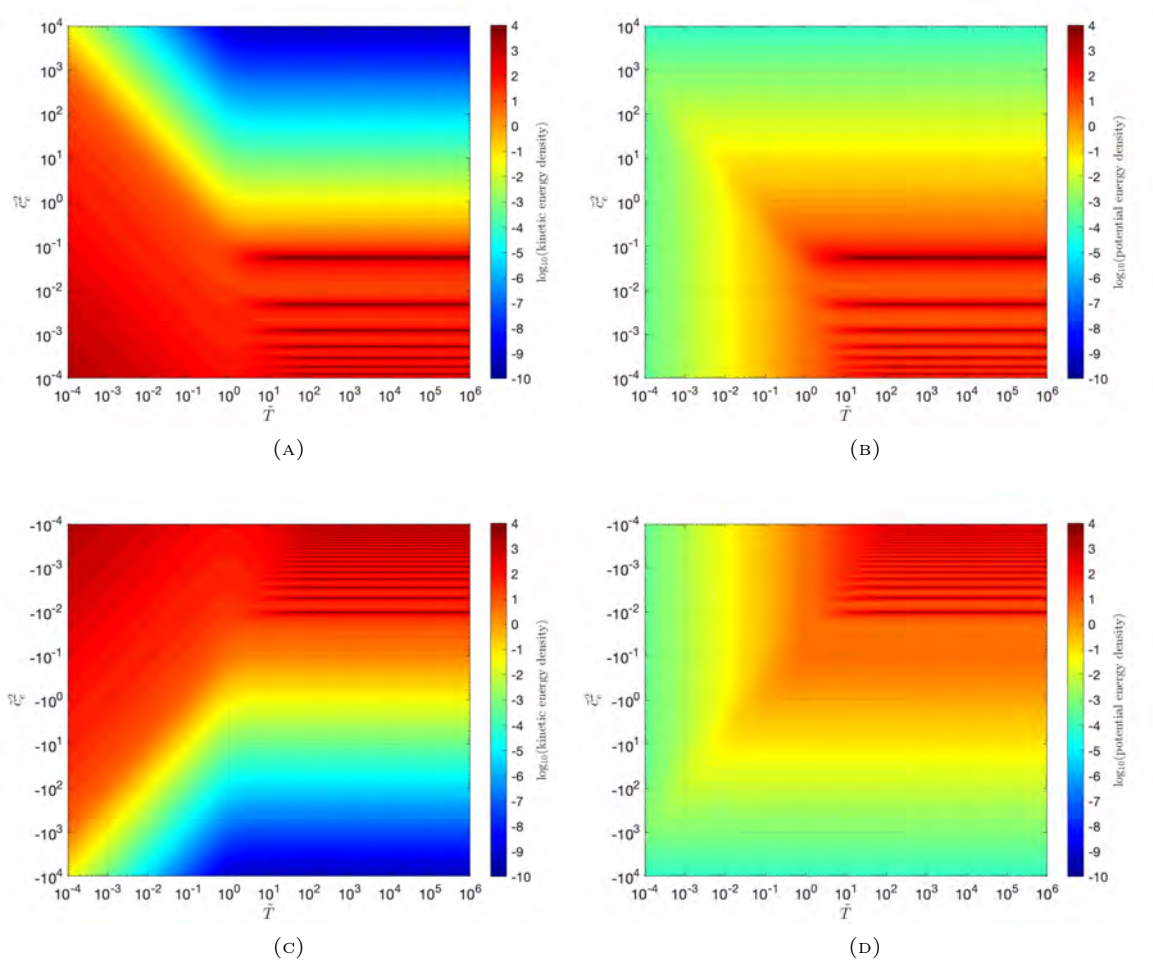

FIGURE 7.3.41

FIGURE 7.3.42. Kinetic energy density (a, c) and potential energy density (b, d) as a function of dissipation time scale $\tilde{T}$ and squared wave speed $\tilde{c}_e^2$ (positive (a) and negative (b) values for $\tilde{c}_e^2$ are displayed). Here $\tilde{T}$ refers to a process where dissipation is proportional to potential energy and the forcing is the G22E component in the nonsynchronous rapid rotation limit described in Section 7.3.2.

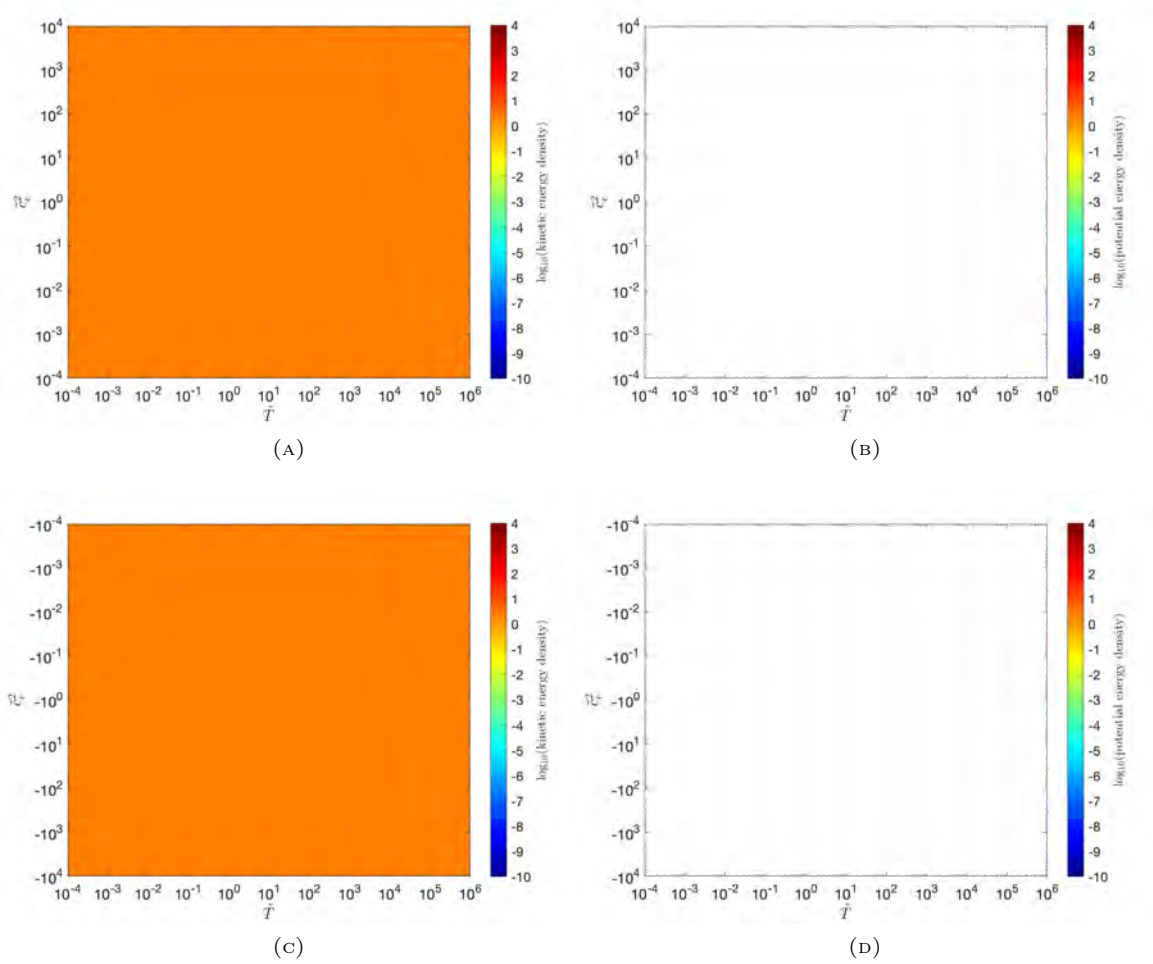

FIGURE 7.3.43

FIGURE 7.3.44. Kinetic energy density (a, c) and potential energy density (b, d) as a function of dissipation time scale $\tilde{T}$ and squared wave speed $\tilde{c}_e^2$ (positive (a) and negative (b) values for $\tilde{c}_e^2$ are displayed). Here $\tilde{T}$ refers to a process where dissipation is proportional to potential energy and the forcing is the G21W component in the nonsynchronous rapid rotation limit described in Section 7.3.2.

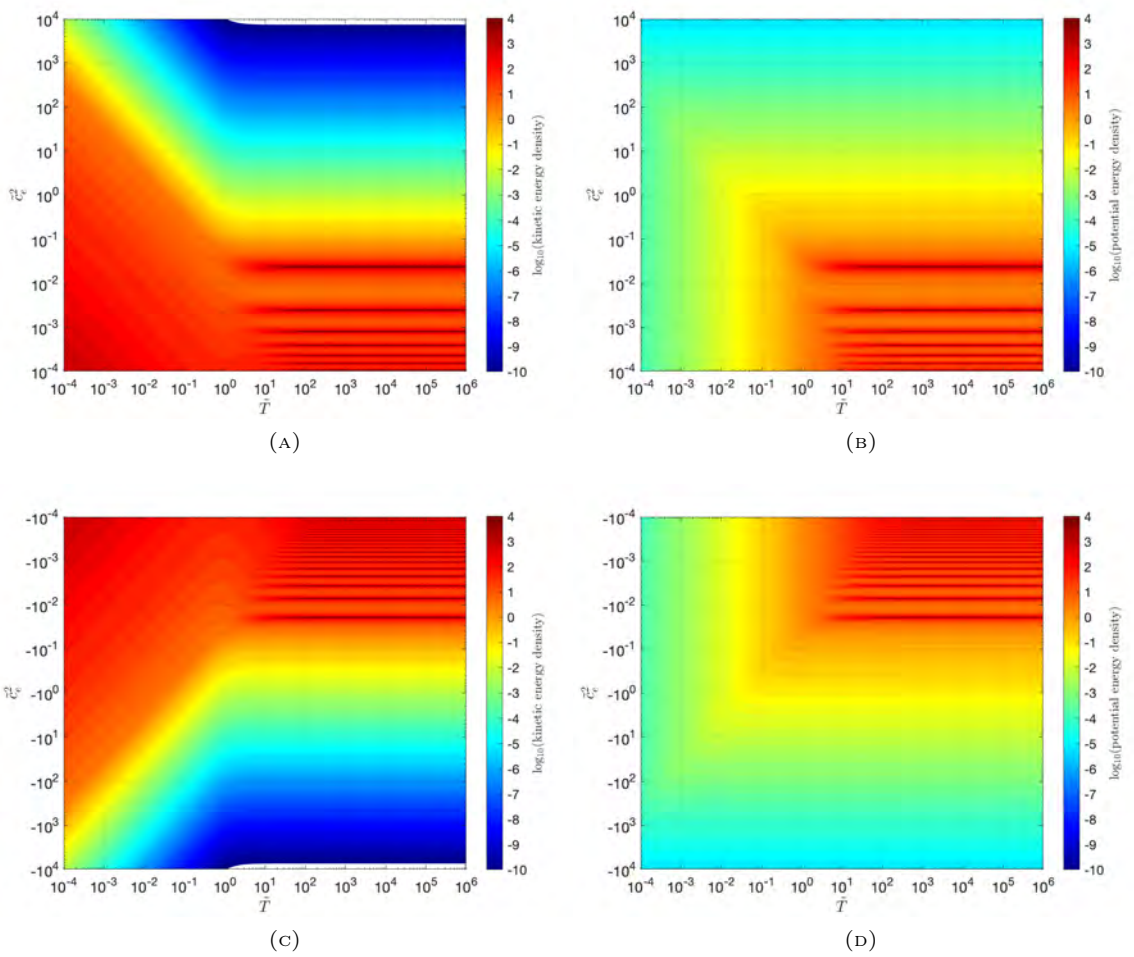

FIGURE 7.3.45. Kinetic energy density (a, c) and potential energy density (b, d) as a function of dissipation time scale $\tilde{T}$ and squared wave speed $\tilde{c}_e^2$ (positive (a) and negative (b) values for $\tilde{c}_e^2$ are displayed). Here $\tilde{T}$ refers to a process where dissipation is proportional to potential energy and the forcing is the G21E component in the nonsynchronous rapid rotation limit described in Section 7.3.2.

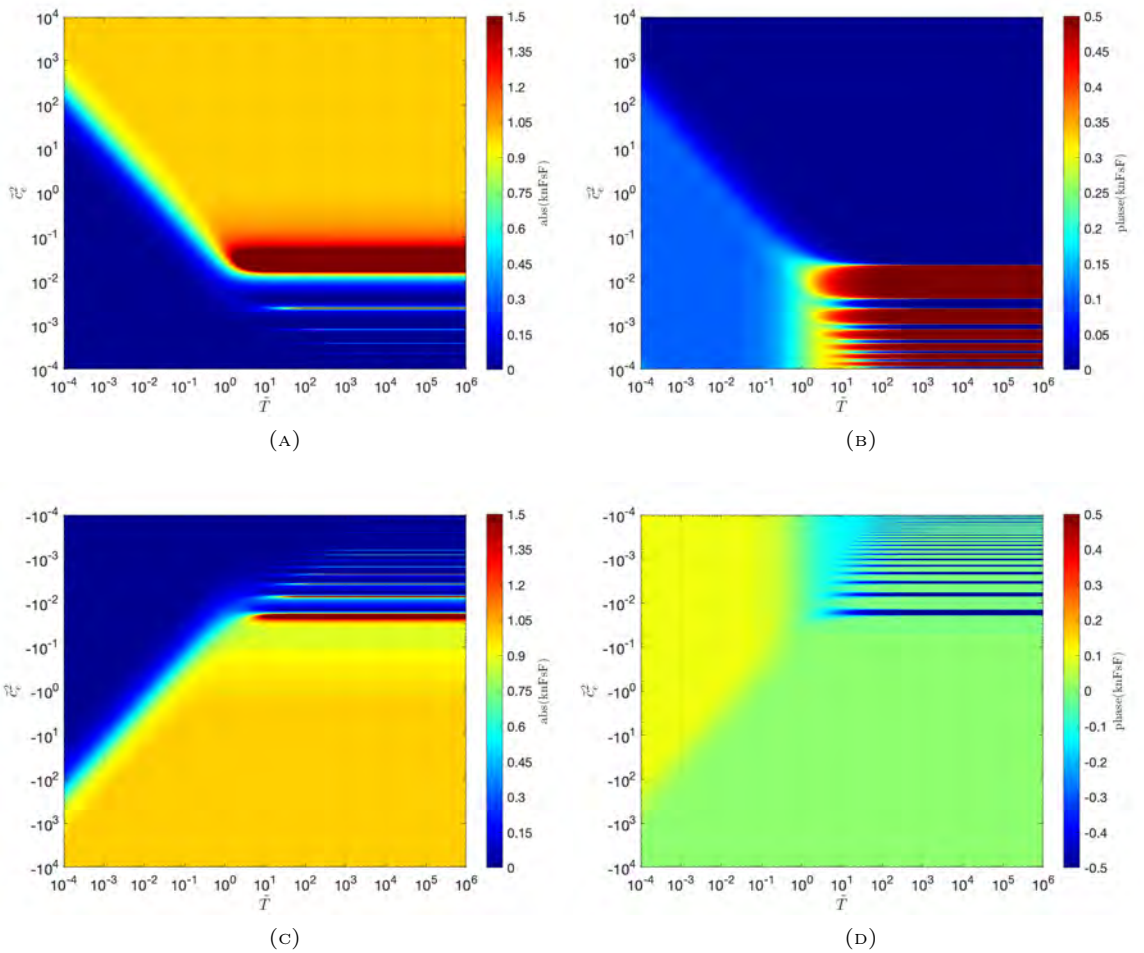

FIGURE 7.3.46. Degree-two admittance (k_2) amplitude (a, c) and phase/(2π) (b, d) as a function of dissipation time scale $\tilde{T}$ and squared wave speed $\tilde{c}_e^2$. Here $\tilde{T}$ refers to a process where dissipation is proportional to potential energy and the forcing is the G20 component in the nonsynchronous rapid rotation limit described in Section 7.3.2.

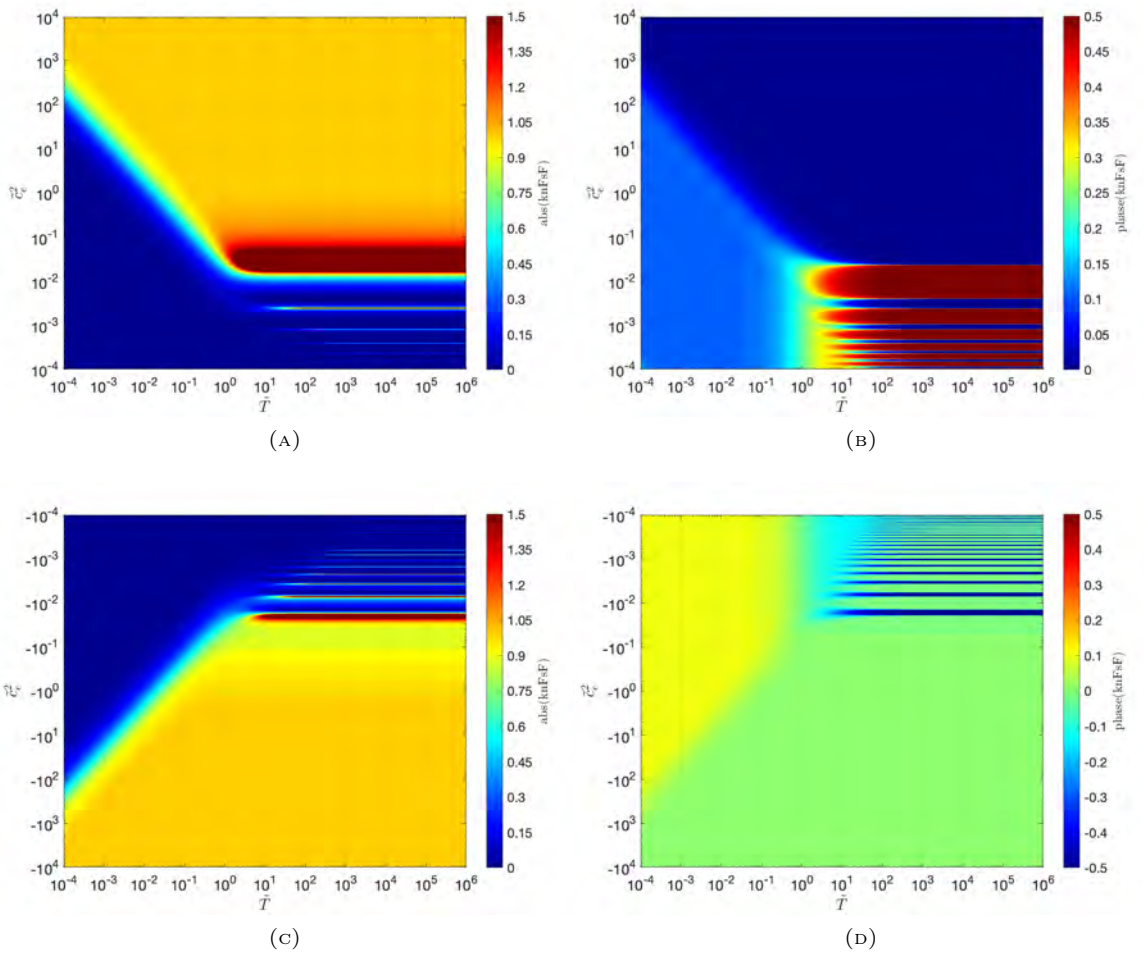

FIGURE 7.3.47. Degree-two admittance (k_2) amplitude (a, c) and phase/(2π) (b, d) as a function of dissipation time scale $\tilde{T}$ and squared wave speed $\tilde{c}_e^2$. Here $\tilde{T}$ refers to a process where dissipation is proportional to potential energy and the forcing is the G22W component in the nonsynchronous rapid rotation limit described in Section 7.3.2.

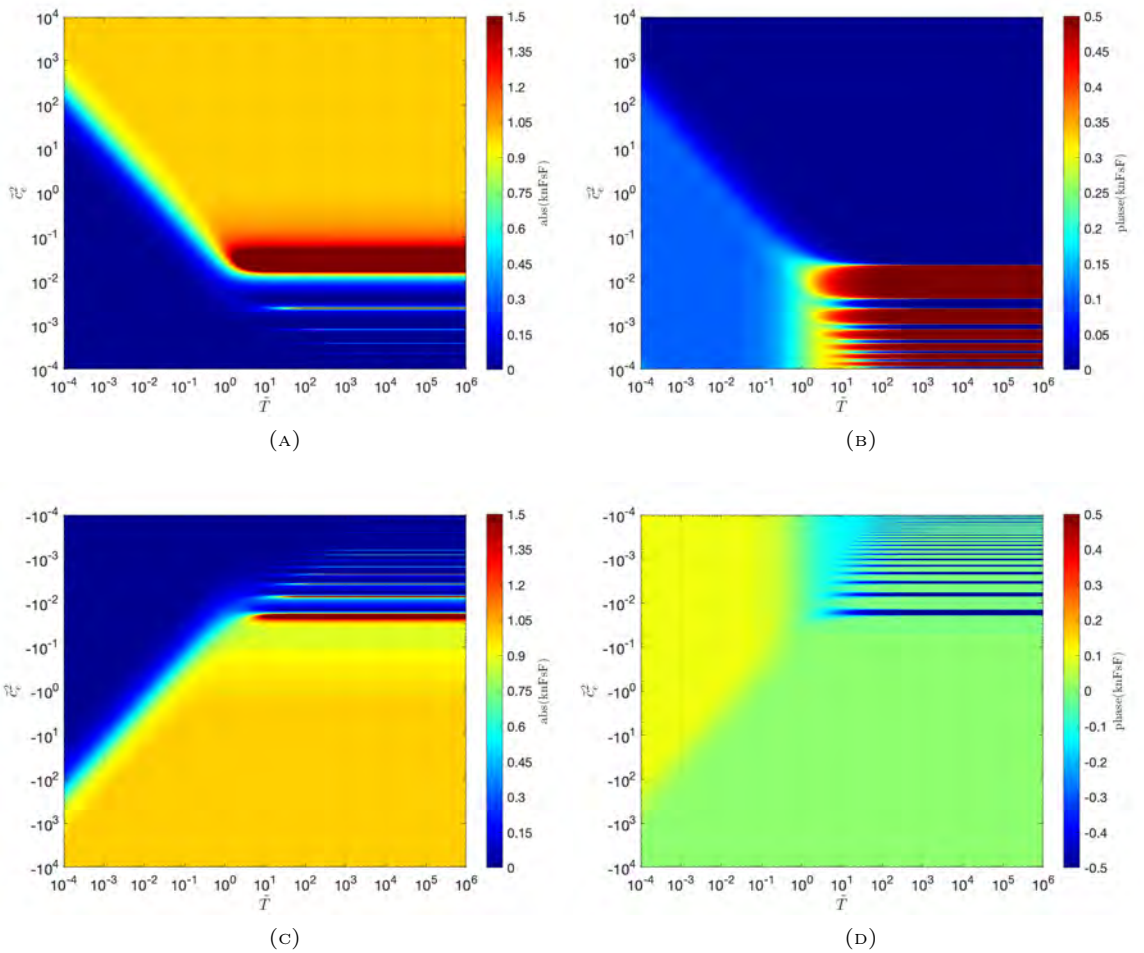

FIGURE 7.3.48. Degree-two admittance (k_2) amplitude (a, c) and phase/(2π) (b, d) as a function of dissipation time scale $\tilde{T}$ and squared wave speed $\tilde{c}_e^2$. Here $\tilde{T}$ refers to a process where dissipation is proportional to potential energy and the forcing is the G22E component in the nonsynchronous rapid rotation limit described in Section 7.3.2.

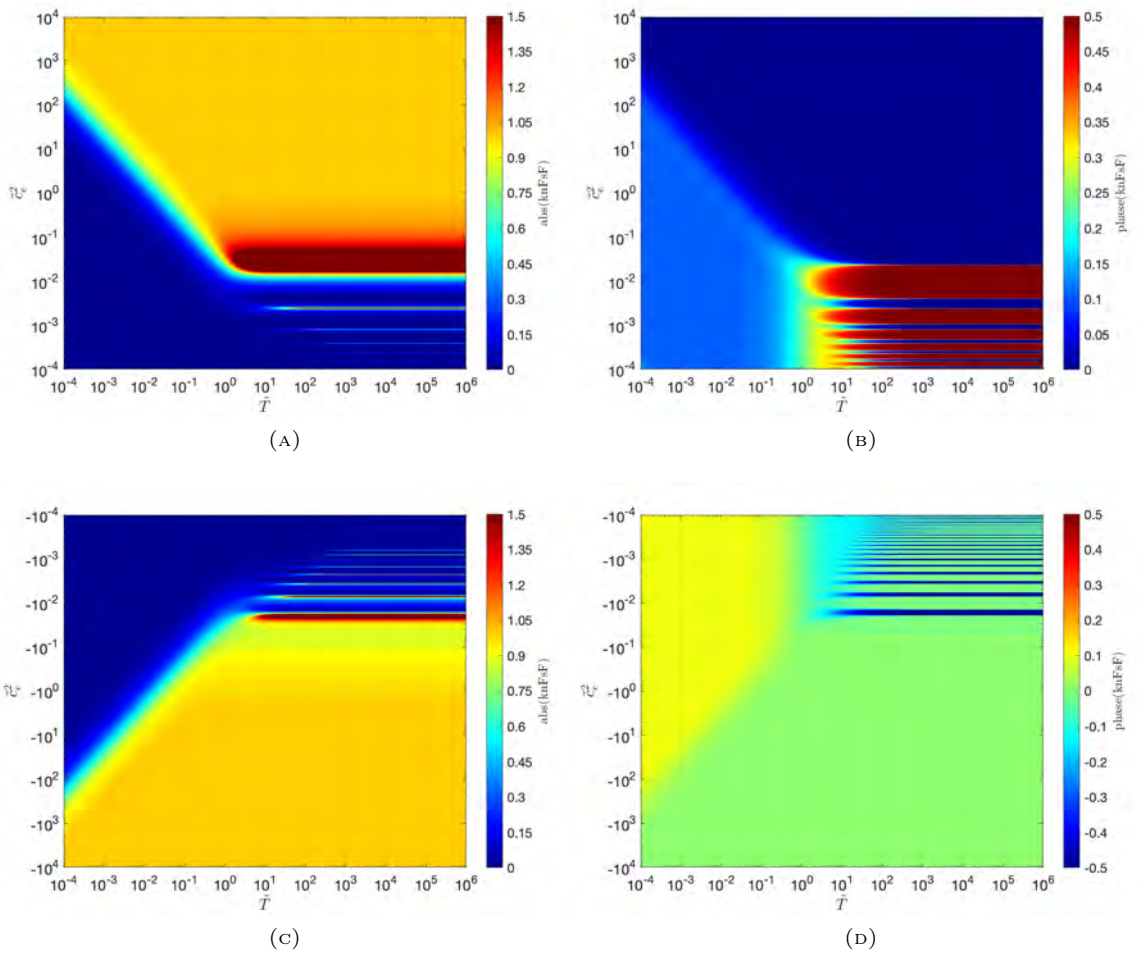

FIGURE 7.3.49. Degree-two admittance (k_2) amplitude (a, c) and phase/(2π) (b, d) as a function of dissipation time scale $\tilde{T}$ and squared wave speed $\tilde{c}_e^2$. Here $\tilde{T}$ refers to a process where dissipation is proportional to potential energy and the forcing is the G21W component in the nonsynchronous rapid rotation limit described in Section 7.3.2.

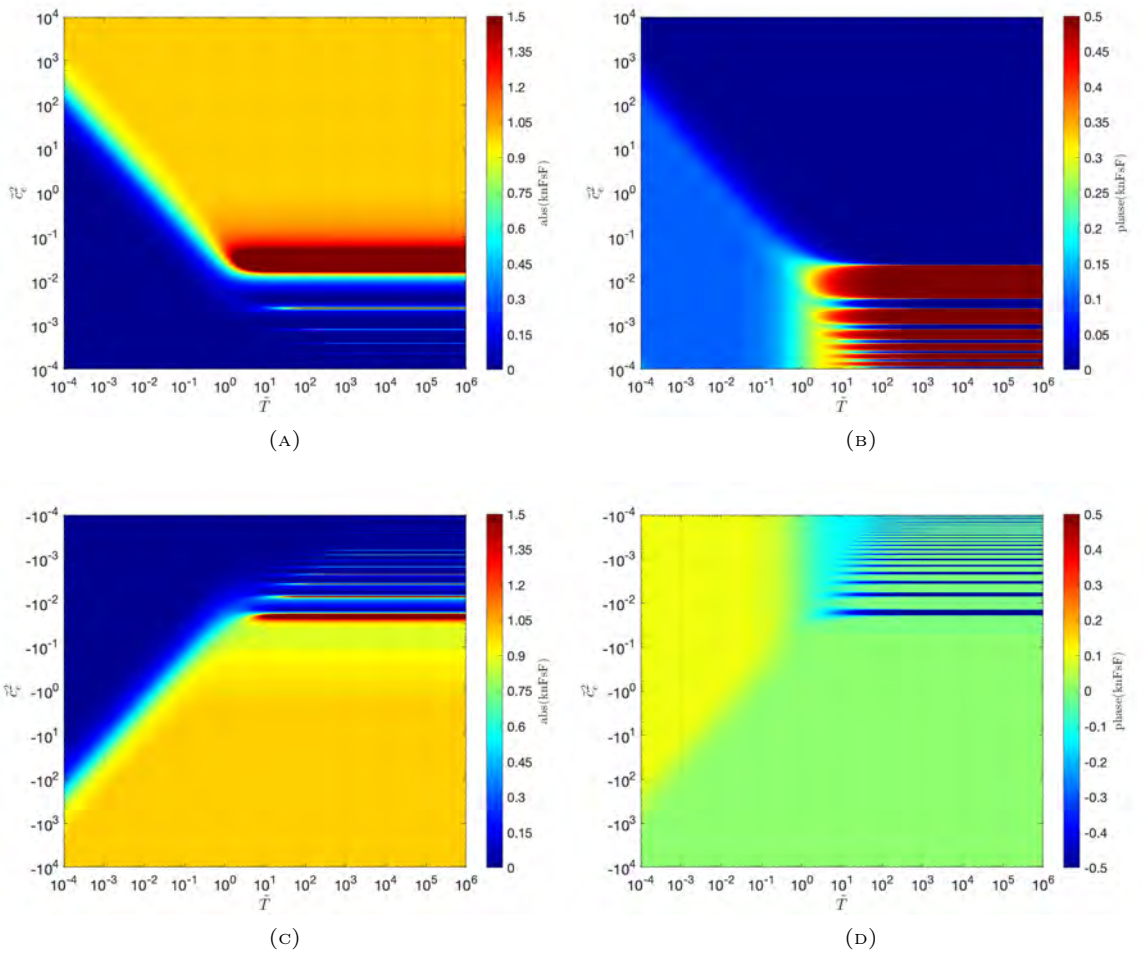

FIGURE 7.3.50. Degree-two admittance (k_2) amplitude (a, c) and phase/(2π) (b, d) as a function of dissipation time scale $\tilde{T}$ and squared wave speed $\tilde{c}_e^2$. Here $\tilde{T}$ refers to a process where dissipation is proportional to potential energy and the forcing is the G21E component in the nonsynchronous rapid rotation limit described in Section 7.3.2.

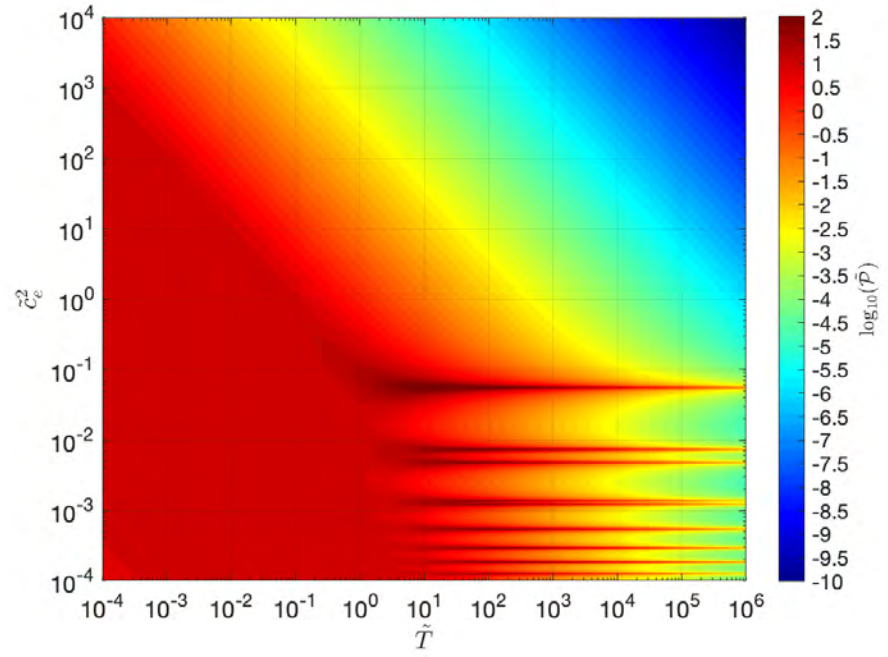

(A)

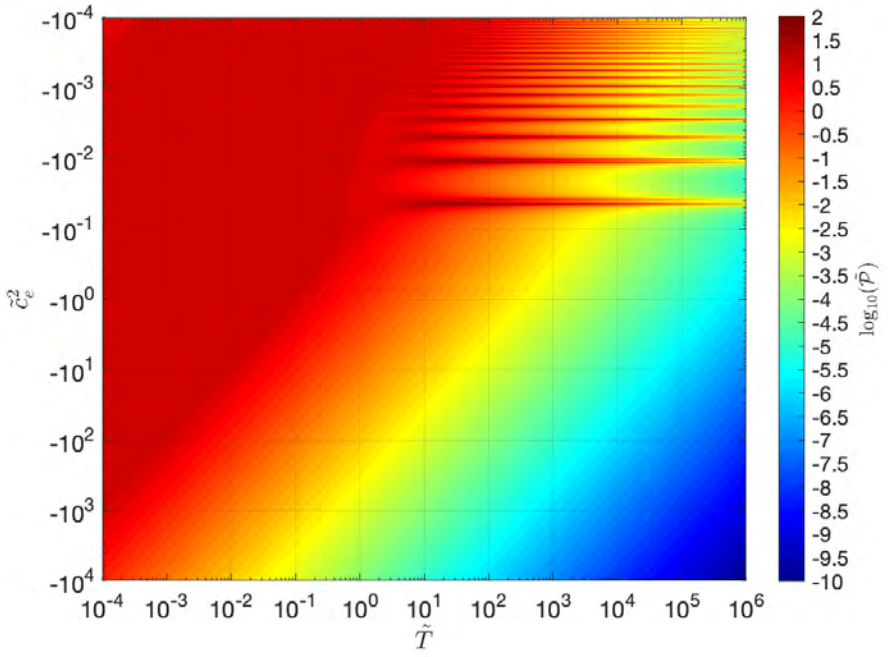

(B)

FIGURE 7.3.51. Tidal power $\tilde{\mathcal{P}}$ as a function of dissipation time scale $\tilde{T}$ and squared wave speed $\tilde{c}_e^2$ (positive (a) and negative (b) values for $\tilde{c}_e^2$ are displayed). Here $\tilde{T}$ refers to a process where dissipation is proportional to potential energy, and the forcing considered is due to the eccentricity of a synchronous-rotation orbit (see Section 7.3.2).

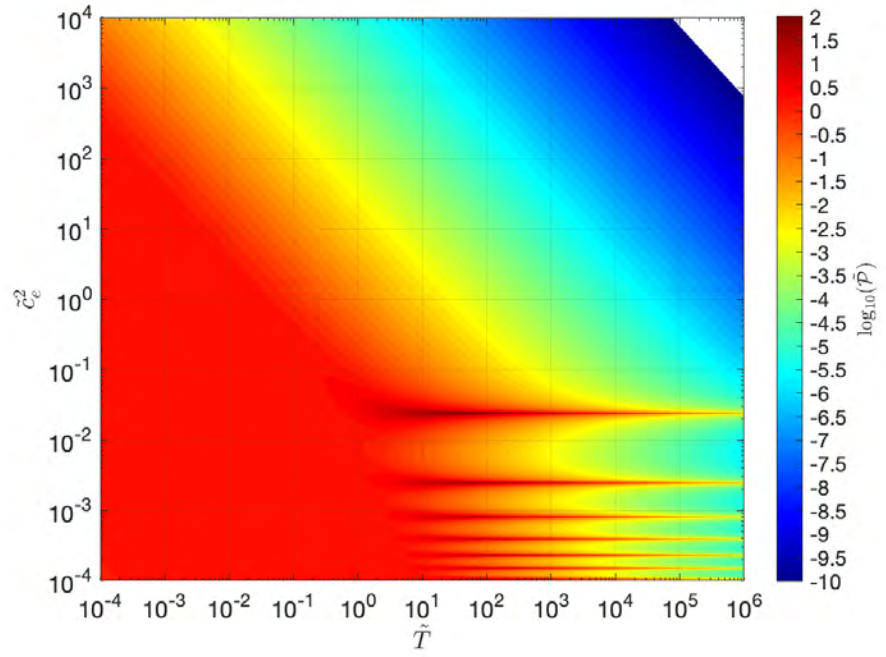

(A)

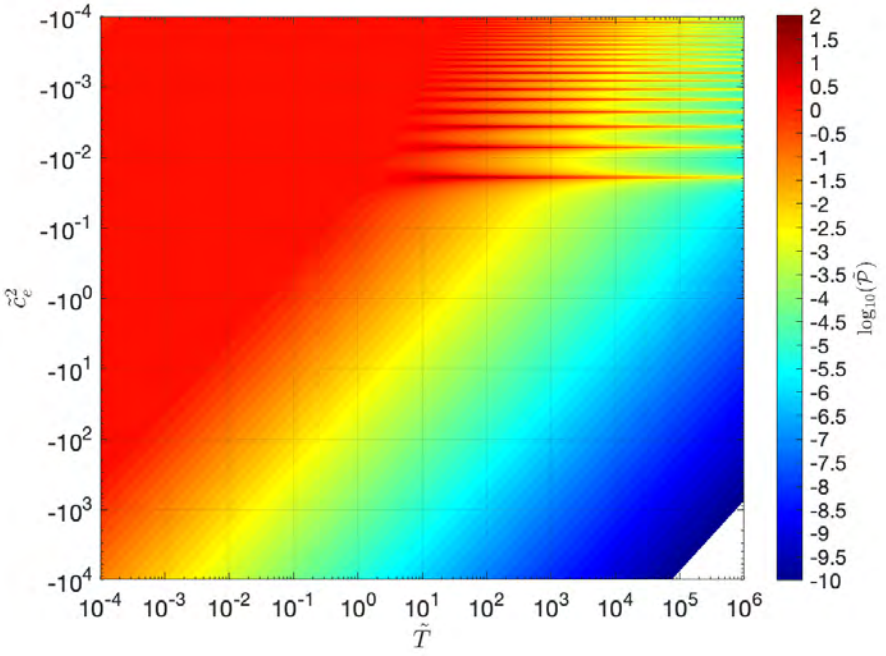

(B)

FIGURE 7.3.52. Tidal power $\tilde{\mathcal{P}}$ as a function of dissipation time scale $\tilde{T}$ and squared wave speed $\tilde{c}_e^2$ (positive (a) and negative (b) values for $\tilde{c}_e^2$ are displayed). Here $\tilde{T}$ refers to a process where dissipation is proportional to potential energy, and the forcing considered is due to the obliquity of a synchronous-rotation orbit (see Section 7.3.2).

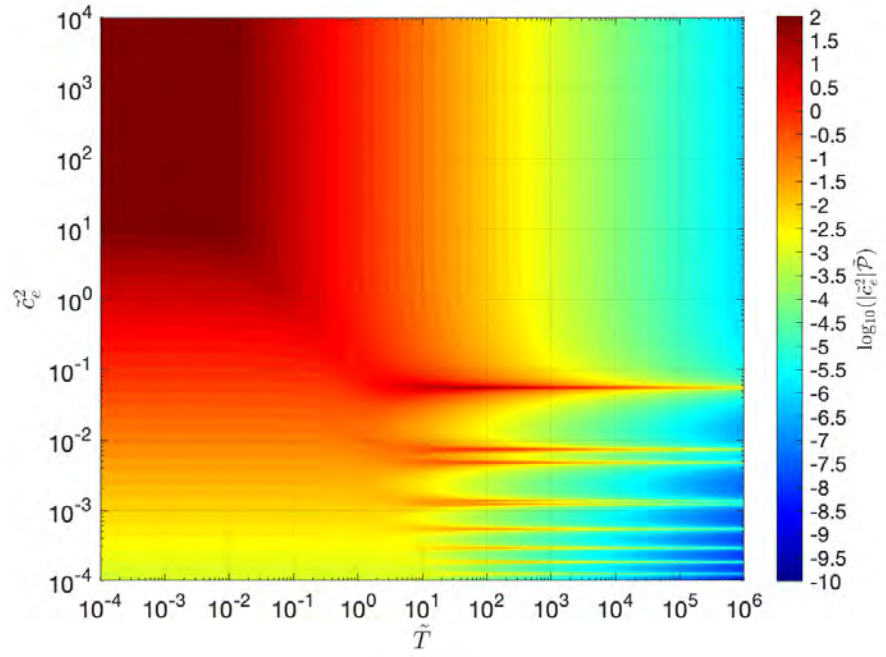

(A)

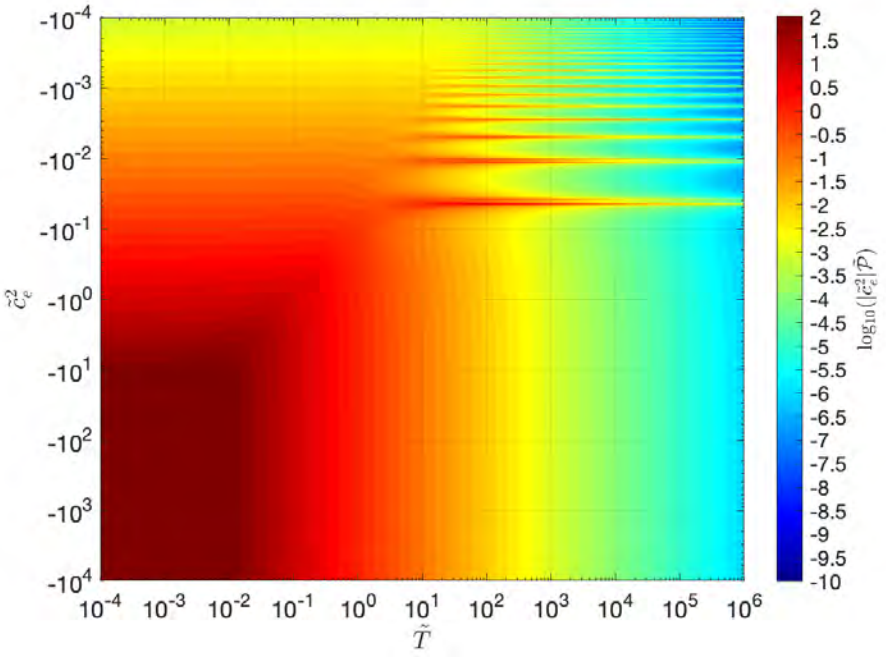

(B)

FIGURE 7.3.53. Tidal power integrated over the fluid thickness as represented by the product $\tilde{c}_e^2\tilde{\mathcal{P}}$, where $\tilde{\mathcal{P}}$ is the total eccentricity component shown in Figure 7.3.51 (a).

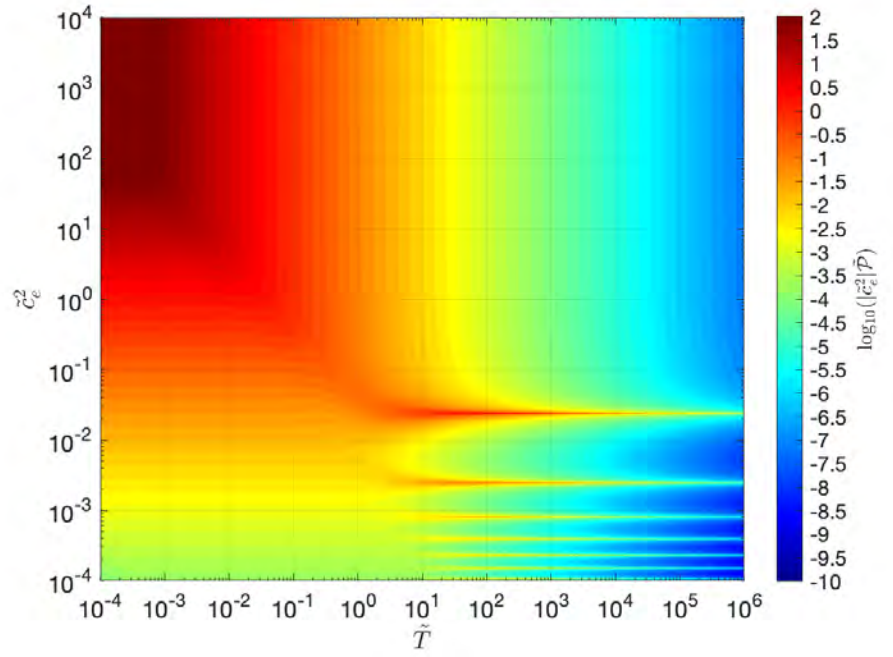

(A)

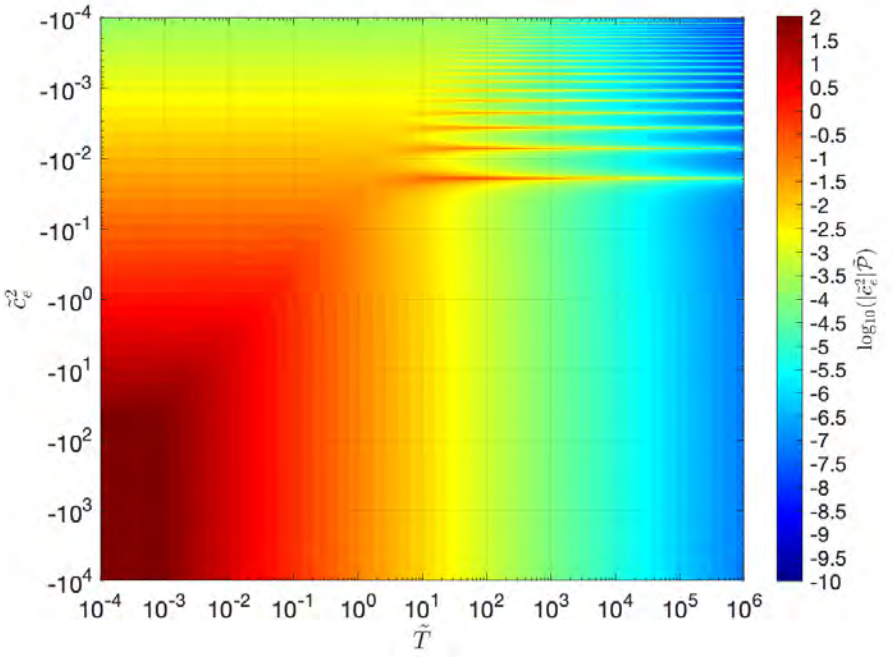

(B)

FIGURE 7.3.54. Tidal power $\tilde{\mathcal{P}}$ as a function of dissipation time scale $\tilde{T}$ and squared wave speed $\tilde{c}_e^2$ (positive (a) and negative (b) values for $\tilde{c}_e^2$ are displayed). Here $\tilde{T}$ refers to a process where dissipation is proportional to potential energy, and the forcing considered is due to the obliquity of a synchronous-rotation orbit (see Section 7.3.2).

Bibliography

M Beuthe. Crustal control of dissipative ocean tides in Enceladus and other icy moons. *Icarus*, 280:278–299, 2016.

E M A Chen, F Nimmo, and G A Glatzmaier. Tidal heating in icy satellite oceans. *Icarus*, 229:11–30, 2014.

PJ Ioannou and RS Lindzen. Gravitational tides in the outer planets. I-Implications of classical tidal theory. *The Astrophysical Journal*, 406:252–278, 1993a.

P.J. Ioannou and R.S. Lindzen. Gravitational tides in the outer planets. II. Interior calculations and estimation of the tidal dissipation factor. *Astrophysical Journal*, 406:252–278, 1993b.

M Longuet-Higgins. The eigenfunctions of Laplace's tidal equations over a sphere. *Philosophical Transactions of the Royal Society of London.*, 262:511–607, 1968.

I Matsuyama. Tidal dissipation in the oceans of icy satellites. *Icarus*, 242:11–18, 2014.

Isamu Matsuyama, Mikael Beuthe, Hamish C F C Hay, Francis Nimmo, and Shunichi Kamata. Ocean tidal heating in icy satellites with solid shells. *Icarus*, 312:208–230, 2018.

R Tyler. Tidal dynamical considerations constrain the state of an ocean on Enceladus. *Icarus*, 211(1): 770–779, 2011.

R Tyler. Comparative estimates of the heat generated by ocean tides on icy satellites in the outer Solar System. *Icarus*, 243:358–385, 2014.

R Tyler and R Käse. A string function for describing the propagation of baroclinic anomalies in the ocean. *Journal of Physical Oceanography*, 31:765–776, 2001.

R H Tyler and R Käse. A 'string function' for describing the propagation of large-scale potential energy anomalies in a rotating fluid. *Geophysical and Astrophysical Fluid Dynamics*, 92(1-2):31–64, July 2000.

RH Tyler. Strong ocean tidal flow and heating on moons of the outer planets. *Nature*, 456(7223):770–772, 2008.

Robert H Tyler. Ocean tides heat Enceladus. *Geophysical Research Letters*, 36(15):L15205, 2009.

Robert H. Tyler. Tidal power and banding in Jupiter. *Planetary and Space Science*, 165:244–249, 2019.

Robert H Tyler and Weijia Kuang. Resonant tidal excitation of internal waves in the Earth's fluid core. *Physics of The Earth and Planetary Interiors*, 232:15–25, 2014.

Robert H Tyler, Wade G Henning, and Christopher W Hamilton. Tidal heating in a magma ocean within Jupiter's moon Io. *Astrophysical Journal Supplement Series*, 218(2), 2015.

APPENDIX A

Vertical Balance

A.1. Uniform-Density Hydrostatic Fluid

Conservation of mass in a fluid layer of thickness h requires

$$\nabla_H \cdot (\rho h \mathbf{u}_H) + \partial_t(\rho h) = \mathfrak{s}, \tag{A.1.1}$$

where $\mathfrak{s}$ is a "source" describing fluxes other than that advected by the flow (e.g. precipitation/evaporation). We also may write $\partial_t h = \partial_t \eta + \partial_t \eta_b$, where η and η_b are the upper and lower boundaries of the layer, respectively. Using this we may rewrite (A.1.1) as

$$\nabla_H \cdot (\rho h \mathbf{u}_H) + \rho \partial_t \eta = \mathfrak{s} + \rho \partial_t \eta_b - h \partial_t \rho. \tag{A.1.2}$$

If the fluid is uniform in density and hydrostatically balanced, then the pressure in the fluid is due only to the displacement of the upper surface, $p = \rho g \eta$, and we may rewrite (A.1.2) as

$$\nabla_H \cdot (\rho h \mathbf{u}_H) + g^{-1} \partial_t p = \mathfrak{s} + \rho \partial_t \eta_b. \tag{A.1.3}$$

In many cases $\partial_t \eta_b$ is zero (e.g. the bottom boundary is fixed). More generally, it may be prescribed and absorbed into the source term $\mathfrak{s}$ (as we shall now assume), or it may depend on the solution in an iterative approach.

Let us now divide through (A.1.3) by ρh_0, where h_0 is an arbitrary constant which may be chosen to reflect the average value for h, for example. We get

$$\nabla_H \cdot \left(\frac{h}{h_0} \mathbf{u}_H \right) + \frac{1}{g \rho h_0} \partial_t p = \mathfrak{s}, \tag{A.1.4}$$

which, recognizing that in this case $\rho = \rho_0$, can be written in nondimensional notation as

$$\tilde{\nabla} \cdot \left(\frac{h}{h_0} \tilde{\mathbf{u}} \right) + \frac{(2\Omega_s r)^2}{g h_0} \tilde{\partial}_t \tilde{p} = \tilde{\mathfrak{s}}. \tag{A.1.5}$$

We see that (A.1.5) is covered by the generic "second relationship" (3.2.1) by simply selecting $L_h \to h/h_0$ and $L_V \to (2\Omega_s r)^2 / (g h_0) = 1/\tilde{c}_0^2$, where $\tilde{c}_0^2$ is the nondimensional shallow-water speed in a fluid of thickness h_0.

In many applications, the fluid thickness h is considered to be uniform and it is convenient to take $h_0 = h$. In this case $L_h \to I$ and, assuming no fluid sources ($\tilde{\mathfrak{s}} = 0$), we may write (A.1.5) as

$$\tilde{\nabla} \cdot \tilde{\mathbf{u}} + \tilde{\nu}^2 \tilde{\partial}_t \tilde{p} = 0, \tag{A.1.6}$$

where the squared slowness $\tilde{\nu}^2 = 1/\tilde{c}_0^2$ is in this case a real, scalar parameter that is prescribed.

A.2. Stratified Incompressible Hydrostatic Fluid

We consider here the case of a stratified, incompressible fluid where the vertical momentum balance is hydrostatic. To include curvature effects in a spherically-symmetric domain, we shall assume that the background vertical stratification is expressed as $\rho_0 = \rho_0(r)$, and that the gravitational acceleration is $g_0 = g_0(r)$.

In this case, temporal variations in the fluid density ρ are caused by advection of ρ_0 by the radial velocity w:

$$\partial_t \rho + w \partial_r \rho_0 = 0. \tag{A.2.1}$$

For an incompressible fluid, mass conservation reduces to the continuity equation

$$\nabla_H \cdot \mathbf{u}_H + r^{-2} \partial_r \left(r^2 w \right) = 0. \tag{A.2.2}$$

For a hydrostatic fluid, the radial momentum equation reduces to

$$\partial_r p = -g_0 \rho. \tag{A.2.3}$$

Combine (A.2.1) and (A.2.3) to obtain

$$w = -\frac{1}{N^2 \rho_0} \partial_r \partial_t p, \tag{A.2.4}$$

where the squared buoyancy frequency, for this incompressible case, is $N^2 = -g_0 \left(\frac{d \ln \rho_0}{dr} \right)$. Combining (A.2.2) and (A.2.4) to remove w gives

$$\nabla_H \cdot \mathbf{u}_H = r^{-2} \partial_r \left(r^2 \left(\frac{1}{N^2 \rho_0} \partial_r \partial_t p \right) \right), \tag{A.2.5}$$

or, in nondimensional form

$$\tilde{\nabla}_H \cdot \tilde{\mathbf{u}}_H = - \left[\left[-\frac{1}{G_s} r \right] \left[2 + \tilde{\partial}_r \right] \left[r \tilde{N}^2 \right]^{-1} \left[-\frac{\tilde{N}^2}{\tilde{g}_0} + \tilde{\partial}_r \right] [G_s] \right] \{ \partial_t \tilde{p} \}, \tag{A.2.6}$$

where $\tilde{N}^2 = N^2/(2\Omega_s)^2$.

We see that (A.2.6) is included in the generic second relationship (3.2.2) provided we chose $L_h = I$ (the identity operator), $\tilde{\mathfrak{s}} = 0$, and

$$L_V \{ \cdot \} = \left[\left[-\frac{1}{G_s} r \right] \left[2 + \tilde{\partial}_r \right] \left[r \tilde{N}^2 \right]^{-1} \left[-\frac{\tilde{N}^2}{\tilde{g}_0} + \tilde{\partial}_r \right] [G_s] \right] \{ \cdot \}. \tag{A.2.7}$$

The operator L_V is presented as factored suboperators in square brackets that are applied sequentially from right to left to the argument in curly brackets. Some of the operators reduce to simple multiplicative factors.

Consider first the particular solution. In this case, we choose $G_s = G_s(r)$ to follow the radial dependence of the forcing $\tilde{\mathfrak{G}}$. For tidal potential forcing of spherical-harmonic degree two, this radial dependence is then r^2. For more generality, consider a trial solution of the form $Y = C_q r^q$, where C_q and q are (potentially complex) constants. Note that $\tilde{\partial}_r Y = qY$. Using (A.2.7), we see

$$L_V Y = \left(-(1+q) \left(\frac{q}{\tilde{N}^2} - \frac{1}{\tilde{g}_0} \right) - \tilde{\partial}_r \left\{ \frac{q}{\tilde{N}^2} - \frac{1}{\tilde{g}_0} \right\} \right) Y. \tag{A.2.8}$$

The particular solution for the tidal response can then be obtained in *TROPF* by prescribing

$$L_V = \left[-(1+q) \left(\frac{q}{\tilde{N}^2} - \frac{1}{\tilde{g}_0} \right) - \tilde{\partial}_r \left\{ \frac{q}{\tilde{N}^2} - \frac{1}{\tilde{g}_0} \right\} \right], \tag{A.2.9}$$

where $q = 2$ for the typical case of a degree-two prescribed tidal potential. In a layer where $\tilde{N}^2$ and $\tilde{g}_0$ vary slowly with radius, the second term may be neglected. If additionally $\frac{q}{\tilde{N}^2} << \frac{1}{\tilde{g}_0}$, we have $L_V \to (1+q)q/\tilde{N}^2$. In any case, we see that the operator L_V reduces to a prescribed scalar parameter (i.e. $L_V = \tilde{\nu}^2_{(q)}$) as in Section A.1.

The particular solution (with $q = 2$) automatically satisfies the conditions $\tilde{p}(r = 0) = 0$ as well as $\tilde{p}(r \to \infty) = 0$, provided ρ_0 decays exponentially with radius. But within a medium where the parameters vary between layers, one may need to add solutions to the homogeneous governing equation (i.e. the governing equation without a forcing term) in order to satisfy the matching conditions between layers. Sometimes the conditions may be given in terms of the radial velocity. For reference, in nondimensional form, (A.1.5) can be written

$$\tilde{w} = \left[-\frac{1}{\tilde{N}^2}\tilde{\partial}_r + \frac{1}{\tilde{g}_0} \right] \tilde{\partial}_t \tilde{p} \tag{A.2.10}$$

which describes how a condition on $\tilde{w}$ may be translated as a condition on $\tilde{p}$.

Note that in calculating the particular solution, q is prescribed from the forcing such that the squared slowness

$$\tilde{\nu}^2 = -(1+q)\left(\frac{q}{\tilde{N}^2} - \frac{1}{\tilde{g}_0}\right) - \tilde{\partial}_r \left(\frac{q}{\tilde{N}^2} - \frac{1}{\tilde{g}_0}\right) \tag{A.2.11}$$

is regarded as prescribed and TROPF solves the equations for the horizontal structure. The same approach is possible for the homogenous solutions if q can be prescribed as representing one of the eigenvalues of a vertical mode, or perhaps the q associated with a fluid layer.

More generally, the homogenous solutions can be obtained by considering one of the eigenvalues of the horizontal "Hough" eigenfunctions $\lambda_j = -\tilde{\nu}_{(j)}^{-2} = -\tilde{c}_{e,(j)}^2$ (see, for example, Section 5.1) and solving the vertical equation subject to the boundary/matching conditions. In this case, we must determine $q_{(j)}$ given $\tilde{\nu}_{(j)}^2$ and from (A.2.11) we can express this relationship as

$$q_{(j)} = \frac{1}{2}\left(\frac{\tilde{N}^2}{\tilde{g}_0} - 1\right) \pm \frac{1}{2}\left(\left(\frac{\tilde{N}^2}{\tilde{g}_0} + 1\right)^2 - 4\tilde{\nu}_{(j)}^2 \tilde{N}^2\right)^{1/2}. \tag{A.2.12}$$

This is a useful expression since $q_{(j)}$ describes the spatial scale (and whether the vertical dependence $r^{q_{(j)}}$ is wavelike or evanescent) associated with the eigenmode j. If, for example, the spatial scale is relatively small then one may see the homogenous solutions as simply adding a boundary layer effect that does not appreciably alter the larger solution given by the particular solution.

A.3. Stratified Compressible Nonhydrostatic Fluid

The equations assumed here to describe the vertical balance are identical to those in Ioannou and Lindzen [1993b] but with additional terms representing heating sources $\mathfrak{J}$ and Newtonian cooling/radiation losses (with parameters γ_t, γ_ρ). Assuming spherical coordinates and a periodic time dependence such that ∂_t can be treated as a complex constant, these equations are the continuity equation,

$$\partial_t \rho + w\partial_r \rho_0 + \rho_0 \chi = 0, \tag{A.3.1}$$

divergence,

$$\chi = \nabla_H \cdot \mathbf{u}_H + r^{-2}\partial_r\left(r^2 w\right), \tag{A.3.2}$$

the radial momentum equation

$$\partial_t w = -\rho_0^{-1}\partial_r p - \rho_0^{-1} g_0 \rho + \partial_r \mathfrak{G}, \tag{A.3.3}$$

and the linearized thermodynamic equation,

$$\gamma_t^{-1}\partial_t p = c_s^2 \gamma_\rho^{-1}\partial_t \rho - g_0^{-1}\rho_0 c_s^2 N^2 w + \Gamma_1 \kappa \rho_0 \mathfrak{J}, \tag{A.3.4}$$

where ρ is mass density, w is radial velocity, $c_s = (\Gamma_1 p_0/\rho_0)^{1/2}$ is the speed of sound, g_0 is gravitational acceleration, $\gamma_t = \left(1 + \frac{\alpha_t}{\partial_t}\right)^{-1}$ and $\gamma_\rho = \left(1 + \frac{\alpha_\rho}{\partial_t}\right)^{-1}$, with attenuation constants α_t and α_ρ, $N^2 = -g_0\left(\frac{d\ln\rho_0}{dr} + \frac{g_0}{c_s^2}\right)$, $\kappa = \left(\frac{\Gamma_1 - 1}{\Gamma_1}\right)$, and $\Gamma_1 = \left(\frac{d\ln p}{d\ln\rho}\right)_s$ is the compressibility assuming constant entropy.

Using the definition of N^2, it is assumed that $\partial_r\rho_0 = -\rho_0\left(N^2/g_0 + g_0/c_s^2\right)$, $\partial_r(p)/\rho_0 = \partial_r(p/\rho_0) - (N^2/g_0 + g_0/c_s^2)(p/\rho_0)$. Then, (A.3.1) can be written as

$$\partial_t \rho = \rho_0\left(\frac{N^2}{g_0} + \frac{g_0}{c_s^2}\right) w - \rho_0 \chi, \tag{A.3.5}$$

and (A.3.3) can be written as

$$\rho = -\frac{\rho_0}{g_0}\partial_t w + \frac{\rho_0}{g_0}\left[\left(\frac{N^2}{g_0}+\frac{g_0}{c_s^2}\right) - \partial_r\right]\frac{p}{\rho_0} + \frac{\rho_0}{g_0}\partial_r \mathfrak{G}. \tag{A.3.6}$$

Combining (A.3.5) and (A.3.4) to remove ρ,

$$\gamma_t^{-1}\partial_t \frac{p}{\rho_0} = \left(\gamma_\rho^{-1} g_0 + \left(\gamma_\rho^{-1}-1\right) g_0^{-1} c_s^2 N^2\right) w - \gamma_\rho^{-1} c_s^2 \chi + \Gamma_1 \kappa \mathfrak{J}. \tag{A.3.7}$$

Combining (A.3.6), and (A.3.4) to remove ρ,

$$\left[\partial_t\partial_t + \gamma_\rho N^2\right] w = -\left[\frac{g_0}{c_s^2}\left(\frac{\gamma_t^{-1}}{\gamma_\rho^{-1}}-1\right) - \frac{N^2}{g_0} + \partial_r\right]\partial_t \frac{p}{\rho_0} + \partial_r\partial_t \mathfrak{G} + \gamma_\rho \frac{g_0 \Gamma_1 \kappa \mathfrak{J}}{c_s^2}. \tag{A.3.8}$$

Combining (A.3.2) and (A.3.7) to remove χ,

$$\nabla_H \cdot \mathbf{u}_H = -\frac{\gamma_\rho}{\gamma_t}\frac{1}{c_s^2}\partial_t \frac{p}{\rho_0} + \left[\frac{g_0}{c_s^2} + \left(1-\gamma_\rho\right)\frac{N^2}{g_0} - \frac{2}{r} - \partial_r\right] w + \frac{\gamma_\rho \Gamma_1 \kappa \mathfrak{J}}{c_s^2}. \tag{A.3.9}$$

Combining (A.3.8) and (A.3.9) to remove w,

(A.3.10)

$$\nabla_H \cdot \mathbf{u}_H = -\left[\frac{\gamma_\rho}{\gamma_t}\frac{1}{c_s^2} + \left[\frac{g_0}{c_s^2} + \left(1-\gamma_\rho\right)\frac{N^2}{g_0} - \frac{2}{r} - \partial_r\right]\left[\partial_t\partial_t + \gamma_\rho N^2\right]^{-1}\left[\frac{g_0}{c_s^2}\left(\frac{\gamma_t^{-1}}{\gamma_\rho^{-1}}-1\right) - \frac{N^2}{g_0} + \partial_r\right]\right]\left\{\partial_t \frac{p}{\rho_0}\right\}$$

(A.3.11)

$$+ \left[\frac{g_0}{c_s^2} + \left(1-\gamma_\rho\right)\frac{N^2}{g_0} - \frac{2}{r} - \partial_r\right]\left[\partial_t\partial_t + \gamma_\rho N^2\right]^{-1}\left\{\partial_r\partial_t \mathfrak{G} + \gamma_\rho \frac{g_0 \Gamma_1 \kappa \mathfrak{J}}{c_s^2}\right\} + \frac{\gamma_\rho \Gamma_1 \kappa \mathfrak{J}}{c_s^2}.$$

Multiplying through by $2\Omega r^2/G_s$ and using definitions in Table 1, (A.3.10) can be written in nondimensional form:

(A.3.12)

$$\tilde{\nabla}_H \cdot \tilde{\mathbf{u}}_H = -\frac{1}{G_s}\left[\frac{\gamma_\rho}{\gamma_t}\frac{1}{\tilde{c}_s^2} - r\left[-\frac{\tilde{g}_0}{\tilde{c}_s^2} + \left(\gamma_\rho - 1\right)\frac{\tilde{N}^2}{\tilde{g}_0} + 2 + \tilde{\partial}_r\right]\left[r\left(\tilde{\partial}_t\tilde{\partial}_t + \gamma_\rho \tilde{N}^2\right)\right]^{-1}\left[\frac{\tilde{g}_0}{\tilde{c}_s^2}\left(\frac{\gamma_\rho}{\gamma_t}-1\right) - \frac{\tilde{N}^2}{\tilde{g}_0} + \tilde{\partial}_r\right]\right]\left\{G_s \partial_t \tilde{p}\right\}$$

(A.3.13)

$$- \frac{r}{G_s}\left[-\frac{\tilde{g}_0}{\tilde{c}_s^2} + \left(\gamma_\rho - 1\right)\frac{\tilde{N}^2}{\tilde{g}_0} + 2 + \tilde{\partial}_r\right]\left[r\left(\tilde{\partial}_t\tilde{\partial}_t + \gamma_\rho \tilde{N}^2\right)\right]^{-1}\left\{\tilde{\partial}_r\left\{G_s \tilde{\partial}_t \tilde{\mathfrak{G}}\right\} + \gamma_\rho \frac{\tilde{g}_0 \Gamma_1 \kappa G_s \tilde{\mathfrak{J}}}{\tilde{c}_s^2}\right\} + \frac{\gamma_\rho \Gamma_1 \kappa \tilde{\mathfrak{J}}}{\tilde{c}_s^2}.$$

Defining the operator

(A.3.14)

$$L_V\left\{\cdot\right\} = \frac{1}{G_s}\left[\frac{\gamma_\rho}{\gamma_t}\frac{1}{\tilde{c}_s^2} - r\left[-\frac{\tilde{g}_0}{\tilde{c}_s^2} + \left(\gamma_\rho - 1\right)\frac{\tilde{N}^2}{\tilde{g}_0} + 2 + \tilde{\partial}_r\right]\left[r\left(\tilde{\partial}_t\tilde{\partial}_t + \gamma_\rho \tilde{N}^2\right)\right]^{-1}\left[\frac{\tilde{g}_0}{\tilde{c}_s^2}\left(\frac{\gamma_\rho}{\gamma_t}-1\right) - \frac{\tilde{N}^2}{\tilde{g}_0} + \tilde{\partial}_r\right]\right]\left\{G_s\left\{\cdot\right\}\right\}$$

and

(A.3.15)

$$\tilde{\mathfrak{s}} = -\frac{r}{G_s}\left[-\frac{\tilde{g}_0}{\tilde{c}_s^2} + \left(\gamma_\rho - 1\right)\frac{\tilde{N}^2}{\tilde{g}_0} + 2 + \tilde{\partial}_r\right]\left[r\left(\tilde{\partial}_t\tilde{\partial}_t + \gamma_\rho \tilde{N}^2\right)\right]^{-1}\left\{\tilde{\partial}_r\left\{G_s \tilde{\partial}_t \tilde{\mathfrak{G}}\right\} + \gamma_\rho \frac{\tilde{g}_0 \Gamma_1 \kappa G_s \tilde{\mathfrak{J}}}{\tilde{c}_s^2}\right\} + \frac{\gamma_\rho \Gamma_1 \kappa \tilde{\mathfrak{J}}}{\tilde{c}_s^2},$$

(A.3.12) can be written as

$$\tilde{\nabla}_H \cdot \tilde{\mathbf{u}}_H = -L_V \tilde{\partial}_t \tilde{p} + \tilde{\mathfrak{s}}, \tag{A.3.16}$$

which we see is covered by the generic second relationship (3.2.2) used in *TROPF*, provided one also assumes $L_h = I$.

As in the example in Section A.2 we consider a trial solution proportional to r^q

(A.3.17)

$$L_V = \tilde{\nu}^2_{(q)} = \frac{\gamma_\rho}{\gamma_t}\frac{1}{\tilde{c}_s^2} + \left(\frac{\tilde{g}_0}{\tilde{c}_s^2} + (1-\gamma_\rho)\frac{\tilde{N}^2}{\tilde{g}_0} - 1 - q\right)\left(\frac{q - \frac{\tilde{N}^2}{\tilde{g}_0} + \frac{\tilde{g}_0}{\tilde{c}_s^2}\left(\frac{\gamma_\rho}{\gamma_t} - 1\right)}{\tilde{\partial}_t\tilde{\partial}_t + \gamma_\rho\tilde{N}^2}\right) - \tilde{\partial}_r\left(\frac{q - \frac{\tilde{N}^2}{\tilde{g}_0} + \frac{\tilde{g}_0}{\tilde{c}_s^2}\left(\frac{\gamma_\rho}{\gamma_t} - 1\right)}{\tilde{\partial}_t\tilde{\partial}_t + \gamma_\rho\tilde{N}^2}\right),$$

which, with $q = 2$ for degree-two forcing, provides the squared slowness parameter $\tilde{\nu}^2$ to be used as input in *TROPF* for obtaining the particular solution for the tidal response.

As in Section A.2, homogeneous solutions may also be needed to satisfy application-specific boundary and/or matching conditions. The nondimensional radial velocity can be obtained from $\tilde{p}$ using (A.3.8) to obtain

$$\tilde{w} = \left[\tilde{\partial}_t\tilde{\partial}_t + \gamma_\rho\tilde{N}^2\right]^{-1}\left\{-\left[\frac{\tilde{g}_0}{\tilde{c}_s^2}\left(\frac{\gamma_t^{-1}}{\gamma_\rho^{-1}} - 1\right) - \frac{\tilde{N}^2}{\tilde{g}_0} + \tilde{\partial}_r\right]\tilde{\partial}_t\tilde{p} + \tilde{\partial}_r\tilde{\partial}_t\tilde{\mathfrak{G}} + \gamma_\rho\frac{\tilde{g}_0\Gamma_1\kappa\tilde{\mathfrak{J}}}{\tilde{c}_s^2}\right\}, \tag{A.3.18}$$

where $\tilde{\mathfrak{J}} = (2\Omega_s G_s)^{-1}\mathfrak{J}$.

APPENDIX B

Propagating Spherical Harmonics

B.1. Expansion of Fields and their Analytical Derivatives and Integrals

B.1.1. Expansion of Fields. Consider a smoothly varying field Ξ with bounded real values defined over the surface of a potentially rotating sphere. We define a coordinate system of colatitude (θ) and longitude (ϕ) whereby the angle θ is defined with respect to the rotation vector (positive spin axis) of the sphere, and ϕ increases in the direction of prograde rotation. (If the sphere is not rotating then these prescriptions for coordinate reference become arbitrary.) Further assume that Ξ is also a smooth function of time. From the latter assumption, a Fourier expansion is permitted; the temporal dependence may be parameterized by the phase $\omega_{(k)}t$, where $\omega_{(k)}$ is the frequency of the kth term in the expansion, and t is time. Without loss of generality, a dual Fourier expansion is permitted whereby the temporal and longitudinal dependencies are represented parametrically by the phase $(s_{(j)}\phi - \omega_{(k)}t)$, where it is assumed that $s_{(j)}$ is a real, non-negative integer and $\omega_{(k)}$ is a real number that may be positive or negative. For simplicity in what follows, let us consider only one of these Fourier components (from here on withholding the (j), (k) indices). Arbitrary Ξ may be represented by an appropriate sum of $\Xi^{s;\omega} = \Xi^{s;\omega}(\theta, \phi, t)$ harmonic components. Terms where the phase $(s\phi - \omega t)$ involves $\omega > 0$ correspond to propagation in the direction of increasing longitude ϕ while terms where $\omega < 0$ correspond to propagation in the direction of decreasing longitude. The sum of a pair of two terms that differ only by the sign of ω represents a standing oscillation in the fixed θ, ϕ coordinate system.

Consider now the further colatitudinal expansion of $\Xi^{s;\omega}$ in terms of Associated Legendre functions. Specifically, let

$$\Xi^{s;\omega} = \Sigma_{n=s}^{\infty} S_n^{s;\omega}, \tag{B.1.1}$$

where

$$\begin{aligned} S_n^{s;\omega} &= P_n^s(\cos\theta)\left(a_n^s \mathrm{e}^{i(s\phi-\omega t)} + a_n^{s*}\mathrm{e}^{-i(s\phi-\omega t)}\right) \\ &= P_n^s(\cos\theta) 2\left(R\left(a_n^s\right)\cos(s\phi-\omega t) - I\left(a_n^s\right)\sin(s\phi-\omega t)\right). \end{aligned} \tag{B.1.2}$$

Here, $S_n^{s;\omega}$ represents the real-valued propagating spherical harmonic function, P_n^s are the Associated Legendre functions of degree n and order (also called rank) s, a_n^s are the complex expansion coefficients (where a_n^{s*} is the complex conjugate of a_n^s), and $R(\cdot)$, $I(\cdot)$ refer to the real and imaginary parts. The expansions above are equivalent to a spherical-harmonic expansion of $\Xi^{s;\omega}$ in a coordinate system rotating with angular speed ω/s. As stated, s is non-negative and so the direction of propagation is controlled by the sign of ω.

The standing wave, for example, can be written as

$$\begin{aligned} S_n^{s;\omega} + S_n^{s;-\omega} =& P_n^s(\cos\theta) 2\left(a_n^s \mathrm{e}^{is\phi} + a_n^{s*}\mathrm{e}^{-is\phi}\right)\cos(\omega t) \\ =& P_n^s(\cos\theta) 4\left(R\left(a_n^s\right)\cos(s\phi) - I\left(a_n^s\right)\sin(s\phi)\right)\cos(\omega t). \end{aligned} \tag{B.1.3}$$

Computationally, is it advantageous to avoid summation loops by using matrix multiplication. Toward this, note that (B.1.1) may be written as

$$\Xi^{s;\omega} = \mathrm{e}^{i(s\phi-\omega t)}(\mathbf{P_n^s})^T\mathbf{a_n^s} + \left\{\mathrm{e}^{i(s\phi-\omega t)}(\mathbf{P_n^s})^T\mathbf{a_n^s}\right\}^*, \tag{B.1.4}$$

where $\mathbf{a_n^s}$ is the column vector of coefficients a_n^s (with $n = s, s+1, s+2...\infty$), $\mathbf{P_n^s}$ is a column vector of Associated Legendre functions $P_n^s(\cos\theta)$, and $\{\cdot\}^*$ provides the complex conjugate. Introducing a complex-valued spherical harmonic function

$$Y_n^{s;\omega} = P_n^s(\cos\theta)\mathrm{e}^{i(s\phi-\omega t)}, \tag{B.1.5}$$

with associated column vector

$$\mathbf{Y}_\mathbf{n}^{\mathbf{s};\omega} = \mathbf{P}_\mathbf{n}^\mathbf{s}\mathrm{e}^{i(s\phi-\omega t)}, \tag{B.1.6}$$

we may write (B.1.1) as

$$\Xi^{s;\omega} = (\mathbf{Y}_\mathbf{n}^{\mathbf{s};\omega})^\mathbf{T}\mathbf{a}_\mathbf{n}^\mathbf{s} + \left\{(\mathbf{Y}_\mathbf{n}^{\mathbf{s};\omega})^\mathbf{T}\mathbf{a}_\mathbf{n}^\mathbf{s}\right\}^* . \tag{B.1.7}$$

Finally, note that the row vectors $(\mathbf{P}_\mathbf{n}^\mathbf{s})^T$ and $(\mathbf{Y}_\mathbf{n}^{\mathbf{s};\omega})^\mathbf{T}$ provide values for only one location and time. To avoid loops over the space/time locations, we now generalize by regarding these row vectors as matrices, where each row is again a row vector of the spherical-harmonic coefficients at specific location and time and the columns range over the various location/time samples. While this avoidance of loops drastically increases computational speed, it also increases the memory requirements. Note that these will be full, not sparse, matrices with $N_{lon}N_{lat}N_tN$ entries, where N_{lon}, N_{lat} are the respective numbers of longitude and latitude grid points, N_t is the number of time instances, and N is the number of spherical-harmonic components. Further note that as N is increased to represent higher harmonics, the need for grid resolution in the mapping also increases. For example with $1/4 \times 1/4$ degree spatial resolution, $N_t = 10$, and $N = 500$, there are about five billion (5191200000) elements.

A compromise over this trade off between computational speed and storage may be flexibly attained as the mapping operation (B.1.7) is the same regardless of what subset of space/time points $(\mathbf{Y}_\mathbf{n}^{\mathbf{s};\omega})^T$ includes, and so we may loop through subsets chosen for convenience and computational performance. Toward this, note that there is redundancy in the longitudinal and temporal dependencies with a propagating spherical harmonic in that it is only the span of the total phase $(s\phi - \omega t)$ that needs to be resolved. In this case, the most computationally efficient approach is that the rows of $(\mathbf{Y}_\mathbf{n}^{\mathbf{s};\omega})^T$ sample latitude and phase. But this can be inconvenient when wanting to choose a common grid for combining multiple spherical-harmonic components (i.e. the choice of N_{lon}, N_{lat} may involve considerations beyond what is strictly required for resolving the component considered). Further, if we regard the operation of mapping of coefficients to a grid as a post-processing step where computational speed is less critical than it is in the core operations of the spherical harmonics, this argues for a convenient choice of the subset chosen for $(\mathbf{Y}_\mathbf{n}^{\mathbf{s};\omega})^T$. Of course for the purpose of mapping, one could loop over the degrees and immediately sum through the elements in a row of $(\mathbf{Y}_\mathbf{n}^{\mathbf{s};\omega})^T$, collapsing the N dimension. Aside from losing the description of the dependence on spherical-harmonic degree in the mapped result, this can be computationally inefficient because of looping over degrees (and N can be large) but also because if the matrix $(\mathbf{Y}_\mathbf{n}^{\mathbf{s};\omega})^T$ is not explicitly built then it cannot be used in multiple matrix operations.

One convenient choice notes that when mapping a propagating spherical harmonic, because the phase varies as $(s\phi - \omega t)$ an explicit description of the temporal dependence is not needed once the description of the longitudinal dependence has been mapped (i.e. a map at $t = 0$ is understood to propagate East/West as described in the opening paragraph of this section). An explicit demonstration of the time dependence then seems needed only as a post-processing element when combining counter-propagating components. A logical choice is then to let $(\mathbf{Y}_\mathbf{n}^{\mathbf{s};\omega})^\mathbf{T}$ become a matrix where each row corresponds to a location at a specified time which may be incrementally advanced in a time loop to produce frames for a movie. These frames can be stored with respect to a third array dimension such that the field arrays become three-dimensional (lon, lat, time).

B.1.2. Analytical Derivatives. The time rate of change of a spherical harmonic component can be written as

$$\begin{aligned}\partial_t S_n^{s;\omega} &= P_n^s(\cos\theta)\left\{(-i\omega a_n^s)\,\mathrm{e}^{i(s\phi-\omega t)} + (-i\omega a_n^s)^*\,\mathrm{e}^{-i(s\phi-\omega t)}\right\} \\ &= P_n^s(\cos\theta)2\left(R\left(-i\omega a_n^s\right)\cos(s\phi-\omega t) - I\left(-i\omega a_n^s\right)\sin(s\phi-\omega t)\right),\end{aligned} \tag{B.1.8}$$

which we see has the same form as (B.1.2), with the coefficient a_n^s simply replaced by $-i\omega a_n^s$. Similarly, the longitudinal derivative is

$$\begin{aligned}\partial_\phi S_n^{s;\omega} &= P_n^s(\cos\theta)\left\{(isa_n^s)\,\mathrm{e}^{i(s\phi-\omega t)} + (isa_n^s)^*\,\mathrm{e}^{-i(s\phi-\omega t)}\right\} \\ &= P_n^s(\cos\theta)2\left(R\left(isa_n^s\right)\cos(s\phi-\omega t) - I\left(isa_n^s\right)\sin(s\phi-\omega t)\right),\end{aligned} \tag{B.1.9}$$

where a_n^s has been replaced by isa_n^s.

The derivative with respect to colatitude is

$$\begin{aligned}\partial_\theta S_n^{s;\omega} &= \partial_\theta P_n^s(\cos\theta)\left(a_n^s\mathrm{e}^{i(s\phi-\omega t)} + a_n^{s*}\mathrm{e}^{-i(s\phi-\omega t)}\right) \\ &= \partial_\theta P_n^s(\cos\theta)2\left(R\left(a_n^s\right)\cos(s\phi-\omega t) - I\left(a_n^s\right)\sin(s\phi-\omega t)\right),\end{aligned} \tag{B.1.10}$$

where we can use the Chain Rule together with Associated Legendre recursion relationships to express $\partial_\theta P_n^s(\cos\theta)$ in terms of Associated Legendre functions of the same degree n but different order s, where we require $s \geq 0$ for consistency with previous assumptions. If $s \geq 1$, we use

$$\left(1-x^2\right)^{1/2}\frac{d}{dx}P_n^s(x) = \frac{1}{2}\left[(n+s)(n-s+1)\,P_n^{s-1}(x) - P_n^{s+1}(x)\right] \tag{B.1.11}$$

to write

$$\partial_\theta P_n^s(\cos\theta) = -\frac{1}{2}\left[(n+s)(n-s+1)\,P_n^{s-1}(\cos\theta) - P_n^{s+1}(\cos\theta)\right], \tag{B.1.12}$$

while if $s < 1$, we use the identity

$$P_n^{-s} = (-1)^s\frac{(n-s)!}{(n+s)!}P_n^s \tag{B.1.13}$$

to rewrite (B.1.12) as

$$\partial_\theta P_n^s(\cos\theta) = -\frac{1}{2}\left[(n+s)(n-s+1)(-1)^{1-s}\frac{(n-1+s)!}{(n+1-s)!}P_n^{1-s}(\cos\theta) - P_n^{s+1}(\cos\theta)\right]. \tag{B.1.14}$$

Now consider the derivatives applied to the arbitrary field $\Xi^{s;\omega}$ rather than just a single spherical harmonic $S_n^{s;\omega}$. The temporal and longitudinal derivatives of the field $\Xi^{s;\omega}$ (see B.1.4) can be expressed as

$$\partial_t\Xi^{s;\omega} = \mathrm{e}^{\mathbf{i(s\phi-\omega t)}}\left(\mathbf{P_n^s}\right)^{\mathbf{T}}\{-i\omega\mathbf{a_n^s}\} + \left\{\mathrm{e}^{\mathbf{i(s\phi-\omega t)}}\left(\mathbf{P_n^s}\right)^{\mathbf{T}}\{-i\omega\mathbf{a_n^s}\}\right\}^*, \tag{B.1.15}$$

$$\partial_\phi\Xi^{s;\omega} = \mathrm{e}^{\mathbf{i(s\phi-\omega t)}}\left(\mathbf{P_n^s}\right)^{\mathbf{T}}\{is\mathbf{a_n^s}\} + \left\{\mathrm{e}^{\mathbf{i(s\phi-\omega t)}}\left(\mathbf{P_n^s}\right)^{\mathbf{T}}\{is\mathbf{a_n^s}\}\right\}^*, \tag{B.1.16}$$

or, using (B.1.15),

$$\partial_t\Xi^{s;\omega} = \left(\mathbf{Y_n^{s;\omega}}\right)^T\{-i\omega\mathbf{a_n^s}\} + \left\{\left(\mathbf{Y_n^{s;\omega}}\right)^T\{-i\omega\mathbf{a_n^s}\}\right\}^*, \tag{B.1.17}$$

$$\partial_\phi\Xi^{s;\omega} = \left(\mathbf{Y_n^{s;\omega}}\right)^T\{is\mathbf{a_n^s}\} + \left\{\left(\mathbf{Y_n^{s;\omega}}\right)^T\{is\mathbf{a_n^s}\}\right\}^*, \tag{B.1.18}$$

which we see differs from (B.1.15) by simply the replacement of the coefficients $\mathbf{a_n^s}$ by modified forms $\{-i\omega\mathbf{a_n^s}\}$ or $\{is\mathbf{a_n^s}\}$. The derivative with respect to colatitude is

$$\partial_\theta\Xi^{s;\omega} = \mathrm{e}^{i(s\phi-\omega t)}(\partial_\theta\mathbf{P_n^s})^T\mathbf{a_n^s} + \left\{\mathrm{e}^{i(s\phi-\omega t)}(\partial_\theta\mathbf{P_n^s})^T\mathbf{a_n^s}\right\}^*, \tag{B.1.19}$$

where

$$\partial_\theta\mathbf{P_n^s} = \frac{1}{2}\left[(n+s)(n-s+1)\,\mathbf{P_n^{s-1}} - \mathbf{P_n^{s+1}}\right] \tag{B.1.20}$$

if $s-1 \geq 0$, while if $s-1 < 0$,

$$\partial_\theta\mathbf{P_n^s} = \frac{1}{2}\left[(n+s)(n-s+1)(-1)^{1-s}\frac{(n-1+s)!}{(n+1-s)!}\mathbf{P_n^{1-s}} - \mathbf{P_n^{s+1}}\right]. \tag{B.1.21}$$

The tangential ('horizontal') component of the nondimensional gradient operator is

$$\tilde{\nabla}_H = \hat{\theta}\frac{1}{\sin\theta}\partial_\theta + \hat{\phi}\partial_\phi \tag{B.1.22}$$

such that

$$\begin{aligned}\tilde{\nabla}_H \Xi^{s;\omega} = &\left(\mathrm{e}^{i(s\phi-\omega t)}(\partial_\theta \mathbf{P}_\mathbf{n}^\mathbf{s})^T \mathbf{a}_\mathbf{n}^\mathbf{s} + \left\{\mathrm{e}^{i(s\phi-\omega t)}(\partial_\theta \mathbf{P}_\mathbf{n}^\mathbf{s})^T \mathbf{a}_\mathbf{n}^\mathbf{s}\right\}^*\right)\hat{\theta} \\ &+ \left(\mathrm{e}^{i(s\phi-\omega t)}(\frac{\mathbf{1}}{\sin\theta}\mathbf{P}_\mathbf{n}^\mathbf{s})^T \{is\mathbf{a}_\mathbf{n}^\mathbf{s}\} + \left\{\mathrm{e}^{\mathbf{i(s\phi-\omega t)}}\left(\frac{\mathbf{1}}{\sin\theta}\mathbf{P}_\mathbf{n}^\mathbf{s}\right)^T \{is\mathbf{a}_\mathbf{n}^\mathbf{s}\}\right\}^*\right)\hat{\phi}.\end{aligned} \tag{B.1.23}$$

Note that the $\partial_\theta \Xi^{s;\omega}$ produces terms with different s.

B.1.3. Analytical Integrals. Let us now consider analytical methods for calculating integrals, particularly integrals of products of two fields. The orthonormality of the Fourier-Legendre bases provide useful simplifications when considering integrals of fields or their products. First, from the form of (B.1.2) it is clear that a spherical harmonic has a vanishing integral when integrated either spatially over the full range of longitude, or temporally over the period $2\pi/\omega$ multiplied by an integer.

Less obvious are integrals involving products of the spherical harmonics. Let us define (similar to B.1.1, B.1.4) a second field

$$\Upsilon^{\nu;\varphi} = \Sigma_{q=\nu}^{\infty} T_q^{\nu;\varphi}, \tag{B.1.24}$$

where

$$T_q^{\nu;\varphi} = P_q^v(\cos\theta)\left\{b_q^v \mathrm{e}^{i(v\phi-\varphi t)} + b_q^{v*}\mathrm{e}^{-i(v\phi-\varphi t)}\right\}. \tag{B.1.25}$$

In matrix notation, (B.1.24) can be written

$$\Upsilon^{\nu;\varphi} = \mathrm{e}^{i(\nu\phi-\varphi t)}(\mathbf{P}_\mathbf{q}^\nu)^T \mathbf{a}_\mathbf{q}^\nu + \left\{\mathrm{e}^{i(\nu\phi-\varphi t)}(\mathbf{P}_\mathbf{q}^\nu)^T \mathbf{a}_\mathbf{q}^\nu\right\}^*. \tag{B.1.26}$$

B.1.3.1. *Temporal Average Over Period.* The temporal average of the product $S_n^{s;\omega}T_q^{v;\varphi}$ over the period $2\pi/\omega$ is

$$\begin{aligned}\frac{\int_0^{(2\pi/\omega)} S_n^{s;\omega}T_q^{v;\varphi}dt}{\int_0^{(2\pi/\omega)} dt} &= \frac{1}{(2\pi/\omega)}\int_0^{(2\pi/\omega)} S_n^{s;\omega}T_q^{v;\varphi}dt = \\ &P_n^s(\cos\theta)P_q^v(\cos\theta)\frac{1}{(2\pi/\omega)}\int_0^{(2\pi/\omega)}\left\{a_n^s b_q^v \mathrm{e}^{i[(s+v)\phi-(\omega+\varphi)t]} + a_n^{s*}b_q^{v*}\mathrm{e}^{-i[(s+v)\phi-(\omega+\varphi)t]}\right\}dt \\ &+ P_n^s(\cos\theta)P_q^v(\cos\theta)\frac{1}{(2\pi/\omega)}\int_0^{(2\pi/\omega)}\left\{a_n^s b_q^{v*} \mathrm{e}^{i[(s-v)\phi-(\omega-\varphi)t]} + a_n^{s*}b_q^{v}\mathrm{e}^{-i[(s-v)\phi-(\omega-\varphi)t]}\right\}dt \\ &= P_n^s(\cos\theta)P_q^v(\cos\theta)\frac{i}{2\pi}\left(a_n^s b_q^v \mathrm{e}^{i(s+v)\phi}\left\{\frac{\mathrm{e}^{-i2\pi\varphi/\omega}-1}{1+\varphi/\omega}\right\} - a_n^{s*}b_q^{v*}\mathrm{e}^{-i(s+v)\phi}\left\{\frac{\mathrm{e}^{i2\pi\varphi/\omega}-1}{1+\varphi/\omega}\right\}\right) \\ &\quad + P_n^s(\cos\theta)P_q^v(\cos\theta)\frac{i}{2\pi}\left(a_n^s b_q^{v*} \mathrm{e}^{i(s-v)\phi}\left\{\frac{\mathrm{e}^{i2\pi\varphi/\omega}-1}{1-\varphi/\omega}\right\} - a_n^{s*}b_q^{v}\mathrm{e}^{-i(s-v)\phi}\left\{\frac{\mathrm{e}^{-i2\pi\varphi/\omega}-1}{1-\varphi/\omega}\right\}\right).\end{aligned} \tag{B.1.27}$$

Note that the terms in curly brackets in the last expression can be indeterminate for some values of φ/ω (e.g. $\varphi/\omega \to 1$). These cases can be evaluated by using L'Hôpital's Rule with differentiation of the numerator and denominator with respect to φ/ω.

Some special cases are as follows:

Case $\varphi = \omega$:

$$\begin{aligned}(\text{B.1.28}) \quad \frac{1}{(2\pi/\omega)}\int_0^{(2\pi/\omega)} S_n^{s;\omega}T_q^{v;\varphi}dt &= P_n^s(\cos\theta)P_q^v(\cos\theta)\left\{a_n^s b_q^{v*}\mathrm{e}^{i[(s-v)\phi]} + a_n^{s*}b_q^v\mathrm{e}^{-i[(s-v)\phi]}\right\} \\ &= P_n^s(\cos\theta)P_q^v(\cos\theta)\left(2R\left(a_n^s\right)R\left(b_q^v\right) + 2I\left(a_n^s\right)I\left(b_q^v\right)\right)\cos\left((s-v)\,\phi\right) \\ &\quad + P_n^s(\cos\theta)P_q^v(\cos\theta)\left(2R\left(a_n^s\right)I\left(b_q^v\right) - 2I\left(a_n^s\right)R\left(b_q^v\right)\right)\sin\left((s-v)\,\phi\right).\end{aligned}$$

Case $\varphi = -\omega$:

$$\begin{aligned}(\text{B.1.29}) \quad \frac{1}{(2\pi/\omega)}\int_0^{(2\pi/\omega)} S_n^{s;\omega}T_q^{v;\varphi}dt &= P_n^s(\cos\theta)P_q^v(\cos\theta)\left\{a_n^s b_q^{v}\mathrm{e}^{i[(s+v)\phi]} + a_n^{s*}b_q^{v*}\mathrm{e}^{-i[(s+v)\phi]}\right\} \\ &= P_n^s(\cos\theta)P_q^v(\cos\theta)\left(2R\left(a_n^s\right)R\left(b_q^v\right) - 2I\left(a_n^s\right)I\left(b_q^v\right)\right)\cos\left((s+v)\,\phi\right) \\ &\quad - P_n^s(\cos\theta)P_q^v(\cos\theta)\left(2R\left(a_n^s\right)I\left(b_q^v\right) + 2I\left(a_n^s\right)R\left(b_q^v\right)\right)\sin\left((s+v)\,\phi\right).\end{aligned}$$

The time average (over period $2\pi/\omega$) of a product of two fields $\Xi^{s;\omega}$ and $\Upsilon^{v;\varphi}$ (rather than just the product of two spherical-harmonic terms, as above), can be described using (B.1.4) and (B.1.24) as

$$\begin{aligned}(\text{B.1.30}) \quad &\frac{\int_0^{(2\pi/\omega)}\Xi^{s;\omega}\Upsilon^{v;\varphi}dt}{\int_0^{(2\pi/\omega)}dt} = \frac{1}{(2\pi/\omega)}\int_0^{(2\pi/\omega)}\Xi^{s;\omega}\Upsilon^{v;\varphi}dt \\ &= \frac{1}{(2\pi/\omega)}\int_0^{(2\pi/\omega)}\left[\mathrm{e}^{i(s\phi-\omega t)}(\mathbf{P_n^s})^T\mathbf{a_n^s} + \left\{\mathrm{e}^{i(s\phi-\omega t)}(\mathbf{P_n^s})^T\mathbf{a_n^s}\right\}^*\right]\circ\left[\mathrm{e}^{i(\nu\phi-\varphi t)}(\mathbf{P_q^\nu})^T\mathbf{b_q^\nu} + \left\{\mathrm{e}^{i(\nu\phi-\varphi t)}(\mathbf{P_q^\nu})^T\mathbf{b_q^\nu}\right\}^*\right]dt \\ &= \frac{1}{(2\pi/\omega)}\int_0^{(2\pi/\omega)}\left\{\left\{\mathrm{e}^{is\phi}(\mathbf{P_n^s})^T\mathbf{a_n^s}\right\}\circ\left\{\mathrm{e}^{i\nu\phi}(\mathbf{P_q^\nu})^T\mathbf{b_q^\nu}\right\}\mathrm{e}^{-i(\omega+\varphi)t} + \left\{\mathrm{e}^{is\phi}(\mathbf{P_n^s})^T\mathbf{a_n^s}\right\}\circ\left\{\mathrm{e}^{i\nu\phi}(\mathbf{P_q^\nu})^T\mathbf{b_q^\nu}\right\}^*\mathrm{e}^{-i(\omega-\varphi)t}\right\} \\ &\quad + \left\{\left\{\mathrm{e}^{is\phi}(\mathbf{P_n^s})^T\mathbf{a_n^s}\right\}\circ\left\{\mathrm{e}^{i\nu\phi}(\mathbf{P_q^\nu})^T\mathbf{b_q^\nu}\right\}\mathrm{e}^{-i(\omega+\varphi)t} + \left\{\mathrm{e}^{is\phi}(\mathbf{P_n^s})^T\mathbf{a_n^s}\right\}\circ\left\{\mathrm{e}^{i\nu\phi}(\mathbf{P_q^\nu})^T\mathbf{b_q^\nu}\right\}^*\mathrm{e}^{-i(\omega-\varphi)t}\right\}^* dt \\ &= \frac{i}{(2\pi)}\left(\left\{\mathrm{e}^{is\phi}(\mathbf{P_n^s})^T\mathbf{a_n^s}\right\}\circ\left\{\mathrm{e}^{i\nu\phi}(\mathbf{P_q^\nu})^T\mathbf{b_q^\nu}\right\}\left\{\frac{\mathrm{e}^{-i2\pi\varphi/\omega}-1}{1+\varphi/\omega}\right\} + \left\{\mathrm{e}^{is\phi}(\mathbf{P_n^s})^T\mathbf{a_n^s}\right\}\circ\left\{\mathrm{e}^{i\nu\phi}(\mathbf{P_q^\nu})^T\mathbf{b_q^\nu}\right\}^*\left\{\frac{\mathrm{e}^{i2\pi\varphi/\omega}-1}{1-\varphi/\omega}\right\}\right) \\ &+\left\{\frac{i}{(2\pi)}\left(\left\{\mathrm{e}^{is\phi}(\mathbf{P_n^s})^T\mathbf{a_n^s}\right\}\circ\left\{\mathrm{e}^{i\nu\phi}(\mathbf{P_q^\nu})^T\mathbf{b_q^\nu}\right\}\left\{\frac{\mathrm{e}^{-i2\pi\varphi/\omega}-1}{1+\varphi/\omega}\right\} + \left\{\mathrm{e}^{is\phi}(\mathbf{P_n^s})^T\mathbf{a_n^s}\right\}\circ\left\{\mathrm{e}^{i\nu\phi}(\mathbf{P_q^\nu})^T\mathbf{b_q^\nu}\right\}^*\left\{\frac{\mathrm{e}^{i2\pi\varphi/\omega}-1}{1-\varphi/\omega}\right\}\right)\right\}^*,\end{aligned}$$

where the symbol '$\circ$' represents the Hadamard product operation (represented as '.*' in Matlab/Octave) and simply describes element-wise multiplication. The special cases corresponding to (B.1.28, B.1.29) become

Case $\varphi = \omega$:

$$\begin{aligned}(\text{B.1.31}) \quad \frac{\int_0^{(2\pi/\omega)}\Xi^{s;\omega}\Upsilon^{v;\varphi}dt}{\int_0^{(2\pi/\omega)}dt} &= \left(\left\{\mathrm{e}^{is\phi}(\mathbf{P_n^s})^T\mathbf{a_n^s}\right\}\circ\left\{\mathrm{e}^{i\nu\phi}(\mathbf{P_q^\nu})^T\mathbf{b_q^\nu}\right\}^*\right) \\ &\quad + \left\{\left(\left\{\mathrm{e}^{is\phi}(\mathbf{P_n^s})^T\mathbf{a_n^s}\right\}\circ\left\{\mathrm{e}^{i\nu\phi}(\mathbf{P_q^\nu})^T\mathbf{b_q^\nu}\right\}^*\right)\right\}^*,\end{aligned}$$

Case $\varphi = -\omega$:

$$\begin{aligned}(\text{B.1.32}) \quad \frac{\int_0^{(2\pi/\omega)}\Xi^{s;\omega}\Upsilon^{v;\varphi}dt}{\int_0^{(2\pi/\omega)}dt} &= \left\{\mathrm{e}^{is\phi}(\mathbf{P_n^s})^T\mathbf{a_n^s}\right\}\circ\left\{\mathrm{e}^{i\nu\phi}(\mathbf{P_q^\nu})^T\mathbf{b_q^\nu}\right\} \\ &\quad + \left\{\left\{\mathrm{e}^{is\phi}(\mathbf{P_n^s})^T\mathbf{a_n^s}\right\}\circ\left\{\mathrm{e}^{i\nu\phi}(\mathbf{P_q^\nu})^T\mathbf{b_q^\nu}\right\}\right\}^*.\end{aligned}$$

Because the time averaged fields are often of interest, let us make a few comments here on the results. The time average of two arbitrary fields $\Xi^{s;\omega}$ and $\Upsilon^{v;\varphi}$ can be calculated analytically from the spherical-harmonic coefficients using the last equality in (B.1.31). We see that terms include only two types of longitudinal dependence—forms proportional to $\mathrm{e}^{i(s-\varphi)\phi}$ and $\mathrm{e}^{i(s+\varphi)\phi}$. In our expansions, it is assumed that both s and φ are non-negative integers. Therefore, there are two important cases that can be distinguished: In the

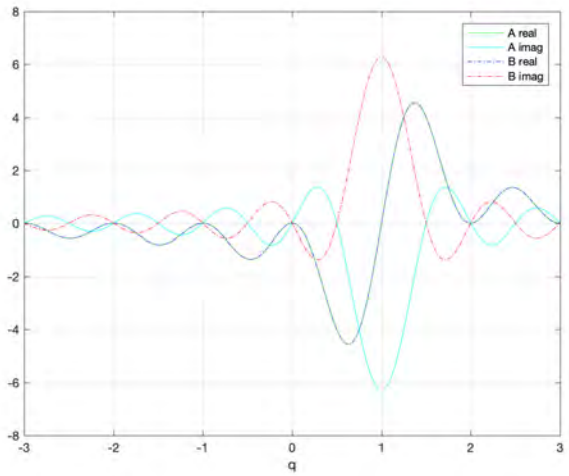

FIGURE B.1.1. The real and imaginary parts of the factors $\left\{\frac{e^{-i2\pi q}-1}{1+q}\right\}$ and $\left\{\frac{e^{i2\pi q}-1}{1-q}\right\}$ as a function of q are shown as 'A' and 'B' respectively. These factors appear in the temporal (Section B.1.3.1) and longitudinal (Section B.1.3.2) integration of field products.

case $s = \varphi$, the field product is independent of longitude. In other cases, the field varies sinusoidally with longitude. When (as below) further averaging along longitude is performed, only terms with $s = \varphi$ contribute to the longitudinal average. More generally, the time average product of $\Xi^{s;\omega}$ and $\Upsilon^{v;\varphi}$ only includes terms proportional to $e^{i(s\pm\varphi)\phi}$.

Finally, notice that the factors from the temporal integration specifically include only $\left(e^{-i2\pi\varphi/\omega}-1\right)(1+\varphi/\omega)^{-1}$ and $\left(e^{i2\pi\varphi/\omega}-1\right)(1-\varphi/\omega)^{-1}$, and factors with a similar form shall show up in the next section when considering longitudinal averaging. As described above, these terms can become indefinite for $\varphi/\omega = \pm 1$ but converge in that case to $-i2\pi$. A more general description of these factors is plotted in Figure B.1.1.

B.1.3.2. *Spatial Average Over Longitude.* The spatial average of the product $S_n^{s;\omega}T_q^{v;\varphi}$ over a full circle of longitude (and recalling that ν, s are both positive integers) is

$$\begin{aligned}
(\text{B.1.33}) \quad \frac{\int_0^{2\pi} S_n^{s;\omega}T_q^{v;\varphi} r\sin(\theta)\,d\phi}{\int_0^{2\pi} r\sin(\theta)\,d\phi} &= \frac{1}{2\pi}\int_0^{2\pi} S_n^{s;\omega}T_q^{v;\varphi}d\phi = \\
&P_n^s(\cos\theta)P_q^v(\cos\theta)\frac{1}{2\pi}\int_0^{2\pi}\left\{a_n^s b_q^v e^{i[(s+v)\phi-(\omega+\varphi)t]} + a_n^{s*}b_q^{v*}e^{-i[(s+v)\phi-(\omega+\varphi)t]}\right\}d\phi \\
&+ P_n^s(\cos\theta)P_q^v(\cos\theta)\frac{1}{2\pi}\int_0^{2\pi/\omega}\left\{a_n^s b_q^{v*} e^{i[(s-v)\phi-(\omega-\varphi)t]} + a_n^{s*}b_q^{v}e^{-i[(s-v)\phi-(\omega-\varphi)t]}\right\}d\phi \\
&= P_n^s(\cos\theta)P_q^v(\cos\theta)\frac{i}{2\pi}\left(-a_n^s b_q^{v*}e^{-i(\omega-\varphi)t}\left\{\frac{e^{i2\pi(s-\nu)}-1}{s-\nu}\right\} + a_n^{s*}b_q^v e^{i(\omega-\varphi)t}\left\{\frac{e^{-i2\pi(s-\nu)}-1}{s-\nu}\right\}\right).
\end{aligned}$$

Note that the terms in curly brackets in the last line have indeterminate forms when $\nu = s$. These can be evaluated using L'Hôpital's Rule.

Case $\nu = s$:

$$\frac{\int_0^{2\pi} S_n^{s;\omega} T_q^{v;\varphi} r\sin(\theta)\,d\phi}{\int_0^{2\pi} r\sin(\theta)\,d\phi} = \frac{1}{2\pi}\int_0^{2\pi} S_n^{s;\omega} T_q^{v;\varphi} d\phi = \tag{B.1.34}$$

$$P_n^s(\cos\theta)P_q^v(\cos\theta)\frac{1}{2\pi}\int_0^{2\pi}\left\{a_n^s b_q^v \mathrm{e}^{i[(s+v)\phi-(\omega+\varphi)t]} + a_n^{s*} b_q^{v*}\mathrm{e}^{-i[(s+v)\phi-(\omega+\varphi)t]}\right\}d\phi$$

$$+ P_n^s(\cos\theta)P_q^v(\cos\theta)\frac{1}{2\pi}\int_0^{2\pi/\omega}\left\{a_n^s b_q^{v*} \mathrm{e}^{i[(s-v)\phi-(\omega-\varphi)t]} + a_n^{s*} b_q^{v}\mathrm{e}^{-i[(s-v)\phi-(\omega-\varphi)t]}\right\}d\phi$$

$$= P_n^s(\cos\theta)P_q^v(\cos\theta)\left(a_n^s b_q^{v*}\mathrm{e}^{-i(\omega-\varphi)t} + a_n^{s*} b_q^v \mathrm{e}^{i(\omega-\varphi)t}\right).$$

B.1.3.3. *Spatial Average Over Colatitude.* When considering area-weighted averages over colatitude, a weighting factor $\sin(\theta)$ is included such that the average is

$$\frac{\int_0^{\pi} S_n^{s;\omega} T_q^{v;\varphi} r\sin(\theta)\,d\theta}{\int_0^{\pi} r\sin(\theta)\,d\theta} = \frac{1}{2}\int_{-1}^{1} S_n^{s;\omega} T_q^{v;\varphi} d(\cos\theta)$$

$$= \frac{1}{2}\int_{-1}^{1}\left\{a_n^s b_q^v \mathrm{e}^{i[(s+v)\phi-(\omega+\varphi)t]} + a_n^{s*} b_q^{v*}\mathrm{e}^{-i[(s+v)\phi-(\omega+\varphi)t]}\right\} P_n^s(\cos\theta)P_q^v(\cos\theta)d(\cos\theta)$$

$$+ \frac{1}{2}\int_{-1}^{1}\left\{a_n^s b_q^{v*} \mathrm{e}^{i[(s-v)\phi-(\omega-\varphi)t]} + a_n^{s*} b_q^{v}\mathrm{e}^{-i[(s-v)\phi-(\omega-\varphi)t]}\right\} P_n^s(\cos\theta)P_q^v(\cos\theta)d(\cos\theta)$$

$$= \left\{a_n^s b_q^v \mathrm{e}^{i[(s+v)\phi-(\omega+\varphi)t]} + a_n^{s*} b_q^{v*}\mathrm{e}^{-i[(s+v)\phi-(\omega+\varphi)t]}\right\}\frac{(n+s)!}{(2n+1)(n-s)!}\delta_{n,q}$$

$$+ \left\{a_n^s b_q^{v*} \mathrm{e}^{i[(s-v)\phi-(\omega-\varphi)t]} + a_n^{s*} b_q^{v}\mathrm{e}^{-i[(s-v)\phi-(\omega-\varphi)t]}\right\}\frac{(n+s)!}{(2n+1)(n-s)!}\delta_{n,q} \tag{B.1.35}$$

where $(\cdot)!$ is the factorial operation, $\delta_{n,q}$ is the Kronecker delta, and the relationship

$$\frac{\int_0^{\pi} P_n^s(\cos\theta)\,P_q^v(\cos\theta)\sin(\theta)\,d\theta}{\int_0^{\pi}\sin(\theta)\,d\theta} = \frac{(n+s)!}{(2n+1)(n-s)!}\delta_{n,q} \tag{B.1.36}$$

has been used.

B.1.3.4. *Spatial Average Over Longitude and Latitude.* The spatial average of the product $S_n^{s;\omega}T_q^{v;\varphi}$ over the global surface is

$$\frac{1}{4\pi}\int_0^{2\pi}\int_0^{\pi} S_n^{s;\omega} T_q^{v;\varphi}\sin(\theta)\,d\theta d\phi = \tag{B.1.37}$$

$$\frac{i}{2\pi}\left(-a_n^s b_q^{v*}\mathrm{e}^{-i(\omega-\varphi)t}\left\{\frac{\mathrm{e}^{i2\pi(s-\nu)}-1}{s-\nu}\right\} + a_n^{s*} b_q^v \mathrm{e}^{i(\omega-\varphi)t}\left\{\frac{\mathrm{e}^{-i2\pi(s-\nu)}-1}{s-\nu}\right\}\right)\frac{(n+s)!}{(2n+1)(n-s)!}\delta_{n,q}.$$

Note that the terms in curly brackets in the last line have indeterminate forms when $\nu = s$. These can be evaluated using L'Hôpital's Rule.

Case $\nu = s$:

$$\frac{1}{4\pi}\int_0^{2\pi}\int_0^{\pi} S_n^{s;\omega} T_q^{v;\varphi}\sin(\theta)\,d\theta d\phi = \left(a_n^s b_q^{v*}\mathrm{e}^{-i(\omega-\varphi)t} + a_n^{s*} b_q^v \mathrm{e}^{i(\omega-\varphi)t}\right)\frac{(n+s)!}{(2n+1)(n-s)!}\delta_{n,q}. \tag{B.1.38}$$

B.1.3.5. *Time Average + Spatial average Over Longitude and Latitude.* When we further take the time average over period $2\pi/\omega$ of the global averaged forms in the last section, we have

$$\text{(B.1.39)}\quad \frac{\omega}{2\pi}\frac{1}{4\pi}\int_0^{2\pi/\omega}\int_0^{2\pi}\int_0^{\pi} S_n^{s;\omega}T_q^{v;\varphi}\sin(\theta)\,d\theta d\phi dt =$$
$$\frac{1}{4\pi^2}\left(a_n^s b_q^{v*}\left\{\frac{\mathrm{e}^{i2\pi\varphi/\omega}-1}{1-\varphi/\omega}\right\}\left\{\frac{\mathrm{e}^{i2\pi(s-\nu)}-1}{s-\nu}\right\} - a_n^{s*}b_q^{v}\left\{\frac{\mathrm{e}^{-i2\pi\varphi/\omega}-1}{1-\varphi/\omega}\right\}\left\{\frac{\mathrm{e}^{-i2\pi(s-\nu)}-1}{s-\nu}\right\}\right)\frac{(n+s)!}{(2n+1)\,(n-s)!}\delta_{n,q}.$$

Case $\nu = s$:

$$\text{(B.1.40)}\quad \frac{\omega}{2\pi}\frac{1}{4\pi}\int_0^{2\pi/\omega}\int_0^{2\pi}\int_0^{\pi} S_n^{s;\omega}T_q^{v;\varphi}\sin(\theta)\,d\theta d\phi dt =$$
$$\frac{1}{4\pi^2}\left(a_n^s b_q^{v*}\left\{\frac{\mathrm{e}^{i2\pi\varphi/\omega}-1}{1-\varphi/\omega}\right\}\{i2\pi\} - a_n^{s*}b_q^{v}\left\{\frac{\mathrm{e}^{-i2\pi\varphi/\omega}-1}{1-\varphi/\omega}\right\}\{-i2\pi\}\right)\frac{(n+s)!}{(2n+1)\,(n-s)!}\delta_{n,q}.$$

Case $\varphi = \omega$:

$$\text{(B.1.41)}\quad \frac{\omega}{2\pi}\frac{1}{4\pi}\int_0^{2\pi/\omega}\int_0^{2\pi}\int_0^{\pi} S_n^{s;\omega}T_q^{v;\varphi}\sin(\theta)\,d\theta d\phi dt =$$
$$\frac{1}{4\pi^2}\left(a_n^s b_q^{v*}\{-i2\pi\}\left\{\frac{\mathrm{e}^{i2\pi(s-\nu)}-1}{s-\nu}\right\} - a_n^{s*}b_q^{v}\{i2\pi\}\left\{\frac{\mathrm{e}^{-i2\pi(s-\nu)}-1}{s-\nu}\right\}\right)\frac{(n+s)!}{(2n+1)\,(n-s)!}\delta_{n,q}.$$

Case $\nu = s$, $\varphi = \omega$:

$$\text{(B.1.42)}\quad \frac{\omega}{2\pi}\frac{1}{4\pi}\int_0^{2\pi/\omega}\int_0^{2\pi}\int_0^{\pi} S_n^{s;\omega}T_q^{v;\varphi}\sin(\theta)\,d\theta d\phi dt \quad = \quad \left(a_n^s b_q^{v*} + a_n^{s*}b_q^{v}\right)\frac{(n+s)!}{(2n+1)\,(n-s)!}\delta_{n,q}.$$

Note that $\left(a_n^s b_q^{v*} + a_n^{s*}b_q^{v}\right) = 2R(a_n^s)R(b_n^s) + 2I(a_n^s)I(b_n^s)$.

The time + space average of a product of two fields $\Xi^{s;\omega}$ and $\Upsilon^{v;\varphi}$ (rather than just the product of two spherical-harmonic terms, as in (B.1.39)) can be written

$$\text{(B.1.43)}\quad \frac{\omega}{2\pi}\frac{1}{4\pi}\int_0^{2\pi/\omega}\int_0^{2\pi}\int_0^{\pi} \Xi^{s;\omega}\Upsilon^{v;\varphi}\sin(\theta)\,d\theta d\phi dt =$$
$$\frac{1}{4\pi^2}\left(\mathbf{a_n^s}\circ\mathbf{b_q^{\nu *}}\left\{\frac{\mathrm{e}^{i2\pi\varphi/\omega}-1}{1-\varphi/\omega}\right\}\left\{\frac{\mathrm{e}^{i2\pi(s-\nu)}-1}{s-\nu}\right\} - \mathbf{a_n^{s\,*}}\circ\mathbf{b_q^{\nu}}\left\{\frac{\mathrm{e}^{-i2\pi\varphi/\omega}-1}{1-\varphi/\omega}\right\}\left\{\frac{\mathrm{e}^{-i2\pi(s-\nu)}-1}{s-\nu}\right\}\right)\frac{(n+s)!}{(2n+1)\,(n-s)!},$$

where we see ratios in curly brackets which can be indeterminate for either $\varphi/\omega \to 1$ or $s = \nu$, and in these special cases we can use L'Hôpital's Rule to write the following:

Case $\nu = s$:

$$\text{(B.1.44)}\quad \frac{\omega}{2\pi}\frac{1}{4\pi}\int_0^{2\pi/\omega}\int_0^{2\pi}\int_0^{\pi} \Xi^{s;\omega}\Upsilon^{v;\varphi}\sin(\theta)\,d\theta d\phi dt =$$
$$\frac{1}{4\pi^2}\left(\mathbf{a_n^s}\circ\mathbf{b_q^{\nu *}}\left\{\frac{\mathrm{e}^{i2\pi\varphi/\omega}-1}{1-\varphi/\omega}\right\}\{i2\pi\} - \mathbf{a_n^{s\,*}}\circ\mathbf{b_q^{\nu}}\left\{\frac{\mathrm{e}^{-i2\pi\varphi/\omega}-1}{1-\varphi/\omega}\right\}\{-i2\pi\}\right)\frac{(n+s)!}{(2n+1)\,(n-s)!}\delta_{n,q}.$$

Case $\varphi = \omega$:

$$\text{(B.1.45)}\quad \frac{\omega}{2\pi}\frac{1}{4\pi}\int_0^{2\pi/\omega}\int_0^{2\pi}\int_0^{\pi} \Xi^{s;\omega}\Upsilon^{v;\varphi}\sin(\theta)\,d\theta d\phi dt =$$
$$\frac{1}{4\pi^2}\left(\mathbf{a_n^s}\circ\mathbf{b_q^{\nu *}}\{-i2\pi\}\left\{\frac{\mathrm{e}^{i2\pi(s-\nu)}-1}{s-\nu}\right\} - \mathbf{a_n^{s\,*}}\circ\mathbf{b_q^{\nu}}\{i2\pi\}\left\{\frac{\mathrm{e}^{-i2\pi(s-\nu)}-1}{s-\nu}\right\}\right)\frac{(n+s)!}{(2n+1)\,(n-s)!}\delta_{n,q}.$$

Case $\nu = s$, $\varphi = \omega$:

$$\frac{\omega}{2\pi}\frac{1}{4\pi}\int_0^{2\pi/\omega}\int_0^{2\pi}\int_0^{\pi}\Xi^{s;\omega}\Upsilon^{v;\varphi}\sin(\theta)\,d\theta d\phi dt \quad = \quad \left(\mathbf{a}_{\mathbf{n}}^{\mathbf{s}}\circ\mathbf{b}_{\mathbf{q}}^{\nu\,*}+\mathbf{a}_{\mathbf{n}}^{\mathbf{s}\,*}\circ\mathbf{b}_{\mathbf{q}}^{\nu}\right)\frac{(n+s)!}{(2n+1)\,(n-s)!}\delta_{n,q}. \tag{B.1.46}$$

APPENDIX C

Nonlinear Solutions

Although the equations *TROPF* solves are linear, one can obtain nonlinear solutions by calculating solutions over a range and then identifying the solutions obeying the nonlinear relationship. For example, consider the simple case with operators $L_h = I$, $L_V = 1/\tilde{c}_e^2$, and $L_{\tilde{\alpha}_d} = L_{\tilde{\alpha}_r} = \alpha$, where we require α satisfy the nonlinear dissipation drag form

$$\alpha = \frac{C_D}{h}|\bar{\mathbf{u}}_H|, \tag{C.0.1}$$

with $|\bar{\mathbf{u}}_H|$ the spatiotemporal average of the flow velocity. The nondimensional form can be written

$$\tilde{\alpha} = (2\Omega_s)^{-1}\left(\frac{G_s}{2\Omega_s r}\right)\frac{C_D}{h}|\bar{\tilde{\mathbf{u}}}_H| = \left(\frac{G_s C_D}{(2\Omega_s)^2 r}\frac{\tilde{c}_e^2}{h}\right)\frac{1}{\tilde{c}_e^2}\left(\tilde{u}_0^2 + 2\bar{\tilde{E}}_k\right)^{1/2}, \tag{C.0.2}$$

where $\bar{\tilde{E}}_k$ is the average kinetic energy density of the solution and $\tilde{u}_0^2$ is a constant representing an additional background squared flow velocity we may wish to add. Using the definition of $\tilde{T}$ (Table 1), we may rewrite this equation as

$$\left(\frac{G_s C_D}{(2\Omega_s)^2 r}\frac{\tilde{c}_e^2}{h}\right) = \frac{|\tilde{\omega}|\tilde{c}_e^2}{\tilde{T}\left(\tilde{u}_0^2 + 2\bar{\tilde{E}}_k\right)^{1/2}}. \tag{C.0.3}$$

If $\tilde{c}_e^2 = gh$, as we would expect for a hydrostatic uniform-density ocean, for example, and assuming g/r is a constant in the fluid, then $\tilde{c}_e^2/h = g/((2\Omega_s)^2 r)$ and (C.0.3) becomes

$$\left(\frac{G_s C_D g}{(2\Omega_s)^4 r^3}\right) = \frac{|\tilde{\omega}|\tilde{c}_e^2}{\tilde{T}\left(\tilde{u}_0^2 + 2\bar{\tilde{E}}_k\right)^{1/2}}. \tag{C.0.4}$$

On a spherical surface, the term on the left is a constant and does not depend on the tidal response solution. The term on the right varies with the solution ($\bar{\tilde{E}}_k$) and also parameters controlling the solution which may appear as coordinates in parameter-space diagrams of solution scenarios. We may then demand that the solution fall on the contour where (C.0.4) is satisfied. In considering generic cases where the value of the left-side term is uncertain, we may include a range of contours in the parameter space diagrams and one may select the appropriate contour for a specific application.

The *TROPF* spherical-harmonic routines assume parameters are spherically symmetric (i.e. they may vary with radius but not longitude and latitude). Hence, there does not seem to be an easy way of extending this to allow nonlinear forms dependent on local values of the solution.

APPENDIX D

Self Gravity and Viscoelastic Ice Membrane

In the formulation to allow for self gravity and/or coupling with a (visco)elastic-membrane ice shell (see [Matsuyama et al., 2018] and references therein), the coefficients for $\tilde{p}$ and $\tilde{p}_h$ (where $\tilde{p}_h$ is $\tilde{p}$ in the absence of self gravity and the ice membrane) are related by

$$\mathbf{p^s_n} = \beta_n \mathbf{p^s_{h,n}} \tag{D.0.1}$$

where β_n is a diagonal matrix of potentially complex coefficients (i.e. the coefficient vector elements $\mathbf{p^s_{h,n}}$ are weighted by β_n).

While the total pressure $\tilde{p}$ (including self gravity and ice coupling) is appropriate in the horizontal momentum equation, $\tilde{p}_h$ should be used in the second relationship (3.2.2) which concerns continuity and mass conservation. The matrix equation representing (3.2.2) is (3.2.12) and should in this case involve $\mathbf{p^s_{h,n}}$ rather than $\mathbf{p^s_n}$. Using (D.0.1), this is then rectified and we return to the standard *TROPF* equations by simply redefining $L_V \rightarrow L_V \beta_n^{-1}$.

Some physical insight into the effect of the weighting by β_n follows easily in the case where L_V (prior to weighting by β_n) is given by $L_V = \tilde{\nu}^2 = 1/\tilde{c}_e^2$, where the squared slowness $\tilde{\nu}^2$ and squared wavespeed $\tilde{c}_e^2$ are simply real scalars. The weighting then gives $L_V \rightarrow L_V \beta_n^{-1} = \tilde{c}_e^{-2} \beta_n^{-1}$. We see then that the effective squared wave speed becomes dispersive (degree dependent). This reflects the physical effect of the ice rigidity adding a restoring force to the ocean that will typically increase the wavespeed of the coupled ocean+ice. When β_n has an imaginary component, then there is also dissipation associated with ocean tidal energy being absorbed by the viscoelastic ice layer. Using (3.2.12) we can write the modified, degree-dependent wave speed as

$$\tilde{c}^2_{e;(n)} = \tilde{c}_e^2 \frac{1}{\mathrm{real}(1/\beta_n)} = \tilde{c}_e^2 \frac{\beta_n \beta_n^*}{\mathrm{real}(\beta_n)}. \tag{D.0.2}$$

Using (3.2.4) we can relate the imaginary component of β_n to the *TROPF* dissipation parameter $\tilde{\alpha}_p$ as

$$\tilde{\alpha}_{p,(n)} = \tilde{\omega} \frac{\mathrm{Imag}\,(1/\beta_n)}{\mathrm{Real}\,(1/\beta_n)} = -\tilde{\omega} \frac{\mathrm{Imag}\,(\beta_n)}{\mathrm{Real}\,(\beta_n)}, \tag{D.0.3}$$

where we have written $\tilde{\alpha}_{p,(n)}$ to emphasize that $\tilde{\alpha}_p$ is degree dependent in this case.

In the case where the β_n entries are equivalent (or can be taken as approximately equivalent), the dissipation due to the ice is identical to the cases covered in previous section where dissipation is proportional to potential energy density (ignoring here also other dissipation terms). Even in the general case of degree-dependent β_n, dissipation is still proportional to potential energy, though with proportionality coefficients varying with degree. Hence, the dissipation due to the viscoelastic membrane is in the family where dissipation is drawn from the potential rather than kinetic energy density.